SCOUR AROUND SPUR DIKES AND BRIDGE PIERS FOUNDED IN COHESIVE SEDIMENT MIXTURES

Ph. D. THESIS

by

AJAY SINGH LODHI

DEPARTMENT OF CIVIL ENGINEERING
INDIAN INSTITUTE OF TECHNOLOGY ROORKEE
ROORKEE – 247 667 (INDIA)
APRIL, 2015

SCOUR AROUND SPUR DIKES AND BRIDGE PIERS FOUNDED IN COHESIVE SEDIMENT MIXTURES

A THESIS

Submitted in partial fulfilment of the requirements for the award of the degree of

DOCTOR OF PHILOSOPHY

in

CIVIL ENGINEERING

by

AJAY SINGH LODHI

DEPARTMENT OF CIVIL ENGINEERING
INDIAN INSTITUTE OF TECHNOLOGY ROORKEE
ROORKEE – 247 667 (INDIA)
APRIL, 2015

INDIAN INSTITUTE OF TECHNOLOGY ROORKEE
ROORKEE

CANDIDATE'S DECLARATION

I hereby certify that the work which is being presented in the thesis entitled **"SCOUR AROUND SPUR DIKES AND BRIDGE PIERS FOUNDED IN COHESIVE SEDIMENT MIXTURES"** in partial fulfillment of the requirements for the award of the degree of Doctor of Philosophy and submitted in the Department of Civil Engineering of the Indian Institute of Technology Roorkee is an authentic record of my own work carried out during the period from July, 2010 to April, 2015 under the supervision of Dr. P. K. Sharma, Associate Professor, Department of Civil Engineering, Dr. G. J. Chakrapani, Professor, Department of Earth Sciences, Indian Institute of Technology Roorkee, Roorkee and Dr. R. K. Jain, Associate Professor, Department of Civil Engineering, Vishwakarma Government Engineering College Chandkheda, Gandhinagar.

The matter presented in this thesis has not been submitted by me for the award of any other degree of this or any other Institute.

Signature of the Candidate

This is to certify that the above statement made by the candidate is correct to the best of our knowledge.

Signature of the Supervisors

The Ph.D. Viva-Voce Examination of **Mr. Ajay Singh Lodhi**, Research Scholar, has been held on ……

Chairman, SRC **Signature of External Examiner**

This is to certify that the student has made all the corrections in the thesis.

Signature of Supervisors **Head of the Department**
Dated:

ABSTRACT

One of the major considerations in the design and construction of a bridge is the scour around its foundation. Many of the bridge failures have been attributed to the scour or the undermining of hydraulic structures (i.e. piers, abutments and spur dikes etc.). Hence, for safe and economic design of hydraulic structures, it becomes essential to estimate the scour depth around such structures with greater accuracy. The accurate estimation of scour depth around bridge piers and spur dikes below the stream bed is important since, that determines the depth of such structures. Several formulae and mathematical models developed for the estimation of the scour depth are still primarily based on theoretical approaches and laboratory tests because of variable field data. Accurate field measurements are difficult to obtain due to the severe three dimensional flow pattern that occur at bridges during flooding, high cost of instrumentation and the costs of getting skilled personnel at bridge sites during period of peak flow. Unrealistic estimation of scour depth may lead to either over expenses in the construction or failure of the structure.

Several studies are available on the scour around spur dikes and abutments in cohesionless sediment mixtures, but very few works have been carried out with cohesive sediments. Estimation of scour depth around spur dikes has attracted considerable research interest. Different prediction methods were presented by Garde et al. (1961), Melville (1992, 1997), Lim (1997), Cardoso and Bettess (1999), Melville and Chiew (1999), Ahmad and Rajaratnam (2000), Kothyari and Ranga Raju (2001), Sarma and Roy (2001), Thompson (2002) and Oliveto and Hager (2002, 2005) etc. The studies of scour around partially submerged spur dike and abutments in cohesionless sediments were conducted by Ettema and Muste (2004), Dey and Barbhuiya (2004, 2005), Giri and Shimizu (2004, 2005), Ezzeldin et al. (2007), Kothyari et al. (2007), Nasrollahi et al. (2008), Fazli et al. (2008), Zhang and Nakagawa (2008), Ghodsian and Vaghefi (2009), Vaghefi et al. (2009), Giri (2010), Uddin and Hossain (2011), and Masjedi and Foroushani (2012), Rashedipoor et al. (2012) and Zhang et al. (2012) etc. The experiments with submerged dikes for the prediction of scour depth were carried out by Kuhnle et al. (1999, 2002), Elawady et al. (2001) and Rodrigue-Gervais et al. (2011) etc.

No studies have been conducted on scour depth around spur dikes (partially submerged and submerged) founded in cohesive sediment mixtures. Only few studies have been conducted on the scour around bridge abutments embedded in cohesive sediment mixtures consisting of clay and sand viz; Monilas and Reiad (1999), Oh et al. (2007), Chen (2008), Abou-seida et al. (2012) and Debnath et al. (2014).

Kand (1993), Ansari (1999), Molinas et al. (1999), Briaud et al. (1999, 2001), Ram Babu et al. (2002), Kho (2004), Brandimate et al. (2006), Debnath and Chaudhuri (2010a, 2010b) and Chaudhuri and Debnath (2013) studied the scour depth around bridge piers embedded in the mixtures of cohesive sediments containing clay, sand and silt. Kumar (2011) and Kothyari et al. (2014) studied scour in the wake region of bridge pier embedded in mixtures of cohesive sediment composed of clay-gravel and clay-sand-gravel mixtures. Very limited investigations have been carried out on scour around spur dikes and bridge piers founded in cohesive sediments with gravel present in it. Thus, there is a need for in-depth study on the effect of presence of cohesive material (clay) in addition to gravel and sand on the process of scour around pier and spur dikes founded in cohesive sediments.

The present investigation was taken up to fill the above mentioned gaps in knowledge.

EXPERIMENTAL SETUP AND PROCEDURE

Extensive experiments were undertaken to study the process of scour around spur dikes (partially submerged and submerged) and pier founded in clay- gravel and clay-sand-gravel mixtures and to quantify the flow and turbulence fields around the spur dikes founded in cohesive sediment mixtures. The experiments were conducted in a fixed bed masonry flume of 25.0m length, 1.0m width and 0.60m depth, which is located at the Hydraulic Engineering Laboratory of Civil Engineering Department, Indian Institute of Technology, Roorkee, India. Experiments were conducted on two longitudinal slopes of the flume bed viz; 0.003 and 0.005. The slope of the flume was changed to 0.005 by pasting the cementing material from upstream to downstream of the flume. The flume had a test section of 4.0m length, 1.0m width and 0.60m depth, starting 12m downstream of the flume entrance.

Locally available clay excavated from a depth of 1.0m below the ground was used as cohesive material. The clay properties were determined as per Indian Standard Code (IS-1498, 1970; IS-2720-29, 1975 and IS-2720-10, 1991). The median size of clay was 0.0014mm as observed by laser particle size analyzer. The geometric standard deviation ($\sigma_g = \sqrt{d_{84}/d_{16}}$) for the same was 2.16. The median size of sand and gravel obtained by sieve analysis were observed to be 0.24mm and 2.7mm respectively, and geometric standard deviation for the same was 1.41 and 1.21 respectively. The relative density of sand and gravel was 2.65. The engineering properties of clay material were: liquid limit (*LL*) = 43%, plastic limit (*PL*) = 22% and plasticity index (*PI*) = 21%, optimum moisture content (*OMC*) = 19%, maximum dry density $(\gamma_d)_{\max}$ = 16.43 kN/m^3, cohesion at *OMC* = 49.23 kN/m^2, angle of friction at *OMC* ((ϕ_c)= 30.7o and relative density 2.65. The mineralogical properties of clay were determined by X-ray diffraction (XRD) test. It was observed the clay were composed of approximately 77.5% Illite, 18% Kaolinite, and 4.5% Montmorillonite.

Cohesive sediments were prepared by mixing clay material with fine gravel and fine sand-fine gravel mixtures (each in equal proportion) in proportions varying from 10% to 50%. The channel bed of cohesive sediments was prepared as per Kothyari and Jain (2008). The unconfined compressive strength of the sediments was determined using laboratory based unconfined compression test apparatus as per IS - 2720-Part X (1991). The bulk unit weight of sediment was computed as per IS-2720-Part XXIX (1975) using standard core cutter method. The value of dry density was computed using the observed value of bulk density and antecedent moisture content. The void ratio was derived from computed value of dry density of cohesive sediments.

Spur dikes with transverse length of 6.10cm, 8.90cm and 11.52cm were used as partially submerged spur dike. However, spur dike with 11.52cm transverse length was used for the submerged dike experiments. In all the experiments, single spur dike was installed at 90^o angle to the direction of flow. Piers with outer diameter 11.52cm and 8.9cm were used for the study conducted in cohesive sediment mixtures. The spur dike or pier was installed 14m downstream of the flume entrance.

The instantaneous three dimensional velocities and turbulence characteristics around the partially submerged and submerged spur dikes were measured by a down

looking 16MHz Vectrino^{+} Acoustics Doppler Velocimeter (ADV) in the three spatial direction *x*, *y* and *z* at a sampling rate of 25Hz. In the data analysis, positive *x*- axis was along the flow direction, the positive *y*- axis was across the left of flow and positive *z*-axis was vertically upward. Intersection point of spur dike, inner face of wall and the original bed is considered as the origin (0, 0, 0) for the grid measurement.

MATHEMATICAL MODELLING FOR TEMPORAL VARIATION OF DEPTH OF SCOUR

A mathematical model for the computation of scour depth in cohesive sediments was developed by using Kothyari et al. (2007) method for the computation of depth of scour in cohesionless sediments as the basis.

Analysis of data on temporal variation of scour depth around spur dikes and piers revealed that d_c/d is inversely proportional to clay percentage(P_c), unconfined compressive strength(UCS), dimensionless cohesion (C_*) and dimensionless angle of internal friction (ϕ_*) for both sediment mixtures. After making a number of trials using all relevant dimensionless parameters, it was found that the following functional relationships for maximum depth of scour could be derived for variation of d_c/d with change in values of (P_c), $(1+C_*/\phi_*)$ and $(1+UCS_*)$.

$$\frac{d_c}{d} = f\left((P_c), \left(1+\frac{C_*}{\phi_*}\right), (1+UCS_*), t_*\right)$$

Here, d_c is depth of scour in cohesive sediment mixtures, d is depth of scour in cohesionless sediment, P_c is clay percentage, UCS_* is dimensionless unconfined compressive strength, C_* is dimensionless cohesion and ϕ_* is dimensionless angle of internal friction. $t_* = t(U_o/d_a)$= time parameter. The variation of scour depth with C_*/ϕ_* did not show significant influence on scour depth in any cases.

Multiple nonlinear regression analysis was used to find out relationship for scour depth around spur dikes (partially submerged and submerged) and pier using all pertinent dimensionless parameters.

Temporal Variation of Depth of Scour around Partially Submerged Spur Dike

For depth of scour at nose of partially submerged spur dike in clay-gravel and clay-sand-gravel mixtures

$$\frac{d_{cun}}{d_{un}} = F_{un}$$

Where, F_{un} = parameter that represents cohesion of clay-gravel and clay-sand-gravel mixtures at nose of the partially submerged spur dike and is expressed as

$$F_{un} = a_o\left[(5\mathrm{P_c})^{a_1}(1+0.001UCS_*)^{a_2}(t_*)^{a_3}\right]$$

Where,

$a_o = 0.00144\,; a_1 = -1.82; a_2 = -0.705; a_3 = 0.335$ for $10\% \le P_c \le 20\%$

(Adjusted R^2= 0.798)

and

$a_o = 1.25\times10^{-6}; a_1 = -4.75; a_2 = -0.25; a_3 = 0.786$ for $30\% \le P_c \le 50\%$

(Adjusted R^2= 0.837)

For depth of scour at the wake of the partially submerged spur dike in clay-gravel and clay-sand-gravel mixtures

$$\frac{d_{cuw}}{d_{uw}} = F_{uw}$$

Where, F_{uw}= parameter that represents cohesion of clay-gravel and clay-sand-gravel mixtures at the wake of the partially submerged spur dike and is expressed as

$$F_{uw} = \mathrm{c}_o\left[(5\mathrm{P_c})^{c_1}(1+0.01UCS_*)^{c_2}(t_*)^{c_3}\right]$$

Where,

$c_o = 0.00195; c_1 = -1.525; c_2 = -0.1067; c_3 = 0.324$ for $10\% \le P_c \le 20\%$

(Adjusted R^2= 0.785)

and

$c_o = 2.96\times10^{-5}; c_1 = -3.633; c_2 = -0.306; c_3 = 0.638$ for $30\% \le P_c \le 50\%$

(Adjusted R^2= 0.792)

The temporal variation of computed depth of scour around partially submerged dike was also compared with the corresponding observations and mostly a satisfactory comparison was noticed.

Temporal Variation of Depth of Scour around Submerged Spur Dike

In the case of scour depth at nose of the submerged spur dike founded in mixtures of clay-gravel and clay-sand-gravel

$$\frac{d_{csn}}{d_{sn}} = F_{sn}$$

Where, F_{sn} = parameter that represents cohesion of clay-gravel and clay-sand-gravel mixtures at nose of the spur dike and is expressed as

$$F_{sn} = \mathrm{b}_o\left[(5\mathrm{P_c})^{b_1}(1+0.01UCS_*)^{b_2}(t_*)^{b_3}\right]$$

Where,

$b_o = 0.0032; b_1 = -1.365; b_2 = -0.444; b_3 = 0.298$ for $10\% \le P_c \le 20\%$

(Adjusted R^2= 0.85)

and

$b_o = 5.7\times10^{-7}; b_1 = -5.535; b_2 = -0.43; b_3 = 0.895$ for $30\% \le P_c \le 50\%$

(Adjusted R^2= 0.95)

In the case of scour depth at wake of the submerged spur dike founded in mixtures of clay-gravel and clay-sand-gravel

$$\frac{d_{csw}}{d_{sw}} = F_{sw}$$

Where, F_{sw}= parameter that represents cohesion of clay-gravel and clay-sand-gravel mixtures at wake of the spur dike and is expressed as

$$F_{sw} = \mathrm{d}_o\left[(5\mathrm{P_c})^{d_1}(1+0.01UCS_*)^{d_2}(t_*)^{d_3}\right]$$

Where,

$d_o = 0.0028; d_1 = -1.024; d_2 = -0.4355; d_3 = 0.331$ for $10\% \le P_c \le 20\%$

(Adjusted R^2= 0.76)

and

$d_o = 6.1\times10^{-7}; d_1 = -4.33; d_2 = -0.281; d_3 = 0.876$ for $30\% \le P_c \le 50\%$

(Adjusted R^2= 0.90)

The temporal variation of computed depth of scour around partially submerged dike was also compared with the corresponding observations and mostly a satisfactory comparison was noticed.

Temporal Variation of Depth of Scour around Pier

For depth of scour at the sides of the pier in clay-gravel and clay-sand-gravel mixtures

$$\frac{d_{cps}}{d_p} = F_{ps}$$

Where, F_{ps} = parameter that represents cohesion of clay-gravel and clay-sand-gravel mixtures at the sides of the pier and is expressed as

$$F_{ps} = \mathrm{m}_o\left[(\mathrm{P_c})^{m_1}(1+UCS_*)^{m_2}(t_*)^{m_3}\right]$$

Where,

$m_o = 0.00024; m_1 = -1.226; m_2 = -0.0914; m_3 = 0.3385$ for $10\% \le P_c \le 20\%$

(Adjusted R^2= 0.844)

and

$m_o = 9.68\times10^{-7}; m_1 = -2.653; m_2 = -0.3785; m_3 = 0.656$ for $30\% \le P_c \le 50\%$

(Adjusted R^2= 0.813)

For depth of scour at the wake of the pier in clay-gravel and clay-sand-gravel mixtures

$$\frac{d_{cpw}}{d_p} = F_{pw}$$

Where, F_{pw} = parameter that represents cohesion of clay-gravel and clay-sand-gravel mixtures at the wake of pier and is expressed as

$$F_{pw} = \mathrm{n}_o\left[(\mathrm{P_c})^{n_1}(1+UCS_*)^{n_2}(t_*)^{n_3}\right]$$

Where,

$n_o = 5.9\times10^{-5}; n_1 = -1.678; n_2 = -0.346; n_3 = 0.342$ for $10\% \le P_c \le 20\%$

(Adjusted R^2= 0.853)

and

$n_o = 2.41\times10^{-8}; n_1 = -2.42; n_2 = -0.253; n_3 = 0.747$ for $30\% \le P_c \le 50\%$

(Adjusted R^2= 0.808)

The comparisons between computed and observed depth of scour at pier sides based on $\overline{D}_a$, σ_a, $\overline{R}_d$ and σ_d indicate that however, differences exists between corresponding computed and observed values, the accuracy of predictions of depth of scour for cohesive sediments is similar to those of Jain and Kothyari (2009 a and 2010) for bed load and suspended load transport in case of cohesive sediment mixtures and Yang et al. (1996); Almedeij and Diplas, (2003) relationships for sediment transport of the cohesionless sediments. Here, $\overline{D}_a$ is average discrepancy ratio based on the average value of the logarithm ratio between computed and observed results, σ_a is standard deviation based on the average value of the logarithm ratio between computed and observed results, $\overline{R}_a$ is average discrepancy ratio based on the difference of computed and observed value and σ_d is standard deviation of the computed results based on difference.

FLOW CHARACTERISTICS AROUND THE PARTIALLY SUBMERGED AND SUBMERGED SPUR DIKES

The flow characteristics around the partially submerged and submerged spur dike in the clay-gravel were analyzed in the form of mean velocity, turbulence intensity, Reynolds stresses and turbulent kinetic energy. Quadrant analysis was also carried out to quantify the contribution of outward interaction, ejection, inward interaction and sweep events out of whole data for a particular z/h value.

At locations (5, 5), (5,10), (10,5) and (10,10) in the flow field of partially submerged and submerged spur dikes, very small values of longitudinal velocity component *u* (negative) were obtained whereas, larger values of *u* were obtained within the flow field bounded by the region *x* = 5 to 20cm and *y* = 15 to 25cm. At the point (5, 15) the value of *u* varied from 1.24 to 1.48 times the approaching flow velocity for partially submerged dike and 1.07 to 1.38 times the approaching flow velocity for submerged dike (velocity profile were measured from bed surface to water surface).

The maximum value of longitudinal component of turbulence intensity occured near the original bed level (z/h = 0.3 to -0.3) just behind the partially submerged spur dike within the region *x* = 5 to 20cm and *y* = 5 to 10cm. Whereas, in the case of submerged spur dike, maximum value of longitudinal component of turbulence intensity

was observed to occur near the original bed level (z/h = 0.5 to -0.25) just behind the submerged spur dike within the region x = 5 to 20cm and y = 5 to 10cm.

The maximum value of Reynolds stress component $\overline{u'w'}$ was observed to occur in the wake zone of partially submerged and submerged spur dikes. The value of Reynolds stresses component $\overline{u'w'}$ is larger for partially submerged spur dike than that for submerged spur dike whereas, the Reynolds stress component $\overline{v'w'}$ did not show significant value around the spur dikes (partially submerged and submerged).

The maximum value of turbulent kinetic energy was observed to occur in the wake zone (bounded by the region x = 5 to 20cm and y = 5 to 10cm) of partially submerged and submerged dike. Outside the scour hole, the values of the turbulent kinetic energy were larger for submerged spur dike than those for partially submerged dike while, within the scour hole the values of turbulence kinetic energy were larger for partially submerged dike than those observed for submerged spur dike.

Quadrant analysis of ADV data showed that the values of outward and inward interaction were higher within the scour hole in partially submerged spur dike as compared to the values of ejection and sweep events, while outside of the scour hole the values of ejection and sweep events were higher as compared to the values of outward and inward interaction events. It was also observed that value of outward and inward interactions increases toward the lower most regions within the scour hole in case of partially submerged dike.

In case of submerged spur dike, the values of outward and inward interaction events were higher at the downstream of the submerged dike (x = 5, 10 and 20cm) than its upstream (x = -15 and -5cm) at an azimuthal plane of y = 5 and 10cm. The trend observed for ejection and sweep events around the submerged spur dike was also similar to that observed around partially submerged spur dike. At outside of the scour hole, small values of ejection and sweep events were measured at the downstream of the submerged dike (x = 10 and 20cm) than its upstream (x = -15 and -5cm) at an azimuthal plane of y = 5 and 10cm. While, within the scour hole at (5, 5) and (5, 10) the ejection and sweep events have maximum value at lower most level and decreases near initial bed level.

ACKNOWLEDGEMENTS

I feel privileged to express my deeps sense of gratitude and sincere regards to Late **Dr. U. C. Kothyari**, Professor of Civil Engineering with whom I started this study. His initial guidance, suggestions and motivations drove me to the completion of this study. At the outset, I wish to express my deep sense of gratitude to my supervisors **Dr. P. K. Sharma**, Associate Professor, Department of Civil Engineering, **Dr. G. J. Chakrapani**, Professor, Department of Earth Sciences, Indian Institute of Technology Roorkee, Roorkee and **Dr. R. K. Jain**, Associate Professor, Department of Civil Engineering, Vishwakarma Government Engineering College Chandkheda, Gandhinagar for their invaluable guidance, thought provoking discussions and untiring efforts throughout the tenure of this work. Their timely help, encouragement, constructive criticism, and painstaking efforts made it possible to present the work contained in this thesis in its present form.

I am very thankful to **Dr. Deepak Kashyap**, Professor and Former Head, Department of Civil Engineering, for providing encouragements and necessary facilities for carrying out the research work. I also want to thank my research committee members **Dr. Z. Ahmad**, Professor, **Dr. K. S. Hari Prasad**, Professor, Department of Civil Engineering and **Dr. Nayan Sharma**, Professor, Department of Water Resource Development and Management for providing insightful and constructive comments.

The assistance extended by lab assistant and supporting staff of Hydraulics Engineering Laboratory, Mr. Molhar Singh, Mr. Rati Ram, Mr. Pramod Kumar, Mr. Chhote Lal, Mr. Vinod Sharma, Mr. Y. S. Pundir, Mr. Ashok, Mr. Bhairav Singh, Mr. Mr. Nadeem, Ajay Saini and others is thankfully acknowledged. I also thankful to Mr. D. R. Saxena, Mr. Suresh Chandra, Mr. Omveer, Mr. Peetamber Singh from Geotechnical Engineering laboratory for providing assistance in the Lab.

I should also acknowledge the help, moral support and companionship of my friends at IIT-Roorkee, especially Nilav Karna, Dr. Ankit Chakravarti, Umesh Kumar Singh, Tarun Kumar Verma, , Himanshu Arora, Himanshu Sharma, Jyoti Choube, Swati Bhawe, Rituraj Shukla, Surendra Chandniha, Bhupesh Jain, Ajmal Hussain, Manish Pandey, Kapil Rohilla, Dr. Deepak Swami, Binita Tiwari, Mrs. Meena Sharma, Aditya

Anupam, Yogesh Shah, Divyesh Patel, Kamlesh, Dr. Amit Rai, Mr. Lokendra Thakur, Kailash Vishnoi, Praveen Patil, Pramod Meena and Sankulp Goel. I also thank to Dr. Nitin Joshi, Dr. Ajay Nagpure and Mrs. Anika Singh for supplying research papers related to my study and their support. Again specially thanks to Mr. Nilav Karna for checking my thesis several times, proving valuable suggestions and all kind of supports.

I would also like to convey my sincere thanks to my teachers of my preceding institute, JNKVV, Jabalpur and PAU, Ludhiana, who have contributed in shaping me what I am today.

It will be unjust on my part to bind in words the spirits of unparalleled sacrifices made by my father **Shri Dashrath Singh Lodhi** and my mother **Smt. Munni Bai** for encouraging me to pursue my studies. I am also thankful to Jawahar Singh and Mrs. Manisha for their encouragement during the thesis. I wish to extend my unconditional love and affection to my son **Atharv** and wife **Kusum** for their help, patience, understanding, encouragement and sacrifice throughout the period of my study. I am very thankful to **Mrs. Meena Kothyari** for her motivation, care, support and help to keep my spirits rejuvenated.

I feel indebted to my parents-in-law, brothers-in law and to all my relatives, who have given me their moral and unconditional support throughout the period of my study.

My humble thanks are for all those who in any manner, directly or indirectly, put a helping hand in every bit of completion of this research work, as it is difficult to name each and everyone. God bless them.

MHRD Fellowship (Institute Fellowship) availed during this period is duly acknowledged.

And above all, I am thankful to the Almighty whose divine grace gave me the required courage, strength and perseverance to overcome various obstacles that stood in my way.

(Ajay Singh Lodhi)

TABLE OF CONTENTS

APPENDICES

LIST OF FIGURES

LIST OF TABLES

LIST OF NOTATIONS

a	Coefficient
Al_2O_3	Aluminium oxide
B	Width of the flume
b	Effective spur width perpendicular to the approach flow direction
C	Clay fraction by dry weight of mixture
CaO	Calcium oxide
C_{comp}	Degree of compaction
C_e	Factor depending on contraction ratio
C_f^n	Standard fatigue strength to rupture of cohesive sediments
Cu	Copper
C_u	Cohesion
C_*	Dimensionless cohesion
C_θ	Factors depending on angle of orientation
D	Diameter of the pier
d_a	Weighted arithmetic mean size of cohesive sediments
d	Instantaneous scour depth in cohesionless sediment
d_c	Scour depth in cohesive sediment
d_{ce}	Equilibrium scour depth in cohesive sediment
d_{cpm}	Maximum depth of scour around pier in cohesive sediment
d_{cpm*}	Dimensionless maximum depth of scour around pier in cohesive sediment
d_{cps}	Instantaneous depth of scour at sides of pier in cohesive sediment mixtures
d_{cpse}	Equilibrium depth of scour at sides of pier in cohesive sediment mixtures

d_{cpw} Instantaneous depth of scour at the wake of pier in cohesive sediment mixtures

d_{cpwe} Equilibrium depth of scour at the wake of pier in cohesive sediment mixtures

d_{csn} Instantaneous depth of scour at nose of the submerged spur dike in cohesive sediment mixtures

d_{csne} Equilibrium depth of scour at the wake of the submerged spur dike in cohesive sediment mixtures

d_{csw} Instantaneous depth of scour at nose of the submerged spur dike in cohesive sediment mixtures

d_{cswe} Equilibrium depth of scour at the wake of the submerged spur dike in cohesive sediment mixtures

d_{cun} Instantaneous depth of scour at nose of the partially submerged spur dike in cohesive sediment mixtures

d_{cune} Equilibrium depth of scour at nose of the partially submerged spur dike in cohesive sediment mixtures

d_{cuw} Instantaneous depth of scour at the wake of the partially submerged spur dike in cohesive sediment mixtures

d_{cuwe} Equilibrium depth of scour at the wake of the partially submerged spur dike in cohesive sediment mixtures

d_{pm} Maximum depth of scour around pier in cohesionless sediment

d_{pne} Equilibrium depth of scour at pier nose in cohesionless sediments

d_{une} Equilibrium depth of scour at nose of the partially submerged spur dike in cohesionless sediments

d_{uje} Equilibrium depth of scour at the junction of wall and partially submerged spur dike in cohesionless sediments

D_r Dispersion ratio

d_{50} Mean particle size

d_* Dimensionless scour depth

D_* Dimensionless grain size

e Void ratio

f_c Lacey's clay factor for cohesive sediments

F_d Actual particle Froude number

F_{di} Densimetric particle Froude number for inception of sediment movement in approach flow

$F_{d\beta}$ Densimetric particle Froude number

Fe_2O_3 Iron Oxide

F_p Parameter representing the cohesion of clay-gravel and clay-sand-gravel mixtures bed for scour around bridge pier

F_{ps} Parameter representing the cohesion of clay-gravel and clay-sand-gravel mixtures bed for scour at sides of the pier

F_{pw} Parameter representing the cohesion of clay-gravel and clay-sand-gravel mixtures bed for scour at the wake of the pier

F_r Approaching flow Froude number

F_{rp} Pier Froude number

F_s Parameter representing the cohesion of clay-gravel and clay-sand-gravel mixtures bed for scour around submerged spur dike

F_{sn} Parameter representing the cohesion of clay-gravel and clay-sand-gravel mixtures bed for scour at nose of the submerged spur dike

F_{sw} Parameter representing the cohesion of clay-gravel and clay-sand-gravel mixtures bed for scour at the wake of submerged spur dike

F_u Parameter representing the cohesion of clay-gravel and clay-sand-gravel mixtures bed for scour around partially submerged spur dike

F_{un} Parameter representing the cohesion of clay-gravel and clay-sand-gravel mixtures bed for scour at nose of the partially submerged spur dike

F_{uw} Parameter representing the cohesion of clay-gravel and clay-sand-gravel mixtures bed for scour at the wake of partially submerged spur dike

F_{w_1} Parameter representing the cohesion of sediment bed (for scour in wake zone of pier for clay-gravel sediment mixtures)

F_{w_2} Parameter representing the cohesion of sediment bed (for scour in wake zone of pier for clay-sand-gravel sediment mixtures)

F_θ Coefficient based on angle of internal friction

g	Acceleration due to gravity
g'	Relative gravimetric acceleration
H_1	Extreme event
h	Approach flow depth
K	Potassium
K_2O	Potassium oxide
K_d	Sediment size factor
K_h	Homogeneity coefficient
K_{yw}	Flow depth-abutment size factor = K_{yb} for piers and K_{yL} for abutments
K_I	Flow intensity factor
K_s	Foundation shape factor
K_θ	Foundation alignment factor
K_σ	Approach channel geometry factor
L_a	Length of abutment perpendicular to direction of flow
LI	Liquidity index
LOI	Loss on Ignition
LL	Liquid limit (%)
L_{down}	Length of scour hole at downstream of spur dike
L_{up}	Length of scour hole at upstream of spur dike
MgO	Magnesium oxide
MnO	Manganese oxide
Na_2O	Sodium oxide
Ni	Nickel
P_2O_5	Phosphorus pentoxide
P_c	Clay percent by weight

P_s	Sand content (volume or mass)
PI	Plasticity index
PL	Plastic limit
OMC	Optimum moisture content
R_{ep}	Pier Reynolds number
R_h	Hydraulic radius
s	Effective spur height
$S_{i,H}$	Occurrence probability
t	Time
SiO_2	Silicon dioxide
T	Time parameter
TiO_2	Titanium dioxide
t_e	Equilibrium time of scour
t_R	Reference time
t_*	Dimensionless time
UCS	Unconfined compressive strength
UCS_*	Dimensionless unconfined compressive strength of cohesive sediment bed
U_{cc}	Permissible (non-scouring) mean velocity for cohesive sediments bed in a plane turbulent flow
U_c	Critical velocity
U_o	Approach flow velocity
u_*	Approach flow shear velocity
u, v, w	Velocity components in longitudinal (x), transverse (y) and vertical (z) directions respectively
u', v', w'	Longitudinal, transverse and vertical component of velocity fluctuation
$\sqrt{\overline{u'u'}}$	Longitudinal component of turbulence intensity

$\overline{u'w'}$	Component of Reynolds stresses
$\overline{v'w'}$	Component of Reynolds stresses
V_{ce}	Equilibrium scour volume
W	Antecedent moisture content
W_*	Moisture content at saturation
W_{r_*}	Moisture content required to saturate the soil sample
W_{ce}	Equilibrium scour width
$\sqrt{\overline{w'w'}}$	Vertical component of turbulence intensity
$\hat{w}$	Optimum molding water content
x, y, z	Distance in x (longitudinal), y (transverse) and z (vertical) directions respectively
z_R	Reference length

GREEK NOTATIONS

α	Contraction ratio
β	Element obstruction
σ_g	Geometric standard deviation
σ_g'	Geometric standard deviation for cohesive sediment mixtures
σ_n	Normal shear stress
ϕ_c	Angle of internal friction of clay
ϕ_{sh}	Angle of internal friction for cohesionless sediment
ϕ_*	Dimensionless angle of internal friction for cohesive sediment mixture
τ_c	Critical shear stress for cohesionless sediments
τ_{cc}	Critical shear stress for cohesive sediments

$\tau_{e,m}$	Critical shear stress for erosion of pure mud
$\tau_{e,s}$	Critical shear stress for erosion of pure sand
τ_s	Bed shear strength
τ_{sh}	Shear strength of cohesive sediment mixture
τ_{sm}	Critical shear stress for erosion of sand and mud mixture
$\hat{\tau}_{s_*}$	Dimensionless bed shear strength
$\tau_{*_{cc}}$	Dimensionless critical shear stress
γ_d	Dry density
γ_s	Specific weight of sediment
γ_w	Specific weight of water
$\Delta\gamma_s$	Difference in the specific weight of the cohesive sediments and fluid
θ_c	Shield's entrainment factor
θ_{down}	Lateral downstream angle
θ_{side}	Lateral side angle of the scour hole
θ_{up}	Lateral upstream angle
Σ	Element shape
Σ_{ca}	Cascade parameter
Σ_s	Submergence
ρ	Fluid density
ρ_s	Sediment density
ν	Kinematic viscosity

ABBREVIATIONS USED

ADV	Acoustic Doppler Velocimeter
C	Clay
CSG	Clay-sand-gravel
G	Gravel
EFA	Erosion Function Appratus
IS	Indian standard
PIV	Particle Image Velocimetry
S	Sand
SG	Sand-gravel
XRD	X- ray diffraction
XRF	X-ray fluorescence

CHAPTER - I

INTRODUCTION

1.1 PRELIMINARY REMARKS

Scour is the natural phenomenon caused by the flow of water that excavates the material from the bed and stream banks, and also carries materials away from the hydraulic structures. One of the major considerations in the design and construction of a bridge is the scour around its foundation. Many of the bridge failures have been attributed to the scour or the undermining of hydraulic structures (i.e. piers, abutments and spur dikes etc.). Hence, for safe and economic design of hydraulic structures, it becomes essential to estimate the scour depth around such structures with greater accuracy. The accurate estimation of the scour depth around bridge piers and spur dikes below the stream bed is important since, it determines the depth of foundation of such structures. Several formulae and mathematical models developed for the estimation of the scour depth are still primarily based on theoretical approaches and laboratory tests. Accurate field measurements are difficult to obtain due to the severe three dimensional flow pattern that occur at bridges during flooding, high cost of instrumentation and the costs of getting skilled personnel at bridge sites during period of peak flow. Unrealistic estimation of scour depth may lead to either over expenses in the construction or failure of the structure.

Studies during the last few decades have shown that the most common cause of bridge failures is the removal of bed material around bridge foundations. In 1973, Federal Highway Administration of USA reported that 383 bridges failed due to catastrophic floods (Federal Highway Administration, 2001). The research showed that 25% of the failures involved pier damage while 75% of it included abutment scour. In 1985, flood in Pennsylvania, Virginia and West Virginia damaged 73 bridges. Similarly, 17 bridges in New York and New England were either damaged or destroyed due to scour by the spring flood of 1987 as stated by the Federal Highway Administration of USA. In 1993, 23 bridge failures, 14 from abutment scour and 2 from pier scour, resulted from floods

caused a damage of $15 million in the upper Missisippi basin. In Georgia, the total financial loss from tropical storm in 1994 was approximately $130 million because more than 100 bridges had to be replaced and repaired due to flooding (Federal Highway Administration, 2001). Kamojjala et al. (1995) detailed the damage and costs of bridge failures associated with the catastrophic flood of the Mississippi River in 1993. Parola et al. (1997) stated that over 400 bridge crossings on federal aid routes and over 2000 non-federal aid bridges were damaged during the 1993 Mid-West flooding. These studies underscore the importance of predicting the depth of scour accurately. Improving the understanding of the scour phenomenon is therefore vital to the engineer responsible in the design of foundations of hydraulic structure.

Scour around a bridge pier, abutment and spur dikes in alluvial channel is still a matter of concern, although there have been significant advances made in this area of research. A series of bridge failures have been reported in the recent past due to pier scour (Kothyari, 2007). Similarly, the scouring/erosion from the bank and bed of rivers and man-made channels are the common problem in the management of water resources. This has revived the interest in advancing our understanding of the scouring process. A spur dike is an elongated structure; one end of which is installed at the bank of a river or stream and the other end projecting into the flow or current (Kuhnle et al. 1999). Spur dikes are used to protect abutment scour and river bank erosion. The spur dikes are generally of irregular shapes. These are designed for partially submerged (non-submerged) conditions and installed in the field. These partially submerged spur dikes are submerged during flood events and acts as submerged dike. When flow passes the spur dike, the natural balance of streams or river is disruped, which causes major disturbance in the pattern of flow around the base of the structure and this disturbance leads to a process of scour (Ezzeldin et al., 2007).

Several studies have been conducted to predict the depth of scour around piers and spur dikes founded in uniform or non-uniform cohesionless sediments and it is well understood at present. However, the river/ stream bank and bed sediment consist of non-cohesive as well as cohesive materials such as a mixture of gravel, sand, and clay (Jain and Kothyari, 2009). Generally mixtures of cohesive sediments are found in upland areas of catchment (Kothyari and Jain, 2008). The process of scour in cohesionless sediment (i.e. sand and gravel) is a function of the submerged weight of particle only, whereas in cohesive sediment the other resisting forces such as electrostatic and Van der Waals

forces play a main role besides the submerged weight of the particles. These forces attract molecules to each other like a magnet; hence resist the scouring (Mitchell, 1993). The bonding forces of cohesive material depend on many factors such as type of clay, clay percentage, moisture content and its drainage conditions present in the mixture of cohesive sediment (Jain and Kothyari, 2009). Due to such properties of cohesive material, the incipient flow conditions and scour depth prediction become very difficult. In case of cohesionless sediment (i.e. sand and gravel) the scour will reach its maximum value in hours while in cohesive sediment mixtures bed, it will take days to reach maximum scour under the similar flow conditions. The scour depth depends on the rate and duration of the scour (Wang et al., 1997).

The flow field around bridge piers and spur dikes is three dimensionally separated vertical turbulent flow. Therefore, the process of scouring around these structures is a complex phenomenon. Presence of cohesive sediment around the structure makes the scouring phenomenon even more complex. Over it, the unsteadiness and possibility of flow reversal at bridge site during the flood add more complexity to the flow field. The local flow structure and the type and properties of the erodible bed govern the scouring pattern around the piers (Raudkivi, 1990). The process of scour around spur dikes and bridge piers is affected by several interdependent variables such as flow, structure shape and its size, and sediment characteristics.

Figure 1.1 depicts a stream bed consisting of cohesive sediment mixture in river Kosi at Kushinagar, Uttarakhand, India and Figure 1.2 depicts the formation of large scour hole around the bridge pier in the same river. Whereas, Fig. 1.3 depicts the practical application of spur dike at river Bhakhra near Haldwani, Uttarakhand India and Fig. 1.4 depicts the failure of spur dikes in same river due to flood in monsoon season.

Fig. 1.1 Bed material of river Kosi at Kushinagar, Uttrakhand (India)

Fig. 1.2 Bride pier scour at river Kosi at Kushinagar, Uttrakhand (India)

Fig. 1.3 Spur dikes installed at river Bhakhra near Haldwani, Uttrakhand (India)

Fig. 1.4 Failure of Spur dikes at river Bhakhra near Haldwani, Uttrakhand (India)

1.2 COHESIVE SEDIMENTS

Non-cohesive and cohesive sediments are distinguished by their median particle size. If the sediment median particle size is larger than 62 microns, they are usually defined as non-cohesive sediments. Non-cohesive sediments do not have significant forces between the adjacent particles (Shan, 2010 and Kumar, 2011). Cohesive sediments include silt and clay particles. The particles usually have shape of a flat plate or a needle and a high specific surface defined as the ratio of surface area to volume (Partheniades, 2007). This indicates that it has a high potential to adsorb ions, which in turn generates attractive or repulsive surface forces. Commonly, the surface forces dominate cohesive sediments entrainment, and the effect of the submerged particle weight is usually negligible (Raudkivi and Tan, 1984).

Due to the small particle size, cohesive sediments are easily suspended in water. With increased dissolved chemicals in water, suspended particles flocculate into flocs. The inherent structure of flocs is quite different from non-cohesive sediments. The latter is composed of individual particles, between which no interactional forces exist. In newly deposited cohesive sediments, the dominant fabric is believed to be open, and the flocs are mainly connected through edge-to-edge and edge-to-face attachment, which is called card-house structure. In consolidated cohesive sediments, flocs are strongly connected through face-to-face attachment, which means high cohesion inside the sediments (Partheniades. 2007). This microcosm property is controlled by the inter-particle forces during the flocculation. Also the forces induced by flow play a dominant role in the deposition and erosion characteristics of cohesive sediments.

1.3 PRESENT STATE OF KNOWLEDGE

The topic of erosion and scour around bridge piers and spur dikes founded in cohesionless sediments have been extensively studied worldwide during last many decades (Garde and Ranga Raju, 2006). Similarly, the flow characteristics around the pier, abutments and spur dikes founded in cohesionless sediments have been studied reasonably well by various investigators in recent past. However, very limited studies have been performed on scouring around pier embedded in cohesive sediment mixture consisting of clay, silt and sand. In recent times, Kumar (2011) conducted a study on

bridge pier scour in clay-sand-gravel mixtures. However, the studies on scour around spur dikes embedded in cohesive sediment mixture of clay, sand and gravel are not available in the literature to the best of the author's knowledge.

The depth of scour around spur dikes and bridge pier is dependent on the resistance of the sediment to scour/ erosion. The critical shear stress of the sediment is an index of such resistance. Therefore, a brief review of the incipient motion of the cohesive sediments is presented here and is followed by a review of literature on the depth of scour around spur dikes (partially submerged and submerged), bridge piers, and flow characteristics around spur dikes.

1.3.1 Incipient Motion of Sediments

Several experimental studies were conducted to determine the critical shear stress of non-cohesive and cohesive sediments by various researchers viz; Dunn (1959), Smerdon and Beasley (1959, 1961), Hong and Xu (1991), Murty and Choudhry (1991), Srivastava and Contractor (1992), Mahapatra and Murty (1994), Yang et al. (1996), Ansari (1999), Dou (1999), Ramesh et al. (2000), Zhang (2000), Jiang et al. (2001), Patel and Rati (2006), Patel et al. (2009 a, b), Lundkvist et al. (2007) etc. Inception of scour occurs if the erosive force generated by the flowing water overcomes the forces between the soil particles (Kuti and Yen 1976, Mirtskhoulava 1991, Annandale 1995, Kessel and Blom 1998, Kothyari and Jain 2008 and Srivastava 2008).

1.3.2 Scour around Spur Dike/ Abutments

The flow pattern at spur dikes and bridge abutment is quite similar since they have essentially same structures and same configurations in the rivers. Several studies are available on scour around spur dikes and abutments in cohesionless sediment mixtures, but only a few are available with cohesive sediment. Estimation of scour depth around spur dike has attracted considerable research interest recently.

Different prediction methods are presented by Garde et al. (1961), Melville (1992, 1997), Lim (1997), Cardoso and Bettess (1999), Melville and Chiew (1999), Ahmad and Rajaratnam (2000), Kothyari and Raju (2001), Sarma and Roy (2001), Thompson (2002) and Oliveto and Hager (2002, 2005). The studies of scour around partially submerged

spur dike and abutments in cohesionless sediments were conducted by Ettema and Muste (2004), Dey and Barbhuiya (2004, 2005 a), Giri and Shimizu (2004, 2005), Ezzeldin et al. (2007), Kothyari et al. (2007), Nasrollahi et al. (2008), Fazli et al. (2008), Zhang and Nakagawa (2008), Ghodsian and Vaghefi (2009), Vaghefi et al. (2009), Giri (2010), Uddin and Hossain (2011), and Masjedi and Foroushani (2012), Rashedipoor et al. (2012) and Zhang et al. (2012). The experiments with submerged dike for the prediction of scour depth were carried out by Kuhnle et al. (1999, 2002), Elawady et al. (2001) and Rodrigue-Gervais et al. (2011).

No such studies have been conducted on depth of scour around spur dikes (partially submerged and submerged) founded in cohesive sediment mixtures. Only few studies have been conducted on the scour around bridge abutments embedded in cohesive sediment mixtures consisting of clay and sand viz; Molinas and Reiad (1999), Oh et al. (2007), Chen (2008), Abou-seida et al. (2012) and Debnath et al. (2014).

1.3.3 Scour around Bridge Piers

The phenomenon of scour around uniform piers founded in cohesionless sediment have been extensively investigated and well documented. Most of the studies have been conducted under clear-water condition. Several researchers have studied the scour depth evolution with uniform sediment viz. Ettema (1980), Kothyari (1989), Yanmaz and Altinbilek (1991), Kothyari et al. (1992, a,b), Graf and Yulistiano (1998), Ansari (1999), Melville and Chiew (1999), Melville and Coleman (2000), Oliveto and Hager (2002, 2005), Yanmaz (2006), Kothyari (2007), Kothyari and Kumar (2010), Pagliara et al. (2010, 2014), Pagliara and Carnacina (2011, a,b). Sediment gradation effect on scour depth in non-uniform sediment has been studied by Ettema (1980), Raudkivi and Ettema (1983), Melville and Sutherland (1988), Kothyari et al. (1992,a), Oliveto and Hager (2002) and Cheng et al. (2004) among many others.

Until recently, no method has been available to estimate the equilibrium scour at bridge piers founded in cohesive soil. The common practice is to use the scour prediction formulas developed for non-cohesive soil to estimate the local scour in cohesive soil as well, although it is well known that the scour mechanism is different in the two cases. Recent bridge surveys conducted by local and federal authorities in the United States, New Zealand and Europe show that the pier scour in cohesive soil is considerably less

than that predicted by the widely used scour prediction formulas such as HEC-18 (Richardson et al., 1991). Although several investigations have been conducted recently to study scour in cohesive soil (e.g. Hosny, 1995; Briaud et al., 1999; Ting et al., 2001 and Ansari et al., 2002); no general-purpose formula is presently available to predict the equilibrium local pier scour in cohesive soil, as these studies are considered to be in the initial stage (Ansari et al., 2002). Experimental study of local pier scour in cohesive soil is challenging due to the complex erosion characteristics of the clay and the difficulty in scaling the properties of the cohesive soil (Ting et al., 2001).

Kand (1993), Ansari (1999), Molinas et al. (1999), Briaud et al. (1999, 2001), Ram Babu et al. (2002), Kho (2004), Brandimarte et al. (2006), Debnath and Chaudhuri (2010a, 2010b) and Chaudhuri and Debnath (2013) are the few who studied the scour depth around bridge piers embedded in the mixtures of cohesive sediments containing clay, sand and silt. Kumar (2011) and Kothyari et al. (2014) studied scour in the wake region of bridge pier embedded in mixtures of cohesive sediment composed of clay-gravel and clay-sand-gravel mixtures.

1.3.4 Flow Characteristics

In the recent past, studies on the flow characteristics over the rough and smooth beds were carried out by Srivastava and Ranga Raju (1983), Mazumder et al. (2006), and Ojha and Mazumder (2010). The studies of flow characteristics around bridge piers founded in cohesionless sediments have been carried out by Melville and Raudkivi (1977), Dey et al. (1995), Ahmad and Rajaratnam (2000), Graf and Istiarto (2002), Muzzammil and Gangadhariah (2003), Dey and Raiker (2007), Kumar (2007, 2012) and Kumar et al. (2012). Flow pattern around spur dikes founded in cohesionless sediments were studied by several researchers viz. Sukhodolov et al. (2004), Duan (2009), Duan et al. (2009), Ghodsian and Vaghefi (2009), Yaeger (2009), Duan et al. (2011), Koken (2011). Studies on flow pattern around the abutments were carried out by Ahmed and Rajaratnam (2000), Barbhuiya and Dey (2003, 2004), Dey and Barbhuiya (2005 a, 2006), Koken and Constantinescu (2014). However, no investigation has been conducted to study the flow characteristics around spur dikes founded in cohesive sediment consisting of clay and gravel.

1.4 OBJECTIVES OF THE PRESENT STUDY

The present study was conducted to determine the process and depth of scour around spur dikes and bridge piers embedded in cohesive sediment mixtures consisting of clay-gravel and clay-sand-gravel. The specific objectives of the present study are:

(i) Identification of correct parameters influencing the depth of scour around spur dikes and bridge piers founded in clay-gravel and clay-sand-gravel mixtures.

(ii) To study temporal variations of scour depth around spur dikes and bridge piers founded in cohesive sediment consisting of clay-gravel and clay-sand-gravel mixtures.

(iii) Development of mathematical model for computation of scour depth around spur dikes and bridge piers founded in cohesive sediment consisting of clay-gravel and clay-sand-gravel mixtures.

(iv) Assessment of flow characteristics around spur dikes founded in cohesive sediment mixture bed.

1.5 LIMITATIONS

The present study is confined under clear water scour conditions. The partially submerged spur dikes having a transverse length (length perpendicular to the direction of flow) of 6.1cm, 8.9cm and 11.52cm were used for the experiments. Only one submerged dike of transverse length 11.52cm with an overtopping ratio (i.e. ratio of approaching flow depth to height of the structure) of 1.40 was used. The circular piers having diameter of 8.9cm and 11.52cm were used in the experiments. The cohesive sediment mixtures were prepared using equal proportion (by weight) of sand and gravel mixed with varying percent of clay. The clay material of single mineral composition was used. The experiments were conducted with uniform gravel and sand having median size of 2.7mm and 0.24mm respectively and a constant width flume was used throughout.

CHAPTER - II

REVIEW OF LITERATURE

2.1 GENERAL

The process of scour around hydraulic structures such as spur dike, abutment and bridge piers is a complex phenomenon. It involves three dimensional flow patterns. Potentially catastrophic events such as enlargement of rivers, damage of highways, bridge failure, and bridge collapse due to excessive scour around spur dikes, abutments and bridge piers causes potential loss of life. Various aspects of the process and phenomenon of scour around hydraulic structures have been studied in the past by several researchers but these studies were mainly confined to cohesionless sediments. Only few studies have been carried out in the past on scour around bridge piers and abutments embedded in cohesive sediments. It is essential to get information on the process and phenomenon of scour, parameters influencing the depth of scour and three dimensional characteristics around spur dikes/abutments and bridge pier. The scouring process and flow pattern around spur dikes and abutments are quite similar since these structures have similar configuration in rivers.

Keeping in view the main objectives of the study, which is to study the scour around spur dikes and bridge piers founded in cohesive sediment mixtures containing clay-gravel and clay-sand-gravel, the literature review has been divided into the following sections:

2.2 Cohesive Sediment and its Characteristics

2.3 Factors affecting Erosion/ Scouring of Cohesive Sediments

2.4 Scour around Spur Dikes/Abutments

- 2.4.1 Partially submerged spur dike/ abutment scour in cohesionless sediments
- 2.4.2 Scour around submerged spur dike in cohesionless sediments
- 2.4.3 Spur dike/ abutment scour in cohesive Sediments

2.5 Scour around Bridge Piers

- 2.5.1 Piers scour in cohesionless sediments
- 2.5.2 Piers scour in cohesive sediments

2.6 Flow Characteristics

2.6.1 Flow pattern around spur dike

2.6.2 Flow pattern around abutment

2.2 COHESIVE SEDIMENT AND ITS CHARACTERISTICS

Sediment containing clay is generally known as cohesive sediment. The sediment having particle size less than 0.062mm is considered as cohesive sediment (Shan, 2010). These particles possess greater specific surface area compared to silt and sand. Due to this, cohesive particles are more active in physiochemical processes. Cohesive sediments are composed of clay, silt, sand and organic matter which have strong forces between particles due to their surface ionic charges. Cohesive sediment contains organic and inorganic minerals (Hayter, 1983). Inorganic mineral contains clay and non-clay minerals. Generally, clay minerals are silica, alumina, montmorillonite, illite and kaolinite and non-clay minerals are quartz, carbonate, feldspar, mica and many more. Particles of clay minerals are flat in shape and their surface carries negative electrical charges. These charges are balanced externally by exchangeable ions (mostly cations). This phenomenon of cations exchange is very important in soil chemistry and soil physics. Clay minerals have the properties of absorbing certain cations, anions and remain in an exchangeable state. These ions (cations and anions) are replaced by other anions and cations of water molecules. The interaction between clay particles and water is the primary mechanism that governs the erosion of cohesive soils. The cation exchange is slower in clay having montmorrilonite minerals while rapid in the kaolinite.

Different types of electrical bonds act among clay particles that are responsible for variation of behavior between cohesive and cohesionless materials. These are

(a) Primary valence bond: These bonds are the strongest bond that holds atoms together in the basic mineral units. These minerals are divided into three categories i.e. ionic, covalent and heterpolar.

(b) Hydrogen bonds: The hydrogen bonds occur when two other atoms as in water molecules strongly attract hydrogen atom. Hydrogen bonds are strong and it prevents the layer to separate in the presence of water.

(c) Van der Waals Bonds (Secondary Forces): These bonds arise from electrical moments existing within the units. Van der Waals bonds contribute to clay strength and cause soils to hold water. Van der Waals forces attract molecules to each other like magnet and hence resist the scouring (Mitchell, 1993).

2.2.1 Effect of Compaction on Cohesive Soils

Fundamentals of compaction of cohesive soil were established by Proctor (1933) and it was concluded that shear strain obtained in compacted soil mainly depends on the method of compaction, water content and compactive effort. The effect of compaction includes elimination of larger pores, breakdown of flocculated aggregates, destruction of shear planes and production of more homogeneous arrangement.

2.2.2 Shear Strength of Cohesive Sediment

The forces acting among the cohesive sediment particles are not yet fully understood. They vary with drainage condition, type of clay, clay percentage, degree of saturation and type of shear application etc. (Ansari, 1999 and Ansari et al., 2003). When clay mixed with sand or gravel or both, the mixture of these also exhibits cohesion. For such cohesive sediments the shear strength τ_{sh} is given by

$$\tau_{sh} = C_u + \sigma_n \tan\phi_c \qquad (2.1)$$

Here, C_u is cohesion, σ_n is normal shear stress and ϕ_c is the angle of internal friction of clay. It is to be mentioned that the parameter of cohesion C_u and ϕ_c depend strongly on the type of shear test, the drainage conditions, rate of application of shear force, pre-consolidation pressure and degree of saturation of sediments (Ansari, 1999). The magnitude of C_u is also controlled by the inter-particle forces which depend on clay contents (quality and quantity), the ion dissolved in water and the stress history (Jain, 2007).

2.3 FACTORS AFFECTING EROSION/ SCOURING OF COHESIVE SEDIMENTS

Several experimental studies have been conducted to determine the critical shear stress of cohesive sediments in laboratory flume and in jet flows by various researchers viz; Sundborg (1956), Dunn (1959), Smerdon and Beasley (1959, 1961), Laflen and

Beasley (1960), Hong and Xu (1991), Yang et al. (1996), Ansari (1999), Dou (1999), Zhang (2000), Jiang et al. (2001), Mazurek et al. (2001, 2003), Lundkvist et al. (2007), Kothyari and Jain (2008). Inception of scour occurs if the erosive forces generated by the flowing water overcome the forces between the soil particles (Kuti and Yen 1976, Mirtskhoulava 1991, Annandale 1995, Kessel and Blom 1998).

Smerdon and Beasley (1961) conducted a flume study on eleven cohesive Missouri soils to relate basic soil properties (plasticity index, dispersion ratio, mean particle size and percent clay) to critical shear stress. Soil samples in the flume were only leveled after placement, but not compacted. With the increase in flow rates, it was observed that a stage was reached when the soil particles started to move. The shear stress corresponding to that stage was considered critical shear stress (τ_{cc}). They developed empirical relations between the soil properties and critical shear stress as

$$\tau_{cc} = 0.16(PI)^{0.84} \tag{2.2}$$

$$\tau_{cc} = 10.2(D_r)^{-0.63} \tag{2.3}$$

$$\tau_{cc} = 3.54\times10^{-28.1d_{50}} \tag{2.4}$$

$$\tau_{cc} = 0.493\times10^{0.0182P_c} \tag{2.5}$$

Where,

τ_{cc} = critical shear stress (Pa)

PI = plasticity index

D_r = dispersion ratio

d_{50} = mean particle size (m)

P_c = percent clay by weight (%).

The relations with PI and D_r were considered the most reliable in the study because the two parameters are directly related to cohesion properties of the soil.

Kamphuis and Hall (1983) conducted several experiments to study the initiation of sediment particle motion under clear water unidirectional flow conditions in consolidated cohesive sediments. In those experiments only clay content and consolidation pressure were varied. It was found that critical shear stress required to start erosion increased with an increase in clay content and consolidation pressure. Similarly, Kothyari and Jain (2008) observed that the critical shear stress of cohesive sediment was

mainly influenced by abundance of clay and unconfined compressive strength of sediment mixtures.

Raudkivi (1990) observed that particle size, clay content, plasticity index and dispersion ratio are the important properties of cohesive sediments which affect the critical shear stress. He concluded that the erosion resistance decreased with an increase of water content since, the inter-particle bonds decrease with increasing the distance between the particles when the soil moisture increases. An opposite conclusion was observed for consolidated clays with an oriented-structure. He observed that the erosion rate decreased with an increase in water content, and opined that the behavior and characteristics of clay water system control the erosion characteristics of cohesive soil.

Hosny (1995) stated that when the clay percentage increases in the soil mixture, it increases the cohesion and erosion resistance and decreases the erosion rate. Mostafa (2003) stated that water is the main agent generating cohesion between clay particles of cohesive soil. Lack of enough water in the soil hampers the redistribution of cations and anions and hence, there exists weak Van der Waals forces within the soil. With an increase in moisture content in the soil, the redistribution of cations and anions increases which on other hand increases the Van der Waal forces. Increase in this force increases the cohesion and this continues till the optimum moisture content is reached. The soil having high plasticity index creates higher resistance to the erosion (Graf, 1984 and Grim, 1962).

Ansari et al. (2007) conducted several experiments to study the condition of incipient motion in cohesive sediment bed consisting of clay-sand mixtures. The cohesive sediment beds were compacted to various dry densities at different antecedent moisture contents. When antecedent moisture content varied from 5% to 27%, clay percentage from 5% to 20%, the range of vane shear strength was obtained as 0.2kN/m^2 to 191kN/m^2. It was observed that the following variables affect the shear stress at incipient motion

$$\tau_{cc} = f(W, W_*, PI, e, \Delta\gamma_s, d_a) \tag{2.6}$$

Based on the dimensional analysis the following relationship was considered for critical shear stress

$$\tau_{*cc} = f\left(\frac{W}{W_*}, e, (1+PI)\right) \tag{2.7}$$

$$\tau_{*_{cc}} = 0.001(1+PI)^{2.89}\left(\frac{W}{W_*}\right)^{0.1} 10^{-(0.64e+2.3)} \tag{2.8}$$

Where, τ_{cc} is the critical shear stress of cohesive sediment mixtures, $\tau_{*_{cc}}$ is dimensionless critical shear stress of cohesive sediment mixtures, W is the antecedent moisture content of cohesive sediments, W_* is the moisture content at saturation (W_* is equal to liquid limit (LL) for plastic sediments), PI is the plasticity index, e is the void ratio, $\Delta\gamma_s$ is the difference in the specific weight of the cohesive sediments and fluid and d_a is the weighted arithmetic mean size of cohesive sediments.

Kothyari and Jain (2008) conducted experiments to study the influence of cohesion on the incipient motion of the cohesive sediment mixture consisting of clay, sand and gravel. They used two types of sediment mixtures in their experiments, (i) clay percentage varying from 10 to 50% was mixed with fine gravel by weight and (ii) clay percentage varying from 10 to 50% was mixed with equal proportion of fine sand and fine gravel by weight. They identified that clay percent, antecedent moisture content, void ratio and unconfined compressive strength of the sediment mixtures bed are main factors affecting the incipient motion of the cohesive sediment mixtures.

They propose a relationship to determine the critical shear stress of the cohesive sediment mixtures containing clay-gravel and clay-sand-gravel ($10\% \le P_c \le 50\%$) as follows

$$\frac{\tau_{cc}}{\tau_c} = 0.94(1+P_c)^{3/2} e^{-1/6}(1+0.001UCS_*)^{9/20} \tag{2.9}$$

Where, τ_{cc} = critical shear stress for cohesive sediment mixtures, τ_c = critical shear stress for cohesionless sediments, P_c = clay percentage, e = void ratio and UCS_* = dimensionless unconfined compressive strength of the cohesive sediment mixtures can be defined as $UCS_* = \frac{UCS}{(\gamma_s - \gamma_w)d_a}$; γ_s is specific weight of sediment, γ_w is specific weight of water.

Ahmad et al. (2011) conducted a study on the critical shear stress for sand and mud mixture. They developed a formulation based on the critical shear for pure sand and pure mud together with fraction content. The formulation given in Eq. 2.10 describes the critical shear stress for the erosion of sand and mud mixture.

$$\tau_{sm} = e^{a\left(1-\frac{1}{P_s}\right)}\tau_{e,s} + (1-P_s)\tau_{e,m} \quad (2.10)$$

Where,

τ_{sm} = critical shear stress for the erosion of sand and mud mixture

P_s = sand content (volume or mass)

$\tau_{e,s}$ = critical shear stress for erosion of pure sand

$\tau_{e,m}$ = critical shear stress for erosion of pure mud

a = an empirical coefficient.

2.4 SCOUR AROUND SPUR DIKES/ ABUTMENTS

Several studies are available on the scour around spur dikes and abutments in cohesionless sediment mixtures, but only a few studies are available with cohesive sediment. Flow pattern around spur dike and abutments are very similar. Estimation of scour depth around spur dike has attracted considerable research interest. Different prediction methods are presented on scour around spur dike and bridge abutments in cohesionless sediments viz; Garde et al. (1961), Gill (1972), Melville (1992, 1997), Lim (1997), Kuhnle et al. (1999, 2002), Cardoso and Bettess (1999), Melville and Chiew (1999), Ahmad and Rajaratnam (2000), Kothyari and Raju (2001), Sarma and Das (2001, 2003), Oliveto and Hager (2002, 2005), Dey and Barbhuiya (2004, 2005 a), Kothyari et al. (2007), Nasrollahi et al. (2008), Fazli et al. (2008), Zhang and Nakagawa (2008), Uddin et al. (2011), Zhang et al. (2012) and Mohammadpour et al. (2013). The scour around abutments embedded in cohesive sediment mixtures consisting of clay and sand were studied by few investigators such as Molinas and Reiad (1999), Oh et al. (2007), Chen (2008), Abou-seida et al. (2012) and Debnath et al. (2014).

2.4.1 Partially Submerged Spur Dike/ Abutment Scour in Cohesionless Sediments

Garde et al. (1961) conducted experiments with right angled spur dikes. They used four sizes of spur dikes with channel contraction ratios $(\alpha = (B - L_a)/B)$ equal to 0.90, 0.835, 0.667, and 0.530 in a 0.60m wide laboratory flume. Here, B is the width of the flume and L_a is the length of the abutment perpendicular to the direction of flow. Bed materials of median size 0.20mm, 0.45mm, 1.00mm and 2.25mm and specific gravity

2.70 were used. The duration of experiments varied between 3 to 5 hours. Using dimensional analysis, they proposed the following equation to predict the scour depth.

$$\frac{h+d_m}{h} = 4\frac{1}{\alpha}F_r^{2/3} \tag{2.11}$$

Where, h is the approach flow depth, d_m = maximum depth of scour in cohesionless sediment, α = contraction ratio and F_r is the approach flow Froude number.

Zaghloul (1983) conducted several experiments to investigate the influence of sediment characteristics, approaching flow conditions and geometry of spur dikes on the maximum depth and pattern of scour around spur dike. It was observed that the Froude number of approaching flow and opening ratio at the location of spur dike significantly affect the maximum scour depth. It was also observed that during the development of scour hole the depth of scour progresses linearly with the logarithm of the time.

Lim (1997) proposed an equation for equilibrium scour depth around vertical-wall abutment under clear-water flow conditions as:

$$\frac{d_e}{h} = K_s 0.9\left(\theta_c^{-0.375}F_{d\beta}^{0.75}\left(\frac{d_{50}}{h}\right)^{0.5}\left\{\left(\frac{L_a}{h}\right)^{0.5}0.9+1\right\}-2\right) \tag{2.12}$$

Where, K_s is the foundation shape factor, θ_c is Shield's entrainment factor, and $F_{d\beta}$ is the densimetric particle Froude number. The duration of experimental run was between 72 to 193 hours. The uniform sand having d_{50}=0.94mm was used. The vertical wall shaped abutment model was constructed with lengths L_a=5cm, 7.5cm, 10cm, 12.5cm, and 15cm. A good agreement was observed between the computed and measured values of scour depth.

Melville (1997) presented an integrated approach to estimate the equilibrium scour depth at an abutment as

$$d_e = K_I K_{yw} K_d K_s K_\theta K_\sigma \tag{2.13}$$

Where,

K is an empirical expression accounting for the various influences on scour depth;

K_{yw}=flow depth-abutment size factor ≡ K_{yb} for piers and K_{yL} for abutments;

K_I =flow intensity factor,

K_d =sediment size factor;

K_s =foundation shape factor;

K_σ =foundation alignment factor;

K_σ =approach channel geometry factor;

K_{yw} and d_e have the dimension of length, while the other K factors are dimensionless.

Kothyari and Ranga Raju (2001) noticed that scour process around a spur dike was similar to that around a pier except that the boundary layer effect induced by the channel wall might cause less scour in the case of spur dikes and abutments.

Kuhnle et al. (2002) conducted a series of experiments with three spur dikes. These dikes were angled at 45^o, 90^o and 135^o to the downstream of channel sidewall. They studied maximum volume of scour hole and maximum bank erosion potential under clear water overtopping flow conditions at various angles of spur dikes. The spur dikes having contraction ratios of 0.125 and 0.250 were used in the experiments. They observed maximum volume of scour hole around spur dike having 135^o angle and highest bed erosion in the vicinity of spur dike at 45^o angle. However, the region around 90^o angled spur dike had least bed erosion in the near bank.

Dey and Barbhuiya (2005,a) presented a semi- empirical model for computation of temporal variation of scour depth around abutments. They used three different sizes of abutments viz; vertical-wall, 45° wing-wall, and semicircular in their experiments. They conducted experiments with uniform and non-uniform sediments under clear water flow conditions. The theory of conservation of mass of sediment was used for developing the model. The results predicted by model showed satisfactory agreement with the observed data on temporal variation of depth of scour in uniform and non-uniform sediments.

Ezzeldin et al. (2007) conducted experiments to study the process and depth of scour around spur dikes. They proposed several equations to compute maximum depth and length of scour hole. They found that scour depth computed from the proposed equations showed good agreement with observed depth of scour in experiments. The proposed equations are

(a) Equation to compute depth of scour

$$\frac{d_m}{h} = C_\theta C_e (6.142F_r - 0.941) \tag{2.14}$$

(b) Equation to compute length of scour at upstream of spur dike

$$\frac{L_{up}}{h} = C_\theta (12.2C_e F_r - 1.4) \tag{2.15}$$

(c) Equation to compute length of scour at upstream of spur dike

$$\frac{L_{down}}{h} = C_e(21.274F_r - 2.263) \tag{2.16}$$

Where, d_m = maximum depth of scour, h = approaching flow depth, F_r = Froude number, C_e and C_θ = factors depending on contraction ratio and angle of orientation respectively, L_{up} = length of scour hole at upstream of spur dike, and L_{down} = length of scour hole at downstream of spur dike.

Kothyari et al. (2007) suggested that, it is more realistic to relate the depth of scour around hydraulic structures to the difference between actual and the entrainment densimetric particle Froude number i.e. $(F_d - F_{d\beta})$. They verified this concept by studying variation of depth of scour with time for different values of $(F_d - F_{d\beta})$ considering a large volume of data from different laboratories. The relationships proposed by them for the determination of temporal variation of scour around spur dikes and bridge pier are

$$d_* = d / z_R = 0.272\sigma_g^{-1/2}(F_d - F_{d\beta})^{2/3}\log T \tag{2.17}$$

Where, F_{di} defined as

$$F_{di} = 2.33D_*^{-0.25}\left(\frac{R_h}{d_a}\right)^{1/6} \quad \text{for } D_* \le 10 \tag{2.18}$$

$$F_{di} = 1.08D_*^{1/12}\left(\frac{R_h}{d_a}\right)^{1/6} \quad \text{for } 10 < D_* < 150 \tag{2.19}$$

$$F_{di} = 1.65\left(\frac{R_h}{d_a}\right)^{1/6} \quad \text{for } D_* \ge 150 \tag{2.20}$$

and $F_{d\beta}$ defined as

For scour around spur dike

$$F_{d\beta} = \left[F_{di} - 1.26\cdot\Sigma\cdot\Sigma_s\cdot\Sigma_{ca}\cdot\beta^{\Sigma/4}\cdot\left(\frac{R_h}{d_a}\right)^{1/6}\right]\sigma_g^{1/3} \tag{2.21}$$

For bridge pier scour

$$F_{d\beta} = \left[F_{di} - 1.26\cdot\beta^{1/4}\cdot\left(\frac{R_h}{d_a}\right)^{1/6}\right]\sigma_g^{1/3} \tag{2.22}$$

Where, d_* = dimensionless scour depth, d = instantaneous scour depth in cohesionless sediment, z_R = reference length $= (hD^2)^{1/3}$ for cylindrical pier $= (hb^2)^{1/3}$ for spur dike, σ_g = geometric standard deviation, T = time parameter, Σ = represents the element shape; Σ_s =

submergence; $\sum_{ca}$ = cascade parameter. For singular spur dikes $\sum_{ca}=1; \sum_{s}=(s/h)^{0.3}$; $\beta=(b/B)$ and $\sum$=5/4, s = effective spur height; b = effective spur width relative to the approach flow direction; R_h=hydraulic radius and D_*= Dimensionless grain size is calculated by $D_*=(g^{'}/\nu^2)^{1/3}d_a$.

Fazli et al. (2008) conducted several experiments to study the depth of scour and flow pattern around spur dike installed at 90^o channel bend. They found that approaching flow Froude number (F_r) is an important parameter for the prediction of maximum depth of scour and height of point bar. These parameters increased with an increase in the Froude number. The depth of scour was also observed to increase with an increase in transverse length of spur dikes (i.e. effective spur width relative to the approach flow direction).

Vaghefi et al. (2009) conducted experiments to study the influence of length of spur dike on amount of scour using a T-shaped spur dike installed at angle of 90° in channel bend. They observed that, the depth and volume of scour as well as ridge height at the downstream of spur dikes increased with an increase in the length of the T-shaped spur dike. The maximum scour depth was located at the upstream nose of spur dike at a distance of about 10 to 20% of the spur dikes length.

Masjedi et al. (2010a) conducted laboratory experiments to study the effects of the Froude number, location and length of spur dike on the depth of scour around spur dike installed at 180^o channel bend. It was found that the depth of scour increased with an increase in Froude number and length of spur dike whereas the same was found to decrease with an increase in wing length of spur dike.

Masjedi et al. (2010b) and Rashedipoor et al. (2012) observed that the maximum depth of scour was highly dependent on the duration of experimental run and it increased with increase in Froude number and spur dike length.

2.4.2 Scour around Submerged Spur Dike in Cohesionless Sediments

Elawady et al. (2001) carried out experiments to investigate the effect of opening and overtopping ratios on depth of scour around submerged spur dike. The overtopping ratio is defined as the ratio of approaching flow depth to height of the structure above the

bed. The opening and overtopping ratios were varied from 0.77 to 0.98 and 1.07 to 5.2 respectively. It was found that spur dike with largest opening ratio formed small scouring area whereas, large depth of scour was observed around spur dike with smallest overtopping ratio.

Rodrigue-Gervais et al. (2011) conducted several laboratory investigations to study the temporal variation of scour around rough surfaced deflectors. Experiments were conducted under three overtopping ratios viz. 1.22, 1.83 and 3.67. Experimental results revealed that depth, length and volume of scour hole increased with an increase in overtopping ratio at constant approaching flow conditions. The process and location of scour hole were different for largest overtopping ratio (i.e. 3.67).

Uddin et al. (2011) carried out laboratory investigations to study the effect of orientation angle of bell mouth submerged groin on scour depth under clear water flow conditions. Experiments were conducted with submerged groin at four different orientations i.e. 60^o, 90^o, 135^o and 150^o. The maximum depth of scour was observed to occur at head of the bell mouth groin installed at 90^o angle while the minimum was observed for 135^o angle. The time to attain equilibrium scour was different for different orientations of submerged groin. The longitudinal and transverse extent of scour was maximum for higher discharge and gradually decreased with decrease in discharge. For the same discharge, maximum scour depth was observed in spur dike oriented at 90^o angle.

2.4.3 Partially Submerged Spur Dike/ Abutment Scour in Cohesive Sediments

Molinas and Reiad (1999) conducted laboratory experiments to study the influence of cohesion on abutment scour. They conducted 121 experiments on vertical wall abutments embedded in cohesive sediment mixtures. Cohesive material consisted of natural montmorrilonite clay and commercial kaolinite clay. In their experiments, clay fraction varied from 0.15 to 0.4 by weight. Clay was mixed with sand fraction of 0.1 to 0.5 by weight. They concluded that the maximum scour depth decreased with an increase of clay fraction and degree of compaction.

Oh et al. (2007) conducted several experiments to study the effect of length of abutment on scour depth in cohesive soil under clear water condition. They used a wing-wall shaped abutment for the experiments. The Porcelain clay was used in the

experiments. It has a median particle diameter d_{50} = 0.003mm, plasticity index PI = 14%, critical velocity U_c = 0.95m/s and critical shear stress τ_{cc} = 1.7N/m^2. The location of scour hole in Porcelain clay was observed to occur at the center of the test section or somewhat downstream of the abutment.

Abou-Seida et al. (2012) conducted laboratory experiments on local scour at bridge abutments on cohesive soil. They used Kaolin clay having median particle size $d_{50} = 0.13\mu m$ and pH ranged from 4.0 to 4.5. Other properties were: liquid limit $(LL) = 46.6\%$, plastic limit $(PL) = 21.4\%$, plasticity index $(PI) = 25.2\%$, optimum moisture content $(OMC) = 21\%$ and moisture of natural clay equal to 0.6%. The experiments consisted of 40 runs with the kaolin clay mixed with silica. They varied clay content, compactions and liquidity indices.

They performed two series of tests; in first test series, the effect of clay content was investigated by keeping the percentage of clay (P_c) at 2, 5, 10 and 20% and in the second test series mixture compaction (C_{omp}) was kept at 57, 69, 80 and 88%. They used the least squares approach to obtain relations among the various variables. They applied their finding in the range of $0.3 \le F_r \le 0.55, 2\% \le P_c(\%) \le 20\%, 57\% \le C_{omp} \le 88\%$, and $0.03 \le LI(\%) \le 0.99$ and proposed different equations for equilibrium scour depth (d_{ce}), scour volume (V_{ce}), scour width (W_{ce}), lateral side slope (θ_{side}) and longitudinal slopes of the scour hole.

The dimensionless equilibrium scour depth is

$$\frac{d_{ce}}{\sqrt{bh}} = 209503\frac{F_r^{1.68} LI^{0.48}}{P_c^{0.35} C_{omp}^{2.36}} \tag{2.23}$$

The equilibrium scour volume V_{ce} is

$$\frac{V_{ce}}{b^3} = 4.0\left(\frac{d_{ce}}{b}\right)^{2.3} \tag{2.24}$$

The equilibrium scour width W_{ce} is

$$W_{ce} = 1.8 d_{ce} \tag{2.25}$$

The lateral side angle of the scour hole θ_{side} (in deg.) is

$$\theta_{side} = 0.74 F_r^{-0.33} P_c^{0.09} C_{omp}^{0.79} LI^{-0.10} \tag{2.26}$$

The lateral upstream angle θ_{up} (in deg.) is

$$\theta_{up} = 2.53 F_r^{-0.02} P_c^{0.07} C_{omp}^{0.59} LI^{-0.06} \tag{2.27}$$

The lateral downstream angle θ_{down} (in deg.) is

$$\theta_{down} = 0.009 F_r^{-1.08} P_c^{0.17} C_{omp}^{1.35} LI^{-0.13} \tag{2.28}$$

The equilibrium time of scour t_e (in hours) is

$$\frac{U_o t_e}{h} = 27000 F_r^{0.58} P_c^{0.12} C_{omp}^{0.82} LI^{-0.05} \tag{2.29}$$

The development of non-dimensional depth of scour in cohesive soil with time is given as

$$\frac{d_{c(t)}}{d_{ce}} = \left(\frac{t}{t_e} \right)^{0.158} \tag{2.30}$$

Debnath et al. (2014) conducted experiments on local scour around abutments in clay/sand-mixed cohesive sediment bed. Out of 117 experiments, 87 experiments were conducted with vertical wall and 30 experiments were conducted with wing wall abutments respectively. Abutments were embedded in bed of cohesive sediment mixtures. It was observed that as water content was less than 24%, the maximum equilibrium scour depth reduced with an augment in clay content in clay-sand mixtures for both types of abutments. Further, it was also concluded that, for water content greater than 24%, the equilibrium scour depth reduced with an augment in clay content up to 50% and thereafter it increased.

2.5 SCOUR AROUND BRIDGE PIERS

2.5.1 Piers Scour in Cohesionless Sediments

An extensive amount of literature exists on scour around bridge piers founded in cohesionless sediments. Several researchers investigated the scour depth evolution with uniform and non-uniform sediment mixtures e.g. Ettema (1980),Yamnaz and Altinbilek (1991), Melville and Chiew (1999, Fukuoka et al. (1994, 1997), Graf and Yulistiano (1998), Raiker and Dey (2005), Kumar and Kothyari (2012), Raudkivi and Ettema (1983) and, Mellville and Sutherland (1988). The methods of estimation of scour depth have been proposed by Melville (1975), Melville and Sutherland (1988), Kothyari et al. (1992 a, b), Melville and Coleman (2000), Yanmaz and Cicekdag (2001), Mia and Nago (2003), Sheppard et al. (2004), Oliveto and Hager (2002, 2005), Kothyari et al. (2007), Hager and

Unger (2010), Uchita and Fukuoka (2010) and Kothyari and Kumar (2012) among many others. Only few studies are mentioned here for completeness.

Oliveto and Hager (2002, 2005) proposed a relationship for the computation of the maximum scour depth d_m at the pier as a function of time *t*. They observed that the densimetric particle Froude number is the dominant parameter controlling the scour process. Particle Froude number is given as $F_d = U_o/(g'd_{50})^{1/2}$, where U_o = velocity of approach flow; $g' = [(\rho_s - \rho)]g$ = relative gravimetric acceleration; ρ_s = sediment density; ρ = fluid density; and d_{50} = median grain size. By combining F_d with parameters for reference length z_R and reference time t_R, they proposed a scour relationship as

$$d_* = d_p / z_R = 0.068 \cdot \sum \cdot \sigma_g^{-1/2} \cdot F_d^{1.5} \cdot \log T \qquad \text{for } F_d > F_{d\beta} \qquad (2.31)$$

Mia and Nago (2003) proposed a design method to predict temporal variation of scour depth. The experiments were conducted with a cylindrical pier founded in uniform sediment bed under steady clear water flow condition. Modified bed load transport theory proposed by Yalin (1977) was used to include the temporal development of shear velocity at pier nose. They stated that the depth of scour hole reached equilibrium when bed shear stress and critical bed shear stress approaches to be equal.

Chang et al. (2004) carried out several experiments to investigate the depth of scour around circular bridge piers under steady and unsteady clear water flow conditions with uniform and non-uniform sediments. They investigated the effect of sediment size on depth of scour around circular pier nose. They developed a mixing layer concept for calculation of equilibrium scour depth in non-uniform sediments. They also proposed a regression formula to estimate the thickness of mixing layer in terms of median size and geometric standard deviation (σ_g) of the bed material when $(\sigma_g \leq 3)$.

Link (2006) conducted laboratory experiments to investigate temporal variation of three dimensional scour hole geometry around circular pier. They used high resolution non-intrusive method to measure time dependent scour hole geometry.

Kothyari et al. (2007) suggested a relationship for a circular bridge pier on the basis of difference between actual and the entrainment densimetric particle Froude number i.e. $(F_d - F_{d\beta})$ explained in section 2.4.1 (Eq. 2.22).

Lu et al. (2011) investigated the scouring around non-uniform cylindrical piers and developed a semi-empirical model for the estimation of scour depth with time. The concept of volumetric extraction of bed material from the scour hole and the formation of primary vortex inside the hole were included in the model development. They validated this model using experimental data of their own along with others. A very good agreement was observed between the results obtained from the proposed model and experiments.

2.5.2 Piers Scour in Cohesive Sediments

Kand (1993) suggested some guidelines to determine the scour depth in cohesive sediments after studying scour around bridges in India founded in clayey strata. He stated that in case of cohesive sediments, a modified value of Lacey's silt factor to be used in Lacey-Inglis method (Garde and Ranga Raju; 2006)

$$f_c = F_\theta (10 + C_u^{1/2}) \tag{2.32}$$

Where, f_c is Lacey's clay factor for cohesive sediments, C_u is cohesion in kN/m^2 and F_Θ is a coefficient based on angle of internal friction.

Briaud et al. (1999) proposed a step by step SRICOS method to compute the scour depth around cylindrical bridge pier embedded in clay. In their experiments, the diameters of cylindrical piers varied from 25 to 76mm and 76 to 229mm in smaller and larger flumes respectively. They used three different types of clay and one type of sand. They developed a new erosion function apparatus (EFA). They computed the initial rate of scour around the pier using the curve generated by EFA. The model proposed by Briaud et al. (1999) was validated by using the observations taken in the Laboratory and field.

Molinas et al. (1999) carried out experiments to investigate the influence of cohesive material properties on local scour around piers. They used sediment mixture composed of fine sand, silt, and montmorillonite clay of medium plasticity. In their experiments, the intensity of compaction varied from 58 to 93%, the initial water content in unsaturated and saturated clay varied from 15 to 20% and 32 to 48% respectively. They observed that the slope of the scour hole in cohesive sediment mixture was steeper than cohesionless sediments. The slope became steeper with an increase in amount of compaction. The slope of scour hole was observed low in compacted unsaturated mixtures and was very similar to that in cohesionless sediments. They also found that the

volume of scour hole decreased with an increase in compaction and initial water content. The high resistance to erosion was offered by saturated mixtures with low initial water content.

Ting et al. (2001) conducted laboratory experiments to study the influence of the Reynolds number, Froude number, and approach flow depth on scour depth around the circular piers embedded in clay. They made a comparison of depth of scour in sand and clay. Three types of clay were used in the experiments and its median size and plasticity index varied from 0.0006mm to 0.0062mm and 14.15 to 39.78 respectively. A total of 43 numbers of experiments were conducted with circular pier having diameter of 25mm and 75mm. They found that the maximum depth of scour hole and its shape is a function of pier Reynolds number. They proposed an equation to estimate the depth of scour.

$$d_{cpm} = 0.12 R_{ep}^{0.682} \tag{2.33}$$

Here, Pier Reynolds number $R_{ep} = U_o D / \nu$.

Ansari et al. (2002) studied the influence of cohesion on scour around bridge piers. They used clay-sand mixture as cohesive sediment in their experiments. They showed the variation of d_{ce}/d_e with W/W_{r_*} and C_*/ϕ_* (Fig. 2.1). It was found that the depth of scour around pier in cohesive sediments initially decreased with an increase in W/W_{r_*} up to 1.0 thereafter it starts increasing with further increase in W/W_{r_*}. They also found that the rate of erosion was least when W/W_{r_*} approaches unity and $PI > 0$. It was also concluded that scour depth in plastic sediments reduces with an increase in C_*/ϕ_*. Here parameter (C_*/ϕ_*) represents the cohesion strength of the sediment mixture. The variation can be shown by following equations

$$\frac{d_{cpm}}{d_{pm}} = 1.51 \left(\frac{W}{W_{r_*}} \right)^{0.35} \left(\frac{C_*}{\phi_*} \right)^{0.2} \qquad \text{for } PI = 0 \tag{2.34}$$

and

$$\frac{d_{cpm}}{d_{pm}} = \frac{6.02 - 10.82 \left(\frac{W}{W_{r_*}} \right) + 5.41 \left(\frac{W}{W_{r_*}} \right)^2}{\left(\frac{C_*}{\phi_*} \right)^{0.2}} \qquad \text{for } PI \geq 4 \tag{2.35}$$

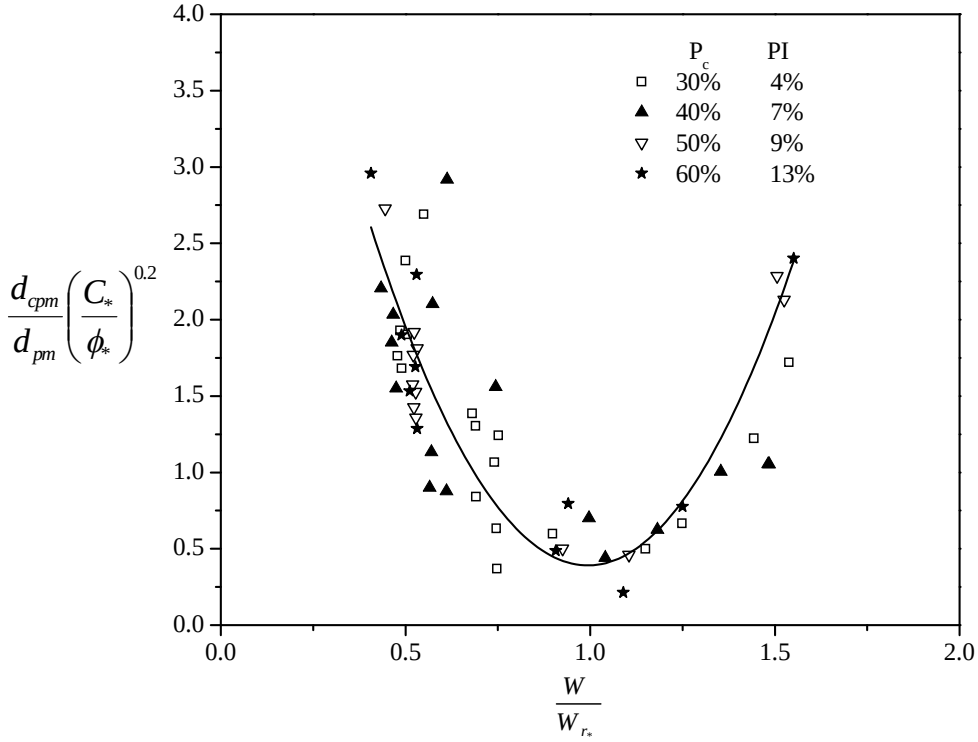

Fig. 2.1 Variation of $\frac{d_{cpm}}{d_{pm}}\left(\frac{c_*}{\phi_*}\right)^{0.2}$ with $\frac{W}{W_{r_*}}$; when *PI* >4 (Ansari et al., 2002)

Ansari et al. (2003) studied the effect of cohesion on the pier scour experimentally. They noted that the maximum scour occurs either at the sides of the pier or downstream of the pier depending on clay properties. They presented a mathematical model to compute the variation of pier scour depth with time in cohesive soil. The model approximately calculated the shear stress under the horseshoe vortex from the size of the horseshoe vortex. The constants of the model were determined from their experimental results and the model was verified with the same experimental data. They related the equilibrium scour depth in cohesive soil to that in non-cohesive soil through regression equations in terms of water content (saturated water content), clay content, the soil angle of repose, and the plasticity index. They suggested that their regression equation could be used at the field scale, assuming that the soil is fully saturated.

Ram Babu et al. (2002) proposed an empirical equation to compute the depth of scour around pile of given diameter and approaching flow velocity. They utilized hyperbolic law to fit the data to obtain ultimate depth of scour. Ram Babu et al. (2003) also developed a simple instrument to measure depth of scour around vertical pile at any instant founded in silty-clay in laboratory experiments. They presented a relationship to

measure depth of scour after considering soil properties, fluid parameters, flow duration and characteristics of the model.

Brandimarte et al. (2006) developed a methodology to study the scour risk at bridge foundation in cohesive soils. They applied the developed methodology for analysis of scour around piers of Woodrow Wilson Bridge on river Potomac in Washington D.C. USA. The sediment deposits in the river mainly consisted of soft clay, silt and silty sand. The proportion of soil (particles less than 0.06 mm) varied from 48 to 71% and plasticity index varied from 33 to 41%. In their study, the scour depth in cohesive soils was estimated by method proposed by Briaud et al. (2001). They also stated that the process of scour in cohesive soil occurs at a slow rate.

Debnath and Chaudhuri (2010,a) conducted experimental investigations on local scour around cylinders embedded in clay and clay-sand mixed beds. The effect of clay percentage and water content present in the sediment mixture on depth of scour hole and on its geometry were investigated in this study. They found that the depth of scour decreases with an increase in clay content at water content less than 24% in clay-sand mixture. While, at water content greater than 27%, the maximum depth of scour decreases with an increase in clay content up to 50% to 70%; thereafter it increases. Various equations were proposed to estimate the depth of scour using regression analysis. The equations are given below

$$d_{cpm*} = 2.05 \mathrm{F}_{rp}^{1.72} P_c^{-1.29} \hat{\tau}_{s*}^{-0.37} \quad \text{for } W = 20\text{-}23.22\% \text{ and } 20\% \le P_c \le 85\% \tag{2.36}$$

$$d_{cpm*} = 3.64 \mathrm{F}_{rp}^{0.22} P_c^{-1.01} \hat{\tau}_{s*}^{-0.69} \quad \text{for } W = 27.95\text{-}33.55\% \text{ and } 20\% \le P_c \le 50\% \tag{2.37}$$

$$d_{cpm*} = 20.52 \mathrm{F}_{rp}^{1.28} P_c^{-0.19} \hat{\tau}_{s*}^{-0.89} \quad \text{for } W = 27.95\text{-}33.55\% \text{ and } 50\% \le P_c \le 100\% \tag{2.38}$$

$$d_{cpm*} = 3.32 \mathrm{F}_{rp}^{0.72} P_c^{-0.62} W^{0.36} \hat{\tau}_{s*}^{-0.29} \quad \text{for } W = 33.60\text{-}45.92\% \text{ and } 20\% \le P_c \le 70\% \tag{2.39}$$

$$d_{cpm*} = 8 \mathrm{F}_{rp}^{0.61} C^{0.58} W^{1.24} \hat{\tau}_{s*}^{-0.19} \quad \text{for } W = 33.60\text{-}45.92\% \text{ and } 70\% \le P_c \le 100\% \tag{2.40}$$

Where, d_{cpm*} is dimensionless maximum depth of scour in cohesive sediment $= d_{scmp} / b$, F_{rp} = Pier Froude number $= U_o / (gD)^{0.5}$, P_c = clay fraction by dry weight of mixture, $\hat{\tau}_{s*}$ = dimensionless bed shear strength $= \tau_s / \rho U_o^2$.

Debnath and Chaudhuri (2010,b) carried out several experiments to investigate the scour around bridge pier in clay-sand mixture bed. The experimental results showed that the clay content present in clay-sand mixture significantly reduces the peripheral expansion and depth of the scour hole. It was observed that initiation of sediment removal in the process of scour commenced from the side of the pier in clay-sand mixture bed. They also found that the depth of scour and peripheral of scour hole increase with an increase in water content in the cohesive sediment.

Dey et al. (2011) presented results of experimental investigation on scour around vertical pile founded in clay and clay-sand mixture beds under waves. They stated that the depth of scour reduces with an augment of clay content in clay-sand mixture. They used Keulegan- Carpenter number for the prediction of variation of equilibrium scour depth in different clay percentages in sediment mixture and they found that it follows potential law.

Kothyari et al. (2014) conducted several experiments to study the depth of scour in wake region of circular pier embedded in cohesive sediment mixtures. The cohesive sediment mixtures were prepared by mixing clay, sand and gravel by weight. The experiments were conducted on two types of sediment mixtures (i) clay percentage varying from 20 to 60% was mixed with fine gravel by weight and (ii) clay percentage varying from 20 to 60% was mixed with equal proportion of fine sand and fine gravel by weight. Using dimensional analysis and after considering all relevant parameters, they proposed the following equation for the computation of scour depth in wake region of piers.

In the case of clay-gravel mixtures

$$\frac{d_{cpw}}{d_p} = \frac{1}{F_{pw1}} \tag{2.41}$$

and in the case of clay-sand-gravel mixture

$$\frac{d_{cpw}}{d_p} = \frac{1}{F_{pw2}} \tag{2.42}$$

Where, d_{cpw} is instantaneous depth of scour around pier in cohesive sediment at the wake of the pier and d_p is instantaneous depth of scour around pier in cohesionless sediment.

F_{pw_1} and F_{pw2} represents the coefficient of cohesion of clay-gravel and clay-sand-gravel sediment mixtures bed and are expressed as

$$F_{pw_1} = \left[(1+P_c)^{5.64}(1+UCS_*)^{0.42}(t_*^{'})^{-0.24}\right]$$

$$F_{pw2} = \left[(1+P_c)^{5.98}(1+UCS_*)^{0.69}(t_*^{'})^{-0.42}\right]$$

Where, $t_*^{'}$ is dimensionless duration of experimental run which can be expressed as

$$t_*^{'} = t\left(\frac{u_*}{d_a}\right) \tag{2.43}$$

Barbhuiya and Chakma (2012) carried out experiments to investigate the influence of consolidation on local scour around bridge pier in cohesive soil. They concluded that the equilibrium scour hole decreased with the increase in dry density of clay and silt content. However, it increases with an increase in sediment size.

Chaudhuri and Debnath (2013) conducted a study on initiation of bridge pier scour and equilibrium scour hole profile in cohesive sediment bed. It was observed that the scour started from the sides of the pier at 45^o to 270^o angle in case of circular pier. However, in case of square pier, the scour commenced from corner of upstream facing wall at 45^o and 315^o angle and moves towards the downstream end. The system of measurement of angles for both the piers is shown in Figure 2.2. They stated that the maximum equilibrium depth of scour and its peripheral expansion decreased with an increase in clay content up to 50% and thereafter it increased. They also found that the expansion of downstream equilibrium scour hole was more than that of upstream.

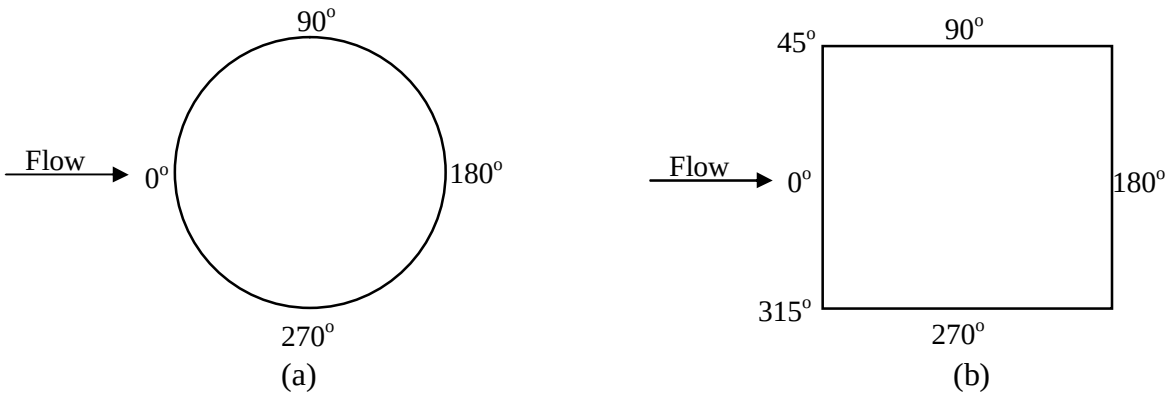

Fig. 2.2 System of measurement of angles for (a) circular pier and (b) Rectangular pier

Link et al. (2013) conducted experiments to quantify the effect of bed compaction on depth of scour around piers embedded in clay-sand mixtures. Experiments were performed in the laboratory flume with natural cohesive sediment. The depth of scour was measured using a non-intrusive high resolution system. They observed that the sediment was scoured in the form of particle by particle and/or aggregate by aggregate and chunks of aggregate. They stated that the maximum depth of scour occured at the wake of the pier with an increase in the ratio of actual to Proctor's optimum molding water content $(\hat{w})$. It was observed that the depth of scour decreased with an increase in water content $(\hat{w})$ up to 2.5. While in case of $\hat{w}$>2.5, depth of scour increases with an increase in water content.

2.6 FLOW CHARACTERISTICS

Several studies have been carried out on flow characteristics in scour hole around spur dikes, abutments and bridge piers founded in cohesionless sediments in recent time. Some studies have been conducted to understand the flow characteristics around bridge piers founded in cohesionless sediments viz; Melville and Raudkivi (1977), Dey et al. (1995), Ahmad and Rajaratnam (2000), Graf and Istiarto (2002), Muzzammil and Gangadhariah (2003), Dey and Raiker (2007), Kumar (2007, 2012). Flow pattern around spur dikes was studied by several researchers viz. Sukhodolov et al. (2004), Duan (2009), Duan et al. (2009), Ghodsian and Vaghefi (2009), Yaeger (2009), Duan et al. (2011), Koken (2011). Studies on flow pattern around abutments were carried out by Ahmed and Rajaratnam (2000), Barbhuiya and Dey (2003, 2004), Dey and Barbhuiya (2005 b, 2006), Koken and Constantinescu (2014). A few of these studies based on three dimensional flow velocities around spur dikes and abutments founded in cohesionless sediment are reviewed here.

2.6.1 Flow Pattern around Spur Dike

Sukhodolov et al. (2004) measured three dimensional turbulent flow velocities around spur dike using Acoustic Doppler Velocimeter at a sampling rate of 25Hz for 100-300s. They used *ExploreV 1.5* software developed by Nortek for the processing of measured instantaneous velocities. The spikes generated in the velocities data were removed and replaced by linear interpolation using 3-sigma filter incorporated in

software. It was observed that the time averaged mean velocities of vertical distribution follow the power law in the deeper part of groin field having depth range of $0.1 < z/h < 0.5$. For the same depth range $0.1 < z/h < 0.5$, the turbulence kinetic energy distributions follow the slope of the semi-theoretical description and it increased at the upper flow layers.

Uijttewaal (2005) carried out laboratory investigations to test the effect of different shapes of groyne on the flow field. They tested four different types of groynes. They arranged groynes in an array of five identical fields. The velocities were measured by Particle Tracking Velocimetry (PTV) around the groynes. Experimental data were used to study the process of vortex formation and detachment near the groyne head. They found that turbulence characteristics at downstream of the groyne can be manipulated by changing the slope of the groyne head and permeability. They also found that flow around groynes becomes more complex in the submerged condition and were dominated by three dimensional effects.

Kuhnle et al. (2008) conducted laboratory experiments to study the flow pattern and process of scour around spur dikes. The three dimensional velocities were measured using Acoustic Doppler Velocimeter around a trapezoidal shaped spur dike installed at fixed flat bed. The observations were taken at a frequency of 50Hz for 5 minutes duration. It was found that the length of the eddy zone was 1.6 times of spur dike length and four times of the dike height at the downstream of spur dike. They stated that the maximum bed shear stresses found to be 2.7 times of the approaching flow shear stresses.

Duan (2009) conducted several laboratory experiments to study the mean and the turbulent flow structure around spur dike by using micro-ADV at a sampling rate of 25Hz. He selected nine vertical profiles with 7-9 points at 1cm spacing for velocity measurements. He measured about 1500 instantaneous velocities at each node. The results are presented in the form of mean velocities, mean and turbulence kinetic energy, turbulence intensities, Reynolds and bed shear stresses. From the measured velocities, it was observed that flow near the water surface is in reverse direction while at the bottom flow remained in a downward direction. In the flow recirculation zone, turbulence kinetic energy, normal stresses and downstream component of Reynolds stresses close to the wake centre of each node reached a maximum value. Reynolds stresses were used to calculate bed shear stresses. It was also stated that maximum bed shear stresses were about three times as large as approaching flow mean bed shear stresses.

Duan et al. (2009) measured the mean and turbulent flow through emergent dike on a flat and scoured bed. The location of deepest scour was observed at downstream of the spur dike tip. He stated that the bed shear stresses in the scoured zone increased by contribution of component of Reynolds shear stresses $-\rho\overline{u'w'}$ and $-\rho\overline{v'w'}$. In case of fixed bed surface, high shear stresses were observed to occur at upstream side of the spur dike due to $-\rho\overline{u'v'}$ component. In scoured bed condition, the stream wise mean velocity reduced while transverse and vertical velocities increased.

Ghodsian and Vaghefi (2009) conducted experiments to study scour and flow field in scour geometry around T-shape spur dike installed at 90^o bend. Experiments were conducted under clear water condition. Flow measurements within the scour hole were taken by ADV-Vectrino at a sampling rate of 50Hz for a period of one to three minutes. The measured values from polar coordinates were converted to Cartesian coordinates. They found that longitudinal velocity components showed a nonlinear variation. However, in the zone between spur dike wing and outer wall of the channel, the magnitude of this velocity was minimum.

Yaeger (2009) conducted experiments to examine the average flow and turbulence characteristics around a series of spur dikes. The experiments were conducted in a laboratory flume of 0.6m width and 12.2m length. The instantaneous velocities in the three spatial directions *x*, *y* and *z* were measured using a 16 MHz Sontek micro-ADV at a sampling rate of 25Hz. Two series of experiments were performed. Three spur dikes were placed perpendicular to the direction of flow and another three dikes were angled into the direction of flow. WinADV software from Sontek was used for post-processing of data. They found that turbulence intensities $\sqrt{\overline{u'u'}}$ and $\sqrt{\overline{v'v'}}$ were most prominent, but $\sqrt{\overline{w'w'}}$ was much lesser than other two. They found the horizontal component of Reynolds stresses $-\rho\overline{u'v'}$ was larger than others two.

Duan et al. (2011) measured three dimensional flow fields around spur dike using micro-ADV. He performed experiments at a sampling rate of 25Hz for duration of about one to two minutes. The observations were taken to study the turbulent burst around the spur dike over the flat and scoured bed. Quadrant decomposition was used to analyze turbulent fluctuations of velocities (u', v', w'). Contributions of extreme events were quantified by the analysis of conditional Reynolds stresses. They observed that sediment

particles are transported by sweep and ejections $(u'>0, w'<0; u'<0, w'>0)$ within the scour hole. The magnitude of w' measured at flat bed was much larger than that measured at fully scoured bed. The extreme events with $H_1 > 2$, the conditional Reynolds stresses $-\rho\overline{u'w'}$ were stronger than $-\rho\overline{v'w'}$. The extreme events with $H_1 > 5$ were rare and only occurred at several locations. The relative contribution to extreme events by $-\rho\overline{v'w'}$ was larger than $-\rho\overline{u'w'}$ within the scour hole.

Koken (2011) conducted several experiments to investigate the turbulent flow structure around spur dikes angled at 60^o, 90^o and 120^o under various flow conditions. Instantaneous three dimensional velocities were measured using Acoustic Doppler Velocimeter at a sampling rate of 25Hz for 30s. It was found that the size, coherence and orientation of horseshoe vortex around spur dike were significantly different. The amplitude of oscillations was much larger in spur dikes angled at 90^o than other two. The total kinetic energy and root mean square of pressure fluctuation induced by horseshoe vortex into the flow were also lager in spur dikes angled at 90^o. Largest recirculation cell was observed in case of 60^o. The scoured area around spur dikes angled at 90^o was 2% and 15% larger than the spur dike angled at 60^o and 120^o respectively.

2.6.2 Flow Pattern around Abutment

Barbhuiya and Dey (2003) conducted laboratory investigations to study the flow field characteristics within scour hole formed around three different types of abutments using Acoustic Doppler Velocimeter (ADV). The observations were taken at a frequency of 50Hz under clear water flow conditions. Rectangular vertical wall, polygonal 45^o wing-wall and semi-circular abutments were used in the experiments. The time averaged three dimensional velocities were measured at vertical/ azimuthal and horizontal planes at the upstream of abutments. They found that primary vortex existed inside the scour hole with downflow. However, the flow field showed reverse flow in the downstream of abutment due to separation of flow.

Barbhuiya and Dey (2004) measured the three dimensional turbulence characteristics around 45^o wing-wall abutment installed in the rigid bed. They used Acoustic Doppler Velocimeter to measure instantaneous velocities at a sampling rate of 50Hz at azimuthal and horizontal planes. The measured data were used to analyze the

Reynolds stresses, turbulence intensity, turbulence kinetic energy and time averaged velocity components. Experimental results revealed the existence of the primary vortex with downflow at the upstream of abutment. They also found recirculation of flow along with strong shedding of wake vortex and high Reynolds stresses in the wake region of abutments.

Dey and Barbhuiya (2006) further investigated the three dimensional turbulent flow characteristics within scour hole around 45^o wing-wall under clear water flow conditions using ADV. They measured three dimensional velocity data, turbulence intensity, time averaged velocity, Reynolds stresses and turbulence kinetic energy at different azimuthal and horizontal planes. They found that flow field was chaotic due to vortex shedding in the downstream of abutment. They used Reynolds stresses and velocity gradients to compute bed shear stress within the scour hole. They stated that bed shear stress increased with the increase in the polar coordinate (θ).

2.7 CONCLUDING REMARKS

The process of scour around spur dikes and bridge piers founded in cohesionless uniform and non-uniform sediments have been studied extensively and are reasonably well understood at present. Similarly, the flow characteristics within the scour hole and on the rigid bed around the pier founded in cohesionless sediment are well explored in recent past. However, the river bed is commonly composed of mixture of cohesive as well as cohesionless sediments like clay, sand and gravel etc. The phenomenon of bridge prier and spur dikes scour is complex. It becomes more complex when these structures are founded in cohesive sediment mixtures. The review presented in this chapter brings out the fact that the process of scour around spur dikes and bridge piers founded in clay-sand mixtures is affected by number of flow and sediment parameters. However, the process of scour around spur dikes founded in cohesive sediments consisting of clay-sand-gravel mixture has not been studied yet, except one on pier scour in such cohesive sediment mixtures by Kumar (2011). Several experimental investigations have been carried out earlier to describe the flow and turbulence characteristics around the pier founded in cohesive sediments. However, no study has been conducted yet to illustrate the flow and turbulence characteristics around spur dike founded in channel bed composed of clay-gravel and clay-sand-gravel sediment mixtures.

CHAPTER - III

MODELLING OF THE PROCESS OF SCOUR AROUND SPUR DIKES AND BRIDGE PIERS FOUNDED IN COHESIVE SEDIMENT MIXTURES

3.1 GENERAL

The main objective of present investigation is to assess the effect of cohesion on the process and depth of scour around spur dikes (partially submerged and submerged) and bridge piers embedded in cohesive sediment mixtures consisting of clay-gravel and clay-sand-gravel. The objective also includes the study of flow characteristics around the spur dikes embedded in cohesive sediment bed. The functional relationships are also developed for the determination of temporal variation of scour depth around spur dikes and bridge piers.

Keeping in view of these objectives, a mathematical model was formulated for the computation of the temporal variation of scour depth around spur dikes and bridge piers embedded in the clay-gravel and clay-sand-gravel sediment mixtures. Quadrant analysis was performed to understand the flow pattern around the spur dike as well as in the scour hole formed around the spur dikes embedded in such cohesive sediment bed.

3.2 ANALYTICAL CONSIDERATIONS

Based on the comprehensive review of literature (Chapter II), it was noted that numerous studies were carried out on the spur dikes and bridge pier scour in cohesionless sediments. However, no study has been conducted on the depth of scour around spur dikes (partially submerged and submerged) embedded in cohesive sediment bed consisting of clay, sand and gravel. Only one study was conducted by Kumar (2011) on bridge pier scour in cohesive sediment bed consisting of clay, sand and gravel.

In nature, the river bed and banks consist of cohesionless as well as cohesive materials such as sand, gravel and clay (Jain and Kothyari, 2009). Hence, it becomes essential to study the process and possible depth of scour around hydraulic structures

founded in the mixtures of cohesionless and cohesive sediments. There are many cohesionless and cohesive parameters which together affect the process and depth of scour around the structures. It is difficult to understand the effect of these parameters analytically. Hence, systematic laboratory experiments were carried out in the present study to understand these processes of scour.

3.3 DIMENSIONAL CONSIDERATIONS

Various analytical and semi-theoretical methods proposed by different investigators revealed that scour depth around spur dike and bridge pier in cohesionless sediments is a function of hydraulic characteristics of flow, sediment characteristics and spur dike/ bridge pier parameters. More often the sediment characteristics used in the cohesionless sediment mixtures are of median size and standard deviation (Kothyari et al., 2014). In case of the mixtures of cohesive sediment, scour depth is influenced by a large number of inter-dependent variables such as clay content, antecedent moisture content, unconfined compressive strength and dry density of the sediment. These variables play a significant role in scouring and erosion process of cohesive sediment mixtures (Jain and Kothyari, 2009, 2010).

In compacted cohesive sediment beds, water content and clay percentage were identified as controlling parameters for abutment scour (Molinas and Reiad, 1999) and bridge pier scour (Molinas et al., 1999; Ansari et al., 2002; Debnath and Chaudhury, 2010a, b). The influence of such variables on scouring phenomenon is difficult to investigate by analytical methods. In cohesive sediments forces such as electrostatic and Van der Waals forces are also important parameters. Electrostatic forces are repulsive forces whereas Van der Waals forces are relatively weak electromagnetic forces. These forces attract molecules to each other like magnet (Mitchell, 1993); and hence resist the scouring.

The depth of scour around spur dikes and bridge piers in cohesive sediments is mainly affected by the following variables:

$$d_c = f\left(P_c, C_u, d_a, \phi_c, \phi_{sh}, e, \gamma_d, \gamma_w, \gamma_s, UCS, d\right) \tag{3.1}$$

Where, d_c is the scour depth in cohesive sediment, C_u is the cohesion, γ_d is dry density, UCS is the unconfined compressive strength, d_a is the arithmetic mean size of cohesive

sediment mixture, e is the void ratio, γ_d is the dry density of sediment mixtures, ϕ_c and ϕ_{sh} are angle of internal friction for clay and cohesionless sediment respectively, γ_w is specific weight of water, γ_s is specific weight of sediment, d is instantneous scour depth in cohesionless sediment. The arithmetic mean size of cohesive sediment mixture (d_a) is calculated by a procedure proposed by Kothyari and Jain (2008), Jain and Kothyari (2009, 2010) and Kothyari et al. (2014).

The variables $P_c, C_u, \phi_c, \phi_{sh}, \gamma_s, \gamma_w, d_a$ and UCS can be written in non-dimensional form as per Buckingham-π theorem (Peerles, 1967; Kothyari and Jain, 2008 and Kothyari et al., 2014)

$$C_* = \frac{P_c\, C_u}{(\gamma_s - \gamma_w) d_a} \tag{3.2}$$

$$\phi_* = \frac{P_c \tan\phi_c + (1 - P_c)\tan\phi_{sh}}{\tan\phi_{sh}} \tag{3.3}$$

Where, C_* is dimensionless cohesion and ϕ_* is dimensionless angle of friction of the mixtures of cohesive sediment. The cohesive sediment mixtures were formed by mixing different proportions of the clay, sand and gravel. Therefore, the parameters C_* and ϕ_* are the main indicators of improved cohesiveness of the cohesive sediment mixtures.

Using dimensional analysis, the variables UCS and t can also be written into dimensionless form as (Kothyari and Jain, 2008 and Kothyari et al. 2014)

$$UCS_* = \frac{UCS}{(\gamma_s - \gamma_w) d_a} \tag{3.4}$$

and

$$t_* = t\left(\frac{U_o}{d_a}\right) \tag{3.5}$$

Where, UCS_* is dimensionless unconfined compressive strength and t_* is the dimensionless time. The term UCS_* represents the scouring resistance of cohesive sediment bed.

Thus, the Eq. (3.1) can be summarized as

$$d_c = f(d, P_c, C_*, \phi_*, \gamma_d, \gamma_w, UCS_*, t_*) \tag{3.6}$$

Using dimensional analysis of the various variables, Eq. (3.6) is arranged in dimensionless form as

$$\frac{d_c}{d} = f\left(P_c, \frac{C_*}{\phi_*}, \frac{\gamma_d}{\gamma_w}, UCS_*, t_*\right) \tag{3.7}$$

Scour depth may be function of $C_*.\phi_*$ as shear strength is directly proportional to the same. However, an attempt has been made to relate scour depth with C_*/ϕ_* which is in agreement with earlier investigators too (Ansari et al., 2002; Jain and Kothyari 2009, 2010; and Kothyari et al., 2014).

The functional form given in the Eq. (3.7) was used to compute the scour depth around spur dikes and bridge piers embedded in the mixtures of cohesive sediment containing clay-gravel and clay-sand-gravel. The depth of scour around spur dikes and bridge piers in cohesionless sediment (d) in the Eq. 3.7 may be obtained by using any suitable relationship proposed by several researchers. In the present study, the value of d is obtained by the relationship proposed by Kothyari et al. (2007). This relationship was proposed for the temporal evolution of maximum depth of scour around hydraulic structures (i.e. bridge pier, abutment, spur dike etc.) using large set of VAW data (Oliveto and Hager 2002, 2005).

3.4 MODELING OF TEMPORAL VARIATION OF SCOUR AROUND SPUR DIKES AND BRIDGE PIERS EMBEDDED IN COHESIVE SEDIMENT MIXTURES

For the design of foundation of any hydraulic structure (i.e. spur dikes, bridge piers, abutments etc.), the realistic estimation of scour depth is essential. The previous literatures have recommended that the estimation of time dependent depth of scour is more important than the estimation of maximum depth of scour for the safe and optimal design of foundation. In real field, most of the hydraulic structures are constructed on the land composed of cohesionless and cohesive sediments.

An attempt has been made in this study to develop a mathematical model for the computation of temporal variation of scour depth around spur dikes and bridge piers founded in mixture of clay-gravel and clay-sand-gravel. The mathematical formulations proposed by Kothyari et al. (2007) were used for the development of the present model.

The transport rate of sediment mainly depends on the resultant shear stress which is the difference of total shear stress and critical shear stress for the incipient motion condition exerted by the flow. Accordingly, Kothyari et al. (2007) suggested that it is more realistic to relate the depth of scour around bridge elements to the difference between actual and the entrainment densimetric particle Froude number i.e. ($F_d - F_{d\beta}$). They verified this concept by studying the variation of depth of scour with time for different values of ($F_d - F_{d\beta}$) after considering a large volume of data from different laboratories.

Oliveto and Hager (2002) had earlier proposed the entrainment conditions represented by $F_{d\beta}$, relative to circular bridge piers and rectangular elements as

$$F_{d\beta} = \phi_\beta F_{di} \tag{3.8}$$

Where, F_{di} is densimetric particle Froude number for incipient motion condition and ϕ_β is ratio between $F_{d\beta}$ and F_{di}. Based on Shields diagram and involving the dimensionless grain size D_*, they proposed relationships to compute F_{di} based on three ranges of D_*.

Following Oliveto and Hager (2002, 2005), Kothyari et al. (2007) also suggested that the sediment entrainment is caused by presence of a flow obstructing element such as spur dike, pier etc. Its effect tends to become small when element width reduces and entrainment process is then governed exclusively by the Shields criterion. The relative depth thus becomes important in addition to channel geometry for the entrainment criterion. The analysis of data of Oliveto and Hager (2002) by Kothyari et al. (2007) resulted in the following relationship for $F_{d\beta}$

$$F_{d\beta} = \left[F_{di} - 1.26\beta^{1/4} \left(\frac{R_h}{d_a}\right)^{1/6} \right] \sigma_g^{1/3} \tag{3.9}$$

with

$$F_{di} = 2.33 D_*^{-0.25} \left(\frac{R_h}{d_a}\right)^{1/6} \qquad \text{for } D_* \le 10 \tag{3.10}$$

$$F_{di} = 1.08 D_*^{1/12} \left(\frac{R_h}{d_a}\right)^{1/6} \qquad \text{for } 10 < D_* < 150 \tag{3.11}$$

$$F_{di} = 1.65\left(\frac{R_h}{d_a}\right)^{1/6} \quad \text{for } D_* \geq 150 \tag{3.12}$$

As the sediment mixtures used in present study are highly non-uniform in nature, arithmetic mean size d_a rather than d_{50} (Kothyari et al., 2007) has been considered for computations in the present study. Therefore, above Equations (2.18) to (2.22) are re-written after replacing d_{50} by d_a. In the present study, geometric standard deviation σ_g (Kothyari et al., 2007) is also replaced by $\sigma_g^{'}$ for cohesive sediment mixtures in Eq. 2.17, where $\sigma_g^{'} = d_{84}/d_{50}$ (Melville and Sutherland, 1988).

Utilizing the data set of Oliveto and Hager (2002, 2005) for pier and abutment scour, a general relationship was presented by Kothyari et al. (2007) for temporal evolution of maximum depth of scour based on the similitude of Froude number. They relate the depth of scour to the difference between the actual and the entrainment densimetric particle Froude numbers as below

$$d_* = d / z_R = 0.272\sigma_g^{'\,-1/2}(F_d - F_{d\beta})^{2/3}\log T \tag{3.13}$$

Using the Eq. (3.13) as the basis, a computational procedure was proposed to determine the temporal variation of depth of scour in cohesive sediment mixtures. The proposed methodology is schematically described in the Fig. 3.1. It illustrates the steps to be followed in the computations. Details of derivation of corresponding relations given in Fig. 3.1 are described in the Chapter V.

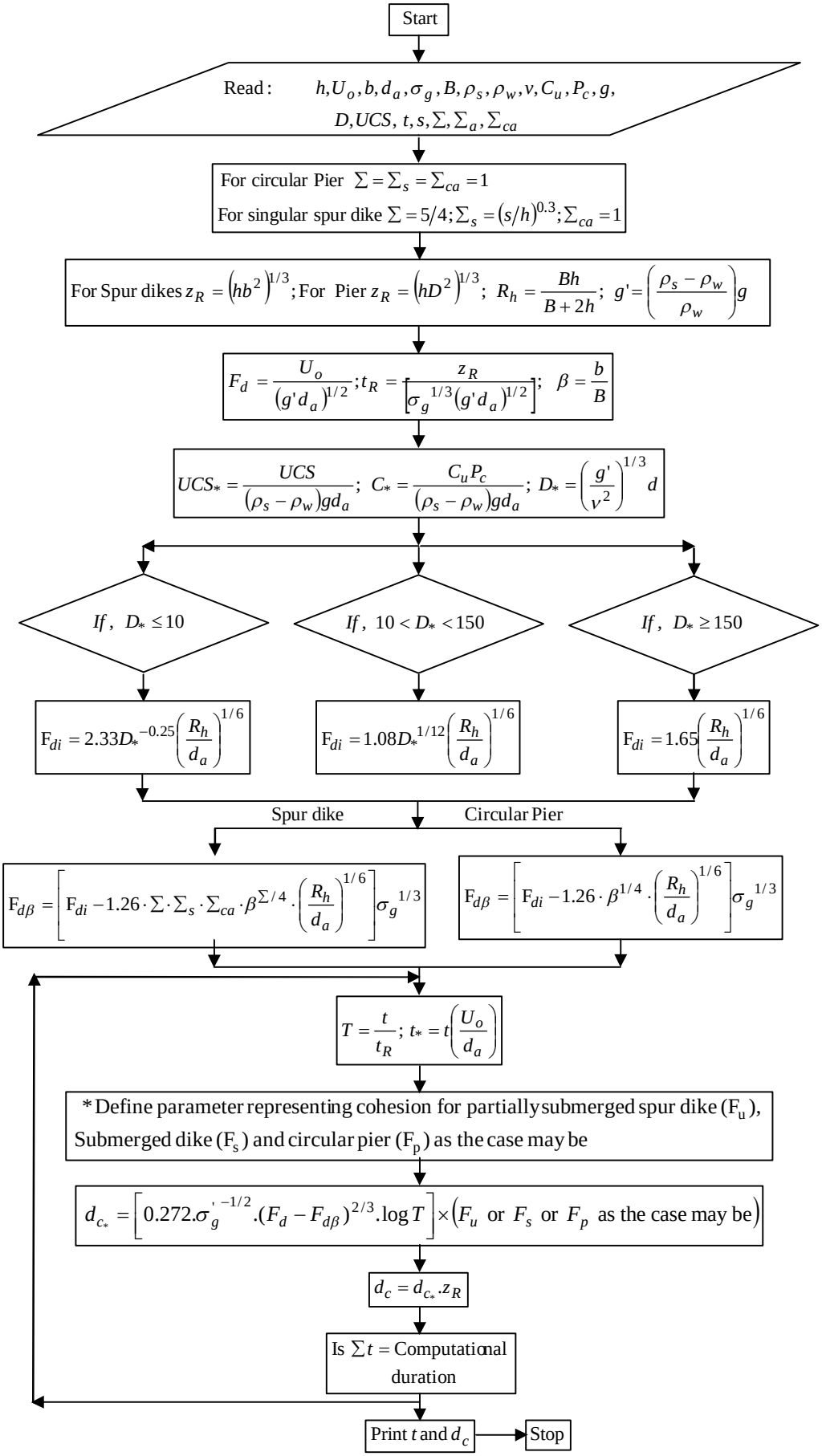

Fig. 3.1 Algorithm for computation of the temporal variation of scour depth around spur dike and bridge pier founded in clay-gravel and clay-sand-gravel mixtures

* Defining cohesion parameter for partially submerged spur dike (F_u), submerged spur dike (F_s) and pier (F_p)

(a) Defining cohesion parameter for partially submerged spur dike (F_u) for nose (F_{un}) and at the wake of the partially submerged spur dike (F_{uw}) in clay - gravel and clay - sand - gravel mixtures

$$F_{un} = a_o\left[(5\mathrm{P_c})^{a_1}(1+0.001UCS_*)^{a_2}(t_*)^{a_3}\right]$$

With, $a_o = 0.00144; a_1 = -1.82; a_2 = -0.705; a_3 = 0.335$ (For $10\% \le \mathrm{P_c} \le 20\%$)

$a_o = 1.25\times10^{-6}; a_1 = -4.75; a_2 = -0.25; a_3 = 0.786$ (For $30\% \le \mathrm{P_c} \le 50\%$)

and

$$F_{uw} = \mathrm{c}_o\left[(5\mathrm{P_c})^{c_1}(1+0.01UCS_*)^{c_2}(t_*)^{c_3}\right]$$

With, $c_o = 0.00195; c_1 = -1.525; c_2 = -0.1067; c_3 = 0.324$ (For $10\% \le \mathrm{P_c} \le 20\%$)

$c_o = 2.96\times10^{-5}; c_1 = -3.633; c_2 = -0.306; c_3 = 0.638$ (For $30\% \le \mathrm{P_c} \le 50\%$)

(b) Defining cohesion parameter for submerged spur dike (F_s) for nose (F_{sn}) and at the wake of the submerged spur dike (F_{sw}) in clay - gravel and clay - sand - gravel mixtures

$$F_{sn} = b_o\left[(5\mathrm{P_c})^{b_1}(1+0.01UCS_*)^{b_2}(t_*)^{b_3}\right]$$

With, $b_o = 0.0032; b_1 = -1.365; b_2 = -0.444; b_3 = 0.298$ (For $10\% \le \mathrm{P_c} \le 20\%$)

$b_o = 5.7\times10^{-7}; b_1 = -5.535; b_2 = -0.43; b_3 = 0.895$ (For $30\% \le \mathrm{P_c} \le 50\%$)

and

$$F_{sw} = \mathrm{d}_o\left[(5\mathrm{P_c})^{d_1}(1+0.01UCS_*)^{d_2}(t_*)^{d_3}\right]$$

With, $d_o = 0.0028; d_1 = -1.024; d_2 = -0.4355; d_3 = 0.331$ (For $10\% \le \mathrm{P_c} \le 20\%$)

$d_o = 6.1\times10^{-7}; d_1 = -4.33; d_2 = -0.281; d_3 = 0.876$ (For $30\% \le \mathrm{P_c} \le 50\%$)

(c) Defining cohesion parameter for circular pier (F_p) for side (F_{ps}) and at the wake of the pier (F_{pw}) in clay - gravel and clay - sand - gravel mixtures

$$F_{ps} = m_o\left[(\mathrm{P_c})^{m_1}(1+UCS_*)^{m_2}(t_*)^{m_3}\right]$$

With, $m_o = 0.00024; m_1 = -1.226; m_2 = -0.0914; m_3 = 0.3385$ (For $10\% \le \mathrm{P_c} \le 20\%$)

$m_o = 9.68\times10^{-7}; m_1 = -2.653; m_2 = -0.3785; m_3 = 0.656$ (For $30\% \le \mathrm{P_c} \le 50\%$)

and

$$F_{pw} = \mathrm{n}_o\left[(\mathrm{P_c})^{n_1}(1+UCS_*)^{n_2}(t_*)^{n_3}\right]$$

With, $n_o = 5.9\times10^{-5}; n_1 = -1.678; n_2 = -0.346; n_3 = 0.342$ (For $10\% \le \mathrm{P_c} \le 20\%$)

$n_o = 2.41\times10^{-8}; n_1 = -2.42; n_2 = -0.253; n_3 = 0.747$ (For $30\% \le \mathrm{P_c} \le 50\%$)

3.5 QUADRANT ANALYSIS

Flow characteristics around spur dike on scoured bed consisting of cohesive sediment mixtures are not studied so far. In present study the quadrant technique (Lu and Willmarth, 1973) has been used to identify the bursting trends in the flow within the scoured profile around the spur dike. The interaction between turbulent bursts and sediment motion can be determined by quadrant analysis (Cava et al., 2005 and Storm and Papanicolaou, 2007). The turbulent bursts events are defined by four quadrants and are classified as

- Outward interaction $(Quardant = I, u' > 0, w' > 0)$.
- Ejection $(Quardant = II, u' < 0, w' > 0)$.
- Inward interaction $(Quardant = III, u' < 0, w' < 0)$ and,
- Sweep $(Quardant = IV, u' > 0, w' < 0)$.

In simple meaning, it is possible to spot an ejection event if a low-speed fluid with $u' < 0$ and an upward velocity $w' > 0$, observed to occur simultaneously (Cellino and Lemmin, 2004). Here, w' is defined as $w' = w - \overline{w}$. Similarly, sweep event can be identified by simultaneously observing a high speed fluid moving towards the bed $u' > 0$ and $w' < 0$ (i.e. w' has downward direction). Two other events are defined as outward interaction when $u' > 0$ and $w' > 0$ and inward interaction when $u' < 0$ and $w' < 0$. These two events are generally observed to be less dominant in the flow field compared to ejection and sweep.

The averaged stream-wise velocities and the vertical velocities were decomposed into the instantaneous velocities following their sign for the quadrant analysis. This approach was proposed by Lu and Willmarth (1973) and is termed as $u'w'$ quadrant splitting scheme. The schematic representation of various quadrants in $u'w'$ plane is shown in Figure 3.2. The cross hatched region in this Figure is called the "hole" and is defined as the one bounded by the curves

$$\left|u'w'\right| = H\sqrt{\overline{u'^2}}\sqrt{\overline{w'^2}} \tag{3.12}$$

Where, H = hole size representing a threshold level as given in Nezu and Nakagawa (1993).

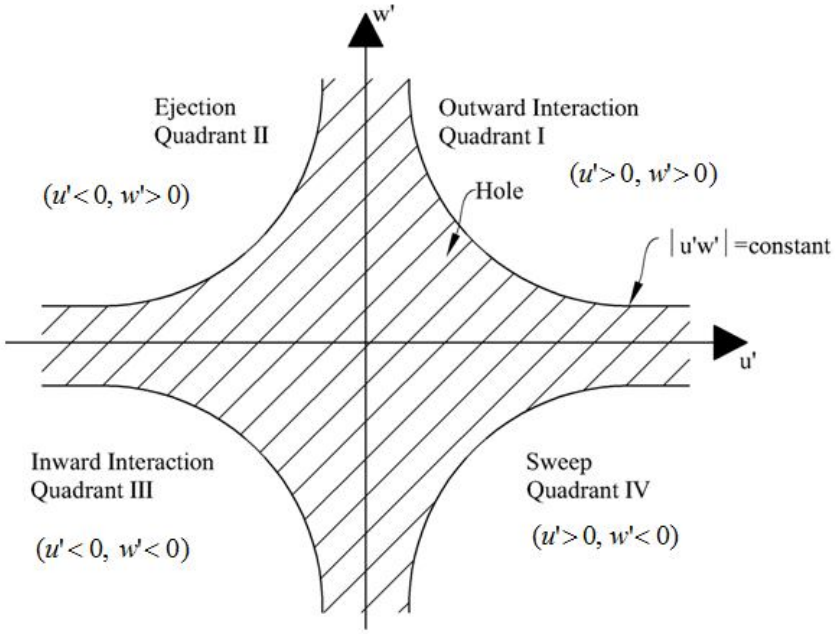

Fig. 3.2 Definition sketch of the $u'w'$ plane (after Nezu and Nakagawa, 1993)

The hole size *'H'* permits to distinguish between strong and weak events. Weak events are included in the case of small value of hole size and only strong events are included in the case of large value of hole size (Cellino and Lemmin, 2004).

3.5.1 Conditional Statistics of Reynolds stress

The organization of vortices in space and time (also called coherent structures) control the wall turbulence. These structures are responsible for the resistance to sediment motion and its transport process (Mazumder and Ojha, 2007). Reynolds stresses contribution and turbulence productions are associated with turbulent events. They are demonstrated by conditional sampling technique (Lu and Willmarth, 1973; Wallece et al., 1972). At any point in a stationary flow, the contribution to the total Reynolds stress from quadrant i, excluding a hyperbolic hole of size H is

$$< u'w' >_{i,H} = \lim_{T\to\infty} \int_0^T u'(t)w'(t)I_{i,H}(u'w')dt \qquad (3.13)$$

Here, angle bracket denotes a conditional average and the indicator function *'I'* follows

$$I_{i,H}(u'w') = \begin{cases} 1 \text{ if } (u'w') \text{ is in the } i^{th} \text{ quadrant and if } |u'w'| > H\overline{|u'w'|} \\ 0, \text{ otherwise} \end{cases}$$

Here, *'H'* is the threshold parameter in the Reynolds stress signal which enables to extract those values of $u'w'$ from the whole set of data which are greater than H times $\overline{|u'w'|}$ values. The threshold parameter *'H'* is used here to get an idea of the relative importance of various quadrant events in generating shear stress of particular strength. The stress fraction for i^{th} quadrant can be defined as

$$S_i, H = < u'w' >_{i,H} / \overline{|u'w'|} \tag{3.14}$$

and it satisfies

$$\sum_{i=1}^{4} |S_{i,0}| = 1 \tag{3.15}$$

Where, $S_{i,H}$ indicatively defines occurrence probabilities of a particular event. As per Ojha and Majumder (2008)

$$S_H = \frac{S_{2,H}}{S_{4,H}} \tag{3.16}$$

Equation (3.16) is a measure of relative dominance of sweep and ejection event.

The above analysis thus enables one to map the flow field under investigation. The quantification of bursting trends (sweep and ejection) in the degraded or scoured profile of channel bed around spur dike/pier should be useful in deciding the methods for scour protections.

3.6 CONCLUDING REMARKS

A non-dimensional form of relationship for the computation of the depth of scour around spur dikes and bridge piers embedded in the mixtures of clay-gravel and clay-sand-gravel is hypothesized. A flow chart explaining the comprehensive procedure for the computation of temporal variation of depth of scour around spur dikes and bridge piers in such cohesive mixtures has also been proposed. The conditional statistics of Reynolds stresses has been described to identify the bursting trends (ejection and sweep) in flow over a scoured bed caused due to spur dikes in cohesive sediment mixture.

CHAPTER - IV

EXPERIMENTAL EQUIPMENT AND PROCEDURE

4.1 GENERAL

To achieve the objectives set for the study, there is a need to collect data for, (i) Identifying the correct parameters influencing depth of scour around spur dike and bridge pier embedded in clay-gravel and clay-sand-gravel sediment mixtures, (ii) Studying the temporal variation of depth of scour around spur dike and bridge pier founded in cohesive sediments consisting of clay-gravel and clay-sand-gravel mixtures, (iii) Studying the flow characteristics in scour hole around spur dike in such cohesive sediments mixtures (iv) Developing the mathematical model for computation of maximum depth of scour around spur dike and bridge pier founded in cohesive sediments consisting of clay-gravel and clay-sand-gravel mixtures.

Keeping in view these objectives, a set of planned laboratory experiments were conducted on the above mentioned aspects using cohesive sediment mixtures consisting of clay-gravel and clay-sand-gravel in various proportions. Experiments were undertaken to understand the influence of cohesion on various processes of scour around spur dike and bridge pier. It was done by systematic variation of percentage of clay in the sediment mixtures. The experiments were carried out in the Laboratory of Hydraulic Engineering Section in the Indian Institute of Technology Roorkee, Roorkee, India. In this chapter, materials and equipment used and the experimental procedure followed for the present study are described.

4.2 SEDIMENTS USED

Three types of sediments i.e. sand, gravel and clay were used in all the experiments in varying proportions. Fine sand and fine gravel were considered as the base sediment in

case of all mixtures. In order to prepare cohesive mixture, clay was added in various proportions to the base sediment. Detailed engineering properties of all the sediments and their mixtures were determined after conducting various tests. The details of the properties are described herein.

4.2.1 Properties of Clay, Sand and Gravel

The clay dug out from 1.0m depth below the ground surface was used in the experiments. The properties of the clay and its mixtures were determined as per Indian Standard Code (IS-1498, 1970; IS-2720-29, 1975 and IS-2720-10, 1991). A laser particle size analyzer was used to find out the median size of clay particle. The median size (d_{50}) of clay, sand and gravel were 0.0014mm, 0.24mm and 2.7mm respectively. The geometric standard deviation ($\sigma_g = \sqrt{d_{84}/d_{16}}$) for the same was 2.16, 1.41 and 1.21 respectively. The relative density of sand and gravel was 2.65. Figure 4.1 depicts particle size distribution curve for clay, sand and gravel. Figure 4.2 (a-c) shows the photographic view of the clay, sand and gravel used in the experiments.

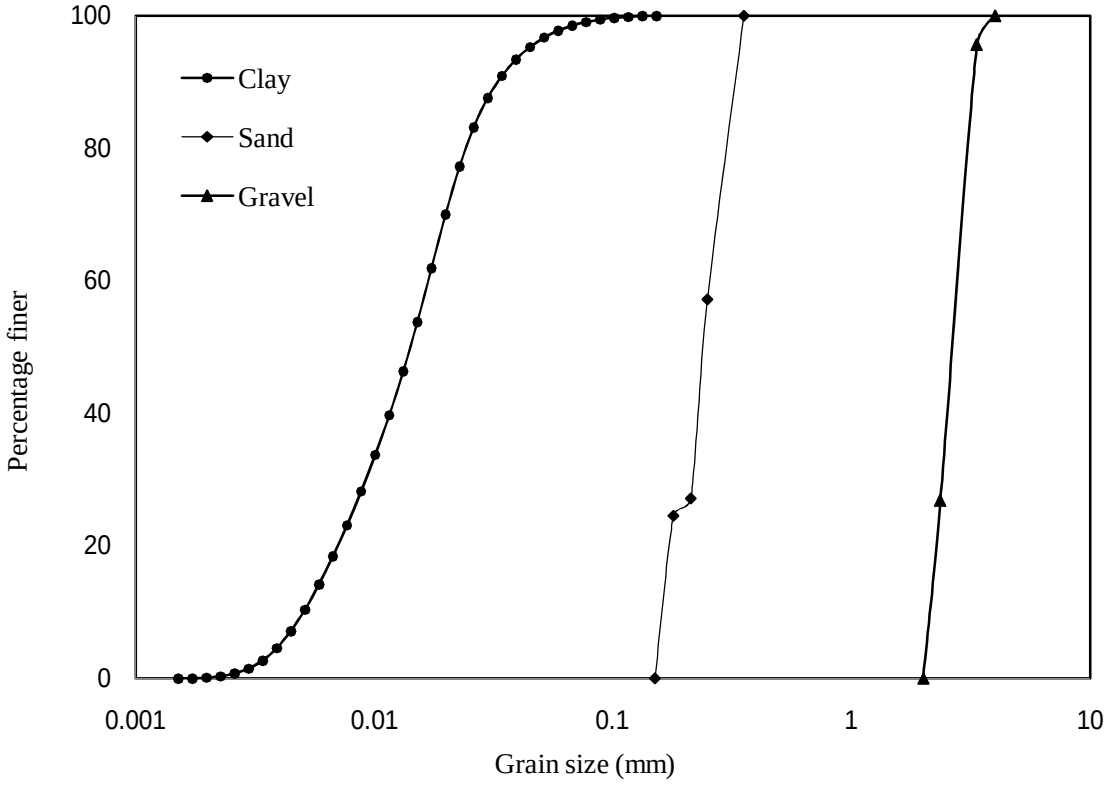

Fig. 4.1 Grain size distribution of clay, sand and gravel

(a) (b) (c)

Fig. 4.2 View of bed materials (a) clay, (b) sand and (c) gravel

The engineering properties of clay material were: liquid limit (*LL*) = 43%, plastic limit (*PL*) = 22% and plasticity index (*PI*) = 21%, optimum moisture content (*OMC*) = 19%, maximum dry density $(\gamma_d)_{\max}$ = 16.43 kN/m^3, cohesion at *OMC*, C_u = 49.23 kN/m^2, angle of friction at *OMC* ((ϕ_c) = 30.7^o and relative density = 2.65.

The X-Ray Fluorescence (XRF) test was conducted to determine the percentage of various oxides present in the different composition of sediment mixtures. The result of XRF test is shown in Table 4.1. The mineralogical properties of clay were determined by X-ray diffraction (XRD) test. The results of the XRD test are shown in Fig. 4.3. The analysis showed the presence of minerals in the clay as Illite = 77.5%, Kaolinite = 18% and Montmorillonite = 4.5%. The running conditions for XRD test are summarized below:

Radiation	*K* (Potassium)	Voltage	40 KV
Target	*Cu* (Copper)	Range	2 KC/s
Filter	*Ni* (Nickel)	Chart speed	1 cm per minute
Scanning angle	4^o to 40^o of 2α	Goniometric speed	1^o of 2 α / minute
Current	30 mA		

Table 4.1: The results of XRF test for various compositions of sediment mixtures

S. No.	Sample Name	Na_2O	MgO	Al_2O_3	SiO_2	P_2O_5	K_2O	CaO	TiO_2	MnO	Fe_2O_3	Sum	LOI
		%	%	%	%	%	%	%	%	%	%	%	%
1	100% Clay	1.14	3.70	17.74	58.18	0.12	3.87	1.07	0.72	0.11	6.95	93.60	6.70
2	100% Sand	0.58	0.44	4.34	90.97	0.02	0.91	0.33	0.19	0.03	1.17	98.98	0.94
3	100% Gravel	1.22	3.01	7.51	72.77	0.09	1.45	3.43	0.35	0.06	2.68	92.57	6.57
4	50 % Sand + 50 % Gravel	0.96	1.67	5.79	81.97	0.04	1.10	1.44	0.26	0.04	1.86	95.13	3.43
5	10% Clay +90 % Gravel	1.16	2.95	9.73	69.60	0.10	1.74	3.33	0.40	0.06	3.29	92.36	6.18
6	20% Clay +80 % Gravel	1.23	3.04	10.07	68.92	0.09	2.01	3.16	0.43	0.07	3.48	92.50	6.29
7	30% Clay +70 % Gravel	1.31	2.87	10.72	70.03	0.08	2.22	2.70	0.46	0.07	3.71	94.17	6.41
8	40% Clay +60 % Gravel	1.28	3.07	12.15	66.24	0.08	2.47	2.64	0.49	0.08	4.39	92.89	6.23
9	50% Clay +50 % Gravel	1.16	3.29	13.26	64.96	0.11	2.79	3.00	0.55	0.08	4.57	93.77	6.91
10	10% Clay+45 % Sand + 45% Gravel	1.07	1.72	7.83	78.53	0.08	1.51	1.61	0.33	0.05	2.49	95.22	3.59
11	20% Clay+40 % Sand + 40% Gravel	1.11	2.33	9.93	73.88	0.06	1.76	1.87	0.37	0.06	2.89	94.26	4.43
12	30% Clay+35 % Sand + 35% Gravel	1.13	2.23	10.20	72.99	0.07	1.99	1.57	0.41	0.07	3.41	94.07	4.37
13	40% Clay+30 % Sand + 30% Gravel	1.13	2.40	11.78	71.49	0.08	2.35	1.45	0.47	0.08	4.09	95.32	4.61
14	50% Clay+25 % Sand + 25% Gravel	1.20	2.87	12.70	67.82	0.09	2.63	1.92	0.51	0.08	4.53	94.35	5.53

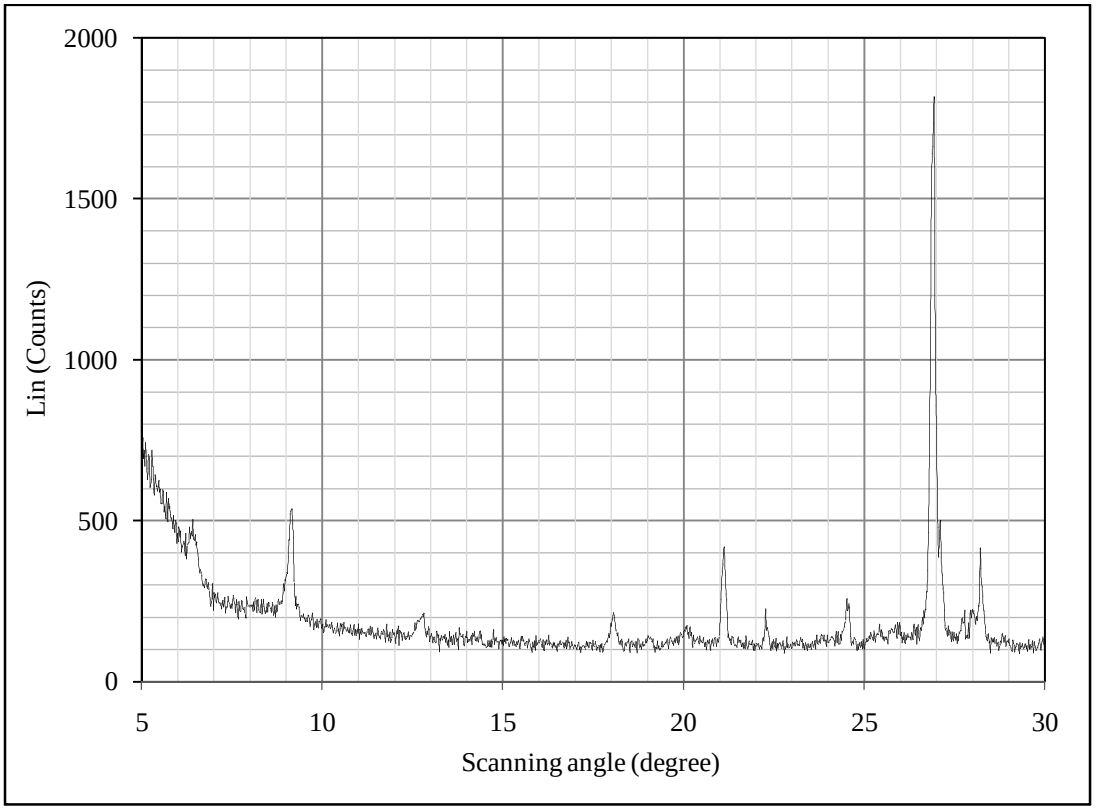

Fig. 4.3 Results of X-Ray Diffraction test for clay

Maximum dry density and optimum moisture content of clay-gravel and clay-sand-gravel mixtures were found out following the standard Proctor compaction test. The results obtained are shown in Fig. 4.4 and Fig. 4.5.

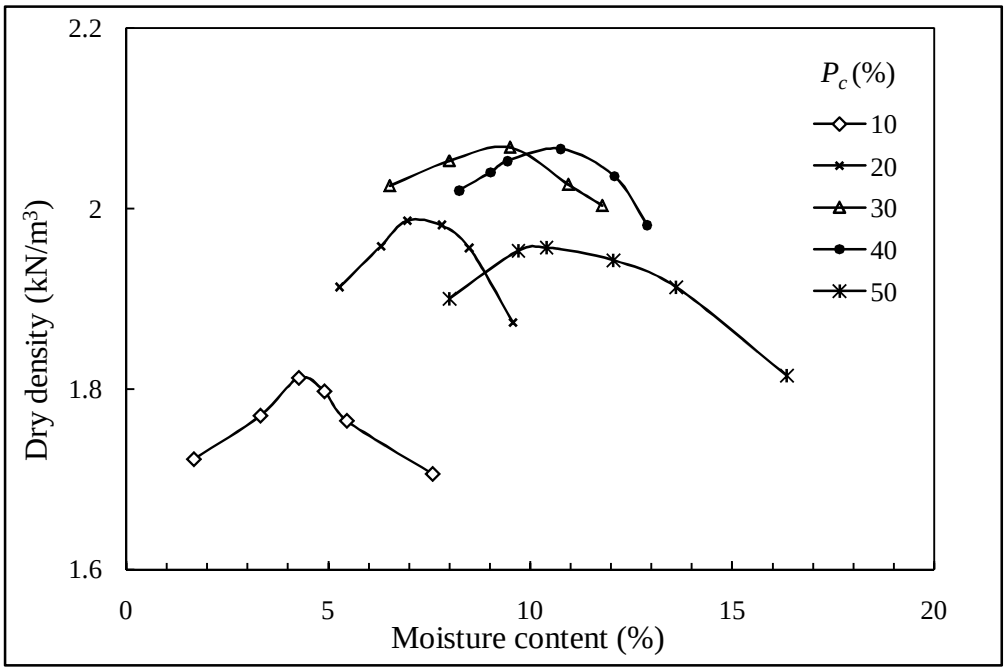

Fig. 4.4 Variation of dry density and optimum moisture content of clay-gravel mixtures for different clay percent by standard Proctor compaction method

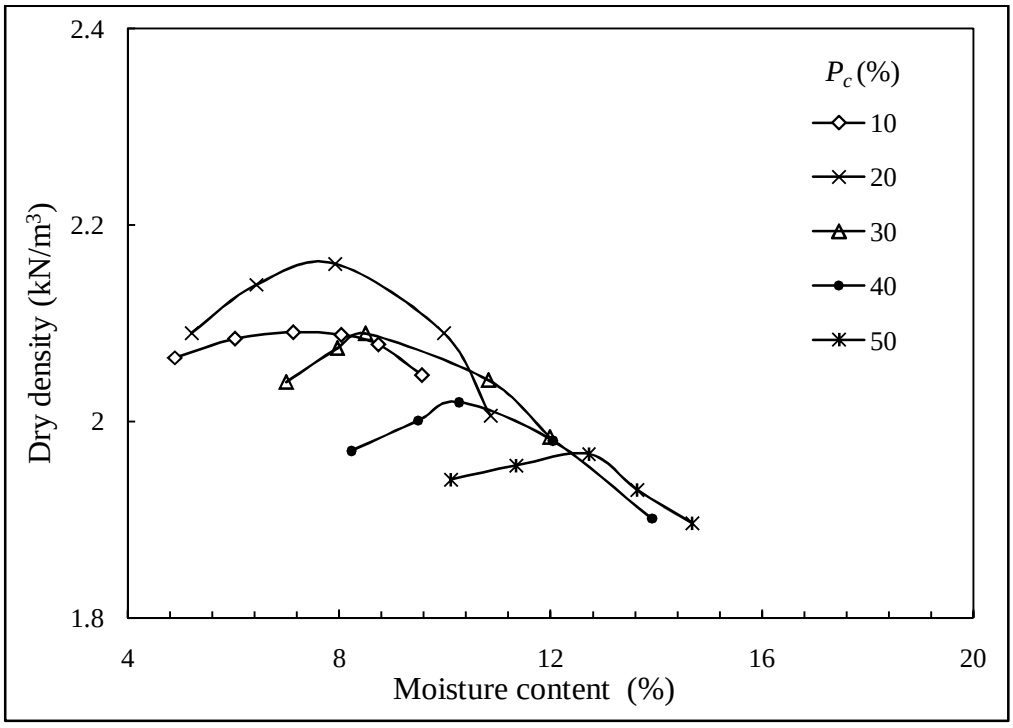

Fig. 4.5 Variation of dry density and optimum moisture content of clay-sand-gravel mixtures for different clay percent by standard Proctor compaction method

4.3 DETAILS OF EXPERIMENTAL SET UP

4.3.1 Flume

Extensive experiments were carried out in a fixed bed masonry flume. It was 25.0m long, 1.0m wide and 0.35m deep. The flume setup has a maximum discharging capacity of 120 l/s. The experiments were conducted on two bed slopes viz; 0.003 and 0.005. The slope of the flume was changed to 0.005 by pasting the cementing material from upstream to downstream of the flume. Flume had 4.0m long, 1.0m wide and 0.60m deep test section. The test section was at 12m downstream of the flume entrance. A constant flow rate was maintained into the flume with the aid of an over head tank. The mixture of cohesive sediment was filled into the test section up to the channel bed level. A layer of sediment being used in the respective experiment was pasted and leveled uniformly in order to create the roughness on the upstream of test section similar to that in the test section. The general view of the experimental setup is shown in Fig. 4.6.

Fig.4.6 Photographic view of the experimental flume

4.3.2 Slope and Discharge Measurement

The slope of the flume was measured with the help of two containers. These containers were connected at their bottom by a long plastic tube. They were positioned on the flume bed at predetermined distant locations along the length of the flume. Sufficient care was taken to remove the air bubbles from the connecting tube. The containers were allowed for sufficient time to equalize water levels in them. The water levels in both the containers were measured by means of a point gauge mounted on rails parallel to the bed surface. The water level difference between these two containers gave the vertical drop of flume for that length. The surveyor's level was also used to cross check the slope of the flume. Both the methods gave results very close to each other. However, slope measured with the former procedure has been adopted for computation purposes. Discharge in the flume was measured by a sharp crested weir installed at the downstream end of the flume. The tail gate provided at downstream end of the flume was used to regulate the depth of flow in it.

4.3.3 Preparation of Cohesive Sediment Bed

Firstly, the clay obtained from the field was dried in the sunlight. It was then ground to convert into powder form. This powder clay was used in the preparation of cohesive sediment mixture. Its proportion was varied from 10% to 50% by weight. Accurately weighed clay powder, sand and gravel were mixed thoroughly. Water was then added into this mixture. It was again mixed uniformly. The prepared mixture was left covered with a polythene sheet for 24 hours. It was done to achieve uniform distribution of moisture throughout the sediment mixture. The sediment mixture was again mixed thoroughly prior to placing it into the test section. The spur dike was then fitted in the groove (provided in the side wall of the flume) prior to filling of sediment into the test section of the flume. The test section was filled with the prepared cohesive sediment mixture. Sediment mixture in the test section was compacted by the dynamic compaction method. The dynamic compaction method was successfully applied by Hanson (1990), Robinson and Hanson (1995), Hanson and Hunt (2006), Kothyari and Jain (2008), Jain and Kothyari (2009) and Kothyari et al. (2014).

The filled sediment mixture was compacted in three different layers of 0.10m thickness each. These layers were compacted with the help of a cylindrical roller of

0.63m length and 0.23m diameter (Fig. 4.7,a). The dead weight of cylindrical roller was 100N and it can be raised up to 200N by filling the water inside it. A wooden rammer was used to compact the sediments at the sides of the channel and area near by spur dike. The rammer was 0.40m long, 0.10m wide and 0.07m thick (Fig. 4.7,b). The previous (existing) layer was made rough using trowel before laying next layer over it to provide proper bonding between the consecutive layers. A sharp edge trowel was used to remove (trim off) additional sediment from the bed. The trimmed bed surface was then smoothened using the wooden template starting from beginning to the end of the test section. The final thickness of sediment bed in the test section was 0.30m.

Upon completion of bed preparation, the samples were taken from three locations for the measurement of bulk density, antecedent moisture content and unconfined compressive strength. The tests were carried out to ensure that placement and compaction of sediment mixture was uniform. The values of bulk density, antecedent moisture content and unconfined compressive strength were found to be alike at all three positions. Finally, the prepared bed of sediment mixture was saturated for 24 hours before the beginning of each experimental run.

Fig. 4.7 A view of compaction of the channel bed by (a) roller and (b) rammer

4.3.4 Spur Dikes

Three spur dikes with transverse length of 6.10cm, 8.90cm and 11.52cm were used in the partially submerged spur dike experiments. However, dike with 11.52cm transverse length was used in the submerged spur dike experiments. The height of the partially submerged spur dikes was 60cm in all cases. The spur dikes were made of 3mm thick metal sheet. In all the experiments, single spur dike was installed at 90^o angle to the direction of flow (Fig. 4.7). The spur dike was installed at 14m downstream to the flume entrance. A 3mm transparent perspex sheet was used to cover the area around the spur dike to prevent scour around spur dike before flow attains the predetermined hydraulic conditions.

4.3.5 Piers

Three sizes of cylindrical iron pipes of outer diameter 11.52cm, 8.9cm and 6.1cm were used in the experiments. All three sizes of piers were used in the case of cohesionless sediment while experiments with cohesive sediment mixtures were conducted with first two sizes of piers viz; 11.52cm and 8.9cm. The surfaces of the pipes were painted to give a smooth finish.

4. 4 MEASUREMENTS

4.4.1 Antecedent Moisture Content

For the measurement of the antecedent moisture content of the prepared bed, three samples were taken from different locations along the test section. These samples were brought to the lab. They were weighed accurately and kept in an oven at a temperature of 105^o for a period of 24 hours. Oven dried samples are again accurately weighed. The difference between the weight of the wet and dry samples gave the moisture content of the bed.

4.4.2 Measurements of Dry Density and Unconfined Compressive Strength

Following the Indian Standard Code (IS: 2720-Part XXIX, 1975), standard core cutter method was used to determine the bulk unit weight of the sediment. The values of measured antecedent moisture content and bulk density were used to calculate the dry

density of the sediment mixture. The computed value of the dry density was used to calculate the void ratio of the cohesive sediment bed.

For the determination of the unconfined compressive strength of the cohesive sediment bed, three cylindrical samples were taken from different locations along the compacted bed. These samples were tested in unconfined compression apparatus to determine the unconfined compressive strength of the bed as per Indian Standard Code (IS: 2720-Part X, 1991).

4.4.3 Flow and Scour Depths Measurements

The approaching flow depth and scour depth were measured by a vertical point (1.2m in length graduated to centimeters and millimeters) with flat bottom having an accuracy of 0.1mm. The flat bottom point gauge was used to avoid the penetration of gauge in the scoured bed while measuring the scour depth.

(a) (b)

Fig. 4.8(a-b) Measurement of unconfined compression strength of sediment mixture sample

4.4.4 Acoustic Doppler Velocimeter

Numerous intrusive and non-intrusive techniques and instruments have been developed to study the flow pattern/ turbulent characteristics in an open channel flow. Out of that, one type is point or probe measurement in which a sensing instrument is inserted into the flow to measure the flow properties. Reddy et al. (2012) used Particle Image Velocimetry (PIV) for turbulence analysis of flow. Another such instrument is the

Acoustic Doppler Velocimeter (ADV). Vectrino^{+} Acoustics Doppler velocimeter (ADV) manufactured by NORTEK, Denmark was used to measure the instantaneous velocities. As the name itself suggests, it is based on the Doppler shift principal. ADV records very accurate three dimensional instantaneous velocities (Kraus et al., 1994). The ADV has one sound emitter transducer and four receiving transducers. The ADV measures the velocity within a sampling volume of approximately 0.09cm^3 located 5cm away from the sensing elements. Owing to this instrumental constraint, the velocity of the top 5cm flow depth was not measured. The sound emitter generates an acoustic signal that is reflected back by sound-scattering particles present in the water, which are assumed to move with the same velocity as of water. The scattered sound signal is detected by the receivers and the flow velocity in three directions is calculated.

The evaluation of ADV for its utility in turbulence analysis showed that ADV can measure the velocity and Reynolds shear stress within ±1% accuracy of estimated true value (Voulgaris and Trowbridge, 1998). Ali and Lim (1986) and Liriano and Day (2000) studied the velocity inside a scour hole using ADV. Dey and Raikar (2007) studied flow through loose gravel bed with ADV. Kumar et al. (2011) studied the flow pattern in the scour hole and in the wake region using ADV. Based on the literature and wide acceptance of ADV, it has been selected for the turbulence analysis in this study. The measurements were taken at any particular point for long durations to ensure that observations become stationary. The instantaneous three-dimensional velocities were measured around the spur dike. Figure 4.9 shows the measurement of data using ADV.

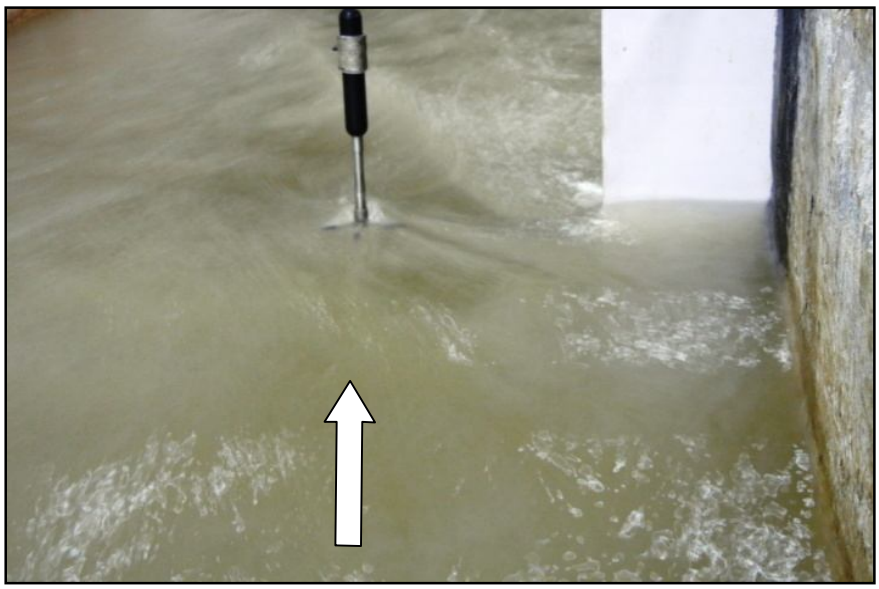

Fig.4.9 Data measurement by Vectrino^{+} ADV

4.5 EXPERIMENTAL PROCEDURE

Experiments are conducted in two series, first to measure the depth of scour in cohesionless and cohesive sediments and second to measure the flow pattern around the spur dikes (partially submerged and submerged) using ADV.

4.5.1 Spur Dike Scour

Before the start of an experimental run, a single spur dike (partially submerged or submerged) was installed 14m downstream of the flume entrance in the groove provided in the side wall of the flume. Spur dike was at 90° angle to the direction of flow. The channel bed with cohesive sediment mixtures was prepared by following the steps explained in section 4.3.3. The area around the spur dike was covered with 3mm thick transparent perspex sheet (Fig. 4.10) in order to prevent any scouring before the flow attains the predetermined flow conditions. Initially, the flume was filled with water at a very low rate. When required flow depth and discharge were achieved in the flume, the perspex sheet was taken out very cautiously ensuring that no scouring takes place during removal of the sheet. The depth of scour was measured at various time intervals.

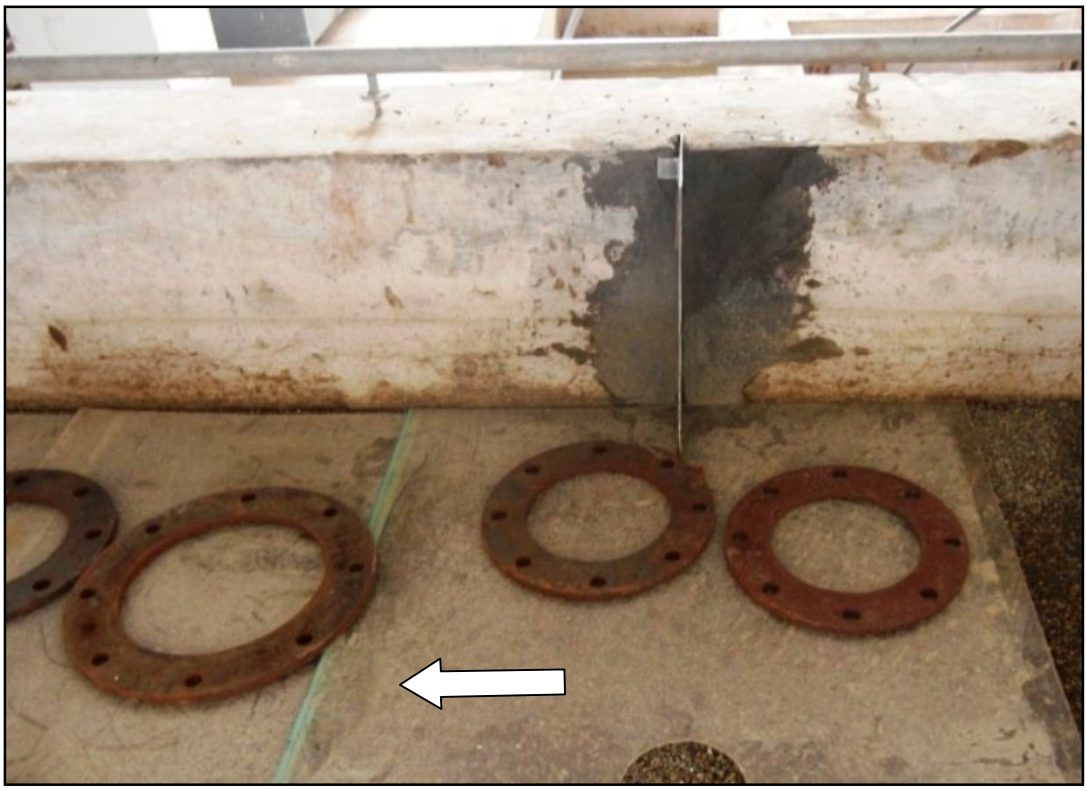

Fig 4.10 Covering nearby area around spur dike by a transparent perspex sheet prior to start of an experimental run

4.5.1.1 Scour around partially submerged spur dike in cohesionless sediments

A total of six experimental runs were carried out in cohesionless sediments (i) gravel (ii) mixture of sand and gravel (in equal proportion by weight). Three partially submerged spur dikes, each of 0.061m, 0.089m and 0.1152m transverse length and 0.60m in height were selected for the experiments. The sediment bed was leveled prior to running the each experiment. All experiments were conducted under clear water condition for a period of 18-20 hours or till equilibrium condition was reached. An equilibrium condition was supposed to achieve when the two consecutive scour depth of measurement were found to same or 1mm difference within 3-4 hours of measurements. The ranges of hydraulic parameters for these experiments are given in Table 4.2. Appendix- A shows the sediment and hydraulic details of the data of cohesionless sediments.

Table 4.2 Range of data for scour around partially submerged dike in cohesionless sediments

$d_a^{'}$ (mm)	h (m)	U_o (m/s)	S_o (-)	d_{une} (m)	d_{uje} (m)
1.47 – 2.70	0.112 - 0.125	0.41 – 0.55	0.003	0.073 – 0.180	0.073 – 0.197

Here, $d_a^{'}$ is the arithmetic mean size of cohesionless sediment (base sediment) and S_o is the bed slope of channel, h is the approaching flow depth, U_o is the approaching flow velocity, d_{une} is the equilibrium depth of scour at the nose of partially submerged spur dike in cohesionless sediments and d_{uje} is the equilibrium depth of scour at the junction of wall and partially submerged spur dike in cohesionless sediment.

4.5.1.2 Scour around spur dikes in cohesive sediments

A total of 40 experimental runs were conducted with spur dikes in cohesive sediment mixtures (30 experiments with partially submerged spur dike and 10 experiments with submerged spur dike). The runs were conducted using three different sizes of partially submerged spur dikes explained in section 4.5.1.1. In addition, a submerged spur dike of 0.1152m transverse length was also used in the experiments conducted on cohesive sediment mixtures. To quantify the influence of cohesion on the depth of scour around spur dike (partially submerged and submerged), the experiments were conducted in two series viz; (a) clay percentage varying from 10 to 50% was mixed with fine gravel by weight and (b) clay percentage varying from 10 to 50% was mixed

with equal proportion of fine sand and fine gravel by weight. The initial dry density and unconfined compressive strength were measured to quantify compaction of the prepared sediment bed.

All experiments were conducted for a period of 24-40 hours or till equilibrium condition was reached. The ranges of hydraulic parameters for partially submerged spur dike are given in Table 4.3 and Table 4.4 for clay-gravel and clay-sand-gravel mixture respectively. Appendix-B and Appendix-C show the sediment and hydraulic details of partially submerged dike embedded in clay-gravel mixtures and clay-sand-gravel mixtures respectively. The ranges of hydraulic parameters for submerged spur dike are given in Table 4.5 and Table 4.6 in case of clay-gravel and clay-sand-gravel mixtures respectively. Data on temporal variation of scour depth at nose (d_{cun}) and at the wake (d_{cuw}) of the partially submerged spur dike in clay-gravel and clay-sand-gravel sediment mixtures is given in Appendix-D.

Appendix-E shows the sediment and hydraulic details of submerged spur dike for the same. Data on temporal variation of scour depth at nose (d_{csn}) and at the wake (d_{csw}) of the submerged spur dike in clay-gravel and clay-sand-gravel sediment mixtures is given in Appendix-F. For documentation, the experimental runs of clay-gravel sediment mixtures were designated as D_pCG1.1, D_sCG3.3, PCG5.5 etc. Here, first character stands for type of structure i.e. partially submerged spur dike (D_p), submerged spur dike (D_s) and pier (P) etc., second character stands for clay (C), third character stands for gravel (G), the fourth character stands for clay percentage and fifth character (after decimal) stands for experiment number. Similarly the experimental runs of clay-sand-gravel mixtures were designated as D_pCSG1.1, D_sCSG4.2, PCSG5.5 etc. Here, SG stands for sand-gravel and meaning of other characters remain same.

Table 4.3 Range of data on scour around partially submerged spur dike in cohesive sediments consisting of clay-gravel mixtures

P_c (%)	d_a (mm)	W (%)	γ_d (kN/m^3)	e (-)	UCS (kN/m^2)	h (m)	U_o (m/s)	S_o (-)	d_{cune} (m)	d_{cuwe} (m)
10-50	1.357-2.431	5.59-17.51	13.22-18.26	0.42-0.92	0.0-16.76	0.072-0.122	0.578-1.222	0.003-0.005	0.0-0.149	0.017-0.128

Here, d_{cune} and d_{cuwe} is an equilibrium depth of scour in cohesive sediment mixtures at nose and at the wake of the partially submerged spur dike respectively.

Table 4.4 Range of data on scour around partially submerged spur dike in cohesive sediments consisting of clay-sand-gravel mixtures

P_c (%)	d_a (mm)	W (%)	γ_d (kN/m^3)	e (-)	UCS (kN/m^2)	h (m)	U_o (m/s)	S_o (-)	d_{cune} (m)	d_{cuwe} (m)
10-50	0.742-1.324	8.46-13.70	17.29-19.11	0.37-0.55	0.0-53.53	0.071-0.135	0.504-1.201	0.003-0.005	0.0-0.150	0.005-0.148

Table 4.5 Range of data on scour around submerged spur dike in cohesive sediments consisting of clay-gravel mixtures

P_c (%)	d_a (mm)	W (%)	γ_d (kN/m^3)	e (-)	UCS (kN/m^2)	h (m)	U_o (m/s)	S_o (-)	d_{csne} (m)	d_{cswe} (m)
10-50	1.357-2.431	5.57-16.80	13.98-20.54	0.27-0.86	0.0-15.14	0.077-0.125	0.555-0.142	0.003-0.005	0.010-0.120	0.036-0.109

Here d_{csne} and d_{cswe} is equilibrium depth of scour in cohesive sediment mixtures at nose and at the wake of the submerged spur dike respectively.

Table 4.6 Range of data on scour around submerged spur dike in cohesive sediments consisting of clay-sand-gravel mixtures

P_c (%)	d_a (mm)	W (%)	γ_d (kN/m^3)	e (-)	UCS (kN/m^2)	h (m)	U_o (m/s)	S_o (-)	d_{csne} (m)	d_{cswe} (m)
10-50	0.742-1.324	8.58-13.92	17.17-18.91	0.37-0.51	0.0-54.61	0.084-0.130	0.489-1.105	0.003-0.005	0.003-0.120	0.026-0.132

4.5.2 Pier Scour

4.5.2.1 Pier scour in cohesionless sediments

Similarly, total six experimental runs were conducted in cohesionless sediments in case of pier in (i) gravel (ii) mixture of sand and gravel (in equal proportion by weight). The experimental runs were conducted using three different sizes of piers. The diameter of piers was 0.061m, 0.089m and 0.1152m. All piers were 0.60m high. A series of experimental runs started with three runs on gravel bed, followed by three runs on bed

composed of equal proportion of sand and gravel. The pier was installed 14m downstream of the flume entrance. All experiments were conducted following the procedure as explained in section 4.5.1. The ranges of hydraulic parameters for these experiments are given in Table 4.7. Appendix-G shows the sediment and hydraulic details of the experimental runs on cohesionless sediments. In cohesionless sediments, the maximum depth of scour was observed at the nose of the pier.

Fig 4.11 Covering nearby area around pier by a transparent perspex sheet prior to start of an experimental run

Table 4.7 Range of data for scour around pier in cohesionless sediments

$d_a^{'}$ (mm)	h (m)	U_o (m/s)	S_o (-)	d_{pne} (m)
1.47 – 2.70	0.112 - 0.125	0.386 – 0.55	0.003	0.048 – 0.166

Here, d_{pne} is an equilibrium depth of scour at the nose of pier in cohesionless sediments.

4.5.2.2 Pier scours in cohesive sediment mixtures

A total of 20 experimental runs were conducted in cohesive sediment mixtures on pier scour. The runs were conducted using two piers of 0.089m and 0.1152m in diameter.

An approach similar to that followed for the quantification of the influence of cohesion on scouring around spur dike was also followed for pier scour.

The ranges of data considered in the experimental investigation are given in Table 4.8 and Table 4.9 for clay-gravel mixtures and clay-sand-gravel mixtures respectively. Appendix-H shows the sediment and hydraulic parameters of cohesive sediments consisting of clay-gravel mixtures collected in the present study, whereas Appendix-I shows the same for cohesive sediments consisting of clay-sand-gravel mixtures. Data on temporal variation of scour depth at sides (d_{cps}) and at the wake (d_{cpw}) of the pier in clay-gravel and clay-sand-gravel sediment mixtures is given in Appendix-J.

Table 4.8 Range of data on scour around bridge pier in cohesive sediments consisting of clay-gravel mixtures

P_c (%)	d_a (mm)	W (%)	γ_d (kN/m^3)	e (-)	UCS (kN/m^2)	h (m)	U_o (m/s)	S_o (-)	d_{cps} (m)	d_{cpw} (m)
10-50	1.357-2.431	5.46-17.36	12.76-18.10	0.44-1.04	0.0-16.11	0.087-0.125	0.573-1.011	0.003-0.005	0.029-0.124	0.013-0.083

Here, d_{cps} and d_{cpw} is an equilibrium depth of scour at side and at the wake of the pier in cohesive sediments mixture bed.

Table 4.9 Range of data on scour around bridge pier in cohesive sediments consisting of clay-sand-gravel mixtures

P_c (%)	d_a (mm)	W (%)	γ_d (kN/m^3)	e (-)	UCS (kN/m^2)	h (m)	U_o (m/s)	S_o (-)	d_{cps} (m)	d_{cpw} (m)
10-50	0.742-1.324	8.37-13.88	17.34-19.61	0.33-0.50	0.0-54.07	0.08-0.127	0.534-1.066	0.003-0.005	0.020-0.140	0.018-0.111

4.5.3 Flow Pattern around Spur Dikes

The study of the flow field, turbulence characteristics and Reynolds stresses were planned within the scour hole around the spur dike. A down looking 16MHz Vectrino$^+$ microADV was used to measure instantaneous velocities in the three spatial direction *x*, *y* and *z* at a sampling rate of 25Hz. In the data analysis, positive *x*- axis was along the flow

direction, the positive *y*- axis was across the left of flow and positive *z*- axis was vertically upward. The ADV measurements were taken in only two experimental runs; one with partially submerged spur dike and another with submerged spur dike embedded in clay-gravel sediment mixture (30% clay + 70% gravel).

Once equilibrium conditions were achieved, the flow was stopped and the bed was allowed for sufficient time to drain out the water. The dried scour hole was fixed by spraying the regin (instant adhesive) over it. After fixing of the scour hole, ADV measurements were taken at various cross sections as shown in Fig.4.12. The origin (0,0,0) is also shown in figure. In all, observations were taken at 68 locations in case of both runs (Fig. 4.12). At each measuring node 1,800 instantaneous three dimensional velocities were recorded. The lowest point of measurement was 5mm above the channel bed. Up to two centimeters from the bed, the measurements were made at 5mm interval, while the interval was kept 1cm in higher region.

The data collected from the ADV had the file extension ".vno". Using the Vectrino Plus software, the ".vno" files were converted to ".adv" files that were readable by the WinADV software. WinADV has the capacity of processing multiple files at a time. After the conversion, the raw data was filtered with using WinADV software by Phase-space threshold despiking method (Goring and Nikora, 2002) and communication errors were filter out. The measured velocities in the processed data file were used to calculate the following turbulence characteristics: (a) mean velocities in the longitudinal, transverse, and vertical directions denoted as u, v, w respectively; (b) Reynolds stresses, $-\rho u'v'$, $-\rho u'w'$, and $-\rho v'w'$ in which u', v' and w' are velocity fluctuations in longitudinal, transverse, and vertical directions, respectively.

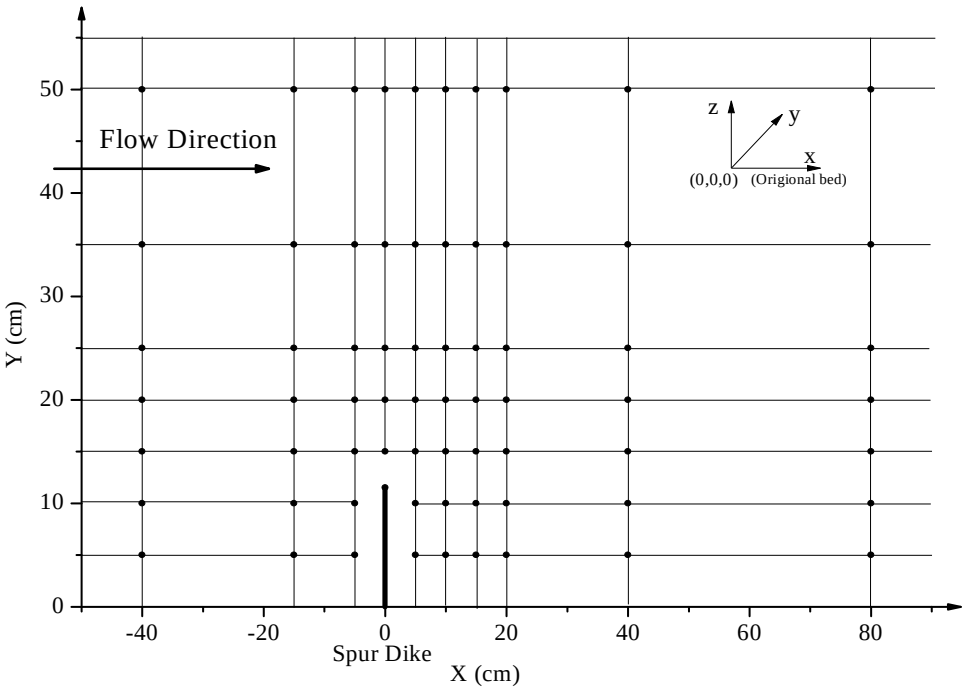

Fig. 4.12 Systematic plot of measuring grid

CHAPTER – V

ANALYSIS OF DATA, RESULTS AND DISCUSSIONS

5.1 GENERAL

Since, no data is available on scour around spur dikes (partially submerged and submerged) founded in cohesive sediment mixtures consisting of clay-gravel and clay-sand-gravel mixtures, the data collected during the present study only were analyzed and results obtained are discussed in this Chapter. The scour around bridge piers founded in cohesive sediment mixtures consisting of clay-gravel and clay-sand-gravel was carried out by Kumar (2011) only, but the clay used for the preparation of mixtures had very low plasticity index (*PI*= 6.16%). Therefore, few more experiments were carried out in the present study with clay having large plasticity index (*PI* = 21%). Based on the functional relationships derived in Chapter-III, new methods are proposed for the computation of maximum depth of scour around spur dikes and bridge piers embedded in cohesive sediment mixtures consisting of clay-gravel and clay-sand-gravel mixtures.

Using the method developed, a computational procedure was evolved to predict temporal variation of depth of scour in such cohesive sediment mixtures. The study of flow structure, turbulence characteristics and Reynolds stresses were done through the analysis of data recorded using ADV around the spur dikes after development of scour. In the present study partially submerged spur dike, fully submerged spur dike and bridge pier were used in the experiments.

Keeping the above discussion in view, the experimental results were divided into following sections:

5.2 Scour around partially submerged spur dike founded in cohesive sediment mixtures
5.3 Scour around submerged spur dike founded in cohesive sediment mixtures
5.4 Scour around bridge piers founded in cohesive sediment mixtures
5.5 Flow characteristics around partially submerged and submerged spur dikes

5.2 SCOUR AROUND PARTIALLY SUBMERGED SPUR DIKE FOUNDED IN COHESIVE SEDIMENT MIXTURES

In the present study, three different sizes of spur dikes, each having transverse length of 6.10cm, 8.90cm and 11.52cm were used for the experiments. All spur dikes were 60cm high. The spur dikes were made of 3mm thick metal sheet. In all the experiments, single spur dike was installed 14m downstream to the flume entrance at an angle of 90^o angle to the direction of flow. A 3mm transparent perspex sheet was used to cover the area around the spur dike to prevent scour around spur dike before the start of experiment. The flume was initially filled with water at very low rate. When required flow depth and discharge were achieved in the flume, the perspex sheet was taken out very cautiously ensuring that no scouring takes place around the spur dike during the removal of sheet. The temporal variation of scour depth was measured by point gauge having an accuracy of ± 0.1mm.

The ranges of different measured parameters and experimental conditions are presented in Appendix-B and Appendix-C for cohesive sediment bed composed of clay-gravel mixtures and clay-sand-gravel mixtures respectively.

5.2.1 Visual Observations

From the laboratory experiments of scouring around partially submerged spur dike founded in cohesionless sediment, it was observed that scouring started from the nose of the spur dike immediately after the beginning of each experimental run. The maximum depth of scour was observed at the junction of wall and spur dike in cohesionless sediment. Similar result was also obtained by Ballio et al. (2010). However, in case of cohesive sediment bed, the scouring started from the wake region of the spur dike as shown in Figs. 5.1(a) and 5.1(b). In cohesive sediment, the maximum depth of scour was observed at wake region of the spur dike.

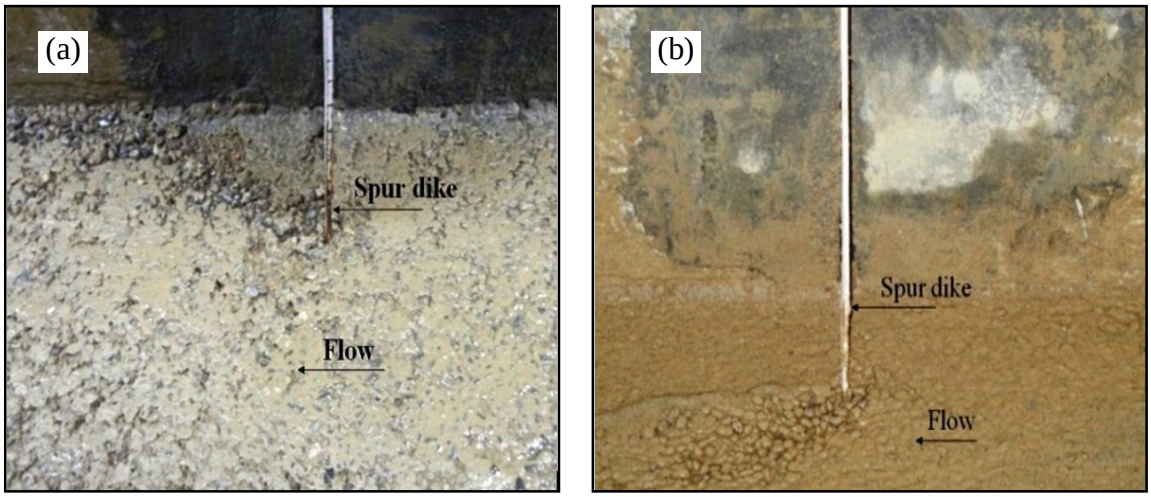

Fig. 5.1 Initiation of scour at partially submerged spur dike in cohesive sediment mixtures (a) 30% Clay + 70% Gravel and (b) 10% Clay + 45% Sand + 45% Gravel

No significant sediment deposition was observed in wake zone of the spur dike in the experiments conducted in cohesive sediment mixtures bed except experiments with 10% clay. It was contrary to experiments conducted on cohesionless sediment bed in which significant deposition was observed to occur at wake region of spur dike. The scour pattern around spur dike was more or less similar to cohesionless sediment at 10% clay content in clay-gravel mixture and $\leq 20\%$ in clay-sand-gravel mixture [See Figs. 5. 2(a) and 5.2(b)]. In such cases, significant scour occurred at upstream of spur dike as well. At 10% clay content, the depth of scour was greater at spur dike nose than that of its wake in both types of cohesive sediment mixtures.

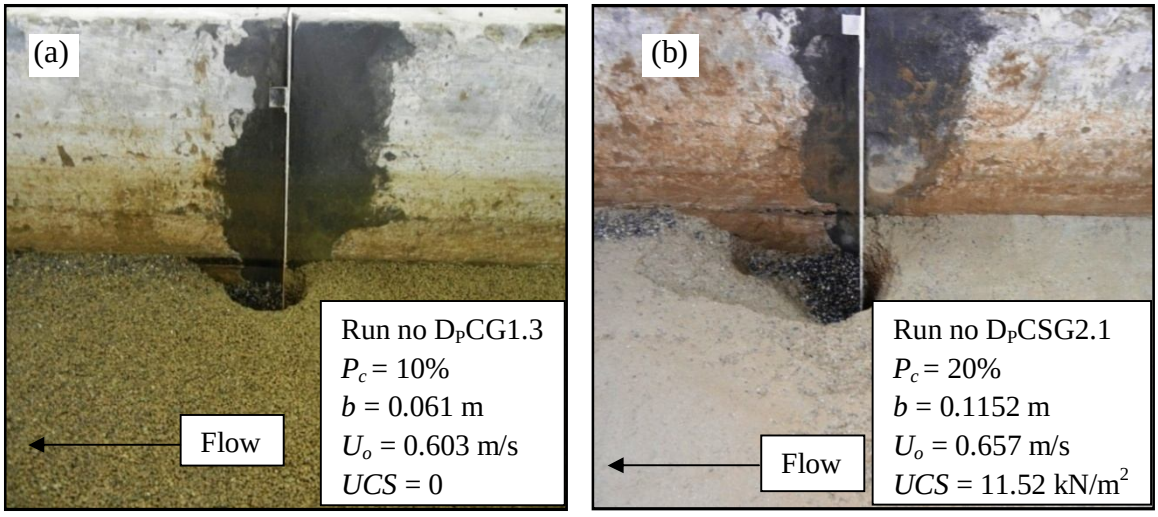

Fig. 5.2 Pattern of scour around partially submerged spur dike in cohesive sediment mixtures (a) 10% Clay + 90% Gravel and (b) 20% Clay + 40% Sand +40% Gravel

At clay content $\leq 20\%$ in cohesive sediment mixture, the scouring took place with removal of individual sediment particles. It was observed that the rate of sediment removal was faster at lower clay percentage in sediment bed as compared to higher clay content. At higher percentage of clay $(\geq 30\%)$ scouring started with removal of sediment in the form of flakes. Similar processes of sediment inception were observed in clay-sand mixture bed by Ansari et al. (2002). It was also observed in the case of detachment and transports of sediment from cohesive sediment bed containing clay-gravel and clay-sand-gravel (Jain and Kothyari 2009, 2010) and in the process of scour around pier (Kothyari et al., 2014). At clay content $\geq 30\%$, smaller scour depth occured at nose of spur dike than that of wake region in both types of cohesive sediment mixtures. Various shapes of scour hole were observed in the cases of different clay content presents in the sediment mixture bed. In case of 30% clay content in sediment bed, a deep vertical scour hole (almost cylinder) was observed at the end of experimental run [see Figs 5.3(a) and 5.3(b)]. The shape of scour hole changes with the augment of clay content in sediment bed. In case of clay content $\geq 40\%$ the depth of scour was observed to reduce. However, the areal extent of scour increased in the wake zone of spur dike as shown in Figs. 5.4(a) and 5.4(b). In case of some experimental runs conducted with the highest clay content $(= 50\%)$ and the smallest transverse length of spur dike, very less or negligible scour depth was noticed to occur at wake region of the spur dike (see Appendix-B and Appendix-C).

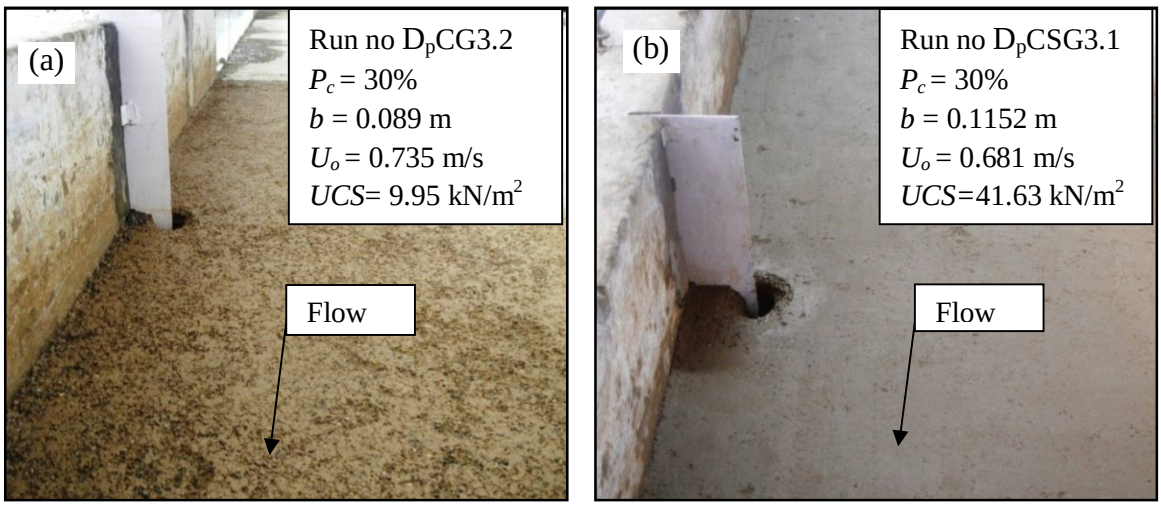

Fig. 5.3 Pattern of scour around partially submerged spur dike in cohesive sediment mixtures (a) 30% Clay + 70% Gravel and (b) 30% Clay + 35% Sand + 35% Gravel

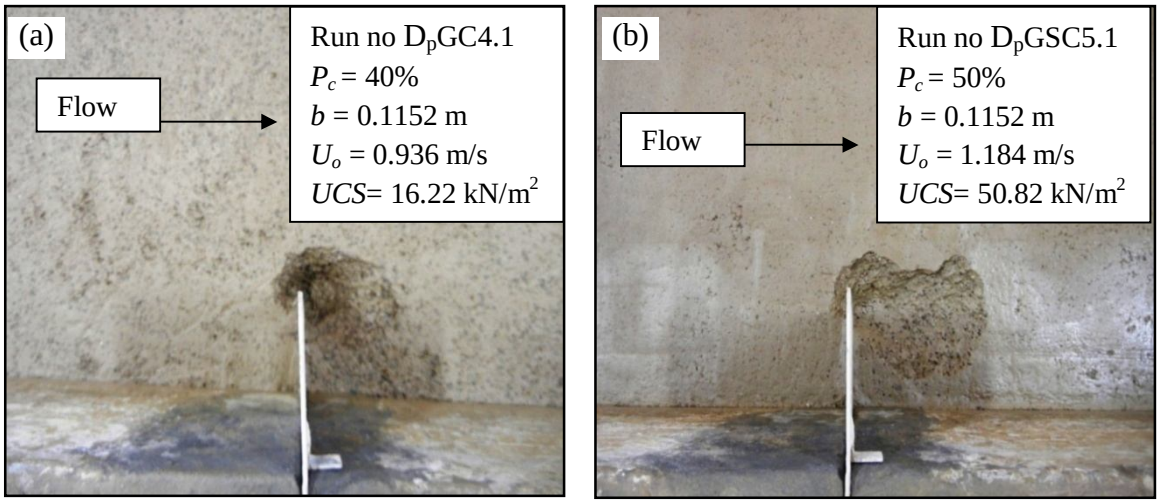

Fig. 5.4 Pattern of scour around partially submerged spur dike in cohesive sediment mixtures (a) 40% Clay + 60% Gravel and (b) 40% Clay + 30% Sand + 30% Gravel

In order to investigate the influence of clay percentage and unconfined compressive strength on the depth of scour at nose (d_{cun}) and at the wake of partially submerged spur dike (d_{cuw}), Figs. 5.5 to 5.8 were prepared. From these Figs. 5.5 and 5.6, it is evident that the maximum scour depth reduced with an augment of clay fraction in cohesive sediment mixtures. Similarly, the scour depth also decreased with an enhancement in unconfined compressive strength of the mixtures of cohesive sediment (Figs. 5.7 and 5.8). Kothyari et al. (2014) also identified the clay percentage and unconfined compressive strength as main parameters to affect scour depth in pier wake zone in mixtures of cohesive sediment composed of clay-gravel and clay-sand-gravel. Jain and Kothyari (2009, 2010) also quantified clay percentage and unconfined compressive strength of the cohesive sediment mixture to act as controlling parameter to affect the transport rate of bed load and suspended load composed of clay-gravel and clay-sand-gravel.

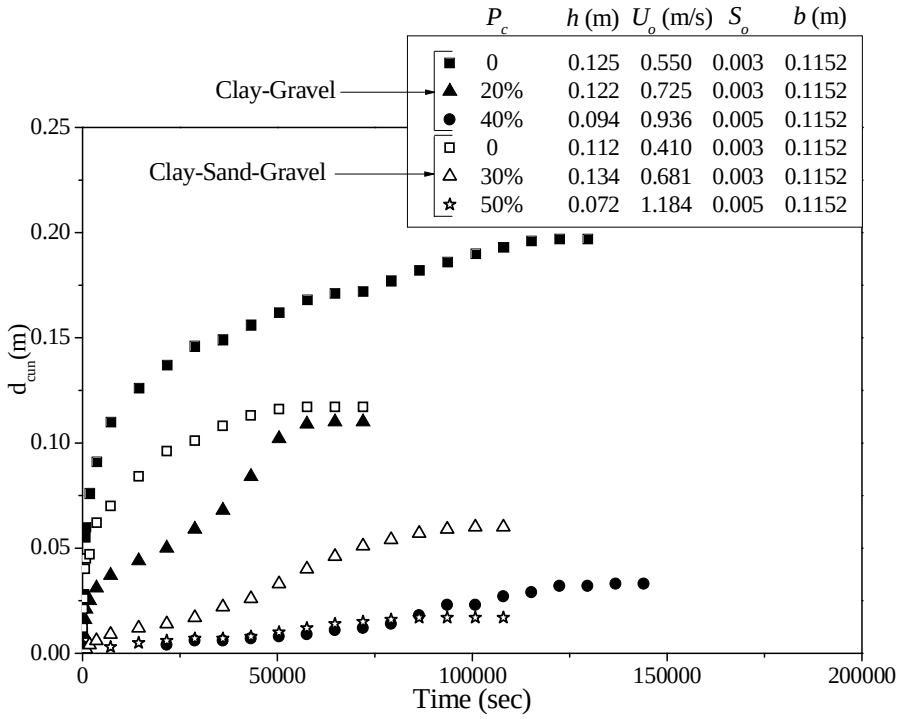

Fig. 5.5 Variation of scour depth with time at nose of the partially submerged spur dike for various clay percentages in clay-gravel and clay-sand-gravel mixtures

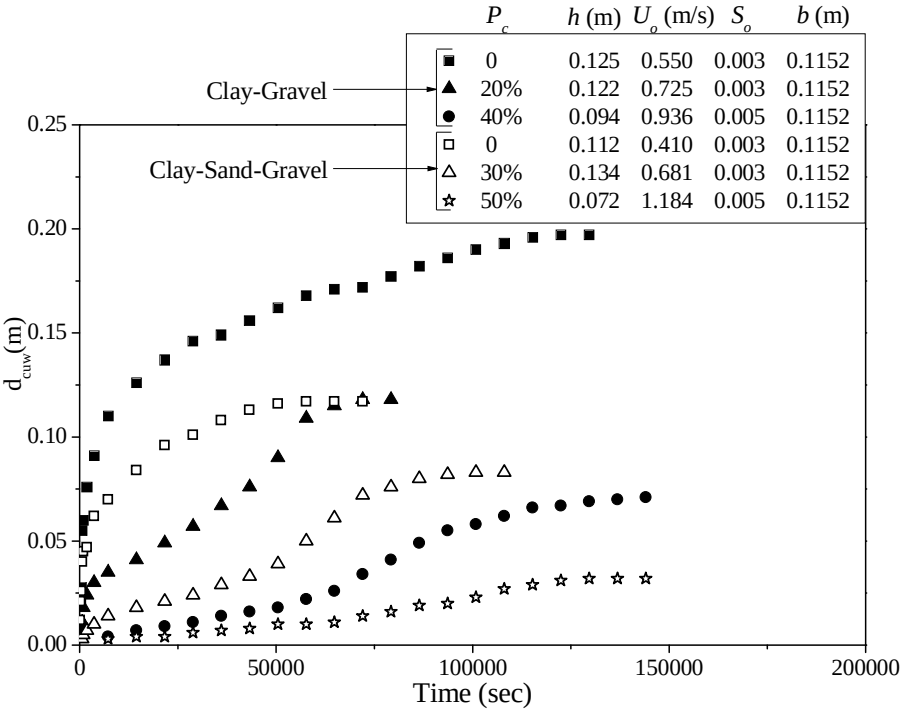

Fig. 5.6 Variation of scour depth with time at the wake of the partially submerged spur dike for various clay percentages in clay-gravel and clay-sand-gravel mixtures

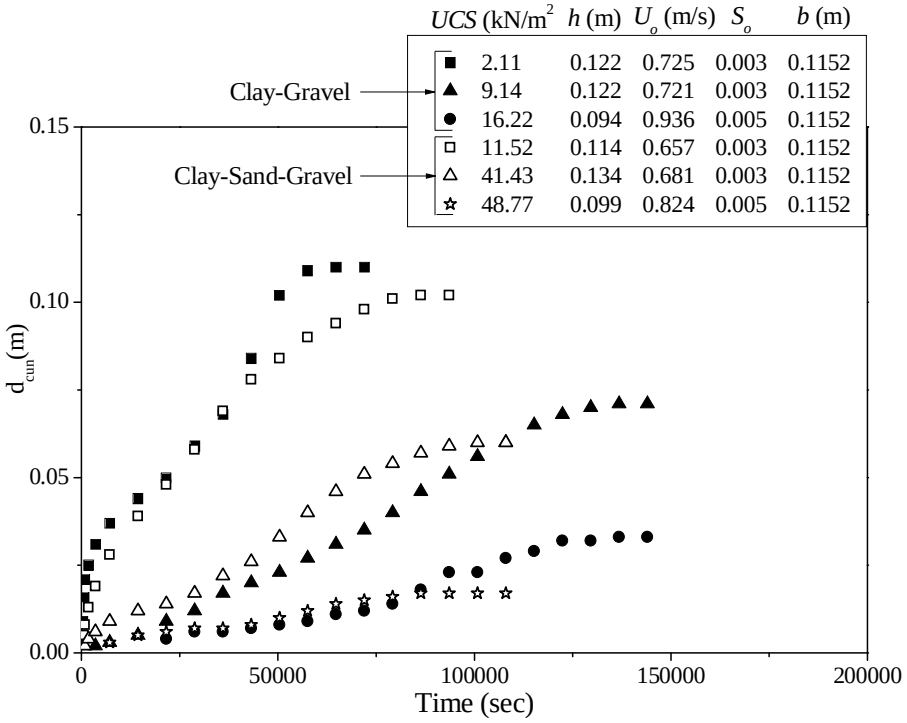

Fig. 5.7 Variation of scour depth with time at nose of the partially submerged spur dike for various clay unconfined compressive strength of clay-gravel mixtures

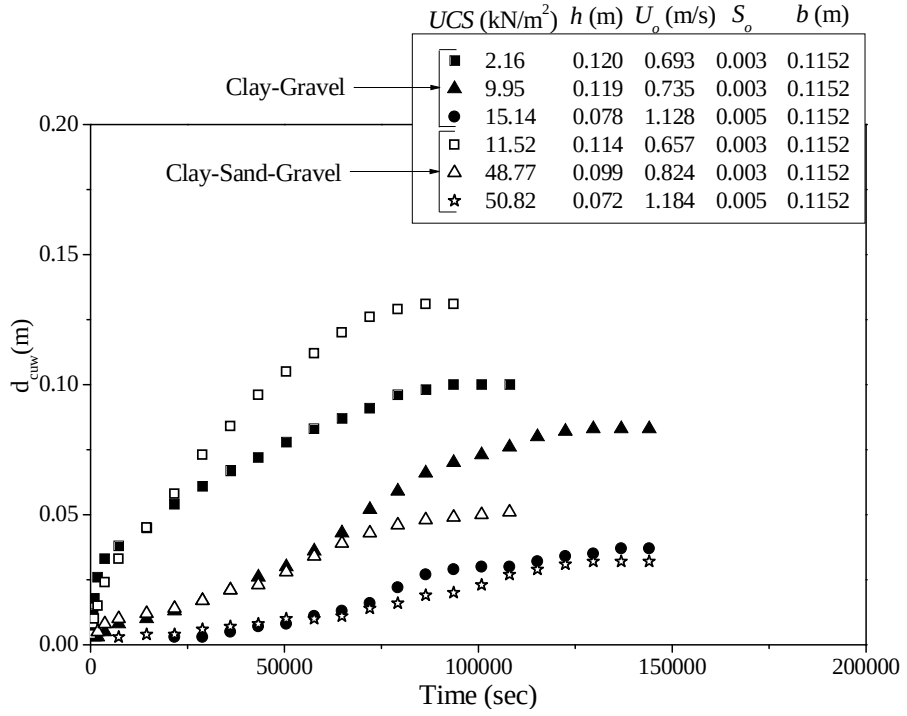

Fig. 5.8 Variation of scour depth with time at the wake of the partially submerged spur wake for various unconfined compressive strength of clay-sand-gravel mixtures

5.2.2 Depth of Scour at Nose and at the Wake of the Partially Submerged Spur Dike in Cohesive Sediment Mixtures

In this section, the effect of cohesive parameters on scour depth around partially submerged dike is analyzed and discussed.

Figures 5.9 and 5.10 present the variation of dimensionless scour depth with time at nose and at the wake of the spur dike for different clay percentage present in sediment bed composed of clay-gravel and clay-sand-gravel. In these figures d_{cun} and d_{cuw} are observed depth of scour at nose and at the wake of spur dike in cohesive sediment mixtures respectively. Very small depth of scour (<1cm) was observed at nose of the spur dike in clay-sand-gravel mixture containing clay $\geq 40\%$ (Appendix- C), hence, these data were dropped from the analysis (Fig. 5.10). The depth of scour was observed to be much smaller in the case of cohesive sediments mixture as compared to same sized (non-uniform) cohesionless sediment. Figures 5.9 and 5.10 show that depth of scour in mixtures of cohesive sediment was considerably different due to the presence of clay in the mixture. However, an organized variation of scour depth with clay percentage present among the mentioned data can be noted from the figures. It is also clear from these figures that the scour depth reduced drastically with an augment of clay percentage in sediment bed.

In order to identify the influence of shear strength of cohesive sediment mixtures on scour depth at nose and at the wake of the partially submerged spur dike, the variation of dimensionless depth of scour with unconfined compressive strength was studied (Figures 5.11 and 5.12). The entire data was classified into three ranges of unconfined compressive strength in the case of both mixtures. It is clearly observed form the figures that the capability to resist the scour in cohesive sediment mixtures enhanced with the augment in unconfined compressive strength. Hence, the scour depth reduced with an augment of unconfined compressive strength of sediment bed. Several investigators such as Robinson and Hanson (1995), Kothyari and Jain (2008), Jain and Kothyari (2009, 2010) and Kothyari et al. (2014) recognized unconfined compressive strength as strength parameter in case of the mixtures of cohesive sediment beds.

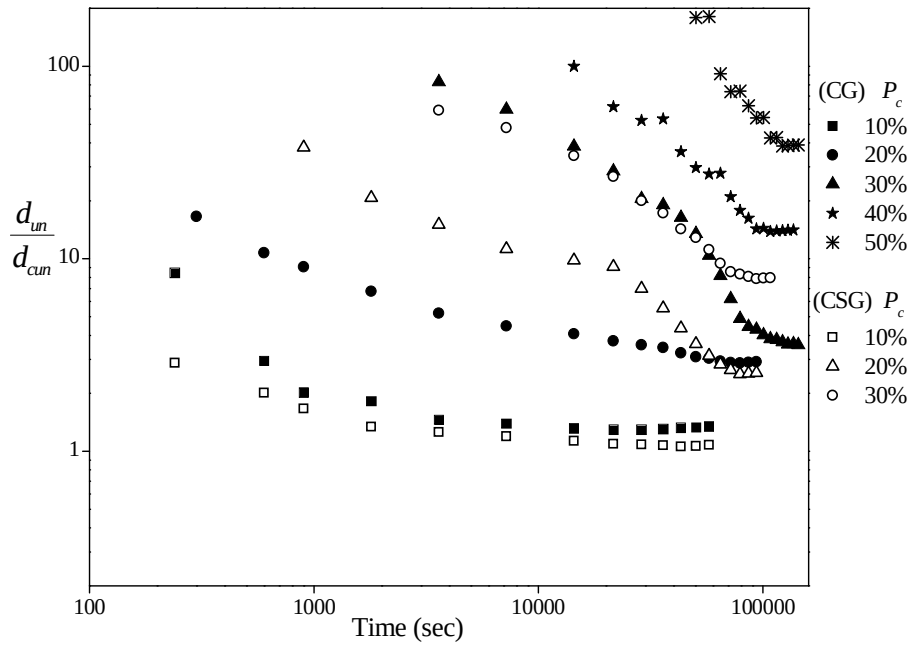

Fig. 5.9 Temporal variation of dimensionless scour depth with clay percentage at nose of the partially submerged spur dike in clay-gravel (CG) and clay-sand-gravel (CSG) mixtures

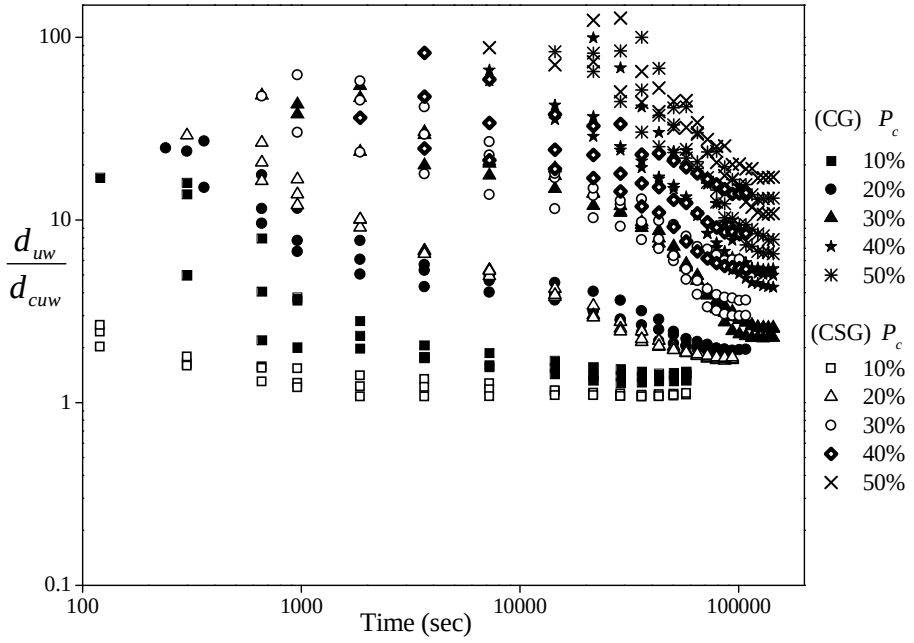

Fig. 5.10 Temporal variation of dimensionless scour depth with clay percentage at the wake of the partially submerged spur dike in clay-gravel (CG) and clay-sand-gravel (CSG) mixtures

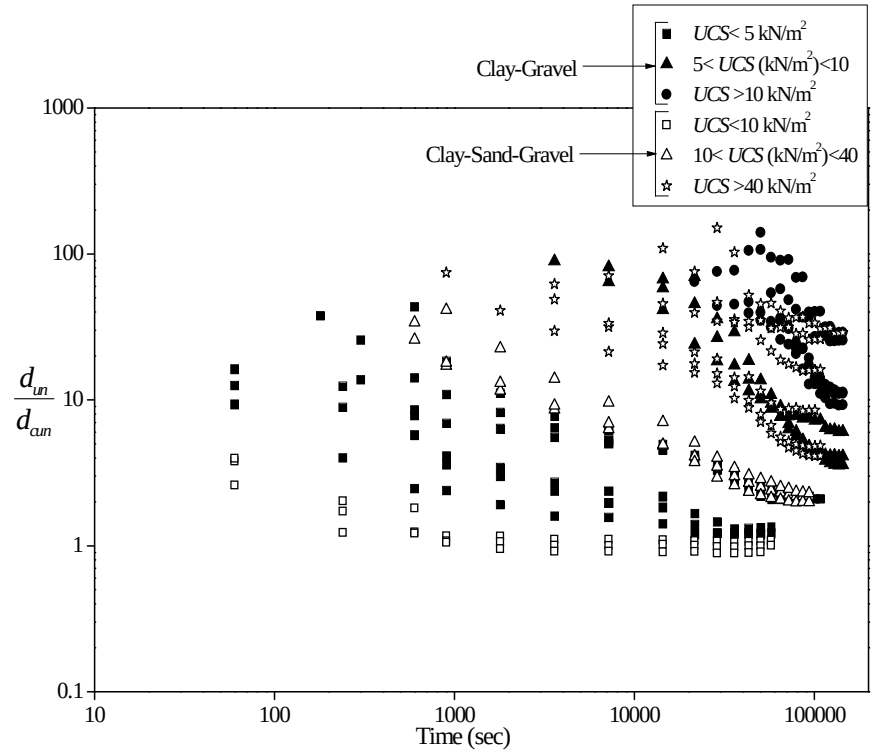

Fig. 5.11 Temporal variation of dimensionless scour depth with *UCS* at nose of the partially submerged spur dike in clay-gravel (CG) and clay-sand-gravel (CSG) mixtures

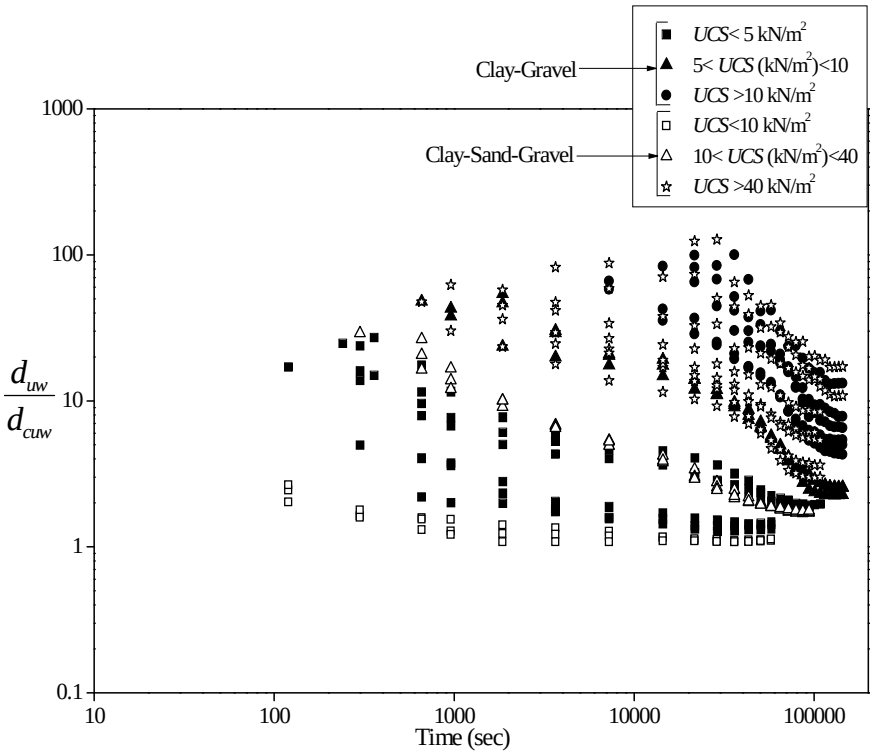

Fig. 5.12 Temporal variation of dimensionless scour depth with *UCS* at the wake of the partially submerged spur dike in clay-gravel (CG) and clay-sand-gravel (CSG) mixtures

The functional relationships for the computation of depth of scour at nose and at the wake of partially submerged spur dike in clay-gravel and clay-sand-gravel mixtures were derived in Chapter- III, which is rewritten here as

$$\frac{d_{cu(n/w)}}{d_{u(n/w)}} = f\left(P_c, \frac{C_*}{\phi_*}, \frac{\gamma_d}{\gamma_w}, UCS_*, t_*\right) \tag{5.1}$$

From Appendix-B and Appendix-C, the range of (γ_d/γ_w) is from 1.34 to 1.94 for the data collected in this study. The analysis of variable (γ_d/γ_w) with scour depth showed that variation (γ_d/γ_w) in this small range could not completely elucidate the variation in scour depth. Therefore, this variable was eliminated from further analysis and new functional relationship can be considered as:

$$\frac{d_{cu(n/w)}}{d_{u(n/w)}} = f\left(P_c, \frac{C_*}{\phi_*}, UCS_*, t_*\right) \tag{5.2}$$

The functional form given in Eq. (5.2) was used to compute the scour depth around partially submerged spur dike in mixture of clay-gravel and clay-sand-gravel. The value of $d_{u(n/w)}$ in the Eq. (5.2) may be obtained by using proper relationship for scour depth at nose or at the wake of partially submerged spur dike in cohesionless uniform and non-uniform sediments as the case may be. In the present study, the relationship suggested by Kothyari et al. (2007) was used for the calculation of scour depth around spur dike in uniform and non-uniform cohesionless sediments.

Other parameters such as vane shear strength and plasticity index were used by Ansari et al. (2002) and, Debnath and Chaudhuri (2010a) as strength parameters for cohesive sediments. Due to presence of gravel in cohesive sediment mixtures in present study, it was difficult to calculate plasticity index (Kothyari and Jain 2008) while vane shear strength was used only in case of soft clayey soils (Kothyari et al. 2014). However, Abou-seida et al. (2012) observed that Froude number, clay content, compaction and liquidity index were the parameters which affected the scour around abutment in clayey soil.

The variation of scour depth with C_*/ϕ_* did not show noteworthy influence on scour depth. A similar result was also observed by Kothyari et al. (2014). Therefore, the

variable C_*/ϕ_* was removed from the further analysis and then Eq. (5.2) can be re-written for computation of scour depth at nose and at the wake of the partially submerged spur dike as:

$$\frac{d_{cu(n/w)}}{d_{u(n/w)}} = f[(P_c),(1+UCS_*),t_*] \tag{5.3}$$

Above relation is applicable to cohesive sediment mixture only. It is important to make use of the variable $(1+UCS_*)$ in place of UCS_* so that Eq. (5.3) is suitable when $UCS = 0$. Analysis of the presently collected data revealed that dimensionless scour depth is inversely proportional to $(1+UCS_*)$ for both sediment mixtures as shown in Fig 5.13 and Fig. 5.14.

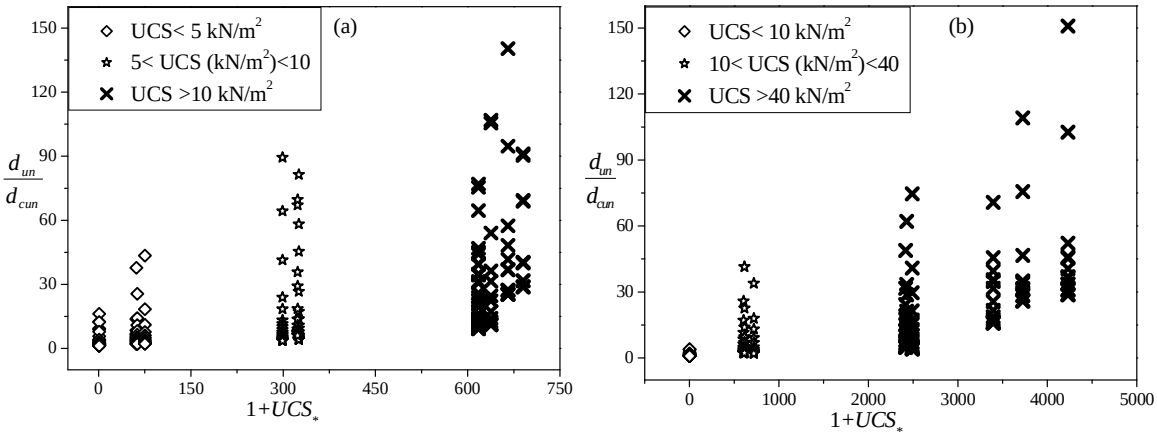

Fig. 5.13 Variation of dimensionless scour depth with $(1+UCS_*)$ at nose of partially submerged spur dike in (a) clay-gravel and (b) clay-sand-gravel mixtures

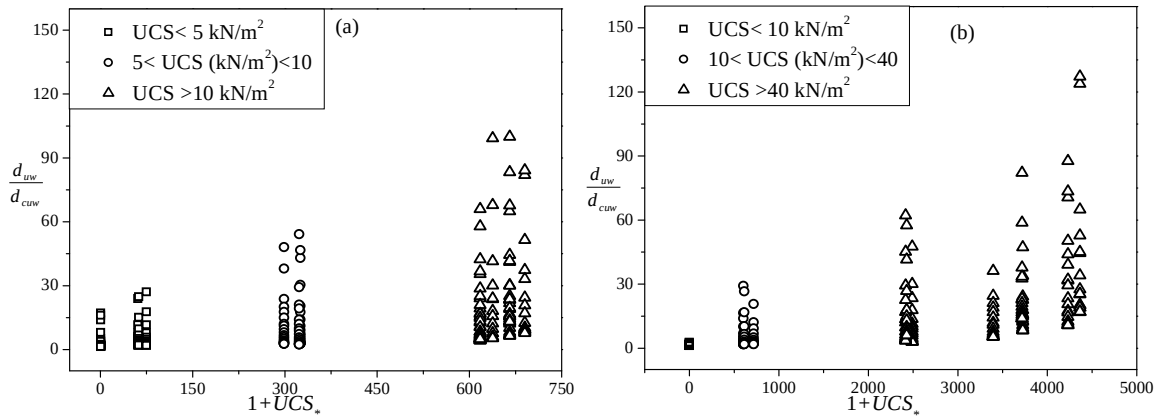

Fig. 5.14 Variation of dimensionless scour depth with $(1+UCS_*)$ at the wake of partially submerged spur dike in (a) clay-gravel and (b) clay-sand-gravel mixtures

The scour depth reduces drastically as clay content in sediment mixture goes beyond 20 % as evident from Figs. 5.9 to 5.10. Therefore, whole data have been analyzed in two ranges of clay percentages to incorporate this effect into analysis. However, scour depth can be considered as a continuous function of clay but accuracy of estimation decreases due to above fact. Debnath and Chaudhuri (2010, a) also proposed various relationships based on various clay contents in sediment bed to estimate scour depth around pier in clay-sand mixtures. Kothyari et al. (2014) also proposed relationships in two ranges of clay to estimate the scour depth in wake zone of pier founded in cohesive sediment mixtures.

Multiple nonlinear regression analysis was used to find out relationship for scour depth at nose and at the wake of partially submerged spur dike using all pertinent dimensionless parameters. Following relationships were obtained for describing the variation of $d_{cu(n/w)}$.

For depth of scour at nose of partially submerged spur dike in clay-gravel and clay-sand-gravel mixtures

$$\frac{d_{cun}}{d_{un}} = F_{un} \tag{5.4}$$

Where, F_{un} = parameter that represents cohesion of clay-gravel and clay-sand-gravel mixtures at nose of the partially submerged spur dike and is expressed as

$$F_{un} = a_o\left[(5\mathrm{P_c})^{a_1}(1+0.001UCS_*)^{a_2}(t_*)^{a_3}\right] \tag{5.4a}$$

With

$a_o = 0.00144\,; a_1 = -1.82; a_2 = -0.705; a_3 = 0.335$ for $10\% \le P_c \le 20\%$

(Adjusted R^2= 0.798)

and

$a_o = 1.25 \times 10^{-6}; a_1 = -4.75; a_2 = -0.25; a_3 = 0.786$ for $30\% \le P_c \le 50\%$

(Adjusted R^2= 0.837)

For depth of scour at the wake of the partially submerged spur dike in clay-gravel and clay-sand-gravel mixtures

$$\frac{d_{cuw}}{d_{uw}} = F_{uw} \tag{5.5}$$

Where, F_{uw}= parameter that represents cohesion of clay-gravel and clay-sand-gravel mixtures at the wake of the partially submerged spur dike and is expressed as

$$F_{uw} = c_o\left[(5P_c)^{c_1}(1+0.01UCS_*)^{c_2}(t_*)^{c_3}\right] \quad (5.5a)$$

With

$c_o = 0.00195; c_1 = -1.525; c_2 = -0.1067; c_3 = 0.324$ for $10\% \le P_c \le 20\%$

(Adjusted R^2= 0.785)

and

$c_o = 2.96\times10^{-5}; c_1 = -3.633; c_2 = -0.306; c_3 = 0.638$ for $30\% \le P_c \le 50\%$

(Adjusted R^2= 0.792)

The comparison between observed depth of scour at nose (d_{cun}) and that computed using Eq. (5.4) is presented in Fig. 5.15. Figure 5.16 shows the same for scour at the wake (d_{cuw}) of partially submerged spur dike using Eq. (5.5).

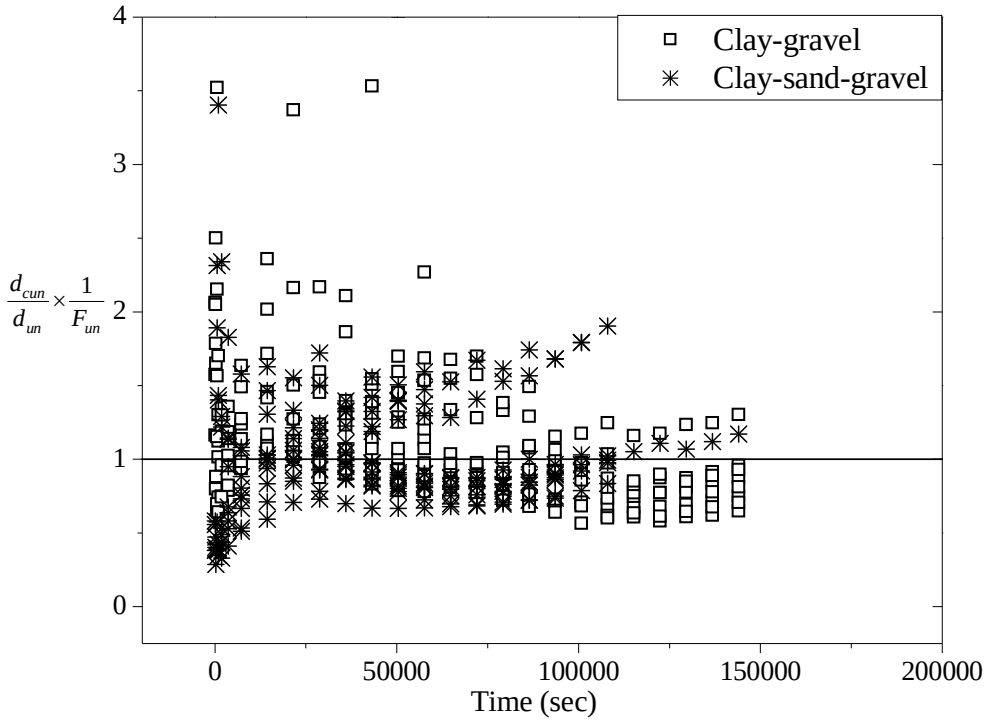

Fig. 5.15 Temporal variation of ratio between observed and calculated depth of scour at nose of the partially submerged spur dike in clay-gravel and clay-sand-gravel mixtures

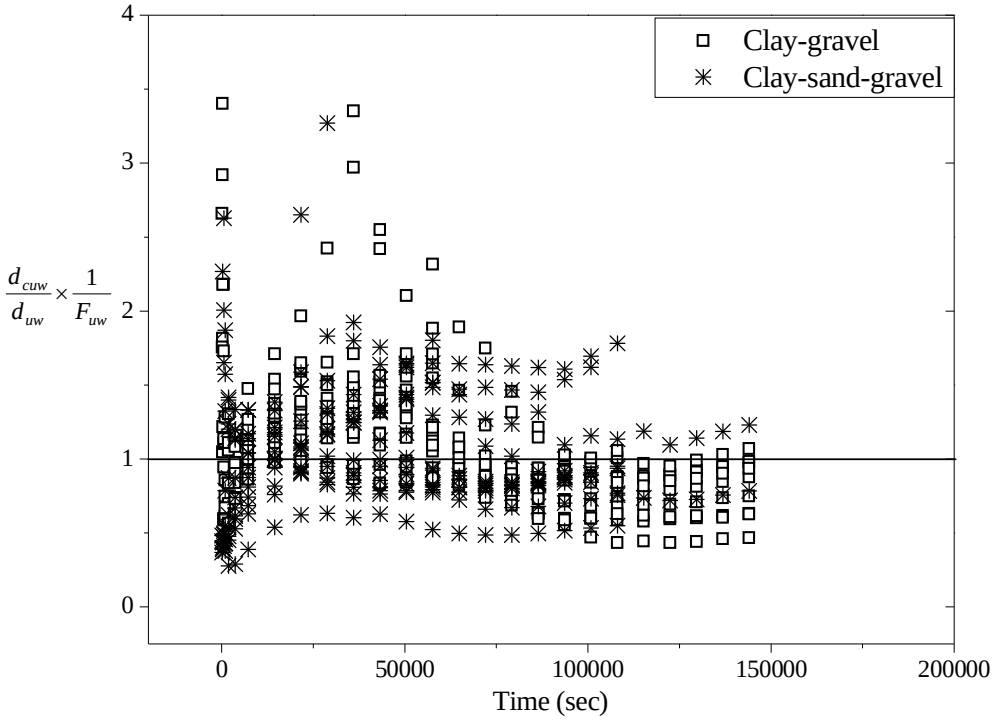

Fig. 5.16 Temporal variation of ratio between observed and calculated depth of scour at the wake of the partially submerged spur dike in clay-gravel and clay-sand-gravel mixtures

The discrepancy ratio and standard deviation given by Yang et al (1996) were used to indicate the goodness of fit between observed scour depth and the values computed using Eq. (5.4) and Eq. (5.5) respectively for the nose and wake of the partially submerged spur dike. These parameters for scour depth at nose and at of the wake region of partially submerged spur dike embedded in cohesive sediment mixtures are defined below

Discrepancy ratio $R_i = \dfrac{d_{cu(n/w)_{c,i}}}{d_{cu(n/w)_{o,i}}}$ (5.6)

Where, $d_{cu(n/w)_{c,i}}$ and $d_{cu(n/w)_{o,i}}$ represents the corresponding values of computed and observed scour depth in mixtures of cohesive sediments at nose and at the wake of partially submerged spur dike respectively.

Mean discrepancy ratio $\overline{R} = \dfrac{\sum_{i=1}^{n} R_i}{N}$ (5.7)

Here N represents the total number of data used in the comparison and

Standard deviation $\sigma = \sqrt{\frac{\sum_{i=1}^{n}(R_i - \overline{R})^2}{N-1}}$ (5.8)

The comparison based on discrepancy ratio and standard deviation between observed and computed values of scour depth at nose and at the wake of partially submerged spur dike in mixtures of cohesive sediment are summarized in Table 5.1.

Table 5.1 Summary of discrepancy ratio and standard deviation between observed and computed value of scour depth at nose and at the wake of partially submerged spur dike in cohesive sediment mixture

Depth of scour at	Percent of data in Range			Mean ($\overline{R}$)	Standard Deviation (σ)	Number of data sets (N)
	0.75-1.25	0.5-2.0	0.33-3			
Nose	54.196	92.565	98.321	1.0767	0.4666	417
Wake	51.771	90.551	98.622	1.0841	0.5032	508

Yang et al. (1996) suggested $\overline{R}_d$, σ_d , $\overline{D}_a$ and σ_a parameters to obtain goodness of fit between observed and calculated values. The parameters $\overline{R}_d$ and σ_d were based on the difference between the observed and their corresponding calculated value, whereas the parameters $\overline{D}_a$ and σ_a on the basis of average value of the logarithm ratio between observed and calculated values. These parameters are given as:

$$\overline{R}_d = \frac{\sum_{i=1}^{N}\left[(d_{cu(n/w)_{c,i}} - d_{cu(n/w)_{o,i}})/d_{cu(n/w)_{o,i}}\right]}{N} \quad (5.9)$$

$$\sigma_d = \sqrt{\frac{\sum_{i=1}^{N}(d_{cu(n/w)_{c,i}} - d_{cu(n/w)_{o,i}})^2}{N-1}} \quad (5.10)$$

For a perfect fit, $\overline{R}_d = 0$ and $\sigma_d = 0$.

Here, $\overline{R}_d$ is average discrepancy ratio and is calculated on the basis of difference of computed and observed value. σ_d is the standard deviation of the computed results based on difference.

$$D_i = \log d_{cu(n/w)_{c,i}} - \log d_{cu(n/w)_{o,i}} \tag{5.11}$$

$$\overline{D}_a = \frac{\sum_{i=1}^{N} D_i}{N} \tag{5.12}$$

$$\sigma_a = \sqrt{\frac{\sum_{i=1}^{N} (D_i - \overline{D}_a)^2}{N-1}} \tag{5.13}$$

For a perfect fit, $\overline{D}_a = 0$ and $\sigma_a = 0$.

Here, D_i is the discrepancy ratio and was calculated on the basis of logarithm ratio between calculated and observed values, $\overline{D}_a$ is average discrepancy ratio and was calculated on the basis of average value of the logarithm ratio between computed and observed values. σ_a is the standard deviation and calculated on the basis of average value of the logarithm ratio between observed and computed values.

The evaluation based on $\overline{D}_a$, σ_a, $\overline{R}_d$ and σ_d parameters between computed and observed values of scour depth at nose and at the wake of partially submerged spur dike in the mixtures of cohesive sediment is summarized in Table 5.2.

Table 5.2 **Comparison of computed and observed values of scour depth at nose and at the wake of the partially submerged spur dike in the mixtures of cohesive sediment based on logarithm ratio and difference between computed and observed results**

Depth of scour at	$\overline{D}_a$	σ_a	$\overline{R}_d$	σ_d	Number of data sets
Nose	-0.00101	0.1651	0.0758	0.0175	417
Wake	-0.00184	0.1757	0.0842	0.0157	508

Figures 5.17 and 5.18 were prepared to show the comparison of observed scour depth and the values calculated from the proposed Eq. 5.4 and Eq. 5.5 for nose and wake of the partially submerged spur dike respectively. It is evident from the figures that the proposed relationship yielded satisfactory outcome with maximum error of two folds for 92.5% of total data for nose and 90.5% of the total data for the wake of the partially submerged spur dike. Although, the scattering of data (Figs. 5.17 and 5.18) is large, but it is acceptable in the perspective of parallel results reported by Kothyari et al. (2014) for pier scour and by Jain and Kothyari (2009, 2010) for transport of cohesive sediments composed of gravel-clay and gravel-sand-clay mixtures. Yang et al. (1996) and, Almedeij and Dilpas (2003) also reported results within the same error range in the case of transport of cohesionless sediment mixtures. However, no other data are available to the best of the author's information on scour depth at nose and at the wake region of partially submerged spur dike founded in cohesive sediment consisting of clay-gravel and clay-sand-gravel mixtures.

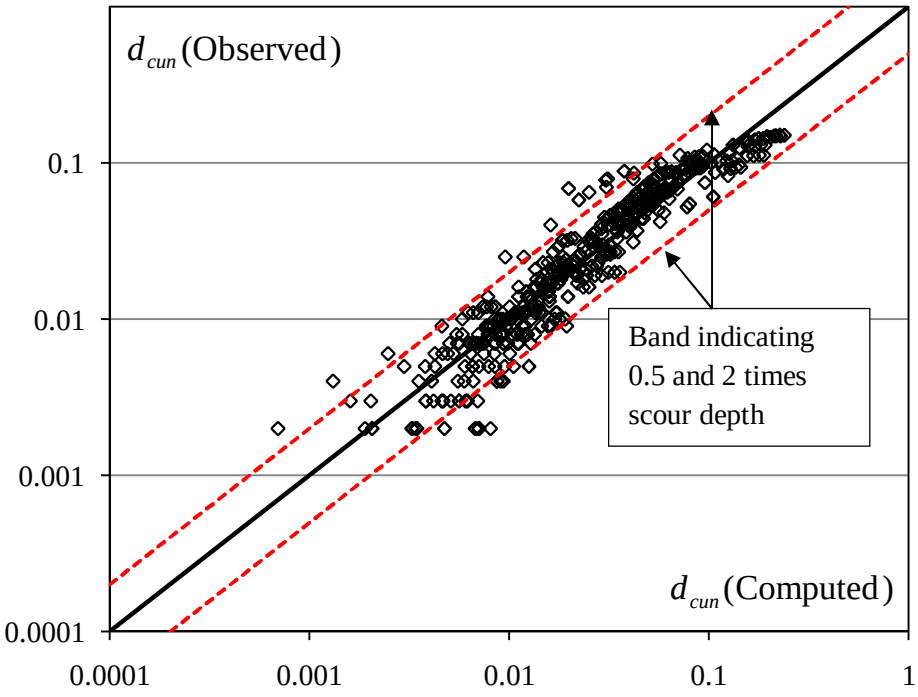

Fig. 5.17 Comparison of computed versus observed depth of scour at nose of the partially submerged spur dike

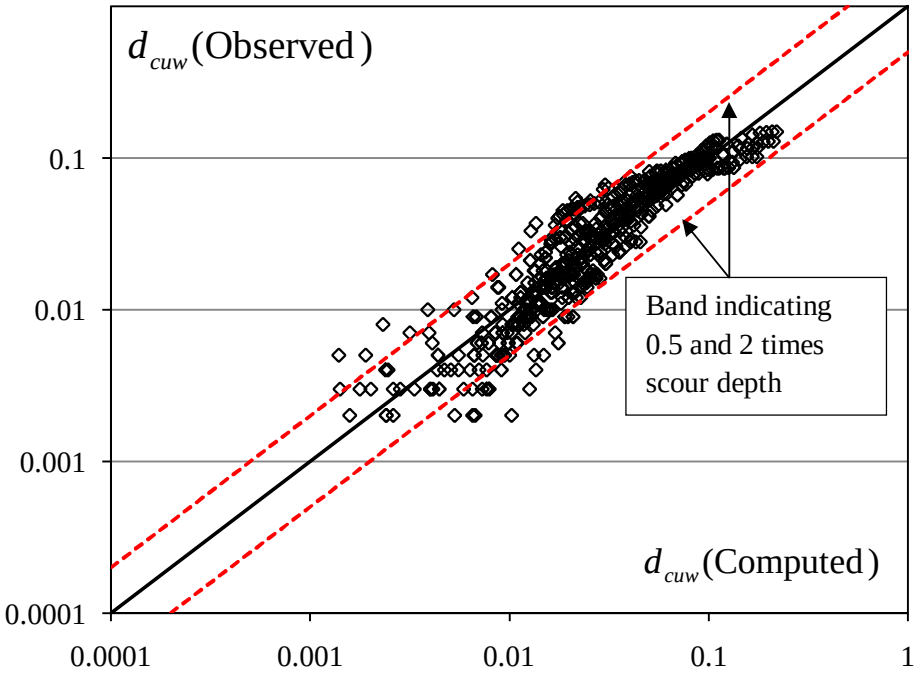

Fig. 5.18 Comparison of computed versus observed depth of scour at the wake of the partially submerged spur dike

5.2.3 Graphical Comparisons for Temporal Variation of Depth of Scour around Partially Submerged Spur Dike in Cohesive Sediments

As mentioned in Chapter-III, the determination of temporal variation of depth of scour is necessary for realistic estimation of design depth of scour. The mathematical formulation presented in Chapter-III was used to establish the relationships for computing the temporal variation of maximum depth of scour at the nose and wake zone of partially submerged spur dike in cohesive sediment mixtures. A graphical comparison between observed and computed temporal variation of depth of scour is presented here.

5.2.3.1 Depth of scour at nose of the partially submerged spur dike in clay-gravel and clay-sand-gravel mixtures

Figures 5.19 and 5.20 show the comparison of observed and computed temporal variation of scour depth at nose of the spur dike in clay-gravel and clay-sand-gravel mixture respectively. Predicted values of scour depth are very close to their respective observed value. As mentioned earlier, the process of scour in cohesive sediment was significantly different from that of cohesionless sediments. In case of cohesive sediment mixtures having lower percentage of clay ($\leq 20\%$), most of the scour occured in the initial 1 to 2 hour of experimental run. When the experiments were conducted with sediment

bed having higher clay percentage 40% to 50 %, the scour in these runs initiated very slowly and even at the end of experimental runs a very small depth of scour was observed. The Figs. 5.19 to 5.20 are presented as an illustration which compares the observed and computed temporal variation of depth of scour at nose of the spur dike in clay-gravel and clay-sand-gravel mixtures. The comparison between observed and computed values is mostly satisfactory as shown in these and many other such figures (not shown here) which in turn confirms the conclusion that present model can predict the depth of scour in clay-gravel mixtures with reasonable accuracy. Poor comparison as depicted by Figs. 5.19 (a, c) for clay-gravel and Fig. 5.20 (a) for clay-sand-gravel were seen to occur in a few runs only.

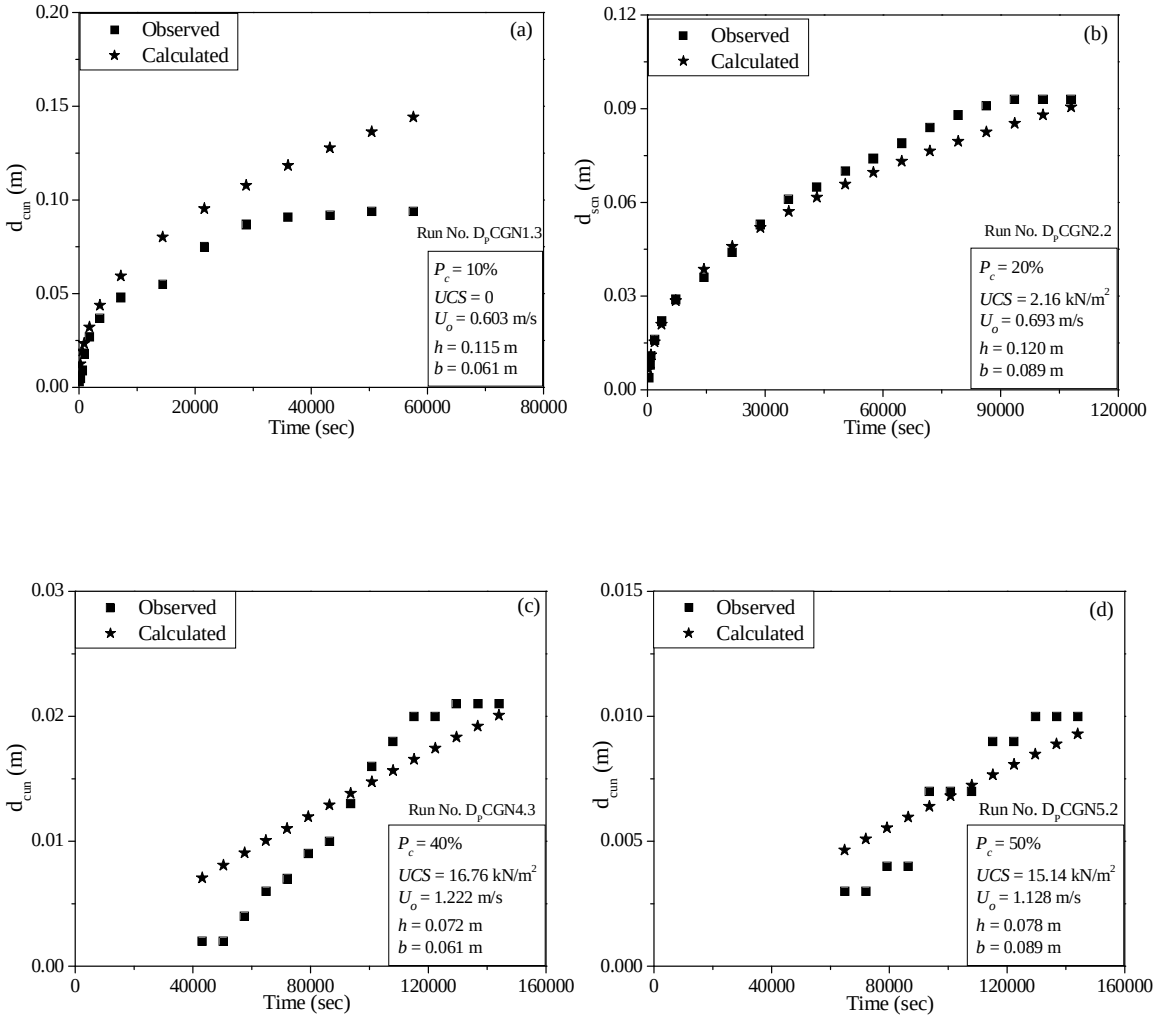

Fig. 5.19 Temporal variation of depth of scour at nose of the partially submerged spur dike in clay-gravel mixture

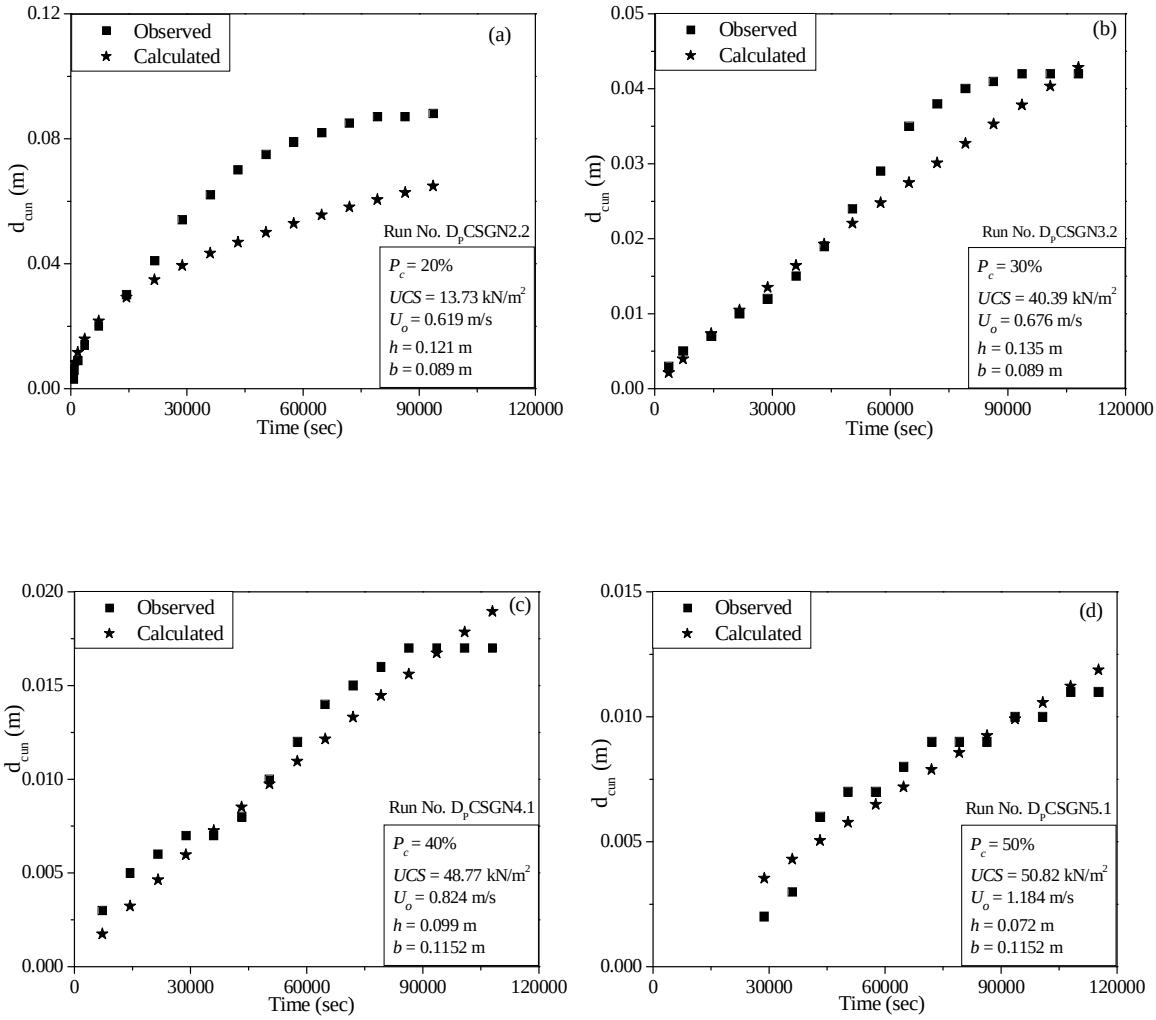

Fig. 5.20 Temporal variation of depth of scour at nose of the partially submerged spur dike in clay-sand-gravel mixture

The comparison of predicted and observed depth of scour shows that the model is able to satisfactorily predict results for the data in this range obtained from the sediment bed consisting of clay-sand-gravel mixtures. The proposed model was similarly applied to all the other data collected in present study and found to be satisfactory (not presented here in detail due to space limitation). It is however worth noting that, in overall the model results have been mostly satisfactory.

5.2.3.2 Depth of scour at the wake of the partially submerged spur dike in clay-gravel and clay-sand-gravel mixtures

The depth of scour at wake of the spur dike was also computed using the proposed model (Eq. 5.5). Figures 5.21 and 5.22 show as an illustration the comparison of observed and computed temporal variation of depth of scour at wake of the spur dike in clay-gravel

and clay-sand-gravel mixture respectively. The results of model were mostly satisfactory in these and in many other runs. A poor comparison between observed and computed values as seen in Figs. 5.21(b) for clay-gravel and 5.22(a) for clay-sand-gravel were seen to occur only for few runs. In case of the highest percentage of clay in the sediment bed, the observed depth of scour was very less which is also well predicted by the proposed model (Fig. 5.21 b).

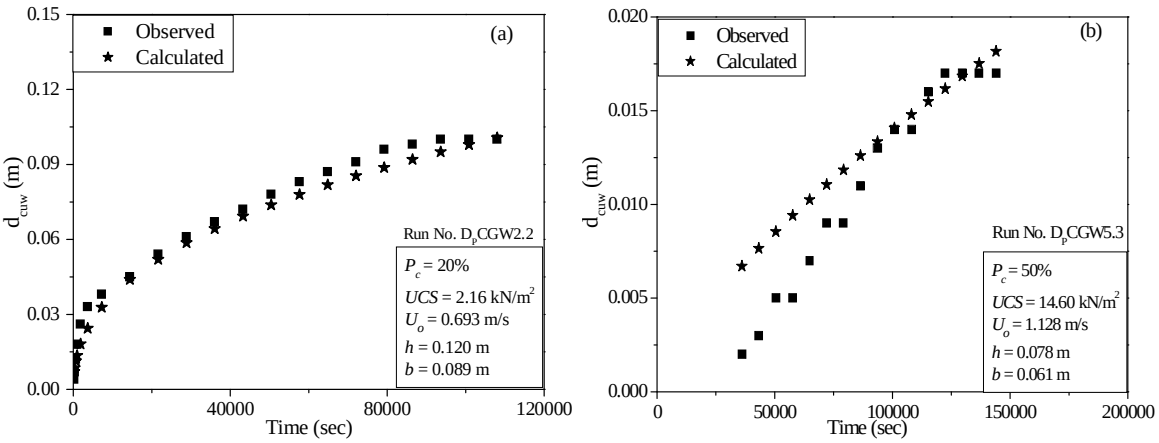

Fig. 5.21 Temporal variation of depth of scour at the wake of the partially submerged spur dike in clay-gravel mixture

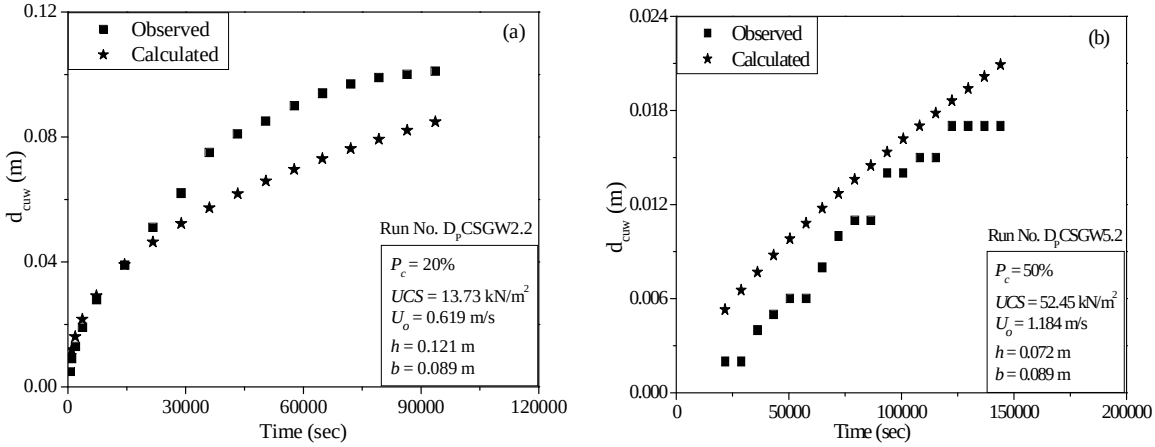

Fig. 5.22 Temporal variation of depth of scour at the wake of the partially submerged spur dike in clay-sand-gravel mixture

5.3 SCOUR AROUND SUBMERGED SPUR DIKE FOUNDED IN COHESIVE SEDIMENT MIXTURES

In the present study, a single metallic spur dike of 3mm thickness and 11.52cm transverse length was installed in the side wall groove provided at 14m downstream of the flume entrance. The dike was installed at an angle of 90° to the direction of flow. The overtopping ratio (ratio of approaching flow depth to structure height above the bed level) for submerged spur dike was maintained at $\cong 1.4$. The temporal variation of scour depth was measured by point gauge having an accuracy of ± 0.1 mm.

5.3.1 Visual Observations

The experiments were conducted with submerged spur dike founded in the mixtures of clay-gravel and clay-sand-gravel. The ranges of different measured parameters and experimental conditions are presented in Appendix-D for cohesive sediment bed composed of clay-gravel and clay-sand-gravel mixtures. From the experiments, it was observed that similar to the scouring in partially submerged spur dike, the scouring for the present case also started from the downstream corner of the wake region (Fig. 5.23).

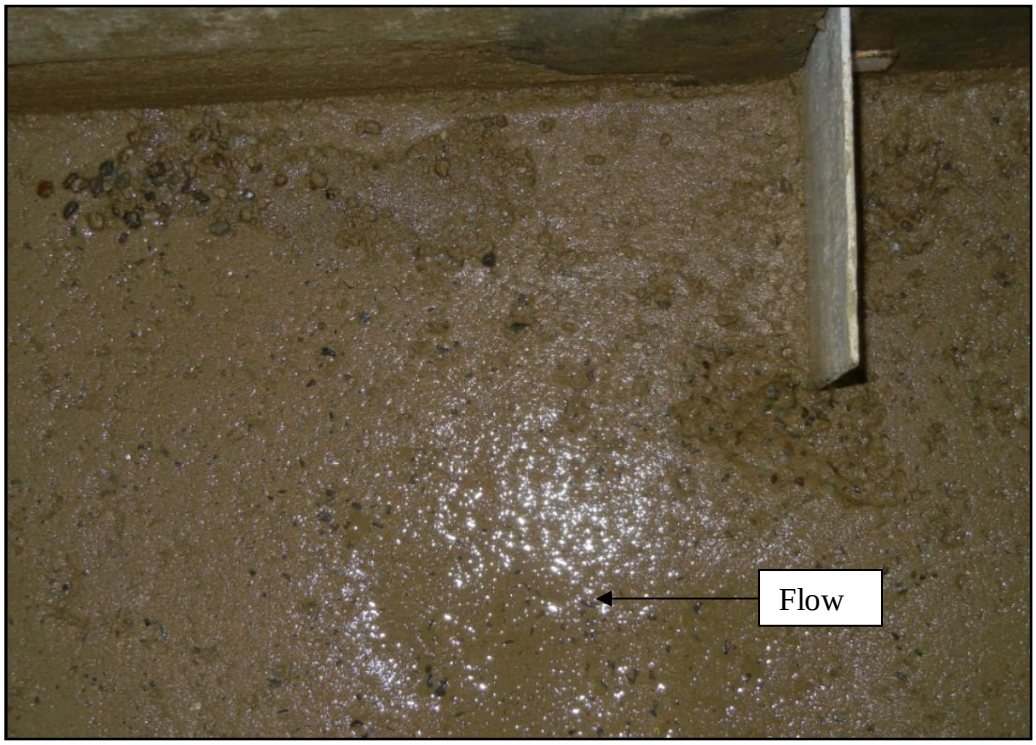

Fig. 5.23 Initiation of scour around submerged spur dike in clay-sand-gravel mixture (20% Clay + 40% Sand + 40% Gravel)

5.3.1.1 Scour in clay-gravel mixtures

Different patterns of scour holes are shown in Fig. 5.24 (a-c) in clay-gravel mixtures. In case of experiments conducted with 10% clay, the observed shape of scour hole around the submerged dike was deep and had a large periphery. In these experiments (when $P_c = 10\%$), the sediments deposition took place in the downstream of submerged dike [Fig. 5.24(a)]. However, in experiments conducted with clay percentage $\geq 20\%$, no sediment deposition occured in the downstream of the spur dike. In case of experiments conducted with higher clay percentage ($\geq 30\%$), the longitudinal and transverse extent of scour hole decreased, and the deep vertical shape (almost cylindrical) of the scour hole was observed [Fig. 5.24(b)]. Experimental runs with the highest clay percentage (=50%) in the sediment bed, the longitudinal and transverse length of the scour hole increased whereas lesser depth of the scour hole was observed [Fig. 5.24(c)].

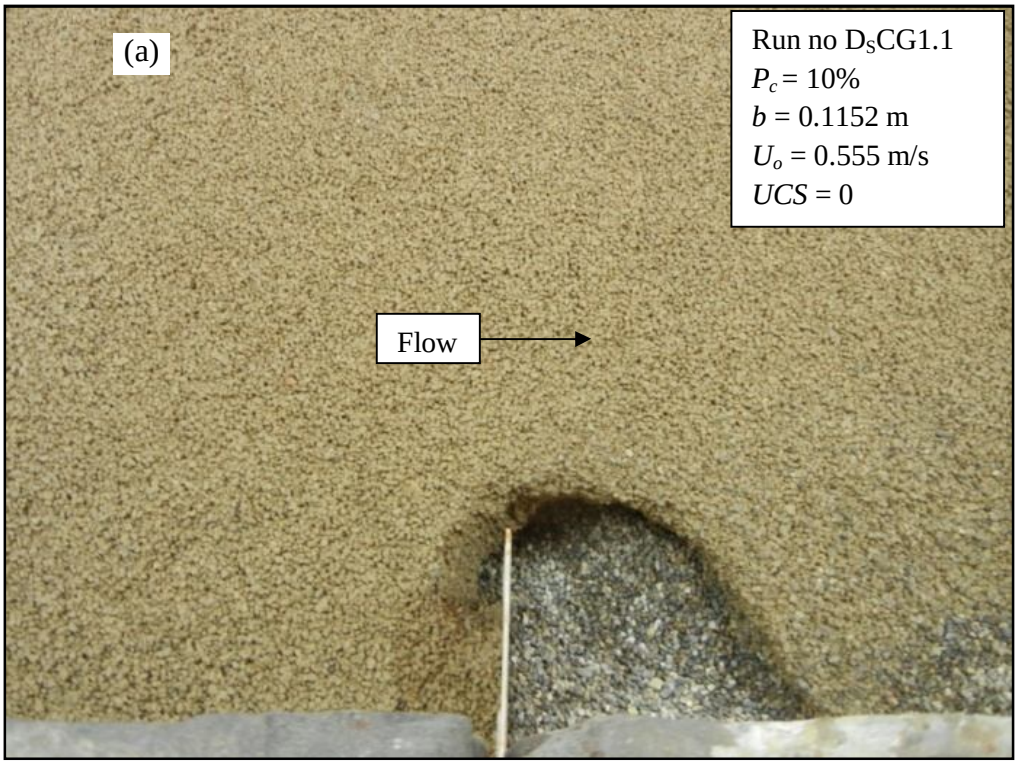

Fig. 5.24(a) Pattern of scour hole around submerged spur dike in cohesive sediment mixture of 10% Clay + 90% Gravel

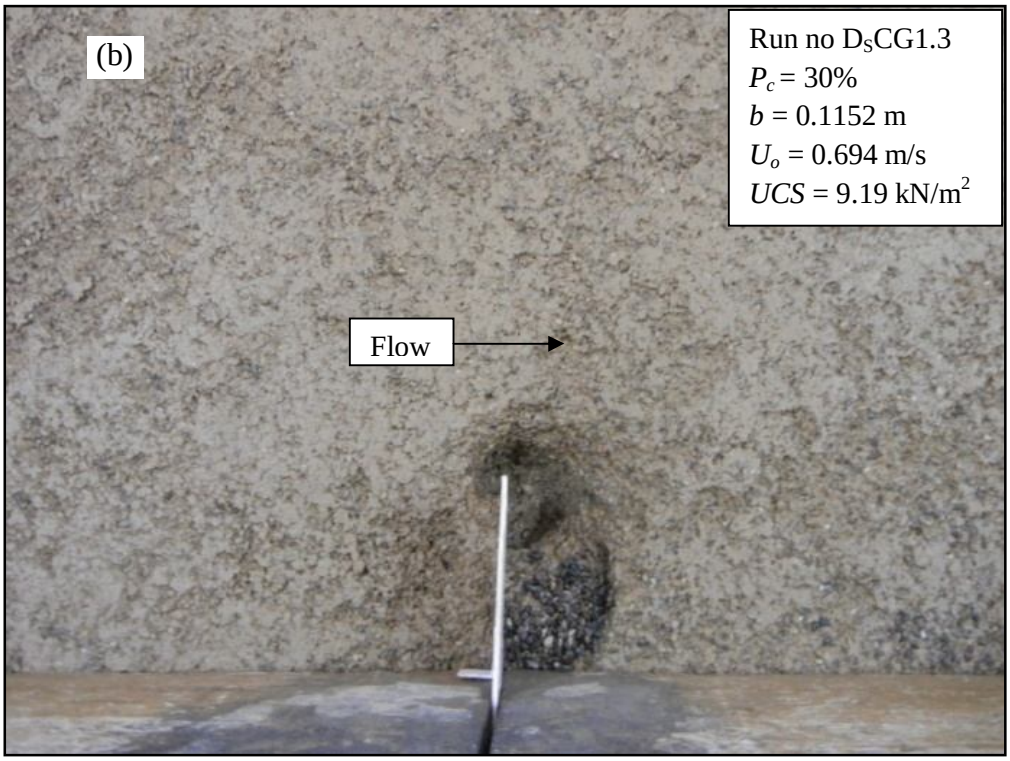

Fig. 5.24(b) Pattern of scour hole around submerged spur dike in cohesive sediment mixture of 30% Clay + 70% Gravel

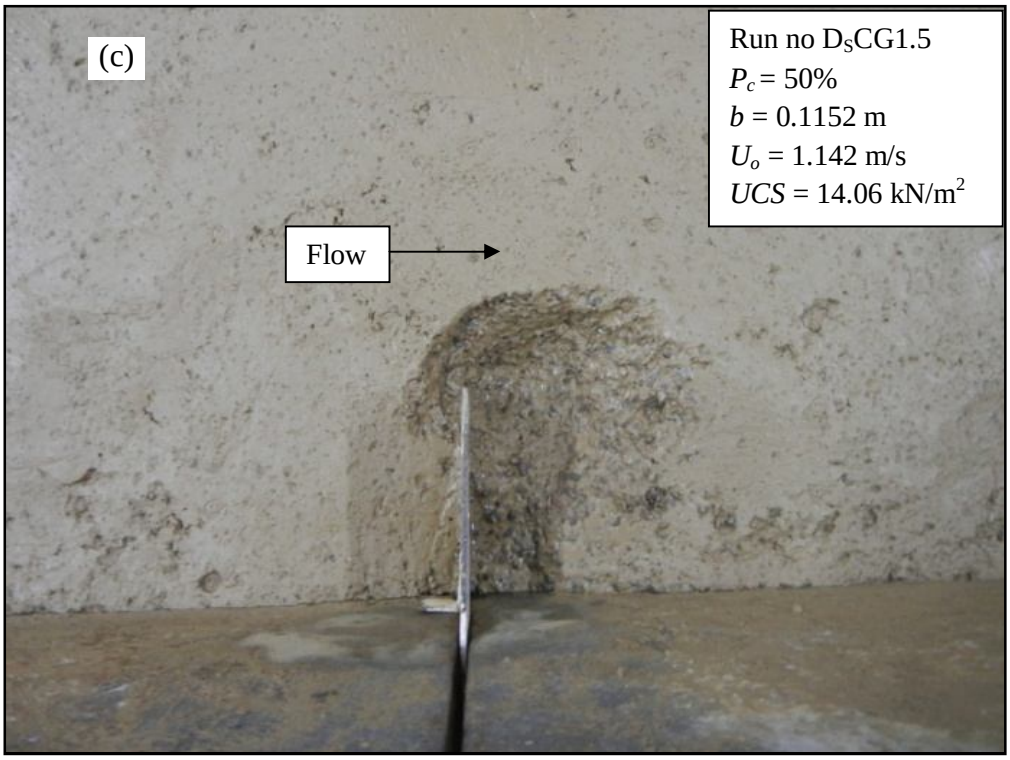

Fig. 5.24(c) Pattern of scour hole around submerged spur dike in cohesive sediment mixture of 50% Clay + 50% Gravel

5.3.1.2 Scour in clay-sand-gravel mixtures

Figure 5.25 (a-c) shows the different patterns of scour hole observed in clay-sand-gravel sediment mixtures. The observations made with submerged spur dike were very similar to those observed in partially submerged spur dike. When experiments conducted with cohesive sediment mixtures having 10% clay content, the maximum scour depth was observed at nose of the spur dike and sediment was observed to deposit at wake region of spur dike. However, in experiments conducted with clay content $\geq 20\%$ the maximum scour depth was observed at wake of the spur dike. Almost cylindrical shape of the scour hole was observed in sediment mixture having 20% clay content [Fig. 5.25(a)]. Scour at the junction of wall and submerged spur dike was also observed in such experiments. In the case of experiments conducted with high clay content $(P_c \geq 40\%)$, very small scour depth (<1cm) was observed at nose of the submerged dike [Fig. 5.25 (b and c)] and maximum scour depth was observed at wake of the spur dike.

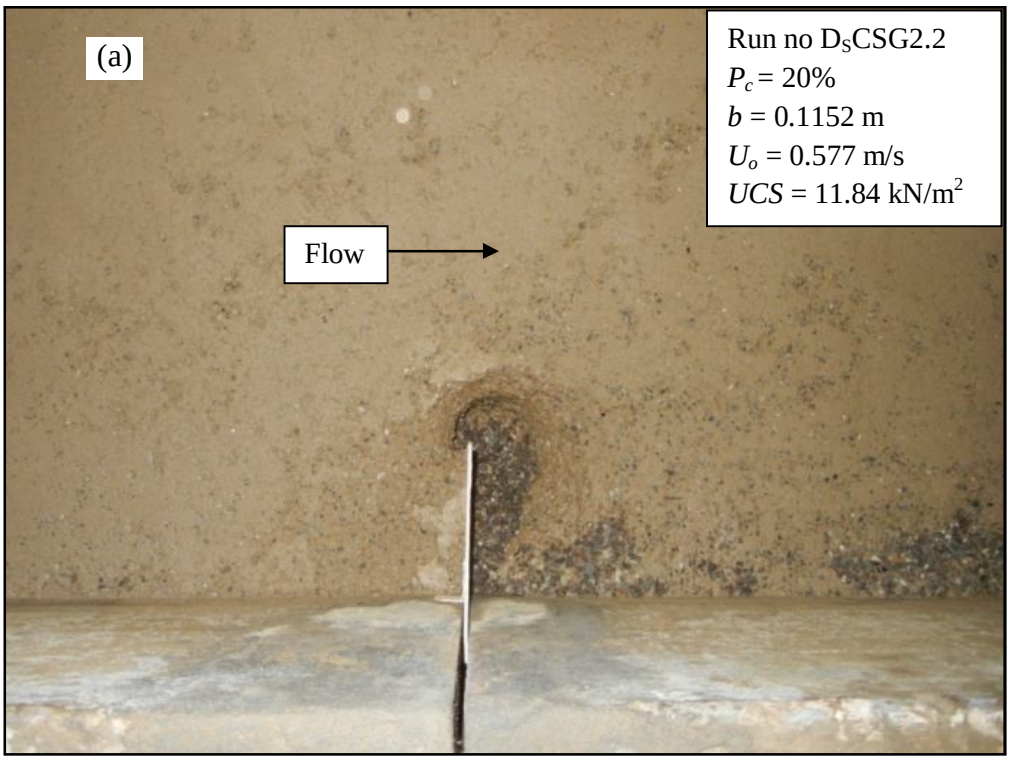

Fig. 5.25(a) Pattern of scour hole around submerged spur dike in cohesive sediment mixture of 20% Clay + 40% Sand + 40% Gravel

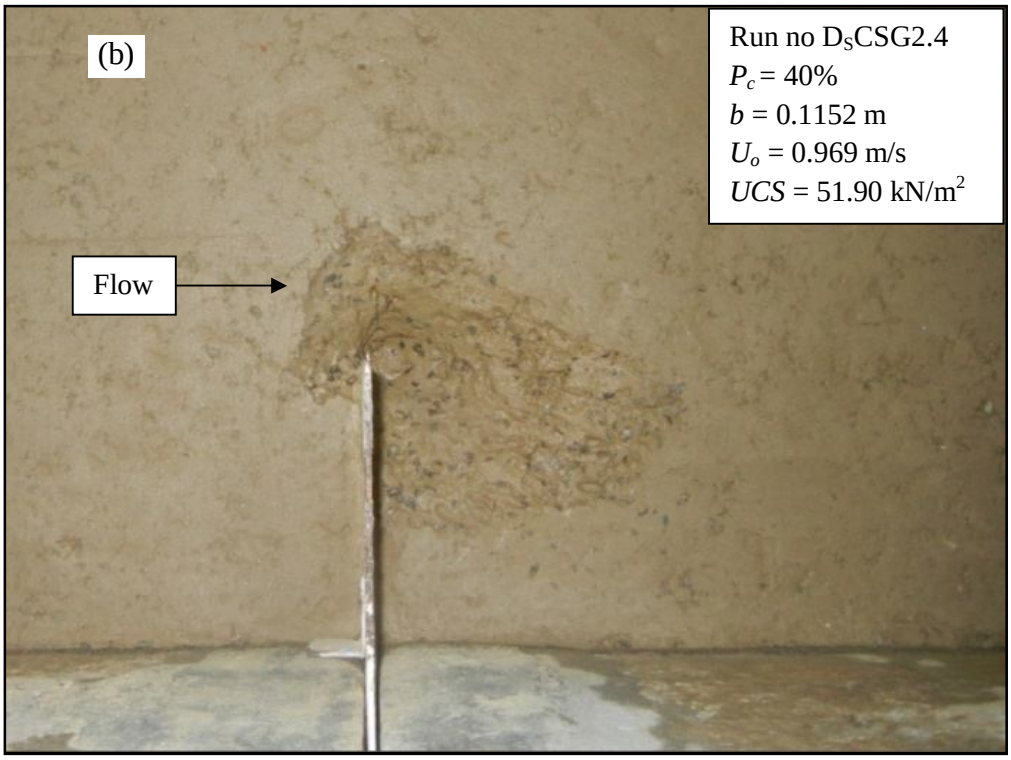

Fig. 5.25(b) Pattern of scour hole around submerged spur dike in cohesive sediment mixture of 40% Clay + 30% Sand + 30% Gravel

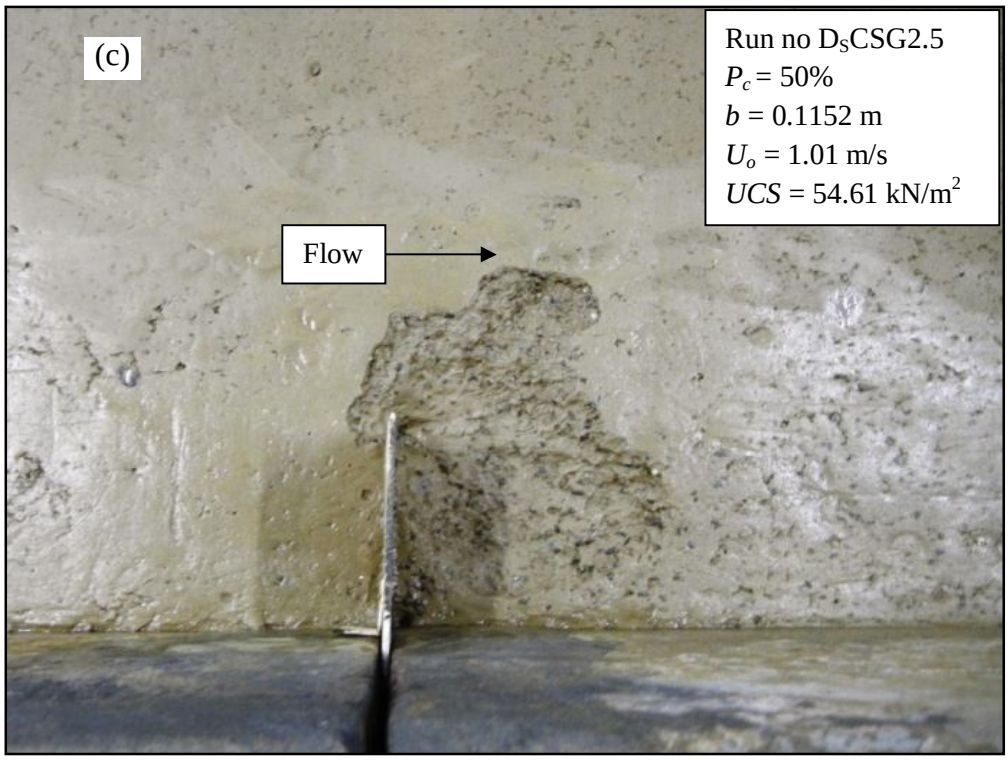

Fig. 5.25(c) Pattern of scour hole around submerged spur dike in cohesive sediment mixture of 50% Clay + 25% Sand + 25% Gravel

To investigate the influence of cohesion on scour depth at nose and at the wake of the submerged dike, Figs. 5.26 to 5.29 were prepared. In these figures (d_{csn}) is scour depth at nose and (d_{csw}) is scour depth at the wake of the submerged dike founded in the mixtures of clay-gravel and clay-sand-gravel. The scour depth at nose and at the wake of the submerged dike decreases with an increase in clay percentage in the mixtures of clay-gravel and clay-sand-gravel (Fig. 5.26 and Fig. 5.27). Similarly, scour depth at nose and at the wake of the submerged dike also decreased with an increase in unconfined compressive strength of clay-gravel and clay-sand-gravel sediment mixture (Fig. 5.28 and Fig. 5.29). Similar results were also obtained in experiments conducted with partially submerged dike embedded in cohesive sediment mixtures.

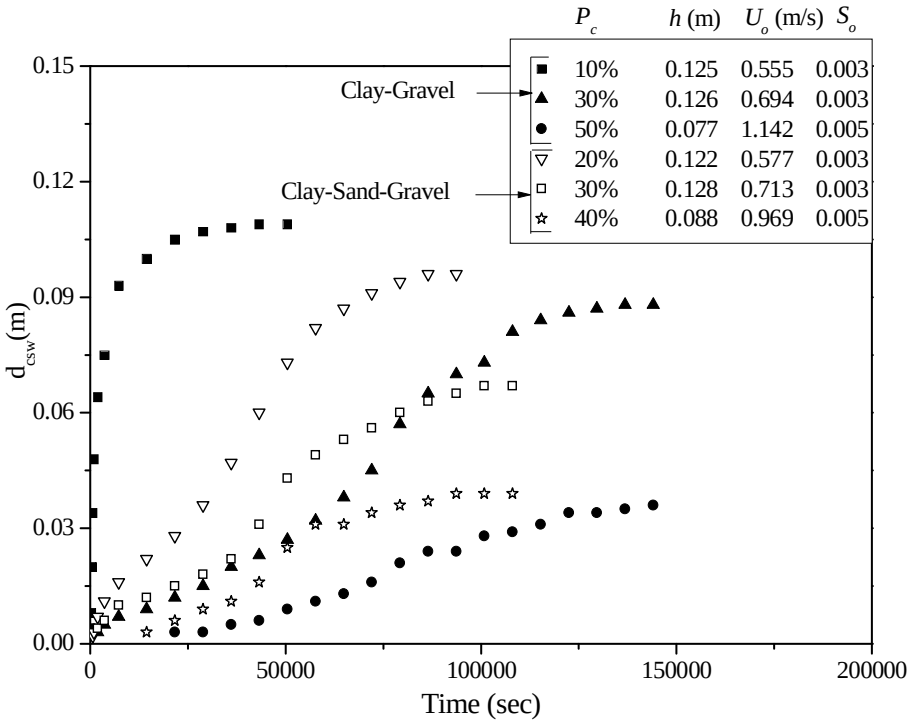

Fig. 5.26 Temporal variation of scour depth with clay percentage at nose of the submerged dike in clay-gravel and clay-sand-gravel mixtures

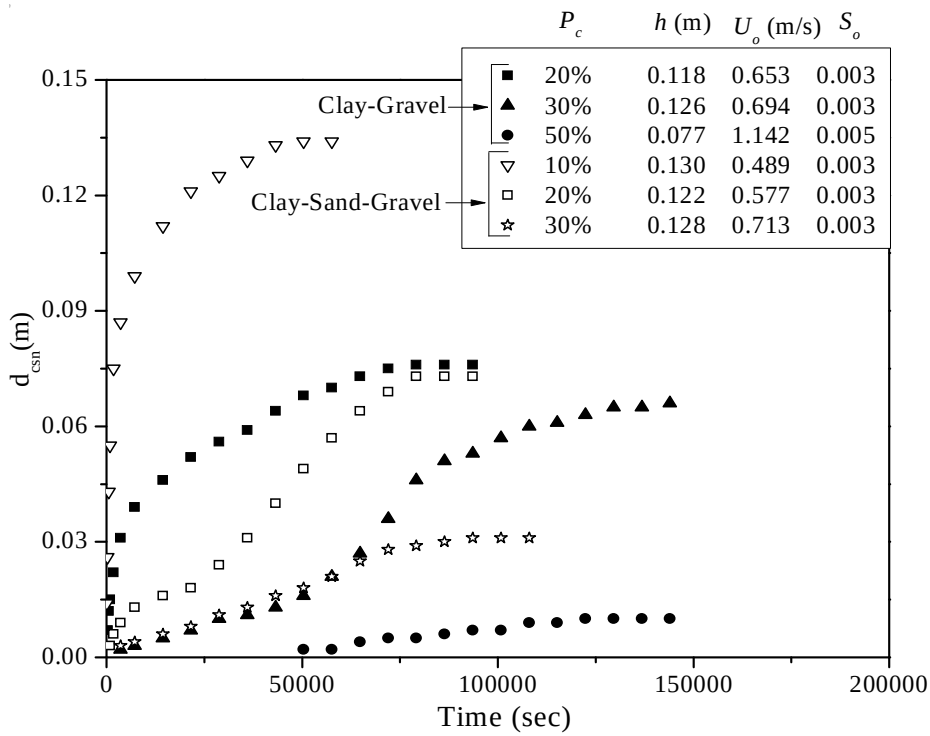

Fig. 5.27 Temporal variation of scour depth with clay percentage at the wake of the submerged dike in clay-gravel and clay-sand-gravel mixtures

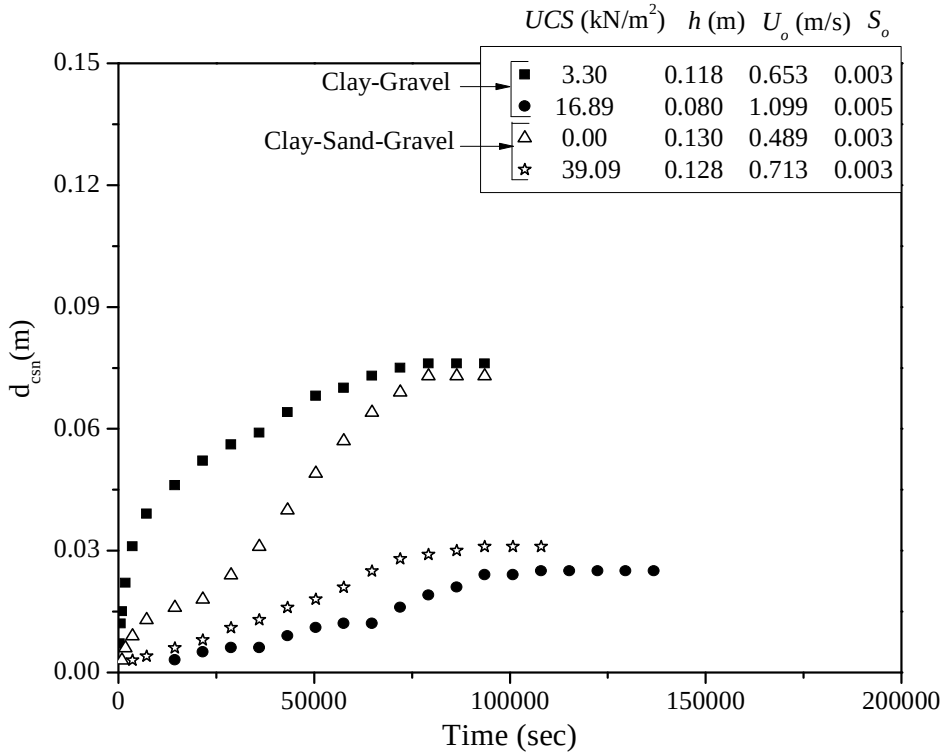

Fig. 5.28 Temporal variation of scour depth with unconfined compressive strength at nose of the submerged dike in clay-gravel and clay-sand-gravel mixtures

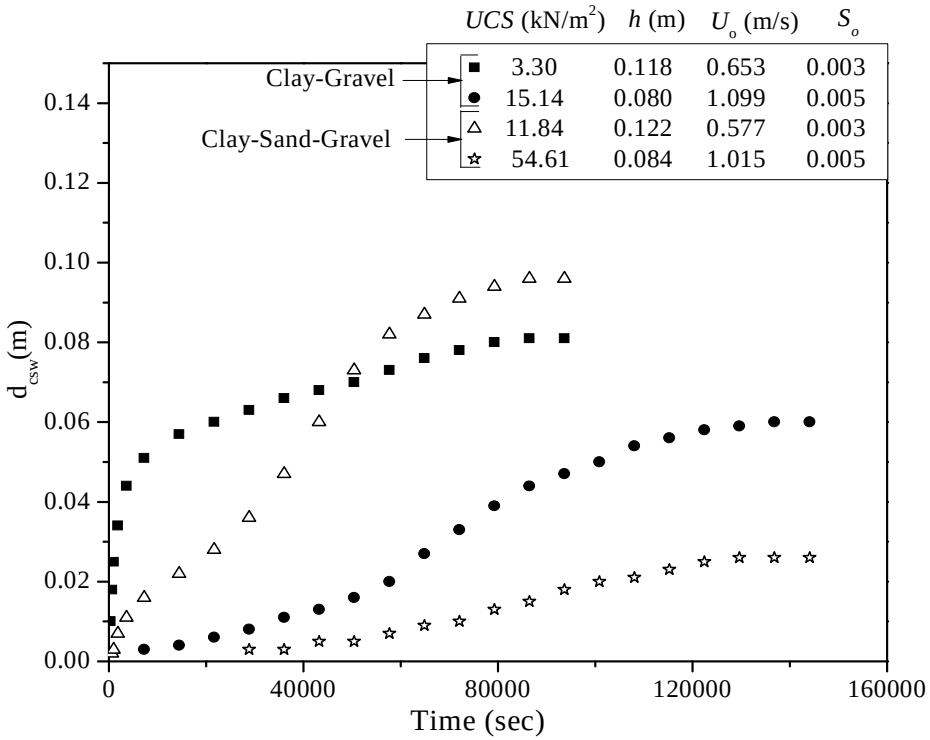

Fig. 5.29 Temporal variation of scour depth with unconfined compressive strength at the wake of the submerged dike in clay-gravel and clay-sand-gravel mixtures

5.3.2 Depth of Scour at Nose and at the Wake of Submerged Spur Dike

The temporal variation of scour depth with various percentage of clay was measured at nose and at the wake of the submerged spur dike founded in clay-gravel and clay-sand-gravel mixtures. Figure 5.30 shows the temporal variation of scour depth at nose of the submerged spur dike whereas Fig. 5.31 shows the same at the wake of submerged dike. These figures clearly revealed that the scour depth at nose (d_{csn}) and at the wake (d_{csw}) of the submerged dike in cohesive sediment mixtures was much smaller than calculated scour depth for cohesionless sediment under same flow conditions and submerged dike size. Very small scour depth (<1cm) occured at nose of the submerged spur dike with 40% and 50% clay content present in the mixture of clay-sand-gravel. Therefore, the experimental runs resulting in scour depth smaller than 1cm was not considered in the calculations and hence not shown in Fig. 5.30. It was clearly observed from these figures that the scour depth at both the locations reduced drastically with the increment of clay percentage in the sediment mixtures bed.

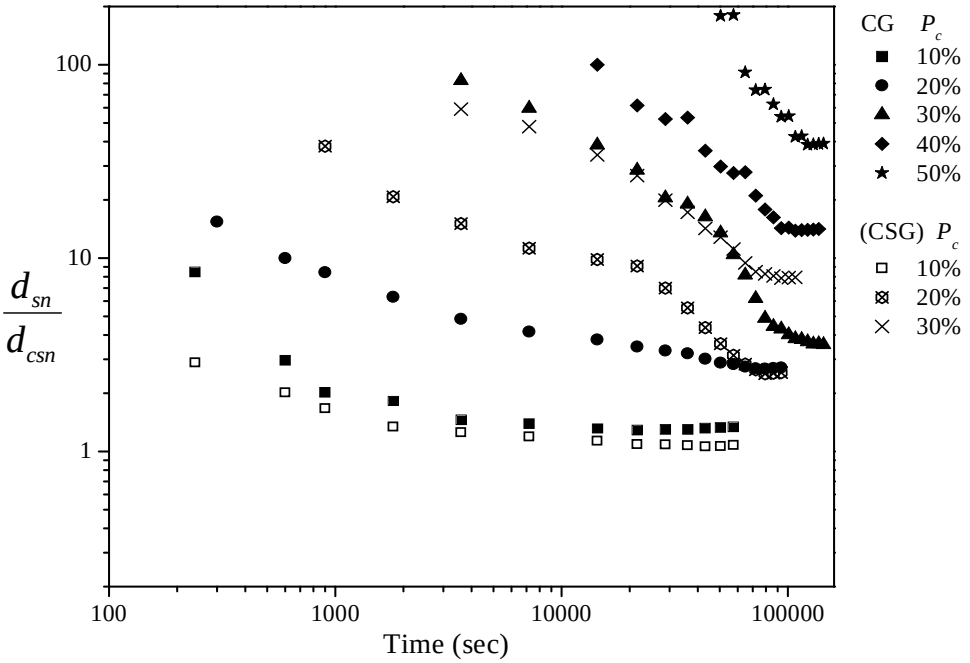

Fig.5.30 Temporal variations of dimensionless scour depth with clay percentage at nose of the submerged dike clay-gravel (CG) and clay-sand-gravel (CSG) mixtures

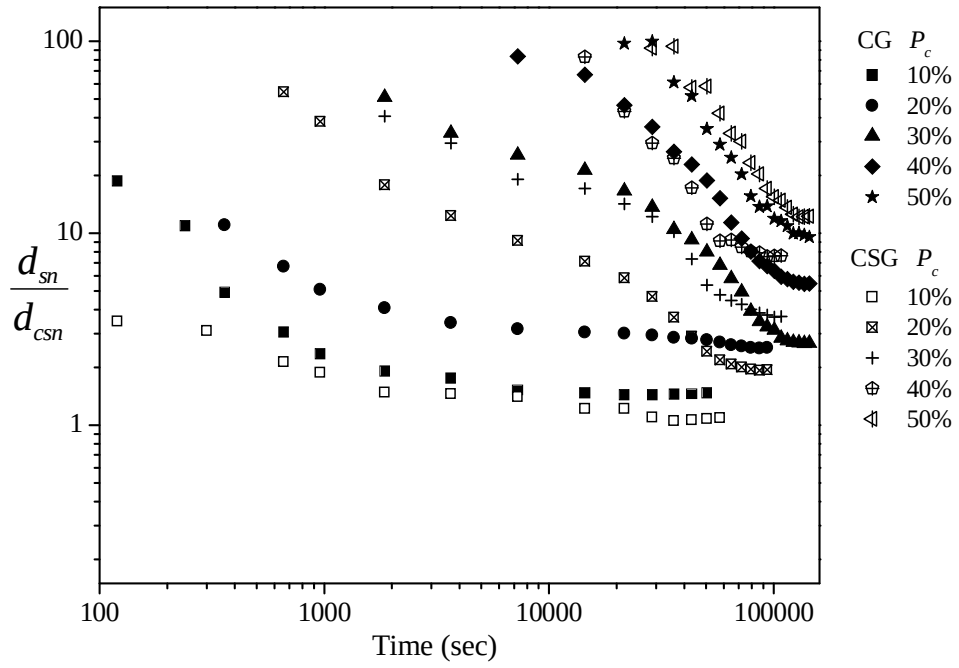

Fig. 5.31 Temporal variations of dimensionless scour depth with clay percentage at the wake of the submerged dike in dike clay-gravel (CG) and clay-sand-gravel (CSG) mixtures

Figures 5.32 and 5.33 were prepared to identify the effect of shear strength of clay-gravel and clay-sand-gravel sediment mixtures on scour depth at nose and at the wake of submerged dike respectively. The variation of scour depth with unconfined compressive strength (*UCS*) was studied. In these figures, the whole data was classified into two ranges of *UCS* for clay-gravel mixtures and three ranges of *UCS* for clay-sand-gravel mixtures. From these figures it is clearly observed that the scour depth reduced with an augment in unconfined compressive strength. The capability to resist the scour depth increased with increase in *UCS* of clay-gravel and clay-sand-gravel mixtures. These results are very similar to that of partially submerged dike founded in cohesive sediment mixtures containing clay-gravel and clay-sand-gravel.

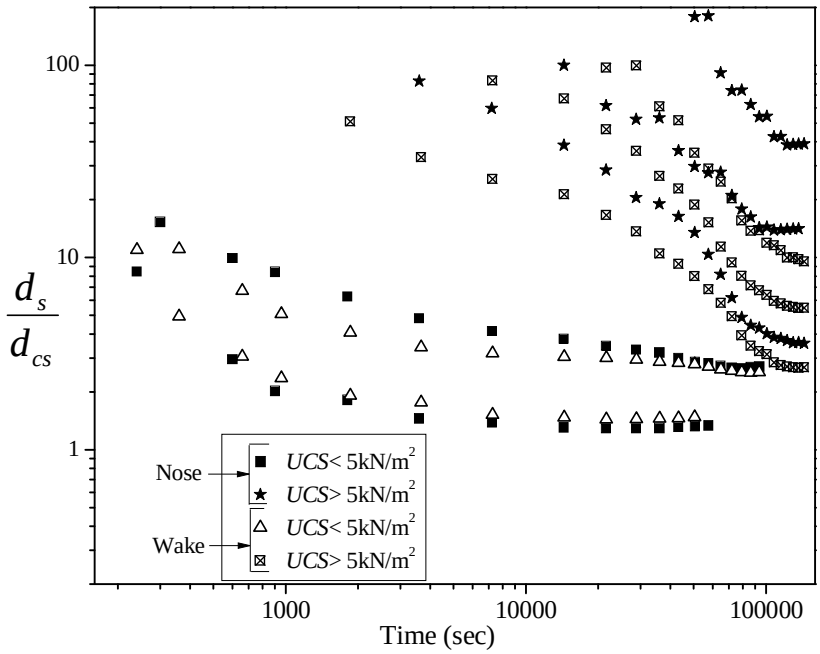

Fig. 5.32 Temporal variations of dimensionless scour depth with *UCS* in clay-gravel (CG) mixture at nose and at the wake of the submerged dike

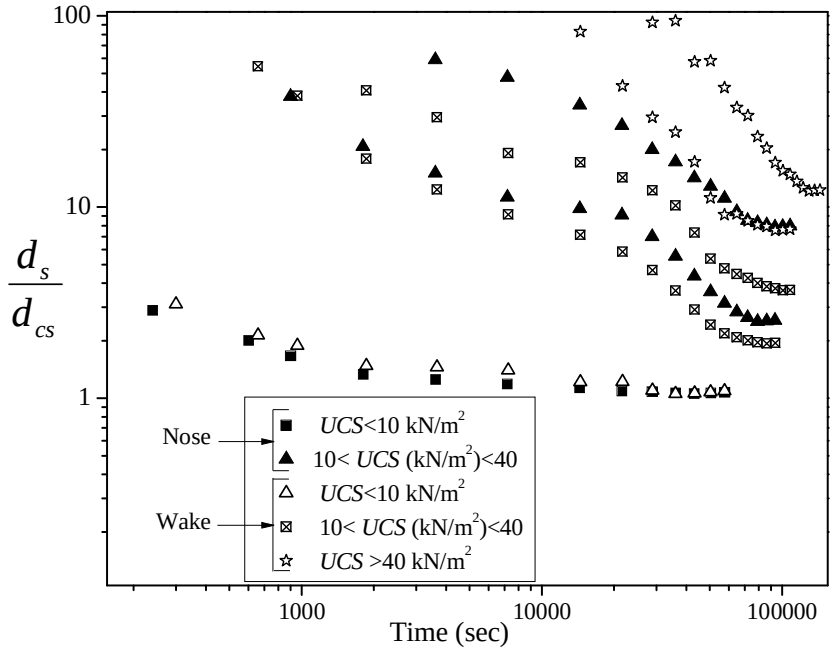

Fig. 5.33 Temporal variations of dimensionless scour depth with *UCS* in clay-sand-gravel (CSG) mixture at nose and at the wake of the submerged dike in clay-sand-gravel mixtures

From the dimensional analysis, the functional relationship for the computation of depth of scour at nose and at the wake of submerged spur dike in clay-gravel and clay-sand-gravel mixtures was derived in Chapter- III, which is rewritten here as

$$\frac{d_{cs(n/w)}}{d_{s(n/w)}} = f\left(P_c, \frac{C_*}{\phi_*}, \frac{\gamma_d}{\gamma_w}, UCS_*, t_*\right) \tag{5.14}$$

From Appendix- E, the range of variable (γ_d/γ_w) is from 1.42 to 2.09 in the present study. The analysis of data indicated that the variable (γ_d/γ_w) in this small range could not fully explain the variation of scour depth around submerged dike. Also the variation of scour depth with C_*/ϕ_* did not show significant influence of the variable C_*/ϕ_* on depth of scour around submerged dike. Similar results were also obtained in section 5.2.2. Therefore, these variables were eliminated from further analysis and new functional relationship can be considered as:

$$\frac{d_{cs(n/w)}}{d_{s(n/w)}} = f\left(P_c, UCS_*, t_*\right) \tag{5.15}$$

Considering all dimensional parameters, the following functional relationship was proposed for the computation of scour depth at nose (d_{csn}) and at the wake (d_{csw}) of the submerged dike founded in the mixtures of clay-gravel and clay-sand-gravel.

$$\frac{d_{cs(n/w)}}{d_{s(n/w)}} = f\left[(P_c), (1+UCS_*), t_*\right] \tag{5.16}$$

It is important to make the use of variables $(1+UCS_*)$ in place of UCS_* so that Eq. (5.16) is also suitable when *UCS* = 0. Above relation is valid for cohesive sediment mixtures only.

Eq. (5.16) was used to find out the scour depth at nose and at the wake of the submerged dike founded in clay-gravel and clay-sand-gravel mixtures. Analysis of the presently collected data (all experimental runs) revealed that scour depth at nose/wake of submerged dike is inversely proportional to P_c (Figures 5.30 and 5.31) and $1+UCS_*$ (Figures 5.34 and 5.35) for both the sediment mixtures. Multiple nonlinear regression analysis was used to find out relationship for scour depth at nose and at the wake of the spur dike using all pertinent dimensionless parameters.

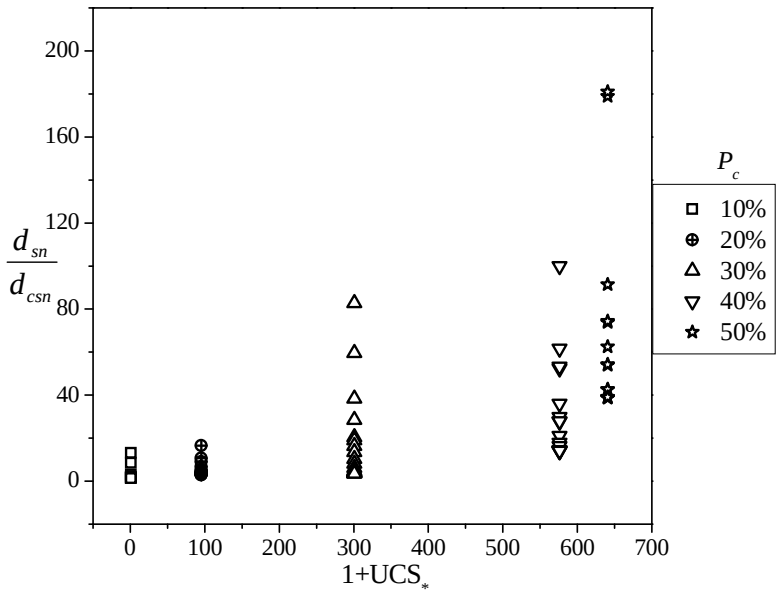

Fig. 5.34 Variation of dimensionless scour depth with $(1+UCS_*)$ at nose of the submerged spur dike in clay-gravel mixtures

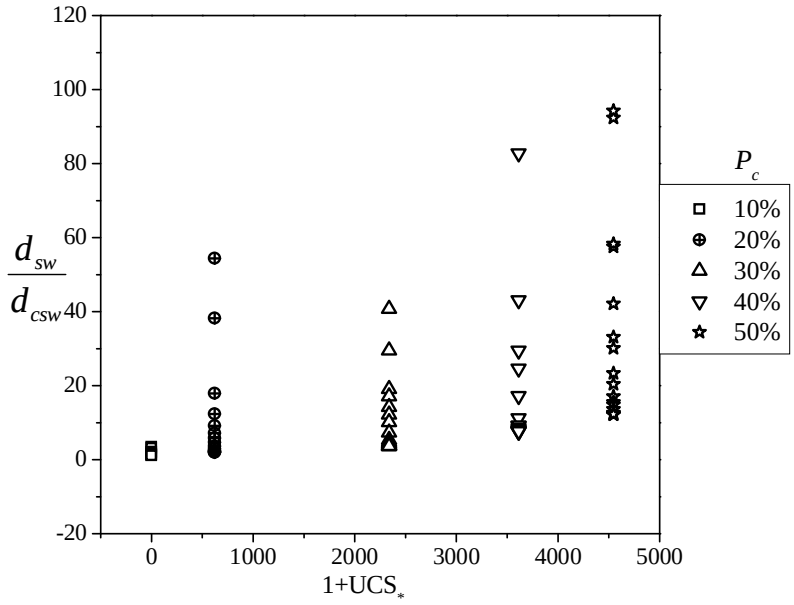

Fig. 5.35 Variation of dimensionless scour depth with $(1+UCS_*)$ at the wake of the submerged spur dike in clay-sand-gravel mixtures

Similar to analysis conducted in the case of partially submerged dike, whole data have been analyzed in two ranges of clay percentages. Following relationships were proposed for describing the variation of scour depth at nose (d_{csn}) and at the wake (d_{csw}) of submerged spur dike.

In the case of scour depth at nose of the submerged spur dike founded in mixtures of clay-gravel and clay-sand-gravel

$$\frac{d_{csn}}{d_{sn}} = F_{sn} \tag{5.17}$$

Where, F_{sn} = parameter that represents cohesion of clay-gravel and clay-sand-gravel mixtures at nose of the spur dike and is expressed as

$$F_{sn} = b_o\left[(5P_c)^{b_1}(1+0.01UCS_*)^{b_2}(t_*)^{b_3}\right] \tag{5.17a}$$

With

$b_o = 0.0032; b_1 = -1.365; b_2 = -0.444; b_3 = 0.298$ for $10\% \le P_c \le 20\%$

(Adjusted R^2= 0.85)

and

$b_o = 5.7\times10^{-7}; b_1 = -5.535; b_2 = -0.43; b_3 = 0.895$ for $30\% \le P_c \le 50\%$

(Adjusted R^2= 0.95)

In the case of scour depth at wake of the submerged spur dike founded in mixtures of clay-gravel and clay-sand-gravel

$$\frac{d_{csw}}{d_{sw}} = F_{sw} \tag{5.18}$$

Where, F_{sw}= parameter that represents cohesion of clay-gravel and clay-sand-gravel mixtures at wake of the spur dike and is expressed as

$$F_{sw} = \mathrm{d}_o\left[(5\mathrm{P_c})^{d_1}(1+0.01UCS_*)^{d_2}(t_*)^{d_3}\right] \tag{5.18a}$$

With

$d_o = 0.0028; d_1 = -1.024; d_2 = -0.4355; d_3 = 0.331$ for $10\% \le P_c \le 20\%$

(Adjusted R^2= 0.76)

and

$d_o = 6.1\times10^{-7}; d_1 = -4.33; d_2 = -0.281; d_3 = 0.876$ for $30\% \le P_c \le 50\%$

(Adjusted R^2= 0.90)

In order to find the goodness of fit between observed and calculated values, discrepancy ratio (R_i), mean discrepancy ratio $(\overline{R}_i)$, standard deviation of the estimate (σ), average discrepancy ratio based on difference $(\overline{R}_d)$, average discrepancy ratio based on logarithm ratio $(\overline{D}_a)$ and, standard deviation of estimate based on difference (σ_d) and logarithm (σ_a) were used and described in previous section 5.2 (Eq. 5.6 to Eq. 5.13).

The comparison between observed and computed values of scour depth at nose and at the wake of the submerged spur dike founded in mixtures of cohesive sediment containing clay-gravel and clay-sand-gravel based on discrepancy ratio and standard deviation is summarized in Table 5.3. Evaluation based on $\overline{D}_a, \sigma_a$, $\overline{R}_d$ and σ_d parameters is presented in Table 5.4.

Table 5.3 Comparison between observed and computed value of scour depth at nose and at the wake of the submerged spur dike in the mixtures of cohesive sediments containing clay-gravel and clay-sand-gravel based on discrepancy ratio and standard deviation

Depth of scour at	Percent of data in Range			Mean ($\overline{R}$)	Standard Deviation (σ)	Number of data sets (N)
	0.75-1.25	0.5-2.0	0.33-3			
Nose	67.175	97.709	100	1.0263	0.2924	131
Wake	50.292	95.906	99.415	0.9827	0.3975	171

Table 5.4 Comparison of computed and observed values of scour depth at nose and at wake of the submerged spur dike in the mixtures of cohesive sediments containing clay-gravel and clay-sand-gravel on the basis of logarithm ratio and difference between computed and observed results

Depth of scour at	$\overline{D}_a$	σ_a	$\overline{R}_d$	σ_d	Number of data sets
Nose	-0.0043	0.1172	0.0264	0.0148	131
Wake	-0.0350	0.1495	-0.0173	0.0145	171

The comparison of observed scour depth and the values calculated from the proposed Eq. (5.17) for nose and Eq. (5.18) for wake of the submerged spur dike are presented in Fig. 5.36 and Fig. 5.37 respectively. It is evident from these Figures that the proposed relationships yielded satisfactory outcome with maximum error of two folds for 97.7% of the total data for nose and 95.9% of total data for wake of the submerged dike respectively. The scattering of data in Fig. 5.36 and Fig.3.37 are large, but it is acceptable in the perspective of parallel results reported by Kothyari et al. (2014) for pier scour and by Jain and Kothyari (2009, 2010) for transport of cohesive sediments containing clay-gravel and clay-sand-gravel. The data shown in Figs. 5.36 and 5.37 are from 10 experimental runs of scour depth measured at different time intervals. However, no other data was available on scour depth at nose and at the wake of the submerged spur dike founded in mixtures of cohesive sediment consisting clay-gravel and clay-sand-gravel to the best of the author's knowledge.

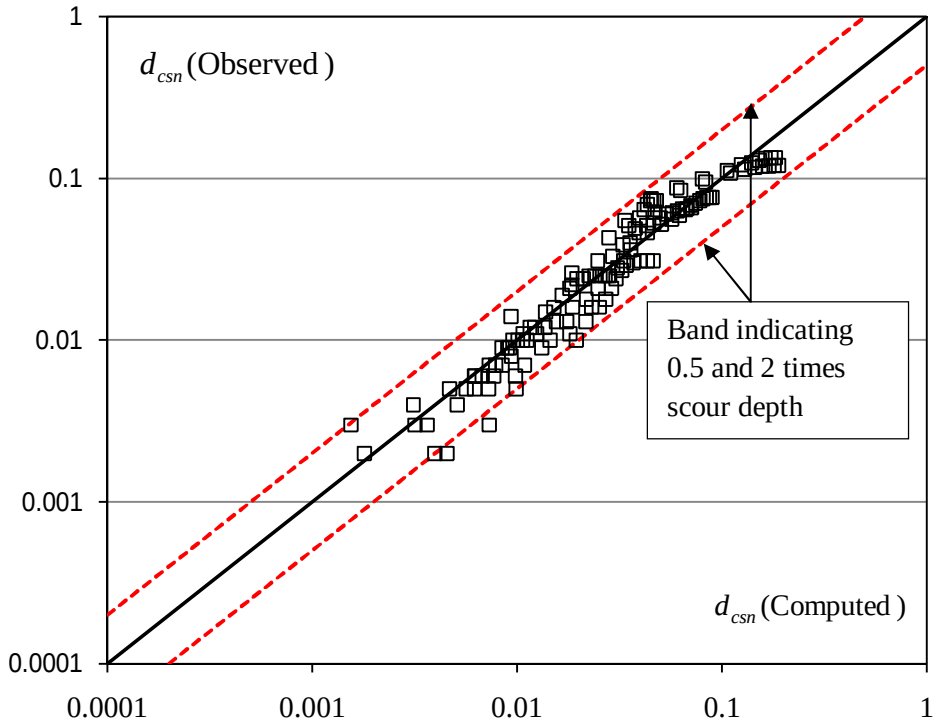

Fig. 5.36 Comparison of computed versus observed scour depth at nose of the submerged spur dike

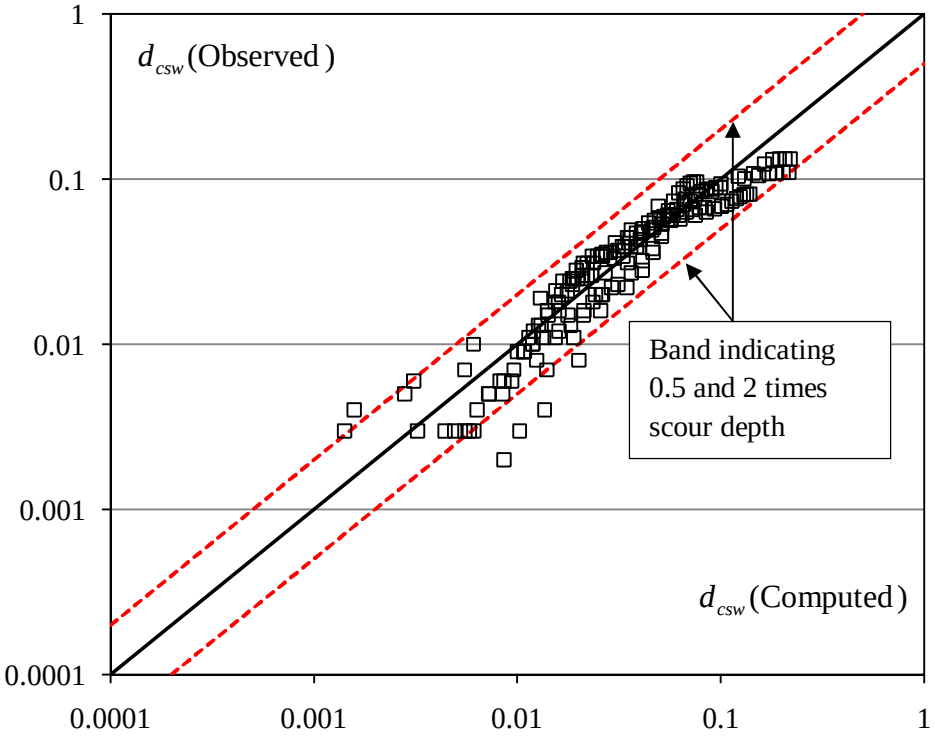

Fig. 5.37 Comparison of computed versus observed scour depth at the wake of the submerged spur dike

5.3.3 Graphical Comparisons for Temporal Variation of Depth of Scour around Submerged Spur Dike in Cohesive Sediments

The mathematical formulation presented in Chapter-III was used to set up the relationships for computing the temporal variation of depth of scour at nose and at the wake of submerged dike in cohesive sediment mixtures. A graphical comparison between observed and computed temporal variation of depth of scour around submerged dike is presented here.

5.3.3.1 Depth of scour at nose of the submerged spur dike in clay-gravel and clay-sand-gravel mixtures

Figures 5.38 and 5.39 are presented as illustrations which compare the observed and computed temporal variation of depth of scour at nose of the spur dike in clay-gravel and clay-sand-gravel mixtures respectively. Predicted values of scour depth were very close to their respective observed values. The comparison between observed and computed values was mostly satisfactory as shown in these and many other such figures (not shown here) which in turn confirms the conclusion that present model can predict the depth of scour in clay-gravel mixtures with reasonable accuracy.

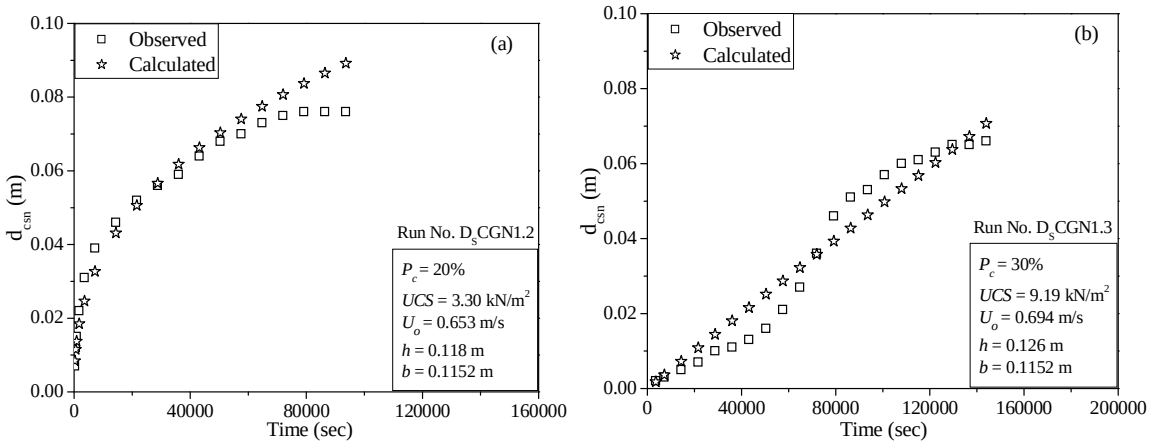

Fig. 5.38 Temporal variation of depth of scour at nose of the submerged spur dike in clay-gravel mixture

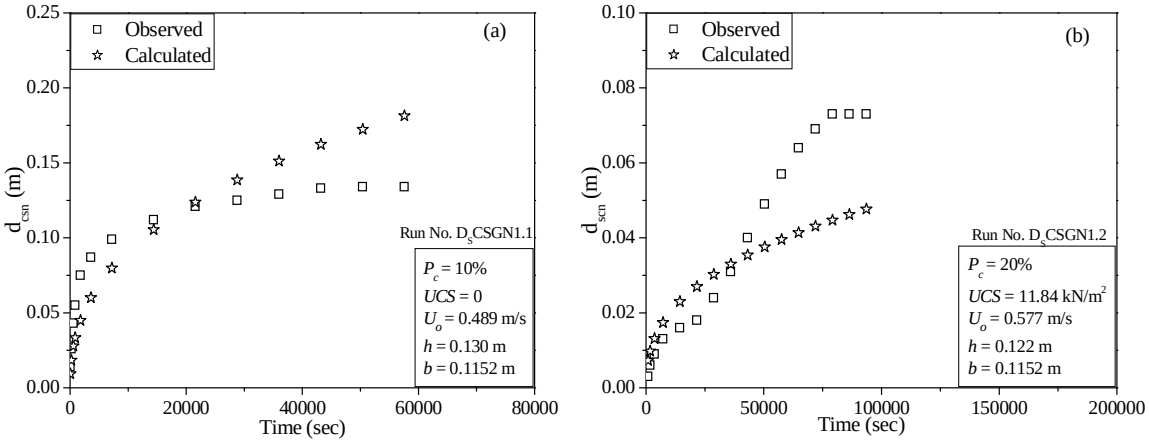

Fig. 5.39 Temporal variation of depth of scour at nose of the submerged spur dike in clay-sand-gravel mixture

5.3.3.2 Depth of scour at the wake of the submerged spur dike in clay-gravel and clay-sand-gravel mixtures

The depth of scour at the wake of the spur dike was also computed using the proposed model (Eq. 5.18). Figures 5.40 and 5.41 show as an illustration the comparison of observed and computed temporal variation of depth of scour at wake of the spur dike in clay-gravel and clay-sand-gravel mixture respectively. The results of model were mostly satisfactory in these and in many other runs. A poor comparison between observed and computed values is seen in Fig. 5.40 (a) for clay-gravel and 5.41 (a) for clay-sand-gravel mixtures.

The proposed model was similarly applied to all the other data collected in present study and the results obtained were similar to those reported here. It is however worth noting that in overall the model results have been mostly satisfactory.

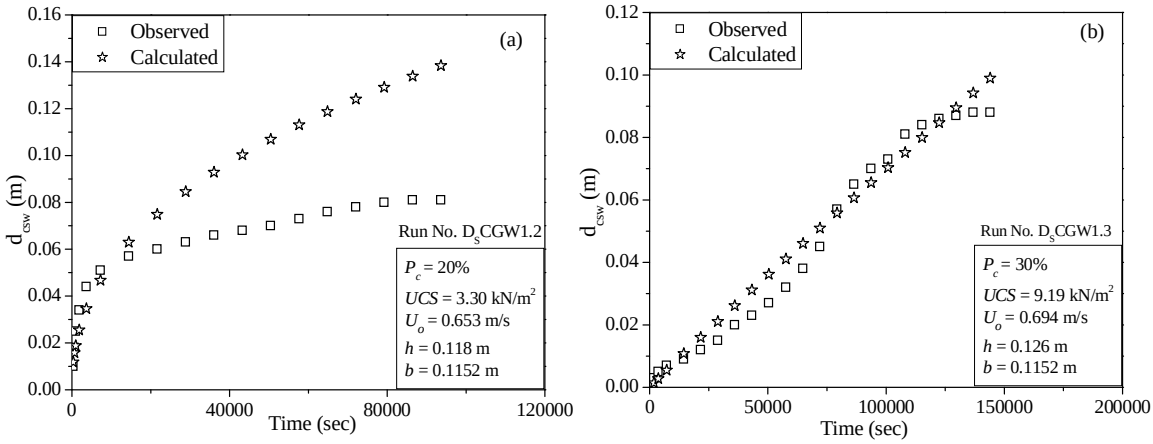

Fig. 5.40 Temporal variation of depth of scour at the wake of the submerged spur dike in clay-gravel mixture

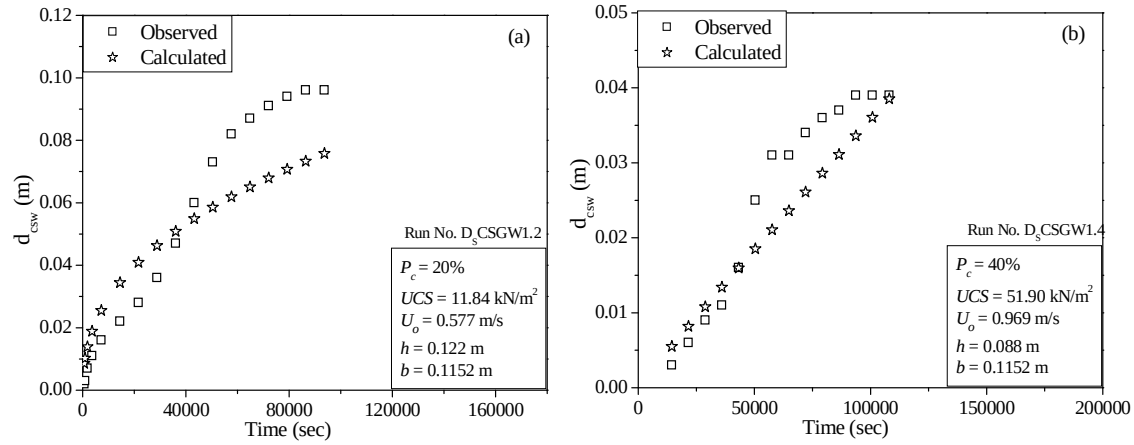

Fig. 5.41 Temporal variation of depth of scour at the wake of the submerged spur dike in clay-sand-gravel mixture

5.4 SCOUR AROUND BRIDGE PIER FOUNDED IN COHESIVE SEDIMENT MIXTURES

In the present study, two cylindrical iron pipes of outer diameter 11.52cm and 8.9cm were used in the experiments. The surfaces of the pipes were painted to give a smooth finish. The temporal variation of scour depth at sides as well as at the wake of the pier was measured by point gauge having an accuracy of ± 0.1 mm. The ranges of different measured parameters and experimental conditions are presented in Appendix-F and Appendix- G for cohesive sediment bed composed of clay-gravel mixtures and clay-sand-gravel mixtures respectively.

5.4.1 Visual Observations

5.4.1.1 Inception of scour around pier

From the laboratory experiments of cohesionless sediment, it was observed that scouring started from the sides of the pier immediately after the beginning of each experimental run and extended towards the nose of the pier. The maximum depth of scour was observed at the nose of the pier in cohesionless sediment. However, in case of cohesive sediment bed, the scouring started from the sides of the pier at a point where separation of flow occured as shown in Figs. 5.42(a) and 5.42(b) and maximum depth of scour was observed at the sides of the pier. Ansari (1999) and Kumar (2011) stated that the scour always initiates from the sides of the pier. Measurement of the shear stress on a rigid flat bed around the pier by Hjorth (1975), Ettema (1980) and Ahmed and Rajratnam (1998) showed that the average shear stress at the pier was approximately ten times the shear stress produced by the approach flow irrespective of the flow condition and the pier size, so long as the contraction caused by the pier is not severe.

From the experiments, it was observed that at clay content $\leq 20\%$ in cohesive sediment mixture, the scour hole formed by the removal individual particles. It was also observed that the rate of sediment removal was faster at lower clay percentage compared to higher clay content. At higher percentage of clay, scouring started with removal of sediment in the form of flakes. Similar process of sediment inception was observed in clay-sand mixture bed (Ansari et al., 2002) and in mixtures of gravel-clay and gravel-sand-clay in scour depth around pier (Kothyari et al., 2014).

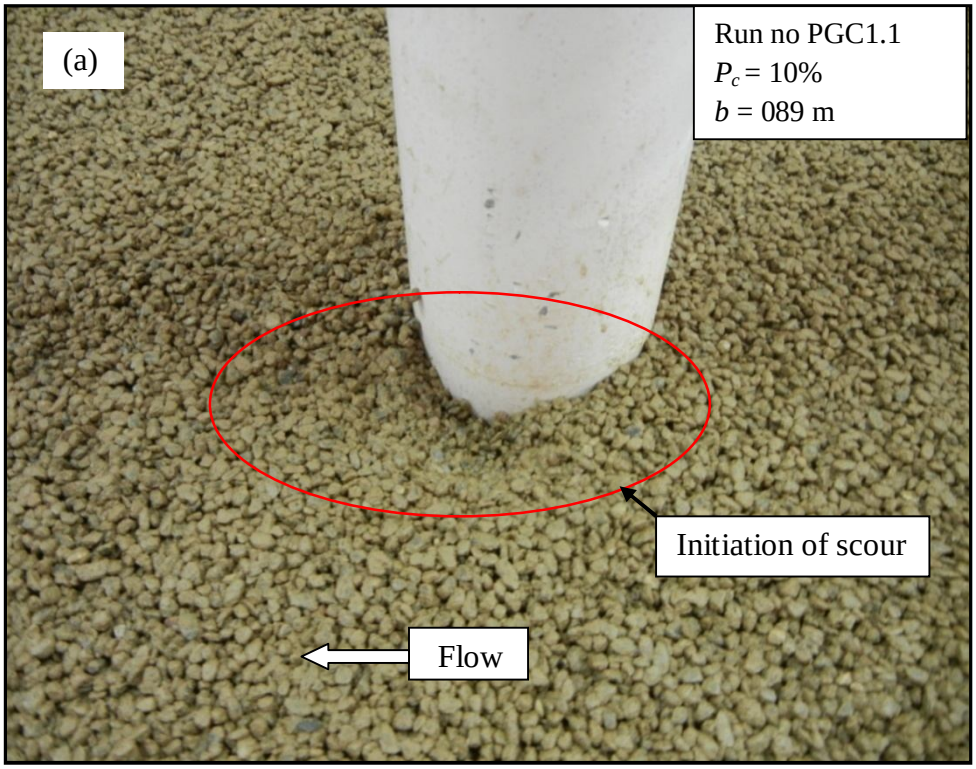

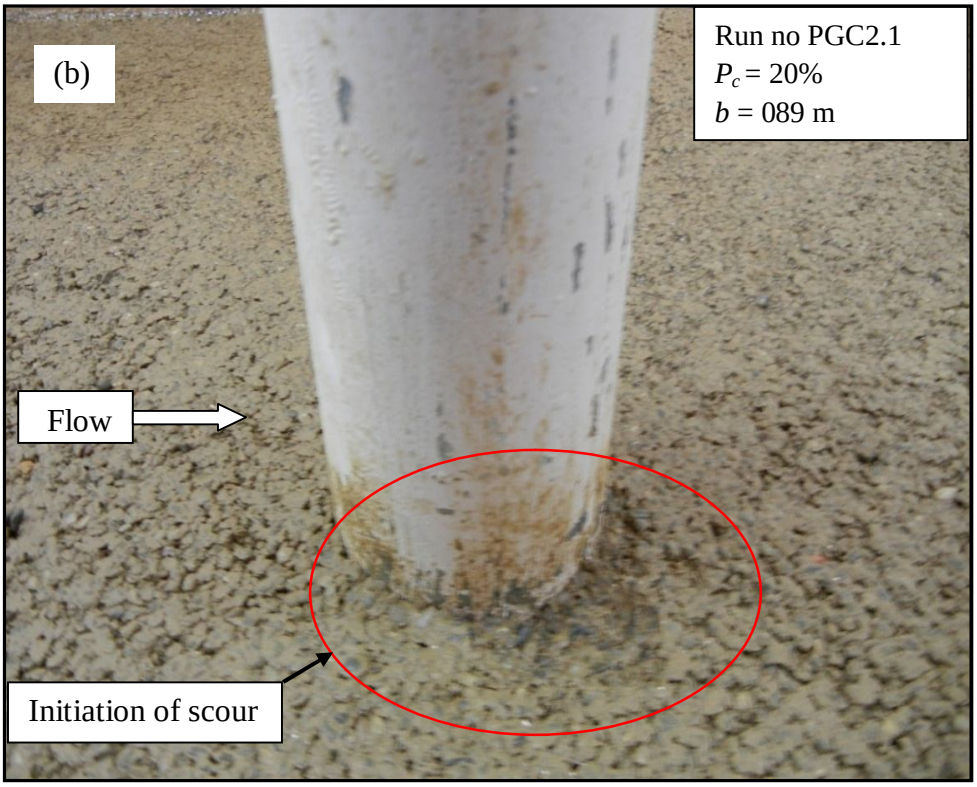

Fig. 5.42 (a-b) Initiation of scour around bridge pier in cohesive sediment mixtures

5.4.1.2 Scour around pier

The pattern of scour around bridge pier was more or less similar to cohesionless sediment at clay content $\leq 10\%$ in clay-gravel and clay-sand-gravel mixture. In such cases the significant scour occured at the nose of the bridge pier and the shape of the scour hole was conical in plan. The maximum depth of scour was observed at nose of the bridge pier in both types of cohesive sediment mixtures (at 10% clay content). No scour depth occured at nose of the pier when clay percent was increased from 20% to 50% in clay-gravel and clay-sand-gravel mixtures. At 20% to 50% clay in clay-gravel and clay-sand-gravel mixtures, the maximum depth of scour was observed to occur at the sides of the pier.

In all cases, no sediment deposition was observed in wake of the pier while the experiments conducted under clear water condition on cohesive sediment mixtures. It was contrary to experiments conducted on cohesionless sediment bed in which significant deposition was observed to occur at wake region of the pier. Different shapes of scour hole were observed with various clay content presents in the sediment mixture of clay-gravel [Figs 5.43 (a-b)] and clay-sand-gravel [Figs 5.44 (a-b)]. The scour hole shape changed with the augment of clay content in sediment bed. At clay content $\geq 40\%$ in sediment mixtures, comparatively larger depth of scour was observed in clay-gravel mixture [Fig. 5.43 (b)] than that in clay-sand-gravel mixture [Fig. 5.44 (a-b)].

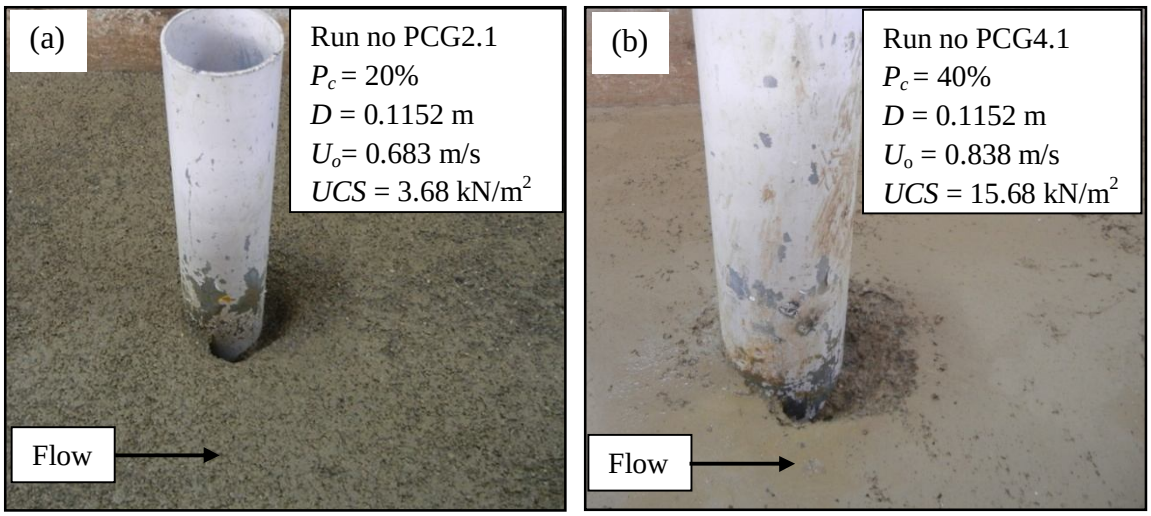

Fig. 5.43 (a-b) Patterns of scour hole around bridge piers in clay-gravel mixtures

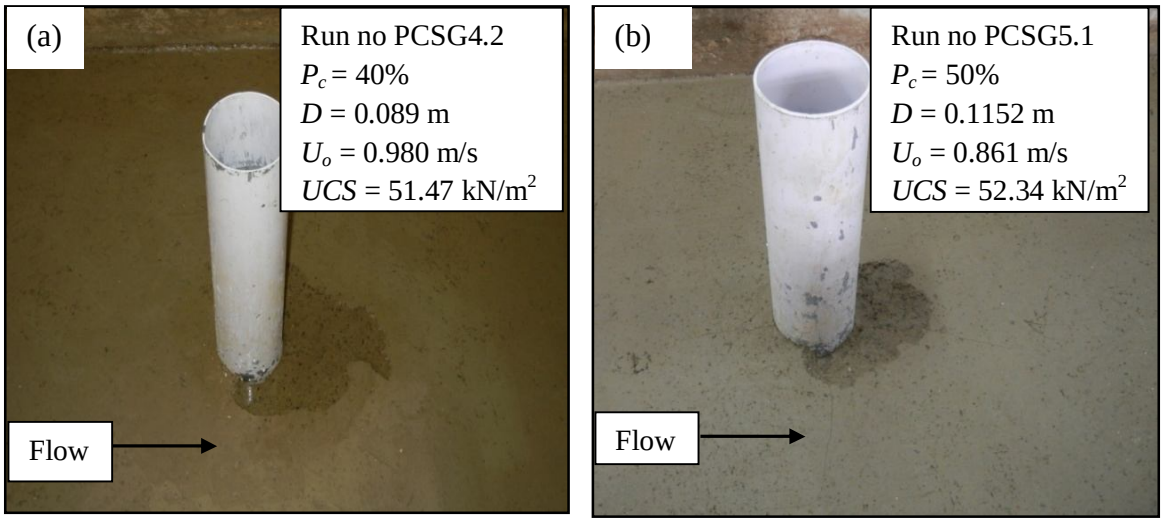

Fig. 5.44 (a-b) Patterns of scour hole around bridge piers in clay-sand-gravel mixtures

5.4.1.3 Influence of clay percentage and unconfined compressive strength on scour depth

To investigate the influence of clay percentage and unconfined compressive strength of the mixtures of cohesive sediment on scour depth at side (d_{cps}) and at the wake (d_{cpw}) of the pier, Figs. 5.45 to 5.48 were prepared. From these figures, it was observed that the maximum scour depth reduced with an increase of clay fraction and unconfined compressive strength in cohesive sediment mixtures. Similar results were also obtained in experiment conducted with spur dike (partially submerged and submerged) embedded in cohesive sediment mixtures consisting of clay-gravel and clay-sand-gravel (described in section 5.2 and section 5.3).

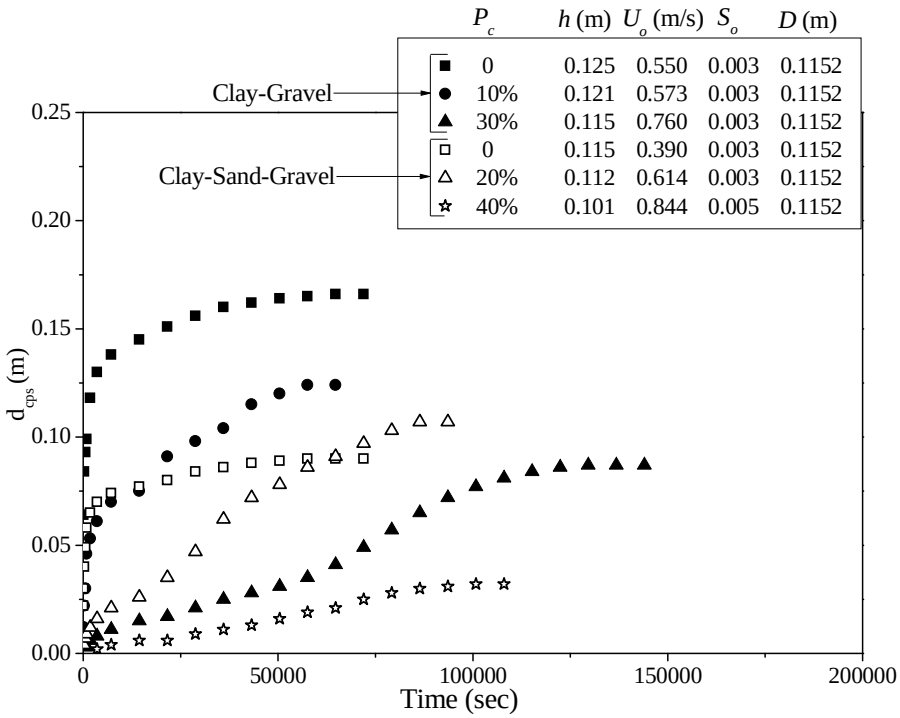

Fig.5.45 Variation of scour depth with time at sides of the pier for various clay percentages in clay-gravel and clay-sand-gravel mixtures

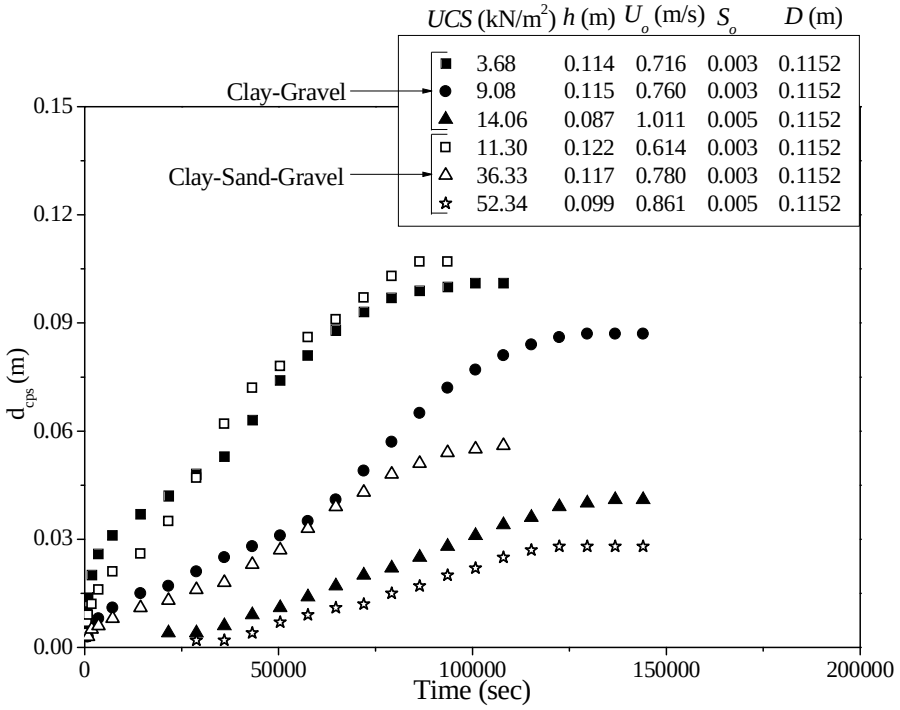

Fig.5.46 Variation of scour depth with time at sides of the pier for various unconfined compressive strength of clay-gravel and clay-sand-gravel mixtures

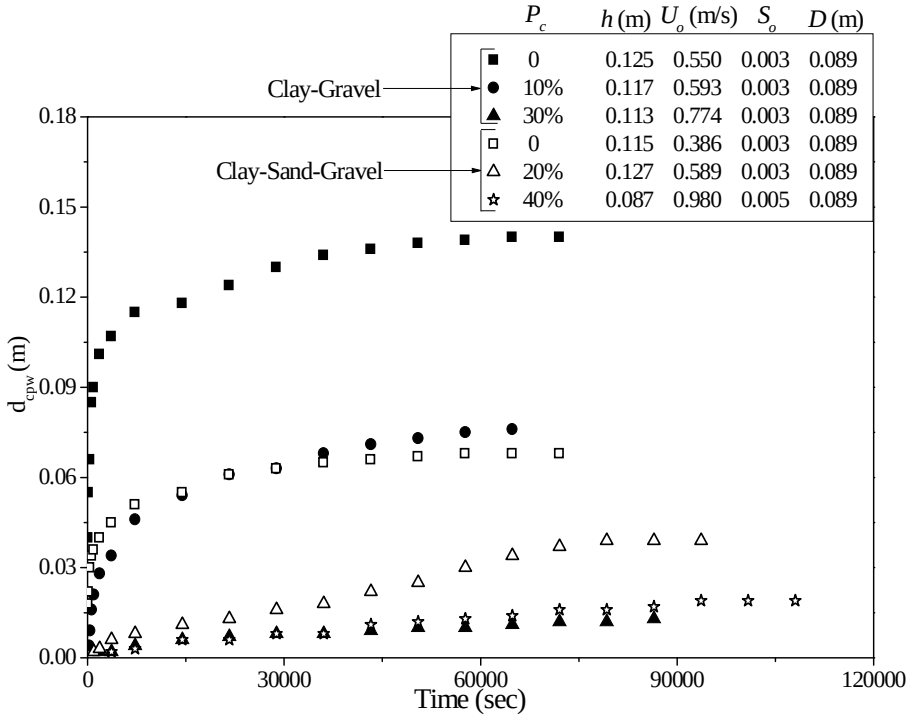

Fig. 5.47 Variation of scour depth with time at the wake of the pier for various clay percentages in clay-gravel and clay-sand-gravel mixtures

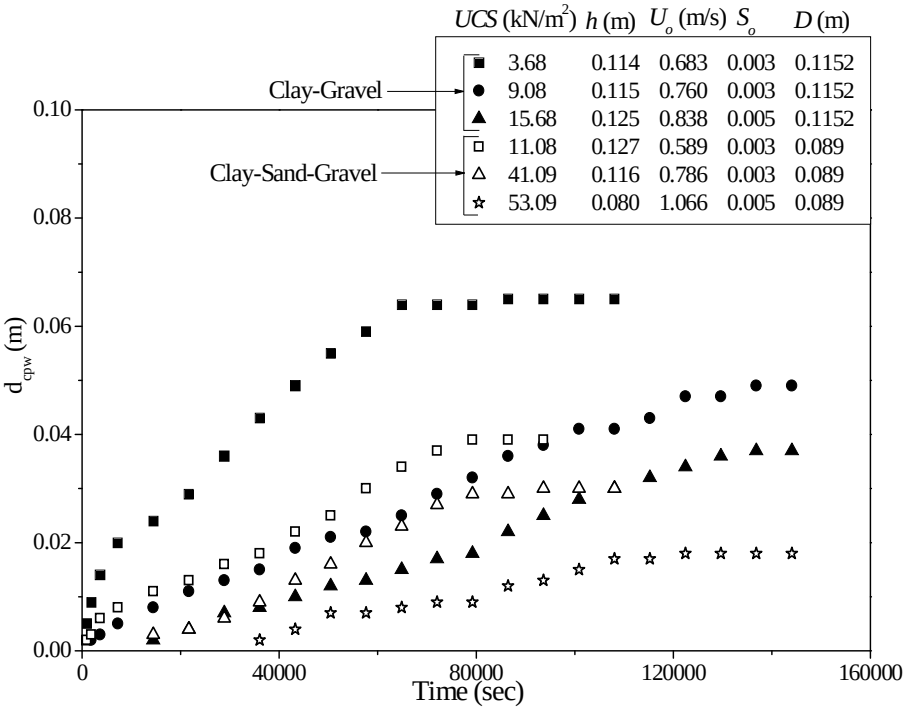

Fig. 5.48 Variation of scour depth with time at the wake of the pier for various unconfined compressive strength of clay-gravel and clay-sand-gravel mixtures

5.4.2 Depth of Scour at Sides and at the Wake of the Pier in Cohesive Sediment Mixtures

To quantify the depth of scour around circular piers founded in cohesive sediments in comparison to those of cohesionless sediments of similar bulk characteristics, Figs. 5.49 and 5.50 were prepared. These figures were prepared using the present experimental data which depict the temporal variation of depth of scour at sides and at the wake of the pier for various percentages of clay present in the bed material consisting of clay-gravel and clay-sand-gravel mixtures respectively. In Figs. 5.49 and 5.50, d_{ps} and d_{pw} are the depth of scour (at sides and at the wake of the pier respectively) computed using Kothyari et al. (2007) model considering the clay-gravel mixture to be cohesionless and; d_{cps} and d_{cpw} are the observed depth of scour at sides and at the wake of pier in cohesive sediment mixtures respectively. It was observed in these figures that the depth of scour in cohesive sediment was much smaller as compared to corresponding values of depth of scour calculated by considering sediments as cohesionless. However, Figs. 5.49 and 5.50 indeed revealed that depth of scour in cohesive sediment mixture was drastically different due the presence of clay in the mixture but a systematic variation with clay content present among the mentioned data was noted. Similar results were also obtained in the experiments conducted with spur dike (partially submerged and submerged) embedded in cohesive sediment mixtures (described in section 5.2 and 5.3).

To quantify the effect of shear strength of cohesive sediments on the depth of scour, the variation of *UCS* with corresponding depth of scour was studied. Figures 5.51 and 5.52 were prepared in which the data was classified as per three ranges of *UCS* in clay-gravel and clay-sand-gravel mixtures. The ability of the cohesive sediment to resist the scour increased with the increase in *UCS* is well illustrated by Figs. 5.51 and 5.52. Such results were reported earlier by Robinson and Hanson (1995) in the context of head cut erosion testing of clay-silt-sand mixtures and by Jain and Kothyari (2009, 2010) in the context of detachment of clay-gravel and clay-sand-gravel mixtures.

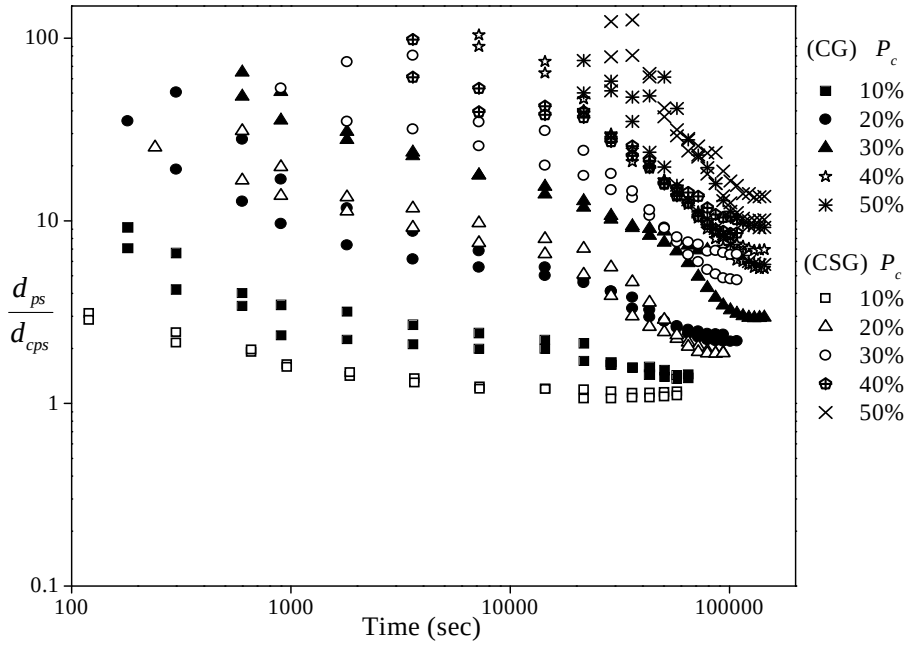

Fig. 5.49 Temporal variation of dimensionless scour depth with clay percentage at sides of the pier in clay-gravel and clay-sand-gravel mixtures

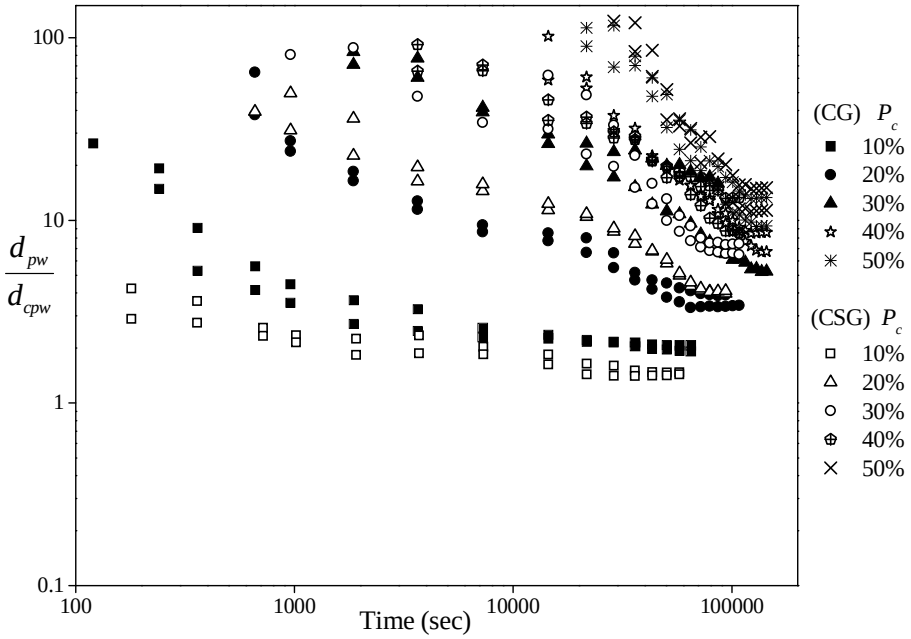

Fig. 5.50 Temporal variation of dimensionless scour depth with clay percentage at the wake of the pier in clay-gravel and clay-sand-gravel mixtures

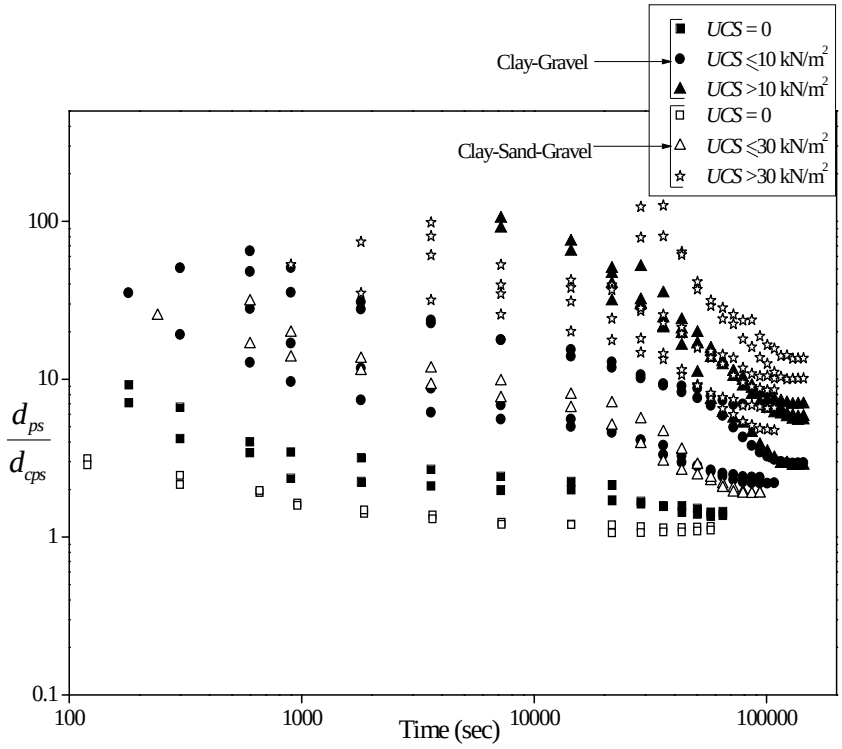

Fig. 5.51 Temporal variation of dimensionless scour depth with UCS at sides of the pier in clay-gravel and clay-sand-gravel mixtures

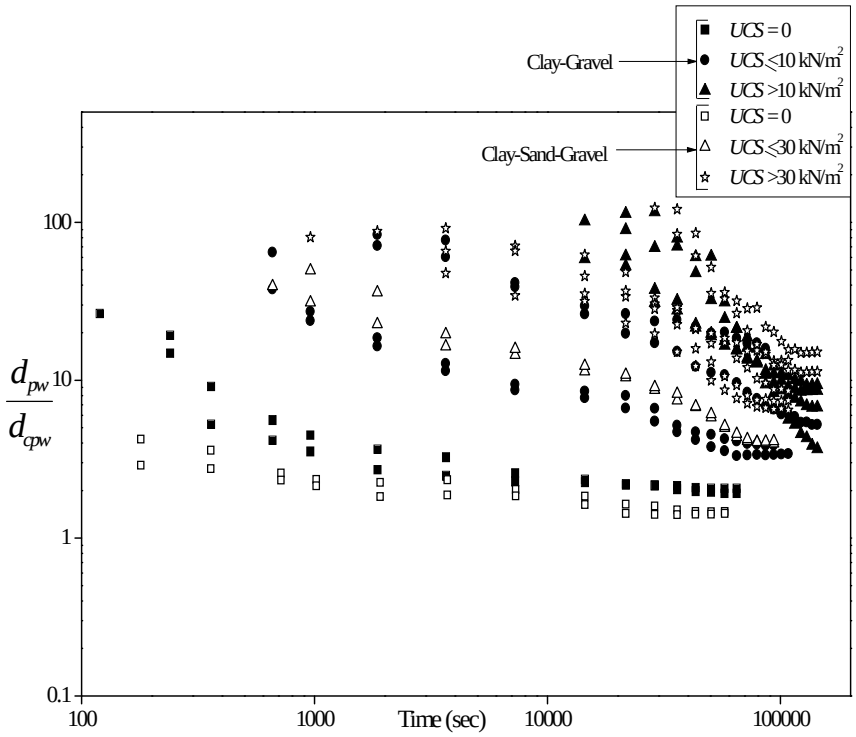

Fig. 5.52 Temporal variation of dimensionless scour depth with UCS at the wake of the pier in clay-gravel and clay-sand-gravel mixtures

The functional relationships for the computation of depth of scour at sides and at the wake of pier in clay-gravel and clay-sand-gravel mixtures derived in Chapter- III, is rewritten here as

$$\frac{d_{cp(s/w)}}{d_{p(s/w)}} = f\left(P_c, \frac{C_*}{\phi_*}, \frac{\gamma_d}{\gamma_w}, UCS_*, t_* \right) \tag{5.19}$$

As observed in Appendix- H and Appendix- I, the range of (γ_d/γ_w) is from 1.30 to 1.99 for the data collected in this study. The analysis of variable (γ_d/γ_w) with scour depth showed that the variation of (γ_d/γ_w) in this small range could not completely elucidate the variation in scour depth around pier. Similar results were also obtained in experiments conducted with partially submerged and submerged spur dike embedded in cohesive sediment mixtures. Therefore, this variable was eliminated from further analysis and new functional relationship can be considered as:

$$\frac{d_{cp(s/w)}}{d_{p(s/w)}} = f\left(P_c, \frac{C_*}{\phi_*}, UCS_*, t_* \right) \tag{5.20}$$

The functional form given in the form of Eq. (5.20) was used to compute the scour depth around pier in mixture of clay-gravel and clay-sand-gravel mixtures. The value of $d_{p(s/w)}$ in the Eq. (5.20) was obtained using relationship suggested by Kothyari et al. (2007) for the calculation of scour depth around pier in uniform and non-uniform cohesionless sediments.

The variation of scour depth with C_*/ϕ_* did not show significant influence of C_*/ϕ_* on scour depth. A similar result was also observed by Kothyari et al. (2014) in pier scour in clay-gravel and clay-sand-gravel mixtures. Therefore, the variable C_*/ϕ_* was also removed from the further analysis and then Eq. (5.20) is re-written for the computation of scour depth at sides and at the wake of the pier as:

$$\frac{d_{cp(s/w)}}{d_{p(s/w)}} = f[(P_c), (1+UCS_*), t_*] \tag{5.21}$$

Above relation is valid for cohesive sediment mixtures only. It is important to make use of the variable $(1+UCS_*)$ in place of UCS_* so that Eq. (5.21) is suitable when (UCS = 0) as well. Equation (5.21) is used to find out the scour depth at sides and at the

wake of the pier founded in cohesive sediment mixtures consisting of clay-gravel and clay-sand-gravel. Analysis of the presently collected data (all experimental runs) revealed that scour depth at sides/ wake of the pier is inversely proportional to P_c (Figures 5.49 and 5.50) and $1+UCS_*$ (Figures 5.53 and 5.54) for both the sediment mixtures.

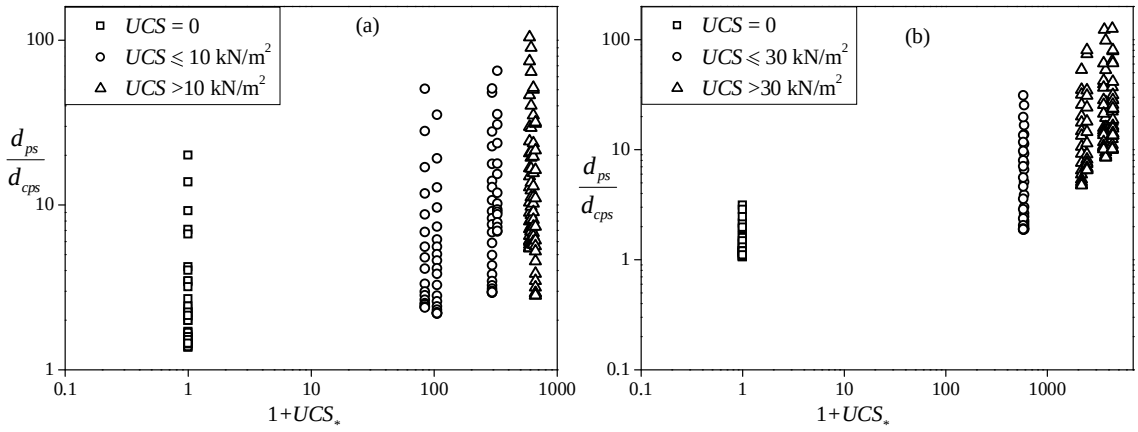

Fig. 5.53 Variation of dimensionless scour depth with $1+UCS_*$ at sides of the pier in (a) clay-gravel and (b) clay-sand-gravel mixtures

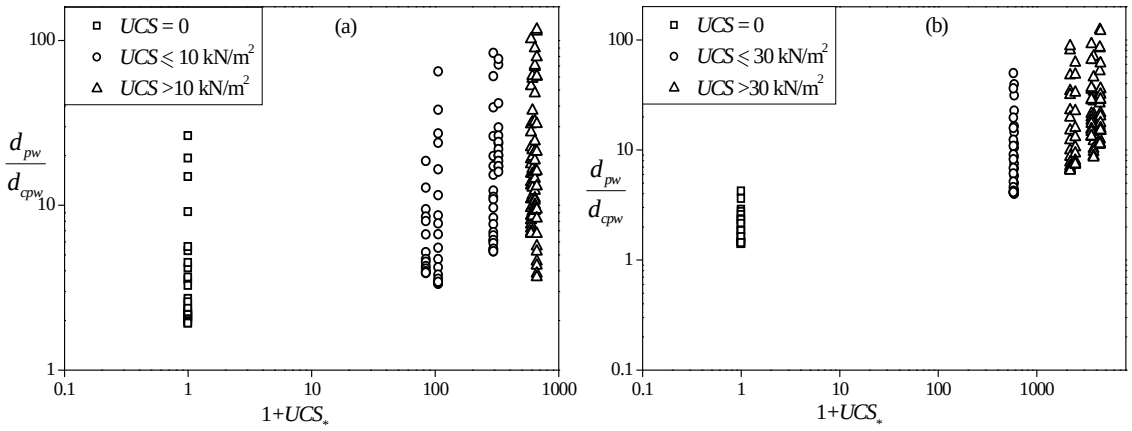

Fig. 5.54 Variation of dimensionless scour depth with $1+UCS_*$ at the wake of the pier in (a) clay-gravel and (b) clay-sand-gravel mixtures

Similar to analysis conducted in the case of spur dikes, whole data have been analyzed in two ranges of clay perecentages. Multiple nonlinear regression analysis was used to find out new relationships for scour depth at sides and at the wake of the pier using all pertinent dimensionless parameters. Following relationships were proposed for describing the variation of (d_{cps}) and (d_{cpw}).

For depth of scour at sides of the pier in clay-gravel and clay-sand-gravel mixtures

$$\frac{d_{cps}}{d_p} = F_{ps} \tag{5.22}$$

Where, F_{ps}= parameter that represents cohesion of clay-gravel and clay-sand-gravel mixtures at sides of the pier and is expressed as

$$F_{ps} = \mathrm{m}_o\left[(\mathrm{P_c})^{m_1}(1+UCS_*)^{m_2}(t_*)^{m_3}\right] \tag{5.22a}$$

With

$m_o = 0.00024; m_1 = -1.226; m_2 = -0.0914; m_3 = 0.3385$ for $10\% \le P_c \le 20\%$

(Adjusted R^2= 0.844)

and

$m_o = 9.68\times10^{-7}; m_1 = -2.653; m_2 = -0.3785; m_3 = 0.656$ for $30\% \le P_c \le 50\%$

(Adjusted R^2= 0.813)

For depth of scour at the wake of the pier in clay-gravel and clay-sand-gravel mixtures

$$\frac{d_{cpw}}{d_p} = F_{pw} \tag{5.23}$$

Where, F_{pw}= parameter that represents cohesion of clay-gravel and clay-sand-gravel mixtures at the wake of pier and is expressed as

$$F_{pw} = \mathrm{n}_o\left[(\mathrm{P_c})^{n_1}(1+UCS_*)^{n_2}(t_*)^{n_3}\right] \tag{5.23a}$$

With

$n_o = 5.9\times10^{-5}; n_1 = -1.678; n_2 = -0.346; n_3 = 0.342$ for $10\% \le P_c \le 20\%$

(Adjusted R^2= 0.853)

and

$n_o = 2.41\times10^{-8}; n_1 = -2.42; n_2 = -0.253; n_3 = 0.747$ for $30\% \le P_c \le 50\%$

(Adjusted R^2= 0.808)

The derived relationships viz; Eqns. 5.4 - 5.5, 5.17- 5.18 and 5.22 - 5..23 are useful to determine the temporal evolution of scour depth around spur dikes/ pier in the field conditions for the known value of clay percentage and unconfined compressive strength of cohesive sediment mixtures. The flow conditions and spur dikes/ pier characteristics are taken care by Kothyari et al. (2007) relationships in the above equations.

The comparison between observed depth of scour at side (d_{cps}) and at the wake (d_{cpw}), and computed depth of scour using Eq. 5.22 and Eq. 5.23 for sides and wake of the pier respectively are presented in Figs. 5.55 and 5.56.

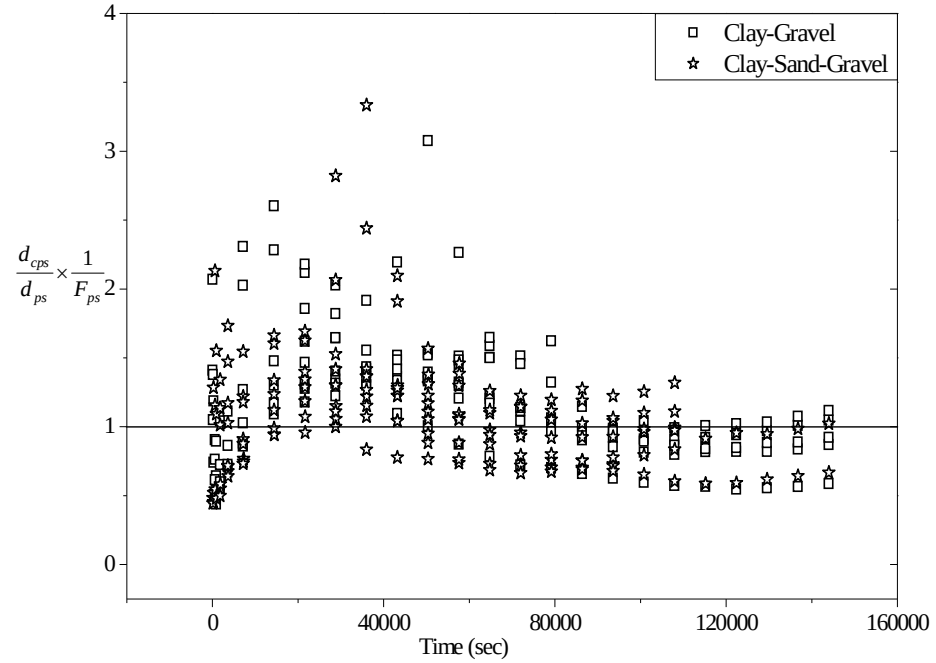

Fig. 5.55 Temporal variation of ratio between observed and calculated depth of scour at sides of the pier in clay-gravel and clay-sand-gravel mixtures

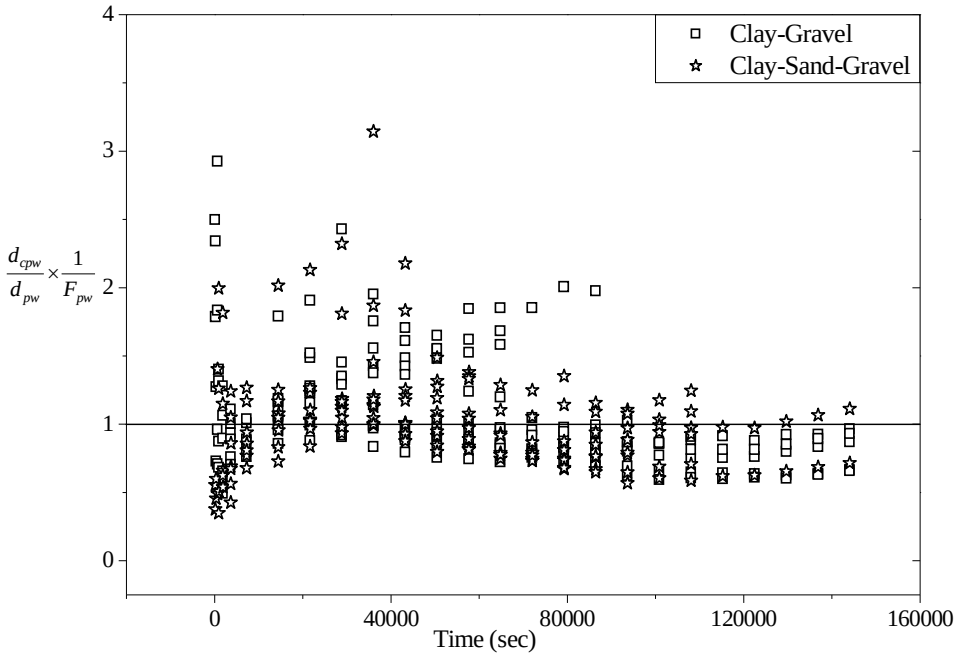

Fig. 5.56 Temporal variation of ratio between observed and calculated depth of scour at the wake of the pier in clay-gravel and clay-sand-gravel mixtures

The goodness of fit between observed and calculated values of scour depth was analyzed by obtaining the following parameters viz; discrepancy ratio (R_i), mean discrepancy ratio $(\overline{R}_i)$, standard deviation of the estimate (σ), average discrepancy ratio based on difference $(\overline{R}_d)$, average discrepancy ratio based on logarithm ratio $(\overline{D}_a)$ and, standard deviation of estimate based on difference (σ_d) and logarithm (σ_a). These parameters have already been described in previous section 5.2 (Eq. 5.6 to Eq. 5.13).

The comparison between observed and computed values of scour depth at sides and at the wake of the pier founded in mixtures of cohesive sediment containing clay-gravel and clay-sand-gravel based on discrepancy ratio and standard deviation is summarized in Table 5.5. Evaluation based on $\overline{D}_a, \sigma_a$, $\overline{R}_d$ and σ_d parameters is presented in Table 5.6.

Table 5.5 Comparison between observed and computed value of scour depth at sides and at the wake of the pier in the mixtures of cohesive sediments containing clay-gravel and clay-sand-gravel based on discrepancy ratio and standard deviation

Depth of scour at	Percent of data in Range			Mean ($\overline{R}$)	Standard Deviation (σ)	Number of data sets (N)
	0.75-1.25	0.5-2.0	0.33-3			
Side	52.57	92.57	99.42	1.1134	0.4309	350
Wake	60.29	94.03	99.70	1.0759	0.4225	335

Table 5.6 Comparison of computed and observed values of scour depth at sides and at the wake of the pier in the mixtures of cohesive sediments containing clay-gravel and clay-sand-gravel on the basis of logarithm ratio and difference between computed and observed results

Depth of scour at	$\overline{D}_a$	σ_a	$\overline{R}_d$	σ_d	Number of data sets (N)
Side	0.01828	0.1551	0.1134	0.01459	350
Wake	0.00457	0.1490	0.0760	0.0103	335

The comparison of observed scour depth and the values calculated from the proposed Eq. (5.22) for sides and Eq. (5.23) for wake of the pier are presented in Fig. 5.57 and Fig. 5.58 respectively. It is evident from these Figures that the proposed relationships yielded satisfactory outcome with maximum error of two folds for 92.5% of the total data for side and 94% of total data for wake of the pier respectively. The scattering of data in Fig. 5.57 and Fig. 5.58 are large, but it is acceptable in the perspective of parallel results reported by Kothyari et al. (2014) for pier scour and by Jain and Kothyari (2009, 2010) for transport of cohesive sediments containing clay-gravel and clay-sand-gravel. Similar results were also obtained in experiments conducted with partially submerged and submerged spur dikes founded in cohesive sediment mixtures.

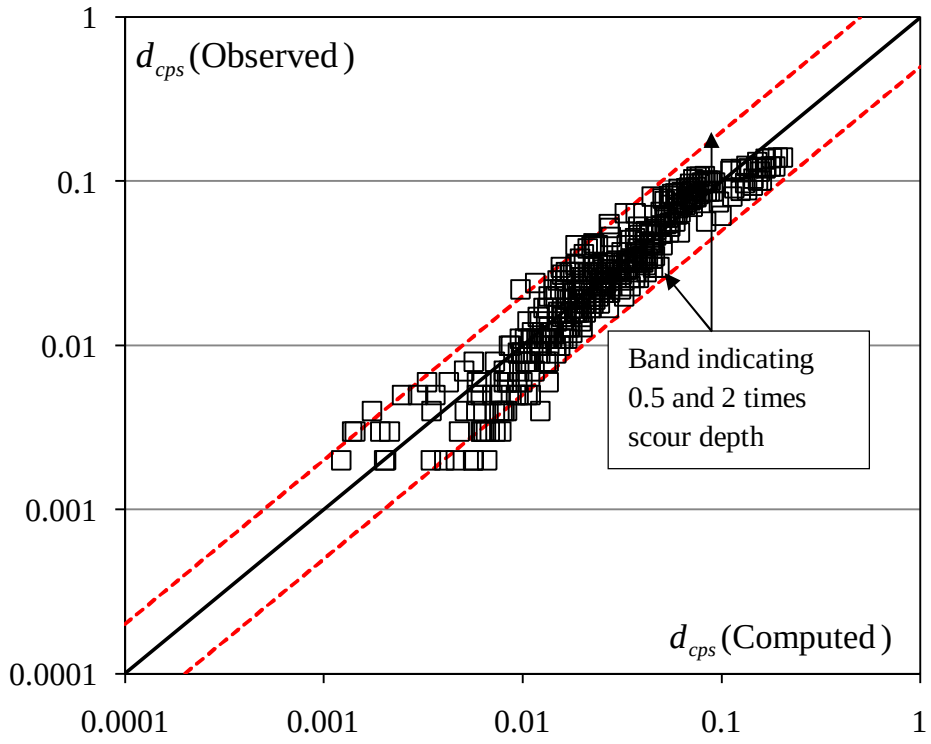

Fig. 5.57 Comparison of computed versus observed depth of scour at sides of the pier

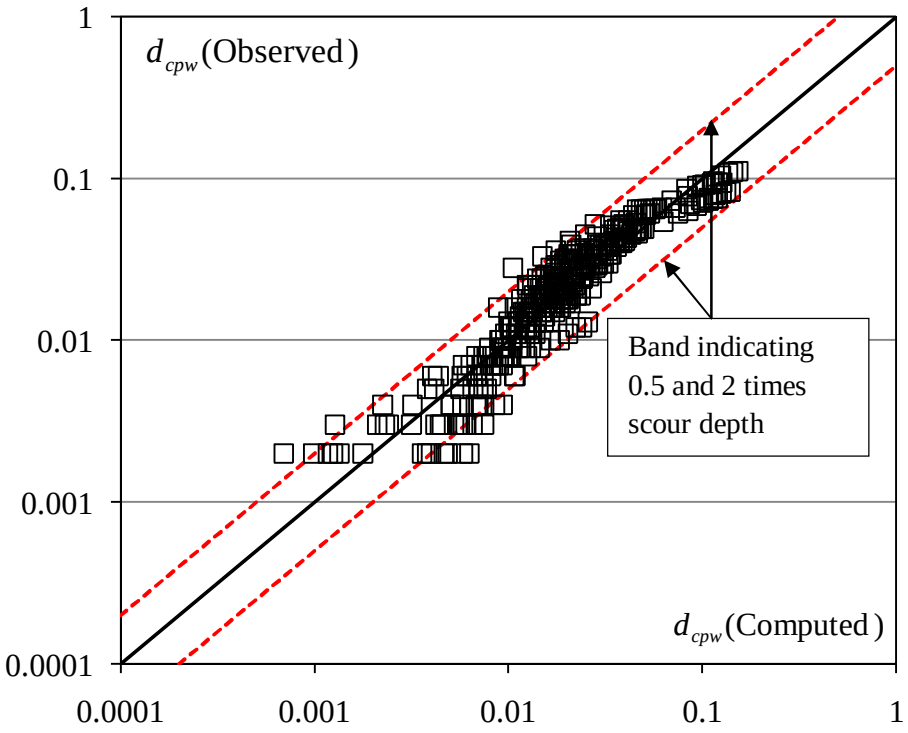

Fig. 5.58 Comparison of computed versus observed depth of scour at the wake of the pier

Scour around hydraulic structures takes place under the dynamic process of entrainment, deposition and transport (Kothyari et al; 2014). The bed shear stress gets altered as soon as erosion starts because of non-uniform erosion pattern and also due to cohesive sediment in suspension which may cause drag reduction (Jain and Kothyari, 2009). As a result, observed scour depth over a time period can be considerably higher and lower than computed scour depth in case of cohesive sediment mixtures. Large scattering of data in Figs. 5.17 to 5.18 in the case of partially submerged spur dike, Figs. 5.36 to 5.37 in the case of submerged spur dike and Figs 5.57 to 5.58 in the case of pier is attributable to this phenomenon.

5.5 FLOW CHARACTERISTICS AROUND PARTIALLY SUBMERGED AND SUBMERGED SPUR DIKES

One of the main objectives of the present investigation is to study the flow pattern around the spur dikes (partially submerged and submerged). To fulfil this objective Vectrino^{+} ADV was used to measure the instantaneous three components of velocity. Measurement of flow structure at different measuring nodes was done as per the experimental details given in the Chapter – IV (Fig. 4.12). The data for cohesive sediments consisting of clay-gravel (30% Clay + 70% Gravel) was chosen for the study of flow pattern around partially submerged and submerged spur dikes. The flow structure studied herein comprises of the vertical distribution of longitudinal velocity, turbulence intensities, Reynolds stresses and turbulence kinetic energy. The discussion on the flow pattern in the scour hole developed in cohesive sediment consisting clay-gravel bed is made. The discussion on quadrant analysis is presented at the last.

5.5.1 Flow Field around Spur Dike

In Chapter-IV, the methodology of measurements through ADV is explained. The flow field was measured at various points as shown in Fig. 4.13. In longitudinal direction flow field was measured at x = -40, -15, -5, 0, 5, 10, 15, 20, 40, and 80 cm from the spur dike. The spur dike was installed at 0 (zero) point, and the negative and positive sign represents the upstream and downstream side of the spur dike, respectively. In the transverse direction for both upstream and downstream, velocity was measured at y = 5, 10, 15, 20, 25, 35 and 50 cm up to the center of the flume by taking right hand side wall of the channel at 0 (zero). The analysis of measuring points existing nearby the spur dike are presented and explained in detail.

5.5.1.1 Vertical distribution of longitudinal velocity

The variation of time averaged component of velocity (longitudinal component u) in various planes is shown in Figs. 5.59 (a-d). The velocity component was normalized by the velocity of approach flow U_o. The vertical distance z (negative and positive value of z represents the depth below and above the initial bed level respectively) was normalized at each location by an approaching flow depth h. Further, it is to be clarified that $z = 0$ denotes the initial level of channel bed (i.e. level of the channel bed before the commencement of scour).

Figure 5.59 (a) and Fig. 5.59 (c) show the vertical distribution of longitudinal velocity around partially submerged and submerged spur dike respectively. The value of longitudinal velocity u was observed to increase towards downstream of dike. It was also observed to increase away from right wall where spur dike was installed. At upstream of the spur dike (partially submerged and submerged) and in the plane y = 5cm and 10cm, the velocity component u was observed to reduce gradually towards the spur dike. Beyond these planes towards left wall the value of u was observed to increase. Very small value of u (negative) is obtained in the region immediate downstream of spur dike (i.e. x = 5 to 10cm and y = 5 to 10cm). In the wake region of spur dike and in the plane y = 15 to 25 cm, large values of velocity component u were obtained from section x = 5cm towards x = 20cm. At these points values of u component varied from 1.15 – 1.55 times of the approaching flow velocity for partially submerged spur dike, whereas, it varied from 0.93 to 1.50 times of the approaching flow velocity for submerged spur dike. At the point (5, 15) the value of u varied from 1.24 to 1.48 times the approaching flow velocity for partially submerged dike and 1.07 to 1.38 times the approaching flow velocity for submerged dike (velocity profiles were measured from bed surface to water surface).

Figure 5.59 (b) and Fig. 5.59 (d) show the vertical distribution of longitudinal velocity at y = 15cm from the right wall at different values of x around the partially submerged and submerged spur dike respectively. From the figures, it is observed that the value of velocity component u decreased from x = -40 to x = - 15; thereafter it increased up to x = 10 for partially submerged dike and x = 20 for submerged spur dike. It again decreased up to x = 80cm in both types of spur dikes. The velocity profile taken at location (10, 15) showed the maximum value of longitudinal velocity component u. The longitudinal velocity at (10, 15, 0.5) and (10, 15, 3) were observed to be 1.48 and 1.45 times the approaching flow velocity respectively for partially submerged spur dike. Similarly, at locations (10,15, 0.5) and (10, 15, 6) the value of u is 1.12 and 1.40 times the approaching flow velocity respectively (whereas it is 1.32 times the approaching flow velocity at 3cm above from the bed surface) for submerged dike . Hence, the value of u was large towards the bed surface for partially submerged dike than submerged spur dike.

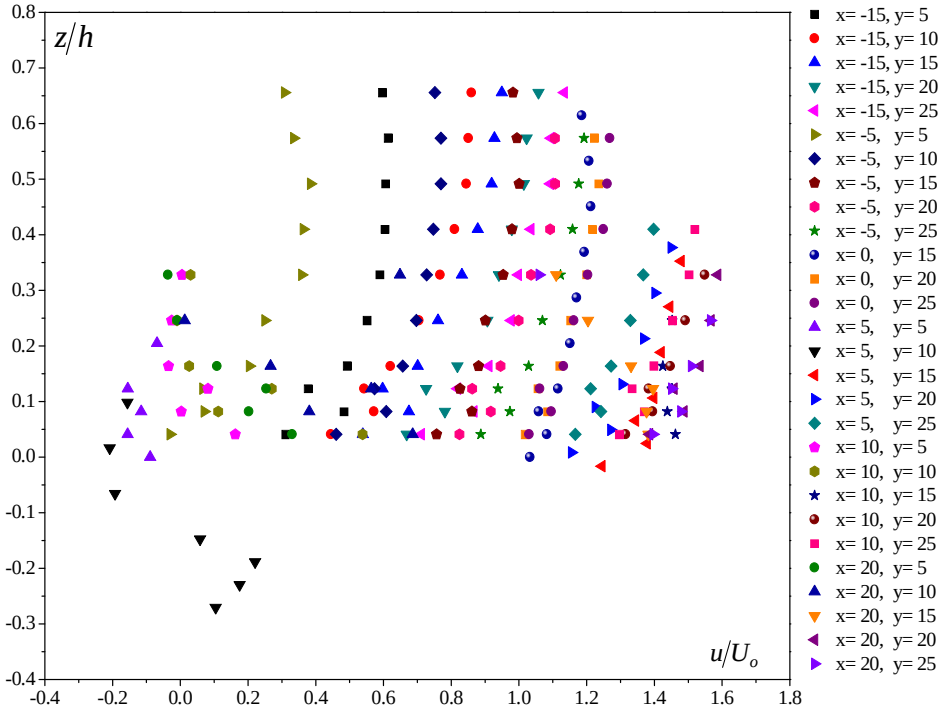

Fig. 5.59 (a) Normalized profiles of longitudinal velocity component u around partially submerged spur dike

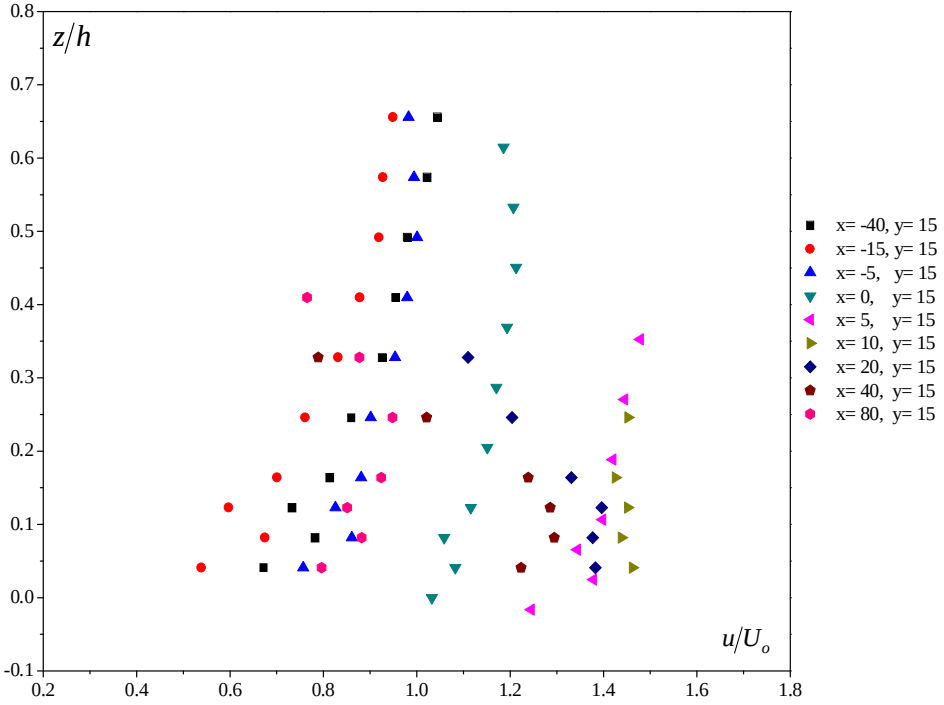

Fig. 5.59 (b) Normalized profiles of longitudinal velocity component u at front of the partially submerged spur dike (y =15)

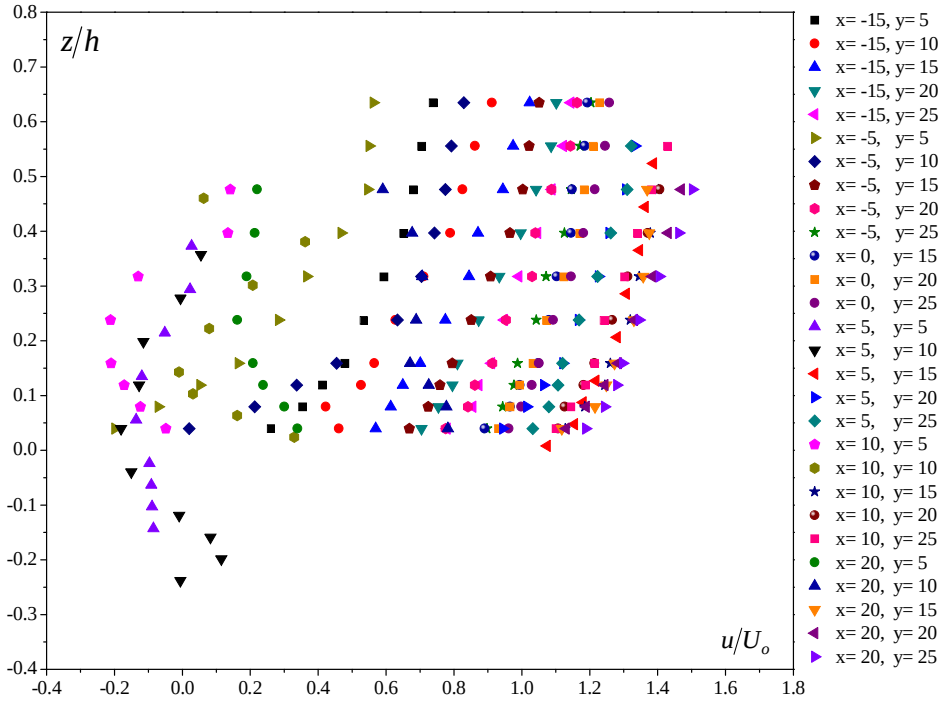

Fig. 5.59 (c) Normalized profiles of longitudinal velocity component u around submerged spur dike

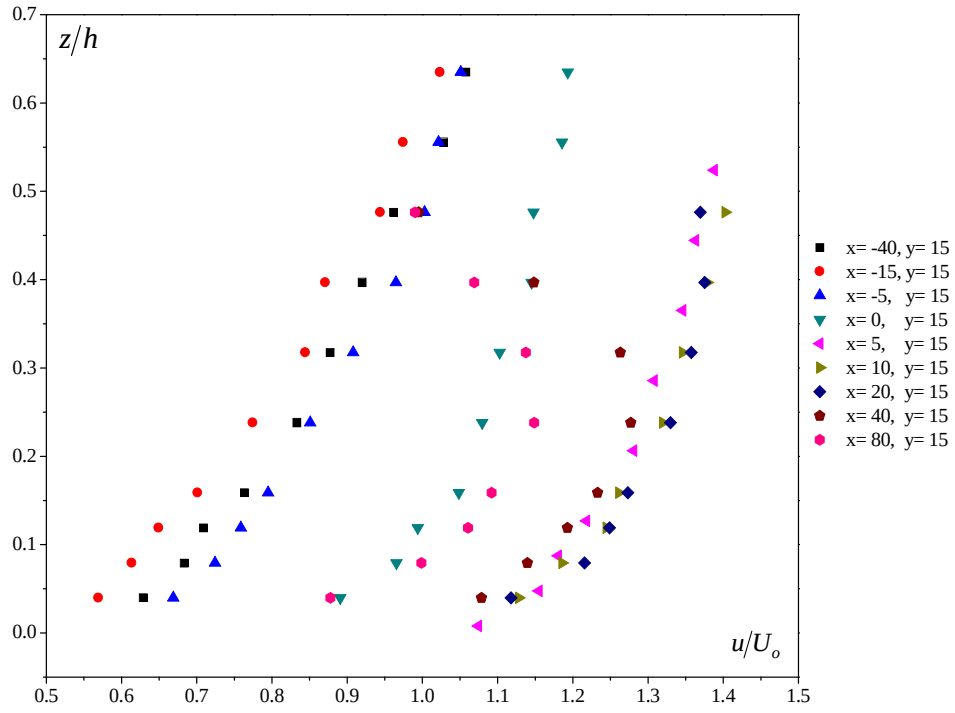

Fig. 5.59 (d) Normalized profiles of longitudinal velocity component u at front of the submerged spur dike (y =15)

5.5.1.2 Turbulence intensity

The variation of normalized longitudinal turbulence intensity $\sqrt{\overline{u'u'}}$ across the flow depth in various planes is shown in Figs. 5.60 (a-b). The turbulence intensity was normalized by the shear velocity u_* in the approach flow. Vertical distance Z was normalized by the approaching flow depth h. Figure 5.60 (a) shows the variation of normalized longitudinal turbulence intensity $\sqrt{\overline{u'u'}}$ across the depth of flow around the partially submerged spur dike. From this figure it was observed that the maximum value of longitudinal component of turbulence intensity occured near the original bed level (z/h = 0.3 to -0.3) in the downstream region bounded by x = 5 to 20cm and y = 5 to 10cm. This indicates the importance of turbulence intensity in sediment detachment for the process of scour to happen. Duan et al. (2009) also observed that the dimensionless longitudinal turbulence intensity $\left(\sqrt{\overline{u'u'}}/u_*\right)$ was larger at the downstream of the spur dike than flat bed. Similarly, Kothyari and Jain (2006) observed a maximum value of turbulence intensity near the original bed surface before the start of detachment in degraded bed profile of clay- gravel mixtures.

Figure 5.60 (b) shows the variation of normalized longitudinal turbulence intensity $\sqrt{\overline{u'u'}}$ across the depth of flow around the submerged spur dike. At the downstream of the submerged dike, the dimensionless longitudinal turbulence intensity $\left(\sqrt{\overline{u'u'}}/u_*\right)$ is larger than flat bed. Turbulence intensity pattern similar to partially submerged dike is also observed around the submerged dike. In the case of submerged dike, maximum value of longitudinal component of turbulence intensity was observed to occur near the original bed level (z/h = 0.5 to -0.25) in downstream region bounded by x = 5 to 20cm and y = 5 to 10cm.

The variation of normalized vertical component of turbulence intensity $\sqrt{\overline{w'w'}}$ across the flow depth around the spur dikes (partially submerged and submerged) is shown in Figs. 5.61 (a-b). The vertical component was also normalized by the value of u_* and vertical distance Z was normalized by the value of h. The variation almost follows the same trend as observed for longitudinal turbulence intensity. However, the magnitude of vertical component was smaller than that of corresponding longitudinal component [Figs.

5.61(a-b)]. Occurrence of maximum value of $\sqrt{\overline{u'u'}}/u_*$ and $\sqrt{\overline{w'w'}}/u_*$ at $z/h \approx 0$ clearly indicates that turbulence intensity is responsible for scour and suspension of sediment particle which is in conformity with the findings of previous investigators (Mazumdar and Ojha, 2007).

From the Figs. 5.60 (a-b), it was observed that the magnitude of dimensionless longitudinal turbulence intensity is larger for the partially submerged spur dike than that of submerged spur dike.

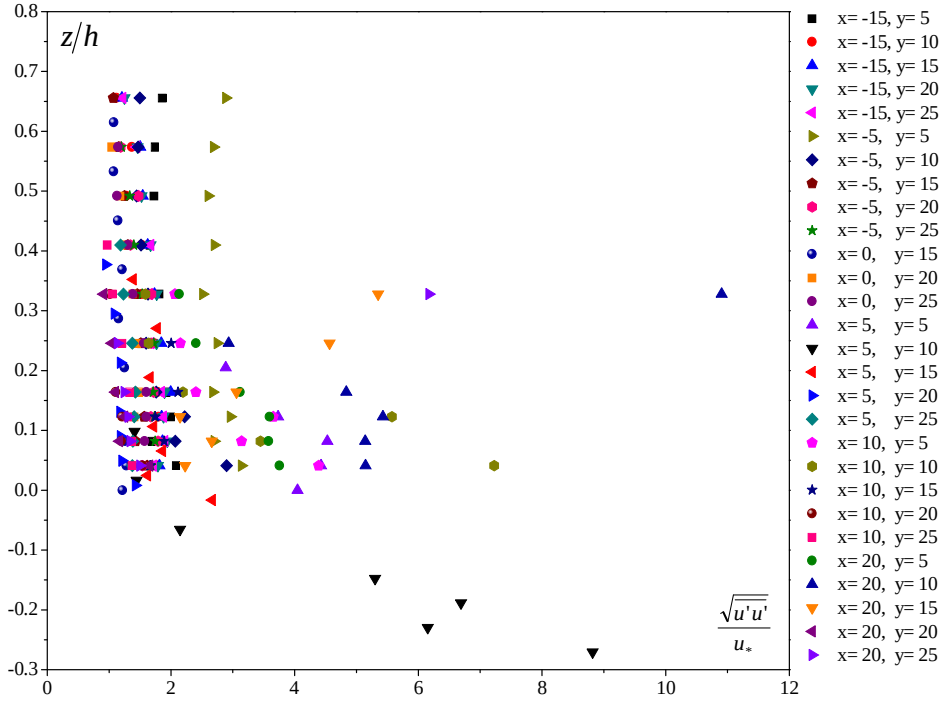

Fig. 5.60 (a) Normalized profiles of turbulence intensities component $\sqrt{\overline{u'u'}}$ measured around partially submerged spur dike

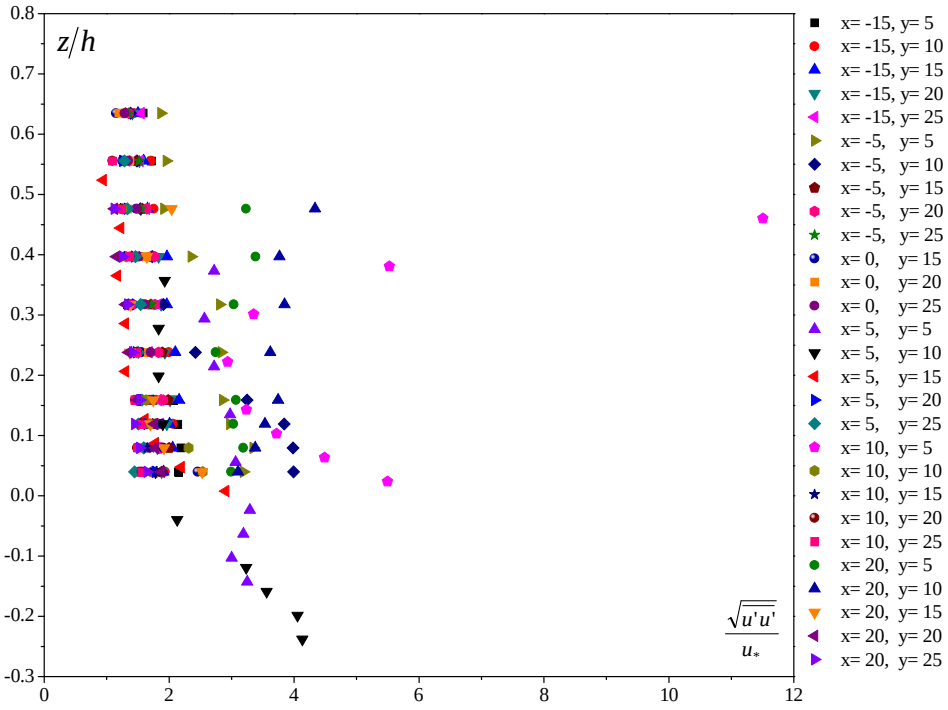

Fig. 5.60 (b) Normalized profiles of turbulence intensities component $\sqrt{\overline{u'u'}}$ measured around submerged spur dike

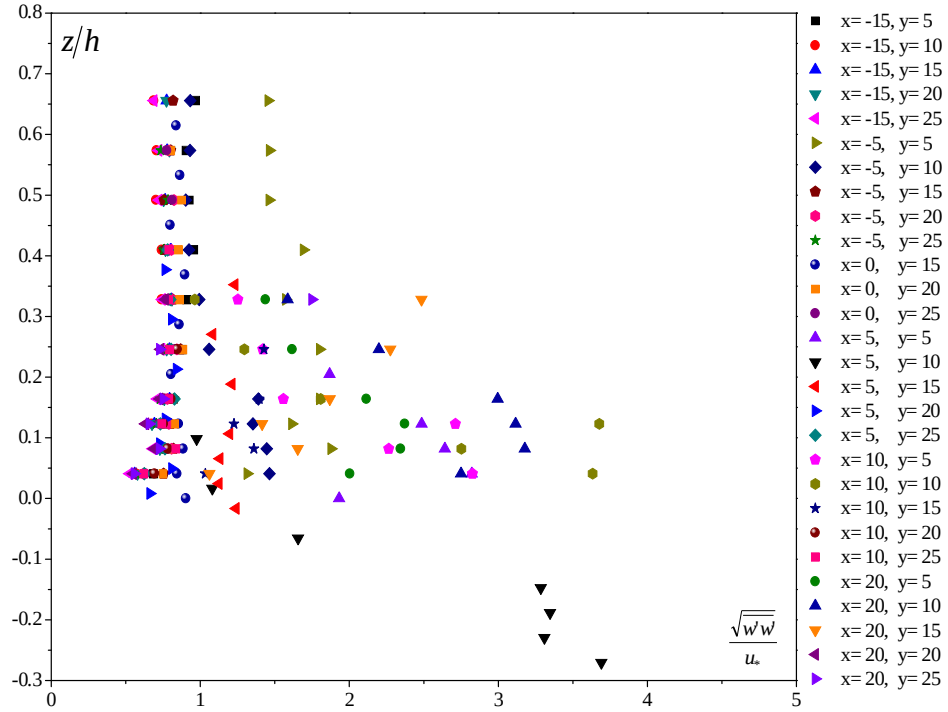

Fig. 5.61 (a) Normalized profiles of turbulence intensities component $\sqrt{\overline{w'w'}}$ measured around partially submerged spur dike

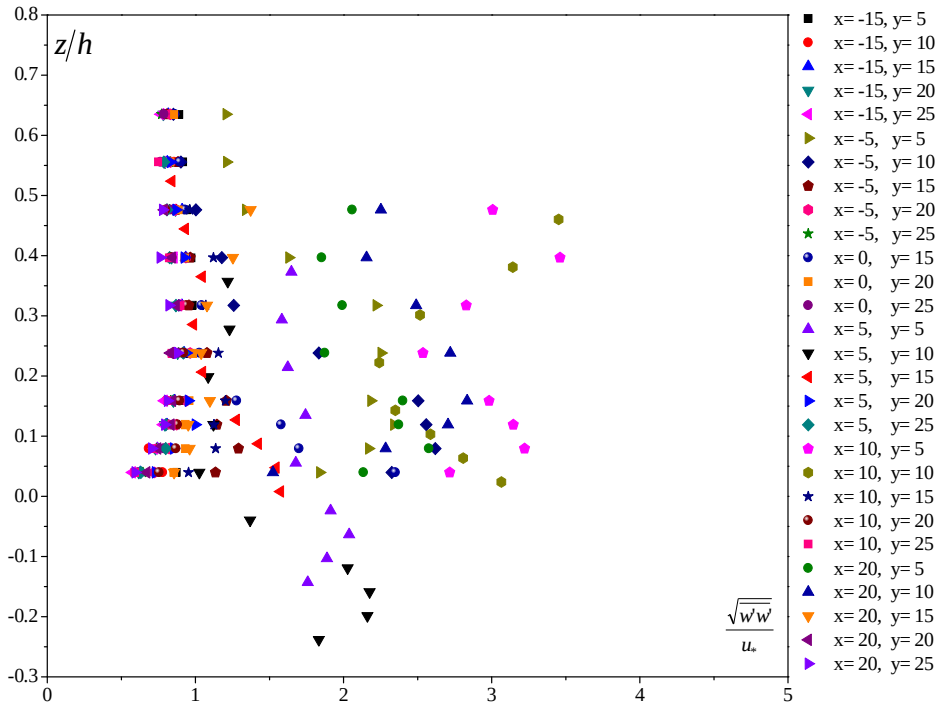

Fig. 5.61 (b) Normalized profiles of turbulence intensities component $\sqrt{\overline{w'w'}}$ measured around submerged spur dike

5.5.1.3 Reynolds stresses

The variation of normalized $\overline{u'w'}$ component of Reynolds stresses along the vertical depth around the partially submerged and submerged spur dikes in various azimuthal planes is shown in Figs. 5.62(a-b). This component of Reynolds stress was normalized by the square of shear velocity of the approach flow i.e. u_*^2. The maximum value of Reynolds stress was observed to occur in the plane y = 5cm and 10cm from section x = 5cm towards x = 20cm of partially submerged and submerged spur dikes [Figs. 5.62 (a-b)]. The Reynolds stresses at the other measuring nodes remained fairly uniform and much smaller. This indicates that turbulence is more prominent in the wake zone of the spur dike than in front of it. Larger scour in the wake zone in comparison to upstream of spur dike in cohesive sediments can be attributed to this reason. Similarly, Kumar (2011) also observed the larger value of Reynolds stresses in the wake zone of the pier than in front of pier embedded in cohesive sediment mixtures consisting of clay-gravel and clay-sand-gravel. From the Figs. 5.62 (a-b) it is also observed that the values of normalized $\overline{u'w'}$ component of Reynolds stresses was larger for partially submerged spur dike than that of submerged dike.

Figures 5.63(a- b) show the variation of $\overline{v'w'}$ component of Reynolds stress across the flow depth around the partially submerged and submerged spur dike in various azimuthal planes. The component of Reynolds stresses were normalized using the square of shear velocity i.e. u_*^2. The component $\overline{v'w'}$ of Reynolds stress obtained around the spur dikes (partially submerged and submerged) does not show significant value [Figs. 5.63 (a-b)]. Kumar (2007) reported that Reynolds stresses components $\overline{u'w'}$ and $\overline{v'w'}$ do not show conclusive trend in the case of scour around compound pier founded in cohesionless sediment. However, Dey and Raikar (2007) reported that there is existence of a core of higher magnitude of turbulence intensities and Reynolds stresses within the scour hole.

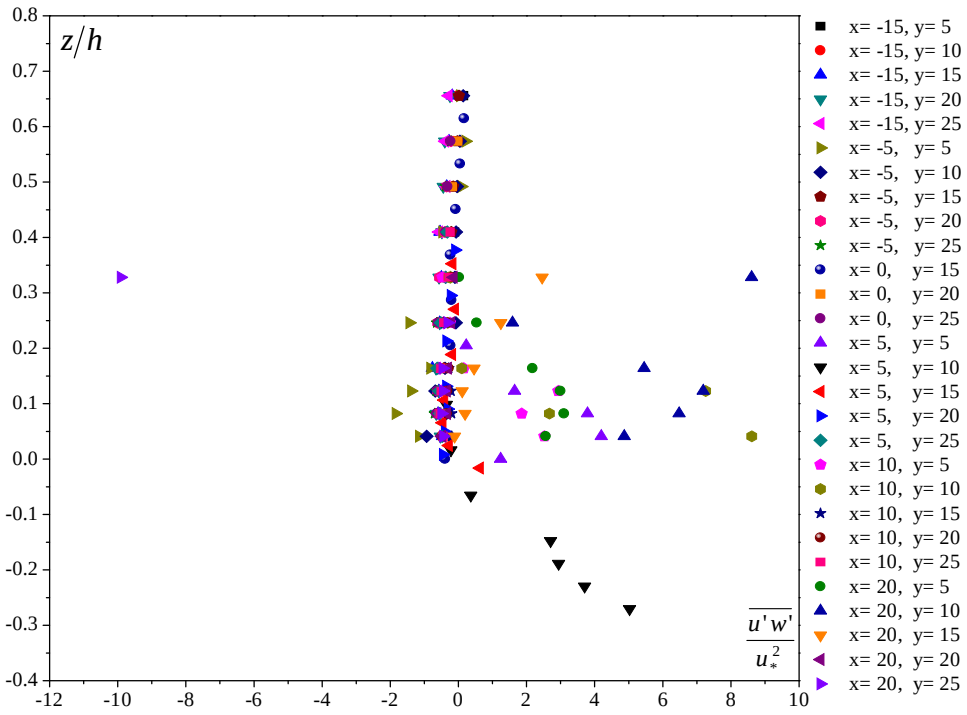

Fig. 5.62 (a) Normalized profiles of Reynolds stresses component $\overline{u'w'}$ measured around partially submerged spur dike

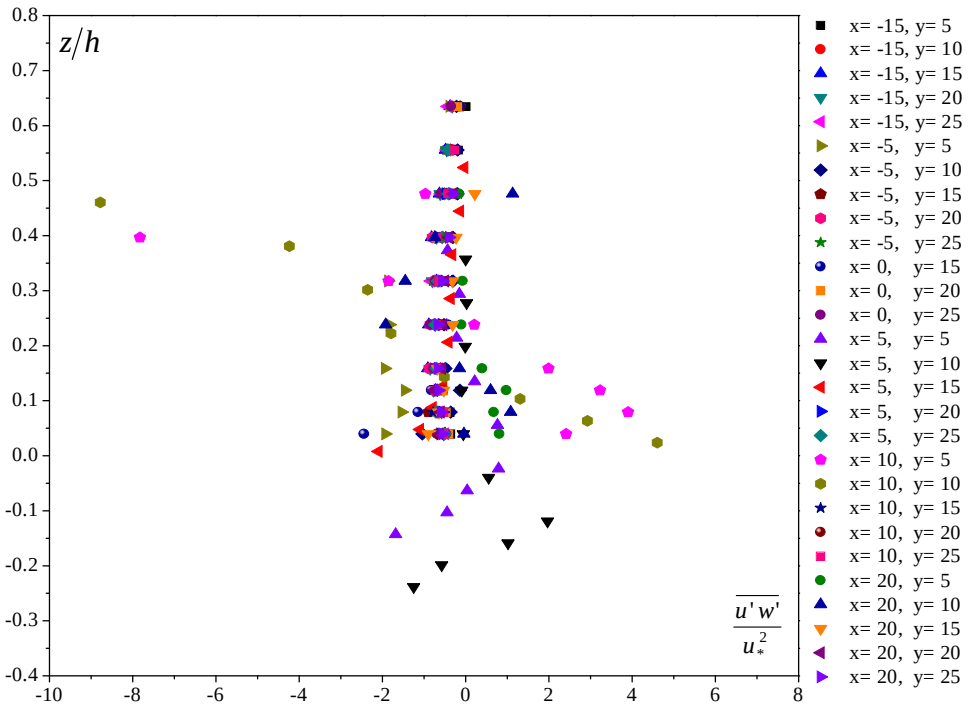

Fig. 5.62 (b) Normalized profiles of Reynolds stresses component $\overline{u'w'}$ measured around submerged spur dike

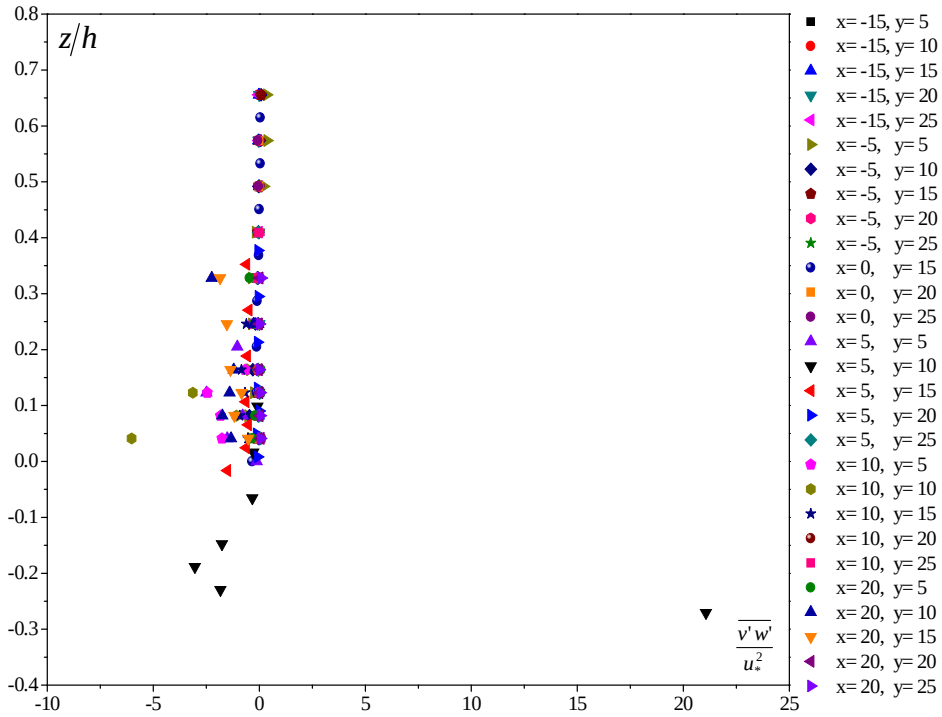

Fig. 5.63 (a) Normalized profiles of Reynolds stresses component $\overline{v'w'}$ measured around partially submerged spur dike

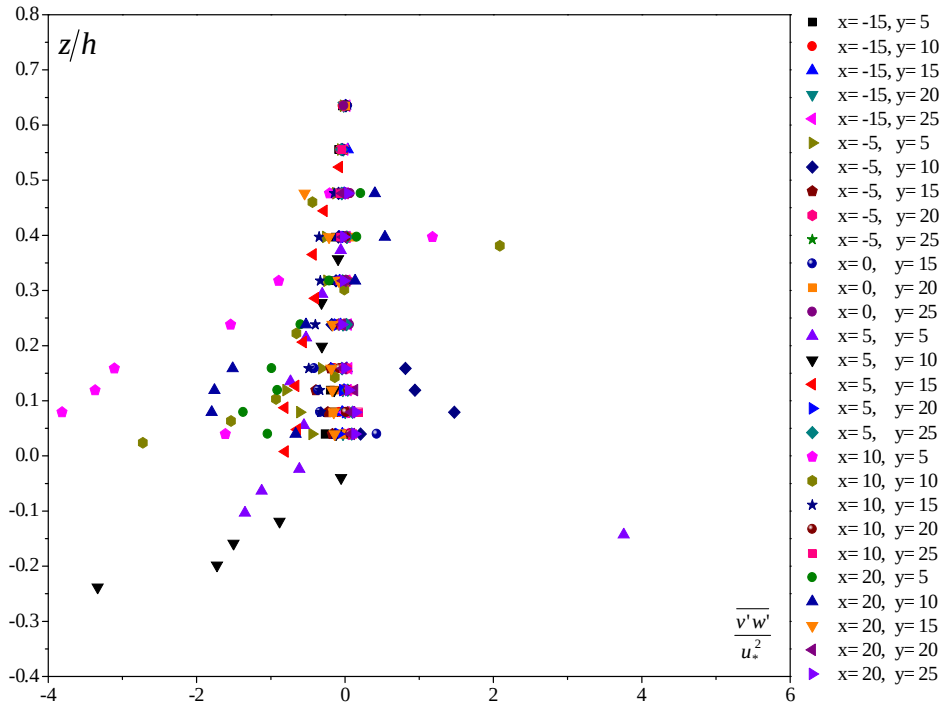

Fig. 5.63 (b) Normalized profiles of Reynolds stresses component $\overline{v'w'}$ measured around submerged spur dike

5.5.1.4 Turbulence kinetic energy

The turbulenence kinetic energy can be expressed as

$$k = \frac{1}{2}\left(\overline{u'u'} + \overline{v'v'} + \overline{w'w'}\right)$$

Figures 5.64 (a-b) show the variation of turbulence kinetic energy across the flow depth around the partially submerged and submerged spur dikes in various azimuthal planes. The value of k was normalized by the square of shear velocity i.e. u_*^2. The turbulence kinetic energy is a qualitative representation of turbulence fluctuations around the spur dike. The maximum value of turbulence kinetic energy was observed to occur in the plane y = 5cm and 10cm from section x = 5cm towards x = 20cm of partially submerged and submerged dike [Figs. 5.64 (a-b)]. The result indicated that maximum turbulence fluctuations occured in the flow within the scour hole near the spur dike. Further away from spur dike, at various measuring nodes, fairly uniform and much smaller value of turbulence kinetic energy was observed. Kumar (2011) also observed maximum value of k near the pier in the wake zone and its value reduced away from the

pier in cohesive sediment mixtures bed. Similarly, Kumar (2007) also observed maximum value of k near the pier in the wake zone and its value reduced away from the pier.

The experimental runs were conducted for partially submerged and submerged spur dike founded in cohesive sediment mixture consisting of clay-gravel mixtures. In comparison, the values of the turbulence kinetic energy outside the scour hole were larger for submerged spur dike than those in partially submerged dike. It was also observed that, within the scour hole, the values of turbulence kinetic energy are larger in case of partially submerged dike than those observed in submerged spur dike.

After the detailed analysis of turbulence intensity, Reynolds stresses and TKE in scour zone around spur dike, it was found that the maximum scour depth developed along the path of the detached layer where the turbulence intensity was the maximum. The higher magnitude of Reynolds stresses and TKE was also observed within the scour hole and it was maximum at the bottom of the scour hole. Similar results were also observed by Duan et al (2009) in the case of scour around partially submerged spur dike and by Dey and Raikar (2007), Kumar (2011) and Kumar (2012) in the case of scour around bridge pier. The magnitudes of turbulence intensity, Reynolds stresses and TKE were higher in case of partially submerged dike than submerged spur dike. Due to this, the depth of scour depth in partially submerged dike found to be larger than submerged dike.

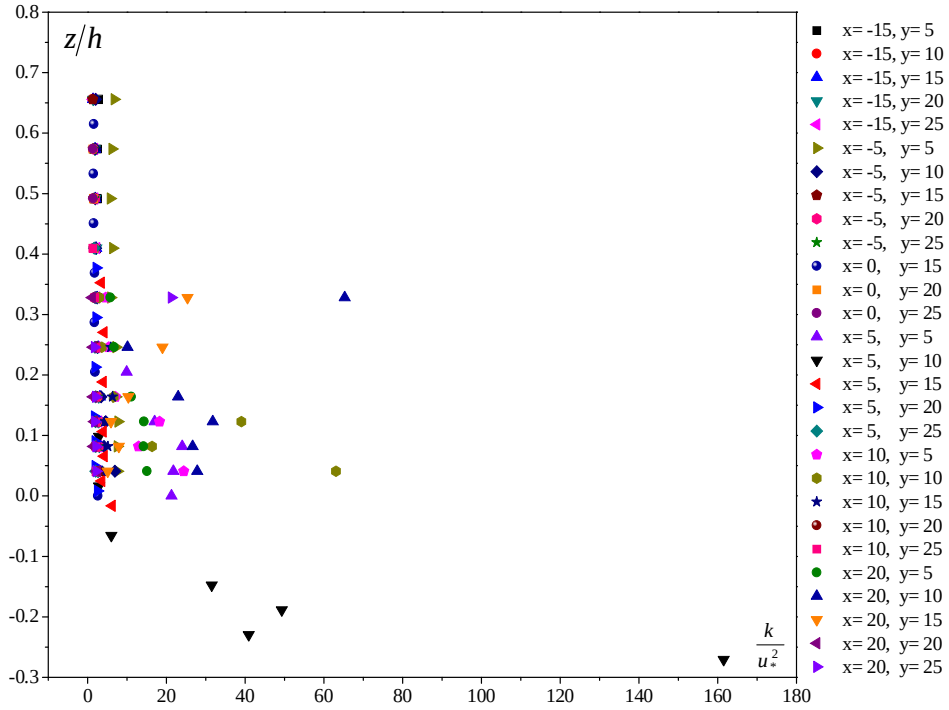

Fig. 5.64 (a) Normalized profiles of turbulence kinetic energy measured around partially submerged spur dike

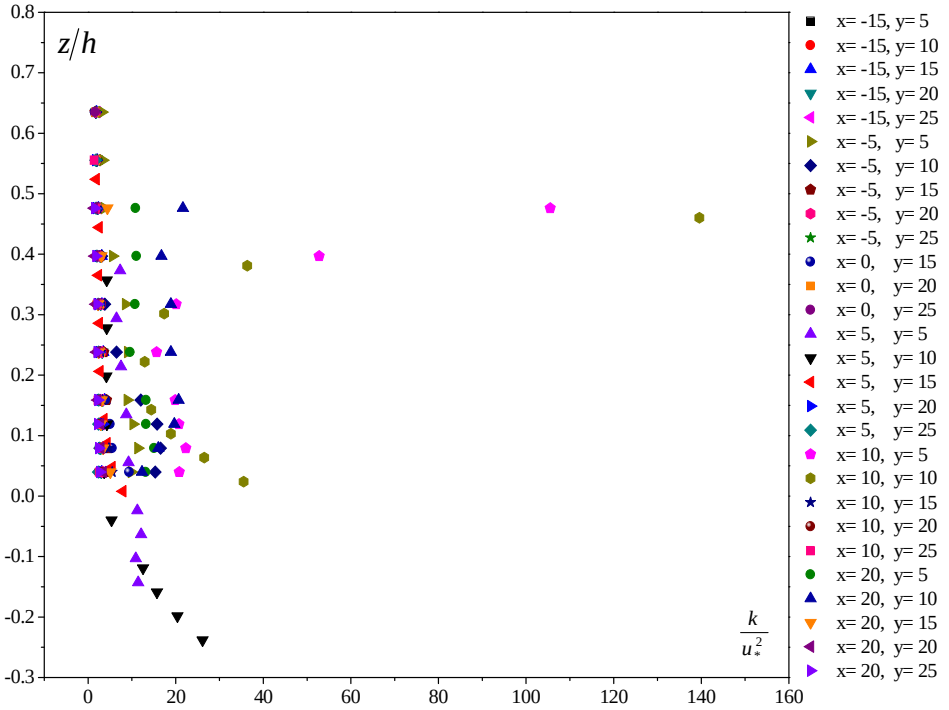

Fig. 5.64 (b) Normalized profiles of turbulence kinetic energy measured around submerged spur dike

5.6 QUADRANT ANALYSIS

To carry out quadrant analysis, the longitudinal fluctuating velocity $u' = u - \overline{u}$ and the vertical fluctuating velocity $w' = w - \overline{w}$ were decomposed following their sign using WinADV software (Nortek, 2000). Data filtration was carried out by Phase-space Threshold method included in the WinADV software and these filtered data was used in further analysis. A code was developed in FORTRAN-90 to obtain the contribution of outward interaction, ejection, inward interaction and sweep events out of whole data for a particular z/h value. As defined in Chapter-III, $S_{i,H}$ indicatively defines occurrence probability of a particular event, the same was obtained using the code developed herein. The occurrence probability for each event over the entire flow depth around the partially submerged and submerged dikes was obtained. The bursting events were computed around the partially submerged spur dike at different measuring node (i.e. x = -15, -5, 0, 5, 10 and 20cm; and y = 5, 10, 15 and 20cm). The negative and positive values of x represent the upstream and downstream of the spur dike respectively. The results presented herein were obtained by performing computations with H = 0 for all events.

5.6.1 Bursting Events around Partially Submerged Spur Dike

The contributions of different bursting events (i.e. outward interaction, ejection, inward interaction and sweep) around partially submerged dike are shown in Figs. 5.65 (a-d) to 5.68 (a-d). From Figs. 5.65 (a-d) and 5.67 (a-d) it is clearly observed that the values of outward and inward interaction were higher at the downstream of the partially submerged dike (x = 5, 10 and 20cm) than its upstream (x = -15 and -5cm) at an azimuthal plane of y = 5 and 10cm. At measuring planes y = 15 and 20cm, small values of outward and inward interaction events were observed.

Figures 5.66 (a-d) and 5.68 (a-d) show distribution of ejection and sweep events around the partially submerged spur dike at various measuring nodes respectively. The small values of ejection and sweep events were measured at the downstream of the partially submerged dike (x = 5, 10 and 20cm) than its upstream (x = -15 and -5cm) at an azimuthal plane of y = 5 and 10cm. The values of ejection and sweep events increased from y = 15 to 20cm in downstream of the spur dike.

From the analysis it was observed that value of outward and inward interactions increases toward the lower most regions within the scour hole in case of partially submerged dike. Similar results were obtained by Kumar (2011) in case of pier scour. The larger value of outward and inward interaction as observed in the lower most measurement layer supports the finding of Nelson et al. (1995), since it denotes a potential for near bed flow to transport more sediments than elsewhere in water column.

5.6.2 Bursting Events around Submerged Spur Dike

The contributions of different bursting events (i.e. outward interaction, ejection, inward interaction and sweep) around submerged spur dike are shown in Figs. 5.69 (a-d) to 5.72 (a-d). Figures 5.69 (a-d) and 5.71 (a-d) show the distribution of outward and inward interaction events around submerged spur dike measured at various nodes respectively. The trend of outward and inward interaction events were very similar to that observed around partially submerged spur dike. The values of outward and inward interaction events were higher at the downstream of the submerged dike (x = 5, 10 and 20cm) than its upstream (x = -15 and -5cm) at an azimuthal plane of y = 5 and 10cm. At measuring nodes y = 15 and 20cm, smaller values of outward and inward interaction events were measured.

Figures 5.70 (a-d) and 5.72 (a-d) show the distribution of ejection and sweep events around the submerged spur dike at various measuring nodes respectively. The trend observed for ejection and sweep events around the submerged spur dike was also similar to that observed around partially submerged spur dike. At outside of the scour hole, small values of ejection and sweep events were measured at the downstream of the submerged dike (x = 10 and 20cm) than its upstream (x = -15 and -5cm) at an azimuthal plane of y = 5 and 10cm. While, within the scour hole at (5, 5) and (5, 10) the ejection and sweep events have maximum value at lower most level and decreases near initial bed level. Their values further increase towards the water surface. Duan et al. (2011), Kumar (2011) and Jain et al. (2015) also found that the ejection and sweep events are more dominant than other two events. The values of ejection and sweep events increased marginally from y = 15 to 20cm in downstream of the submerged spur dike.

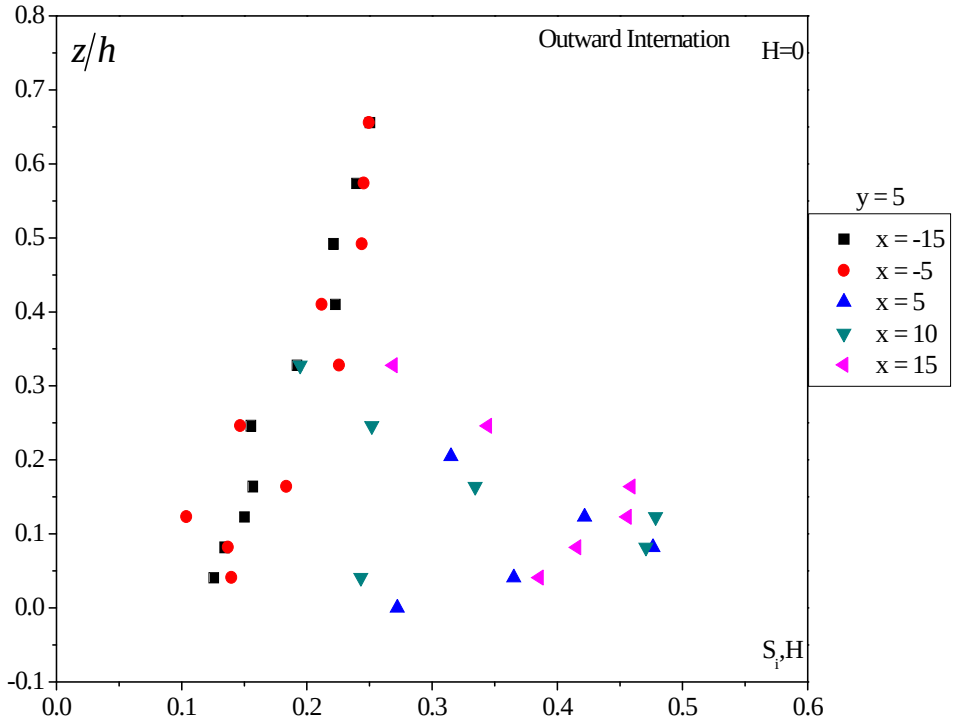

Fig. 5.65 (a) Distribution of outward interaction event at various measuring nodes around the partially submerged dike at y = 5cm

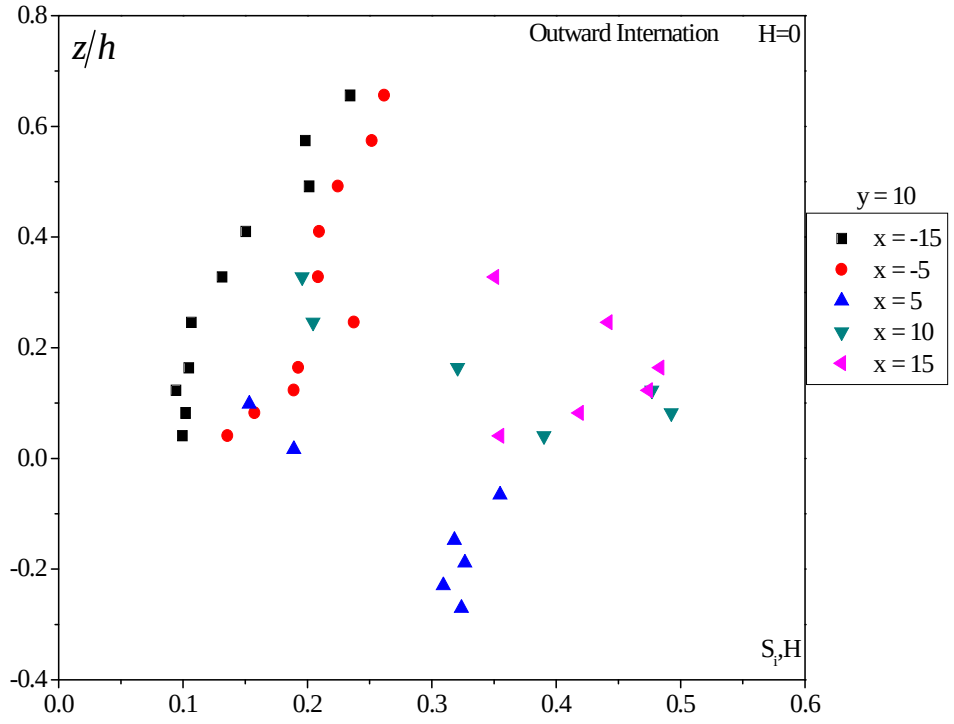

Fig. 5.65 (b) Distribution of outward interaction event at various measuring nodes around the partially submerged dike at y = 10cm

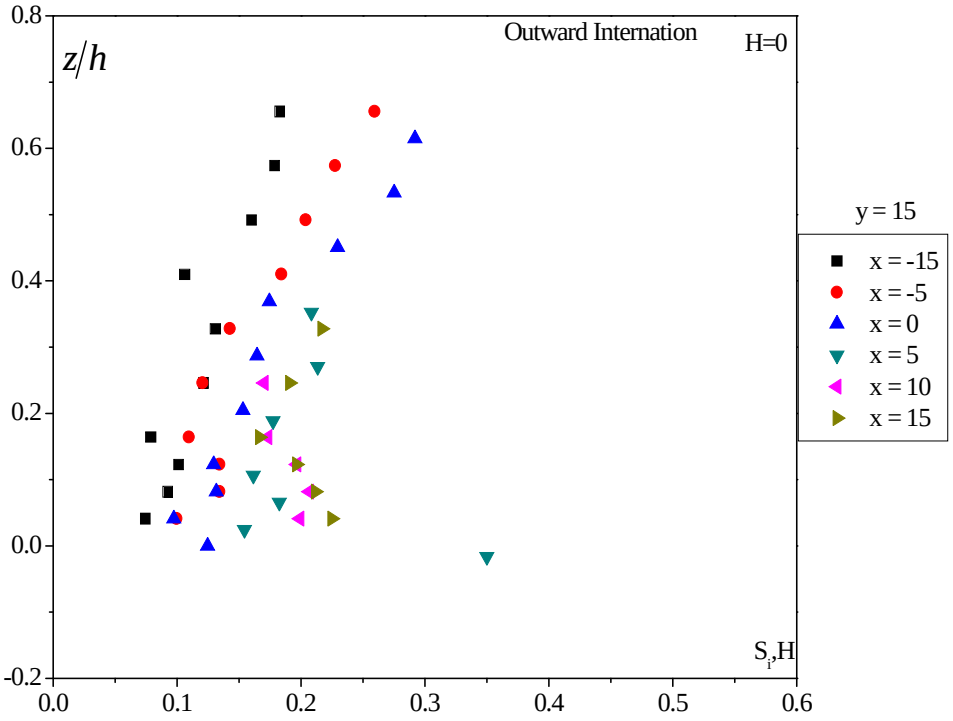

Fig. 5.65 (c) Distribution of outward interaction event at various measuring nodes around the partially submerged dike at y = 15cm

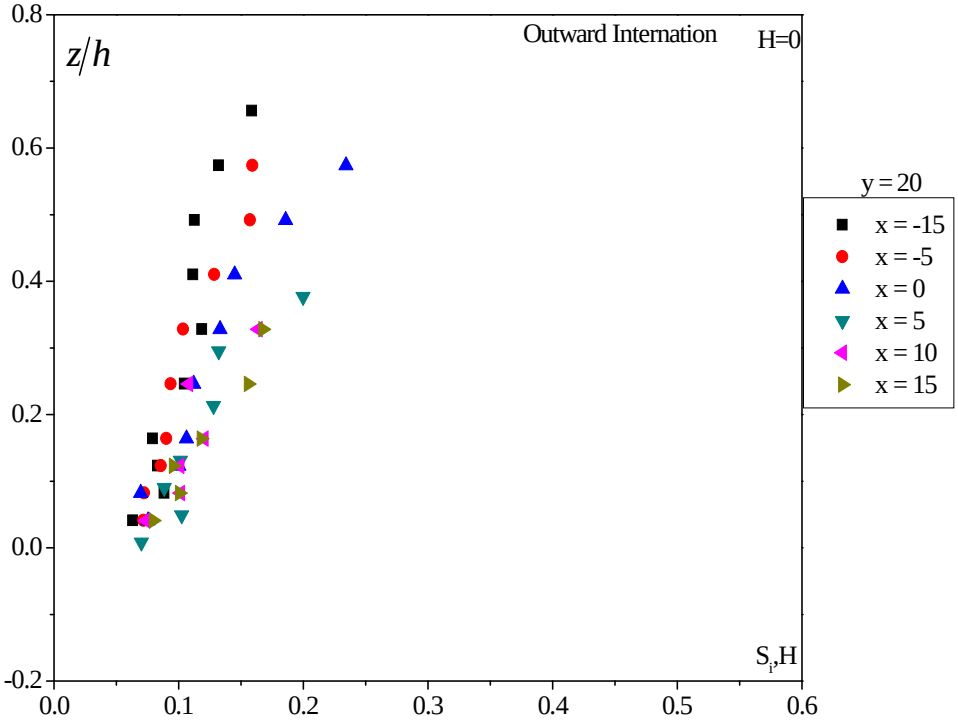

Fig. 5.65 (d) Distribution of outward interaction event at various measuring nodes around the partially submerged dike at y = 20cm

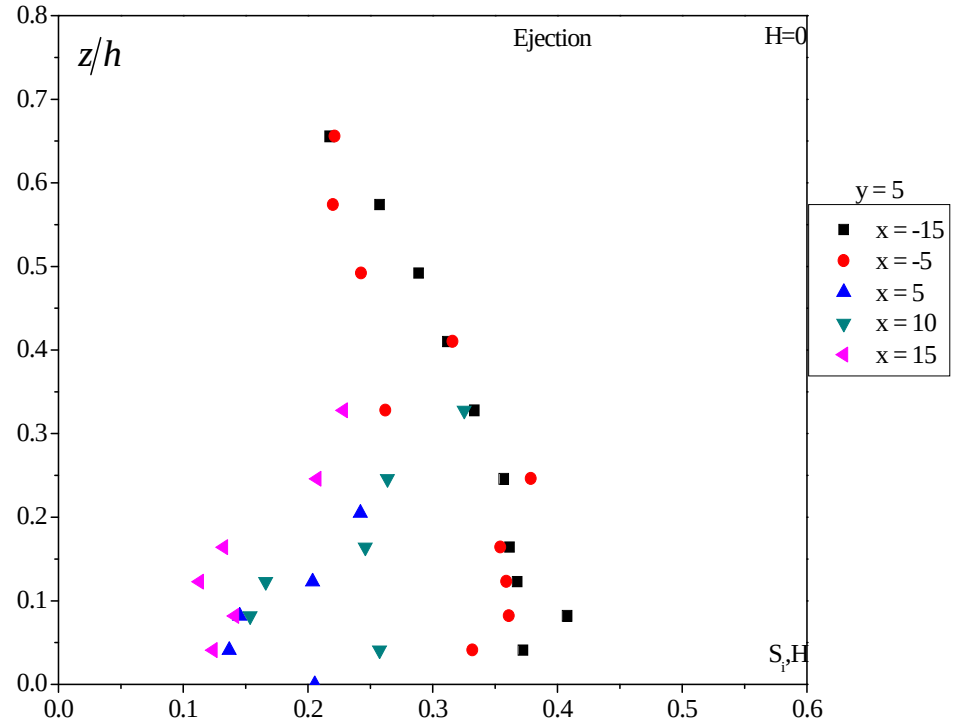

Fig. 5.66 (a) Distribution of ejection event at various measuring nodes around the partially submerged dike at y = 5cm

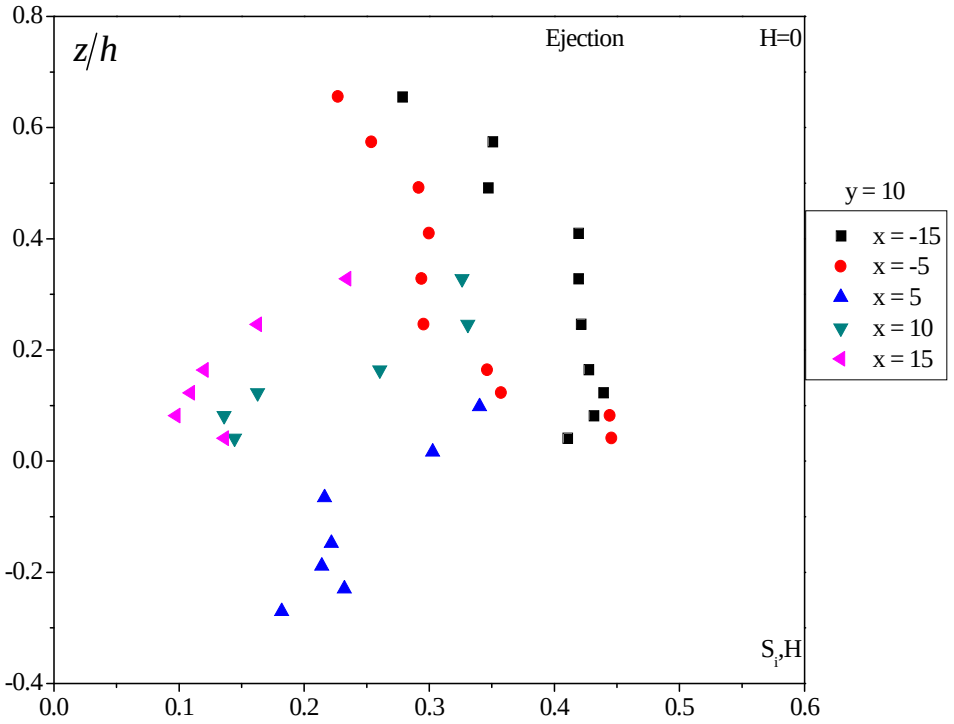

Fig. 5.66 (b) Distribution of ejection event at various measuring nodes around the partially submerged dike at y = 10cm

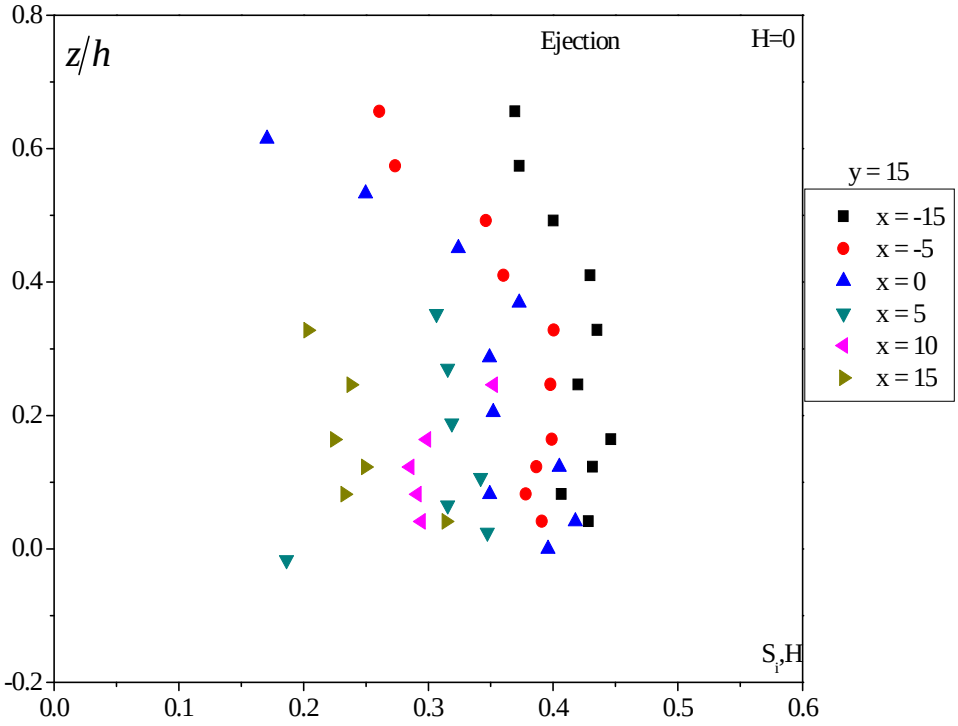

Fig. 5.66 (c) Distribution of ejection event at various measuring nodes around the partially submerged dike at y = 15cm

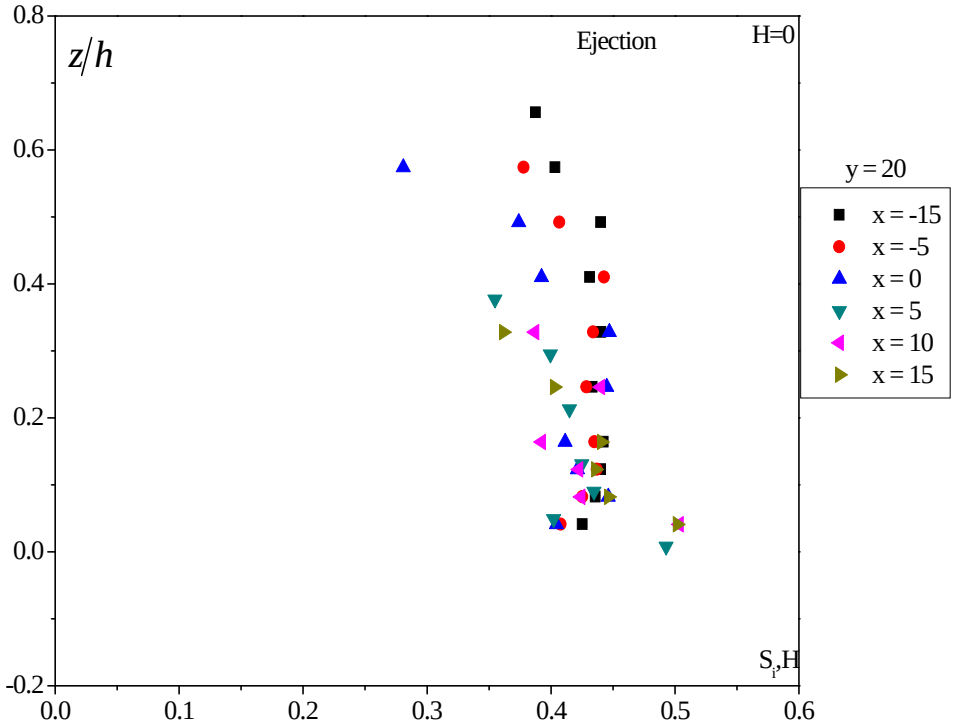

Fig. 5.66 (d) Distribution of ejection event at various measuring nodes around the partially submerged dike at y = 20cm

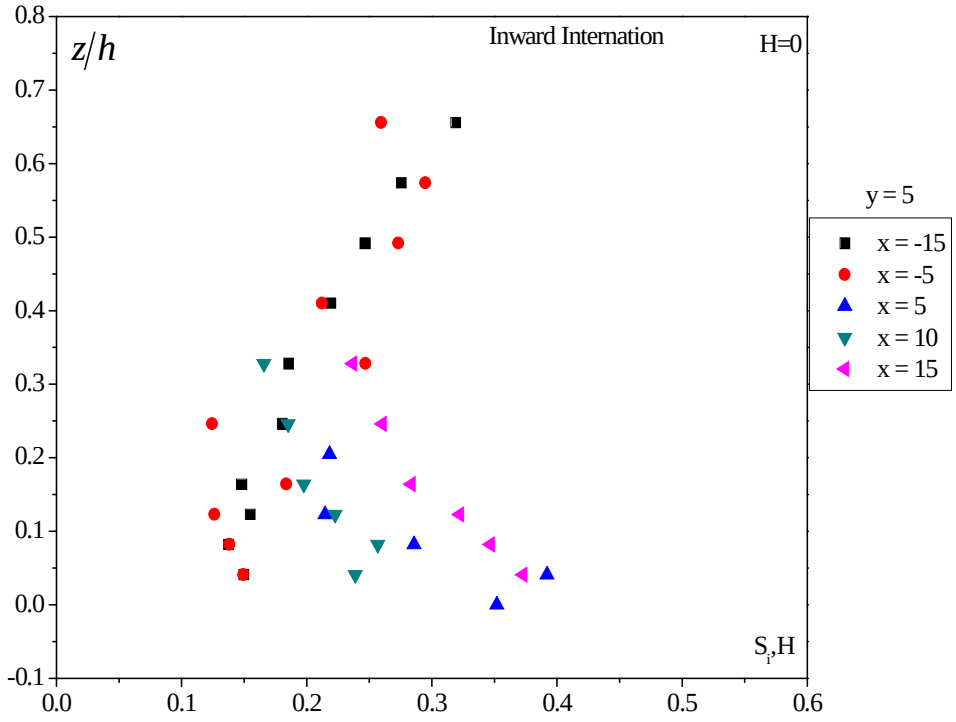

Fig. 5.67 (a) Distribution of inward interaction event at various measuring nodes around the partially submerged dike at y = 5cm

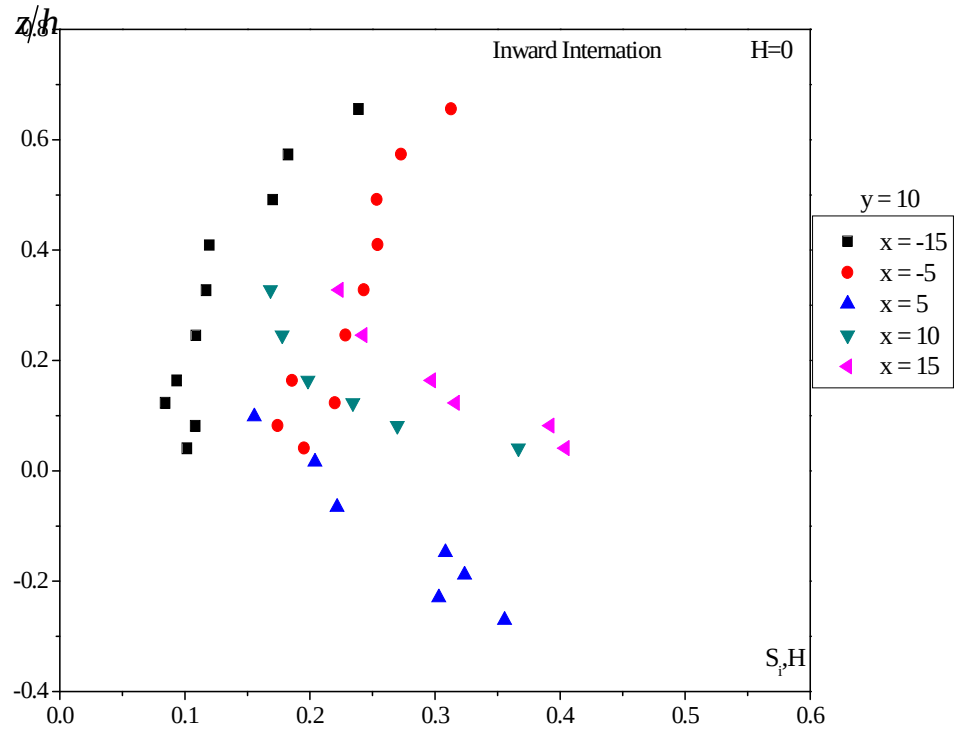

Fig. 5.67 (b) Distribution of inward interaction event at various measuring nodes around the partially submerged dike at y = 10cm

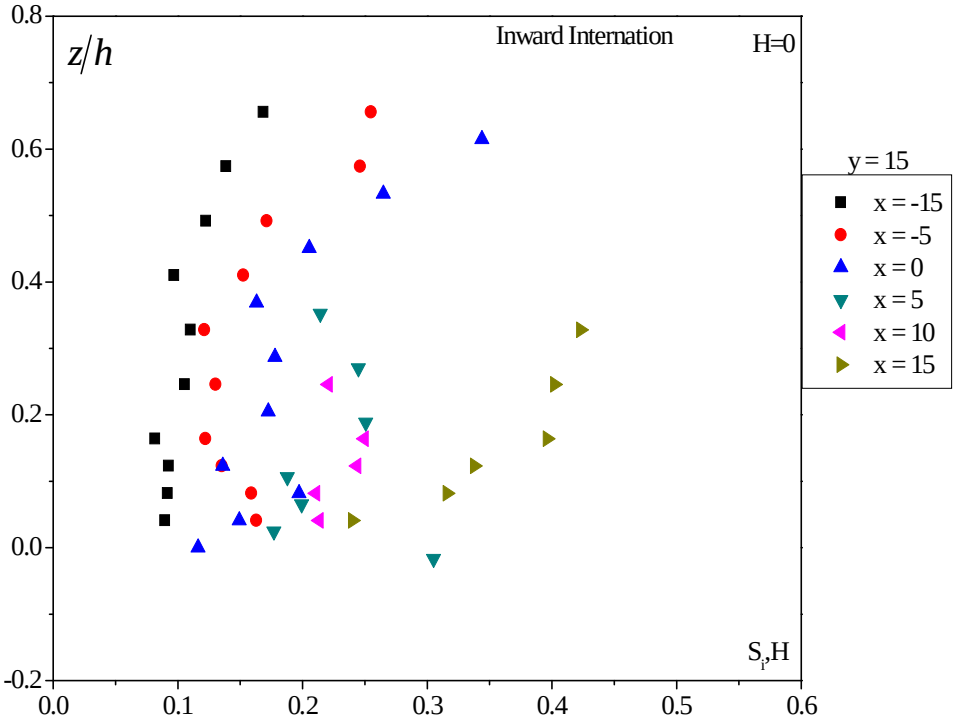

Fig. 5.67 (c) Distribution of inward interaction event at various measuring nodes around the partially submerged dike at y = 15cm

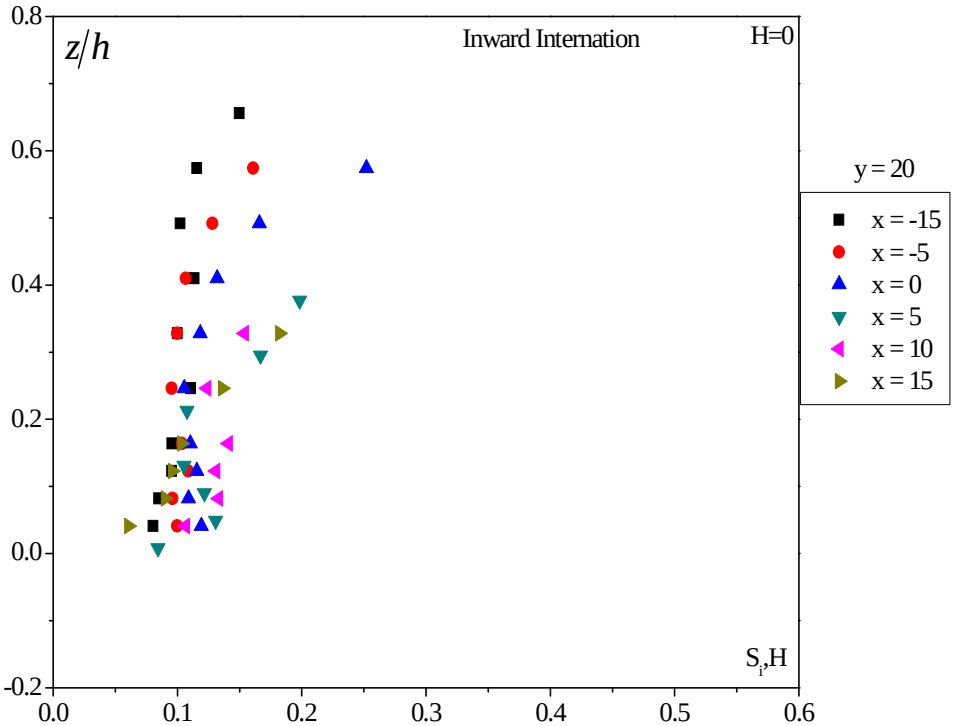

Fig. 5.67 (d) Distribution of inward interaction event at various measuring nodes around the partially submerged dike at y = 20cm

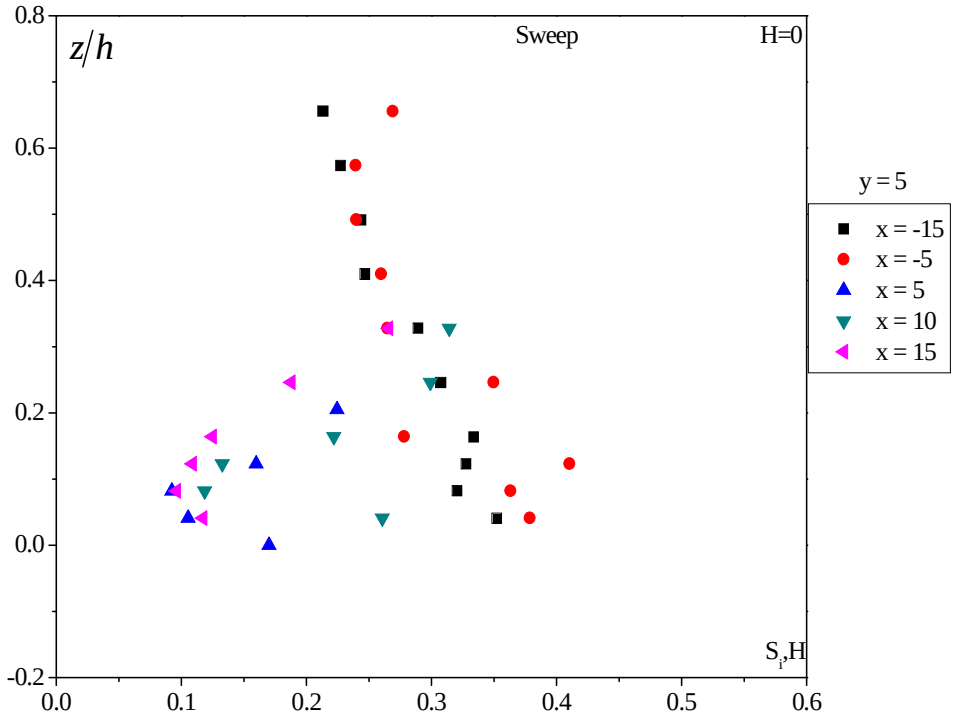

Fig. 5.68 (a) Distribution of sweep event at various measuring nodes around the partially submerged dike at y = 5cm

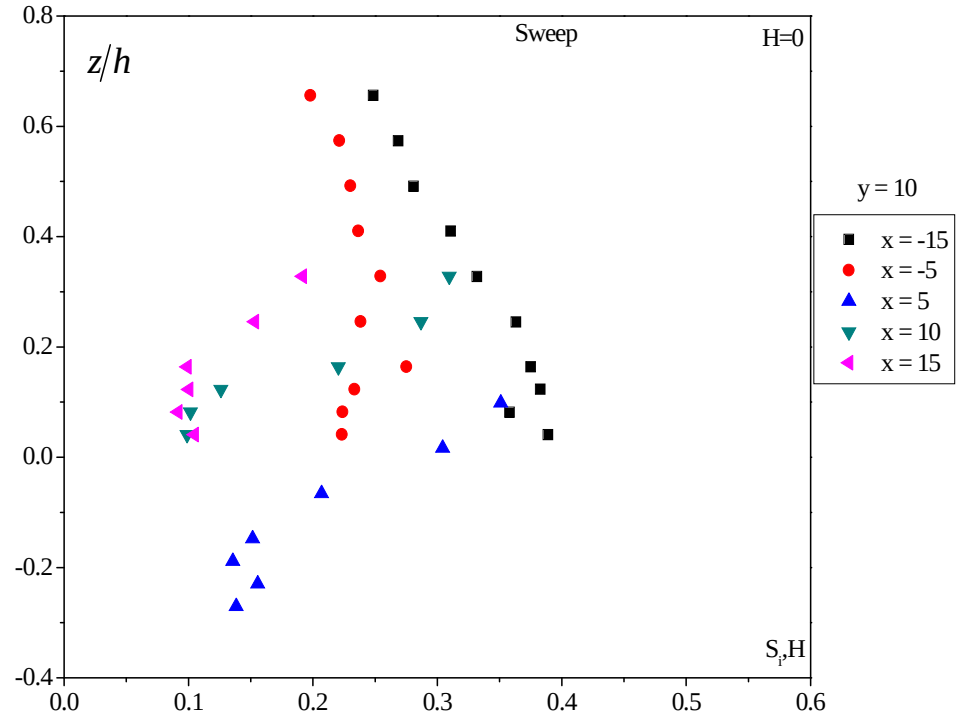

Fig. 5.68 (b) Distribution of sweep event at various measuring nodes around the partially submerged dike at y = 10cm

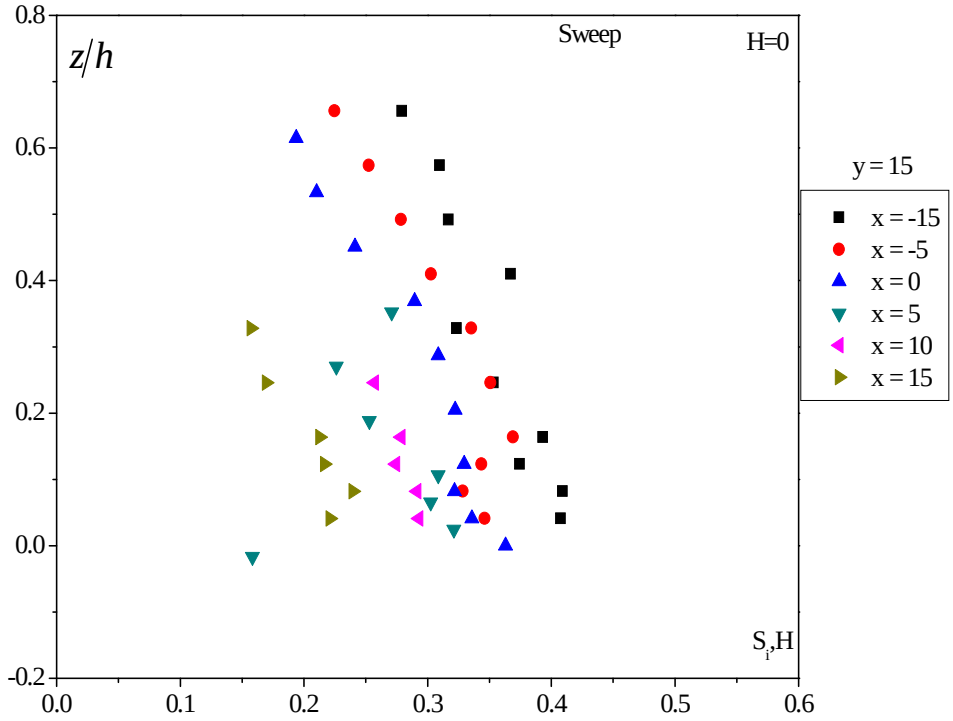

Fig. 5.68 (c) Distribution of sweep event at various measuring nodes around the partially submerged dike at y = 15cm

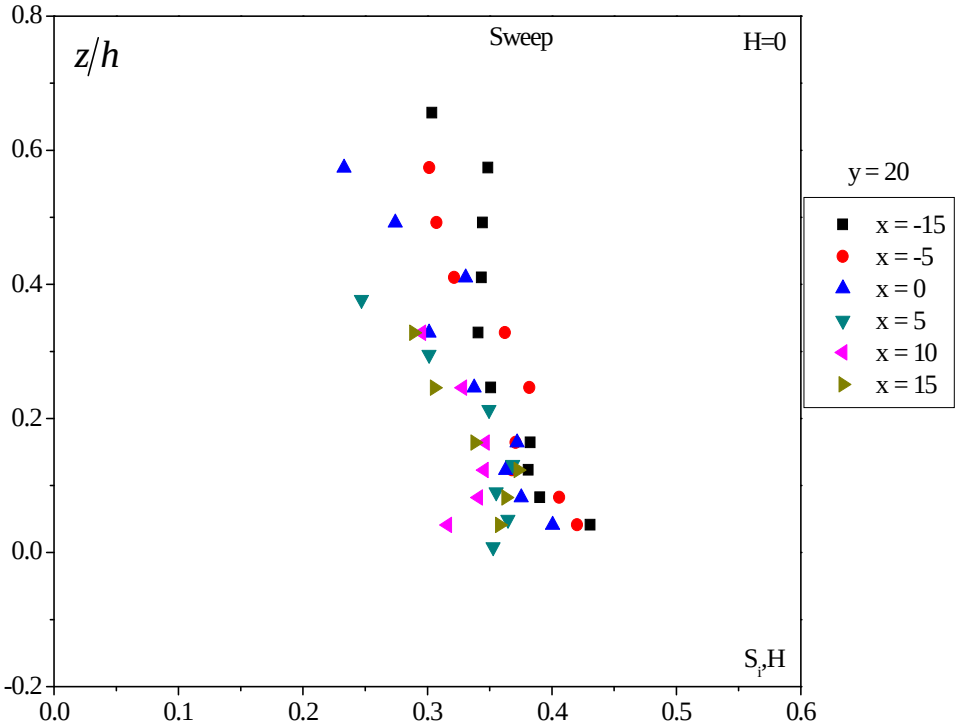

Fig. 5.68 (d) Distribution of sweep event at various measuring nodes around the partially submerged dike at y = 20cm

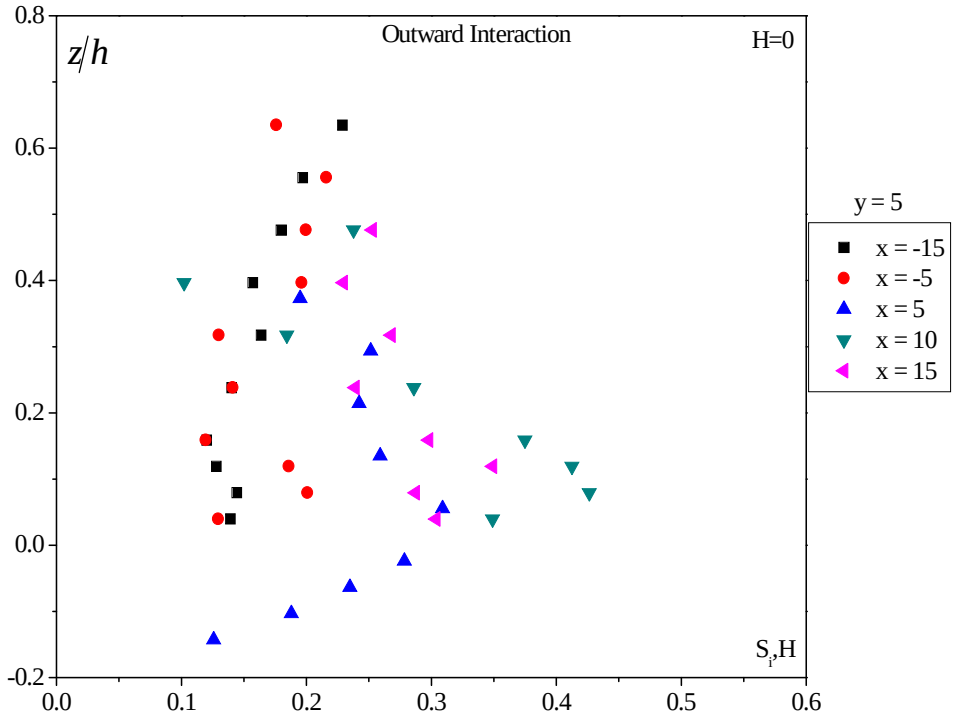

Fig. 5.69 (a) Distribution of outward interaction event at various measuring nodes around the submerged dike at y = 5cm

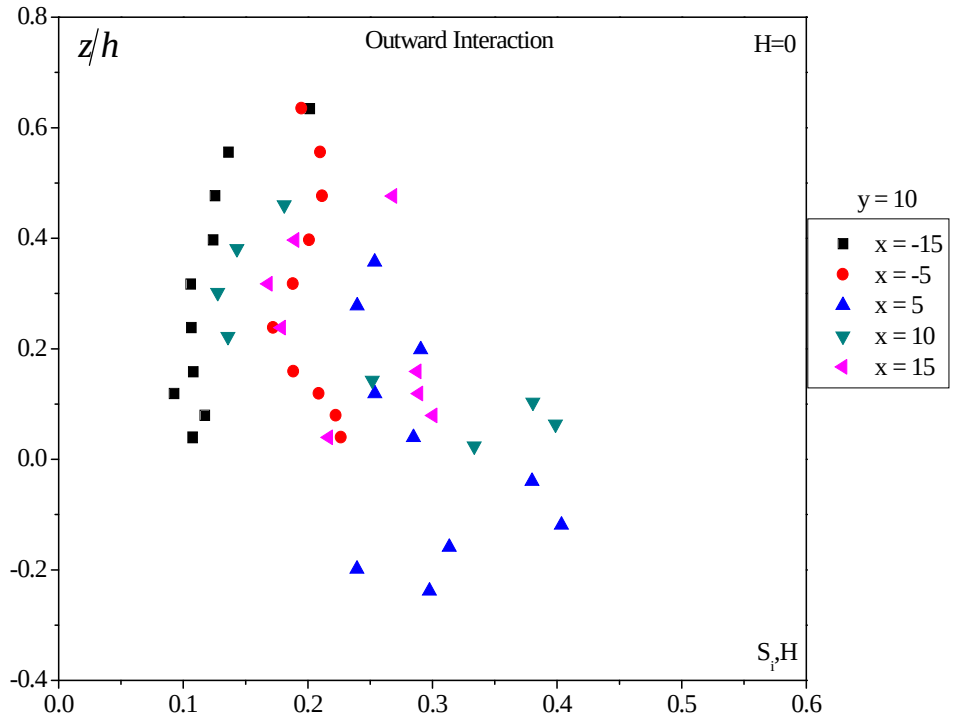

Fig. 5.69 (b) Distribution of outward interaction event at various measuring nodes around the submerged dike at y = 10cm

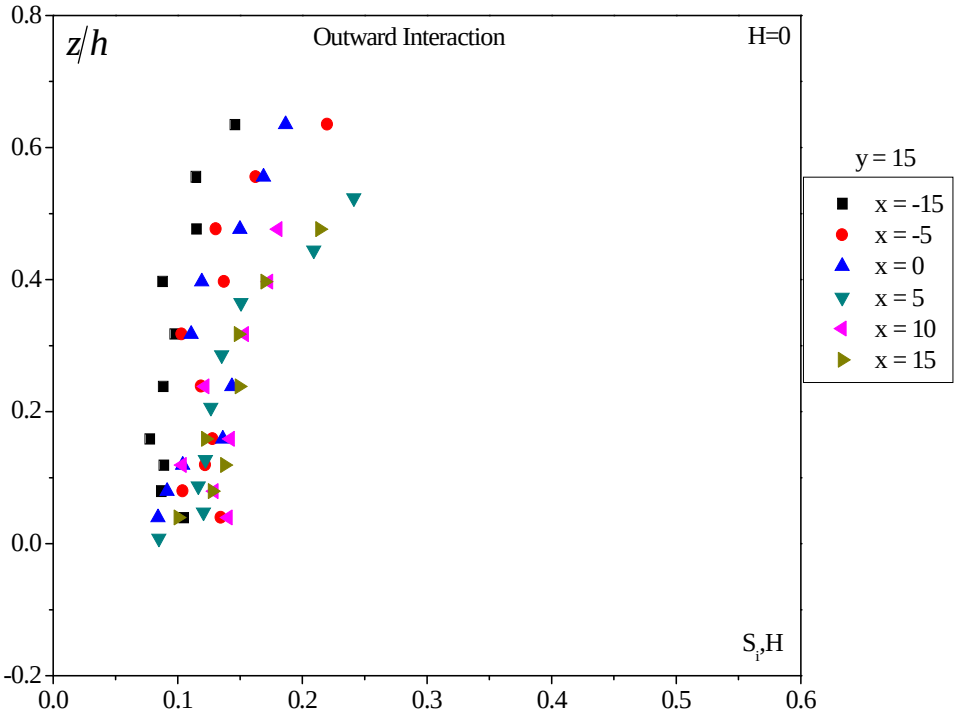

Fig. 5.69 (c) Distribution of outward interaction event at various measuring nodes around the submerged dike at *y* = 15cm

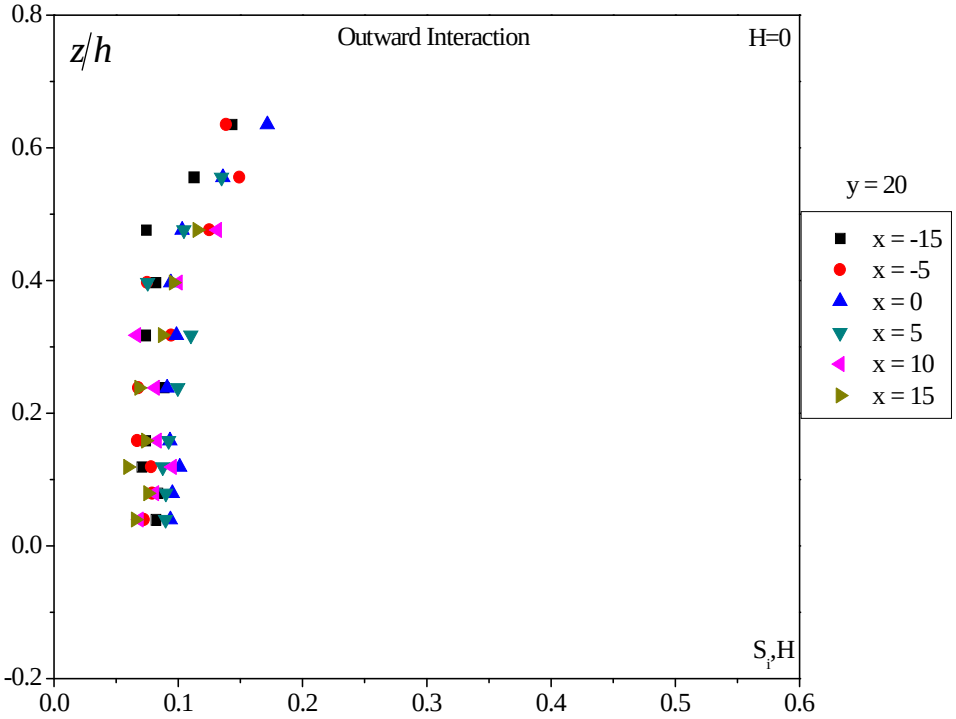

Fig. 5.69 (d) Distribution of outward interaction event at various measuring nodes around the submerged dike at *y* = 20cm

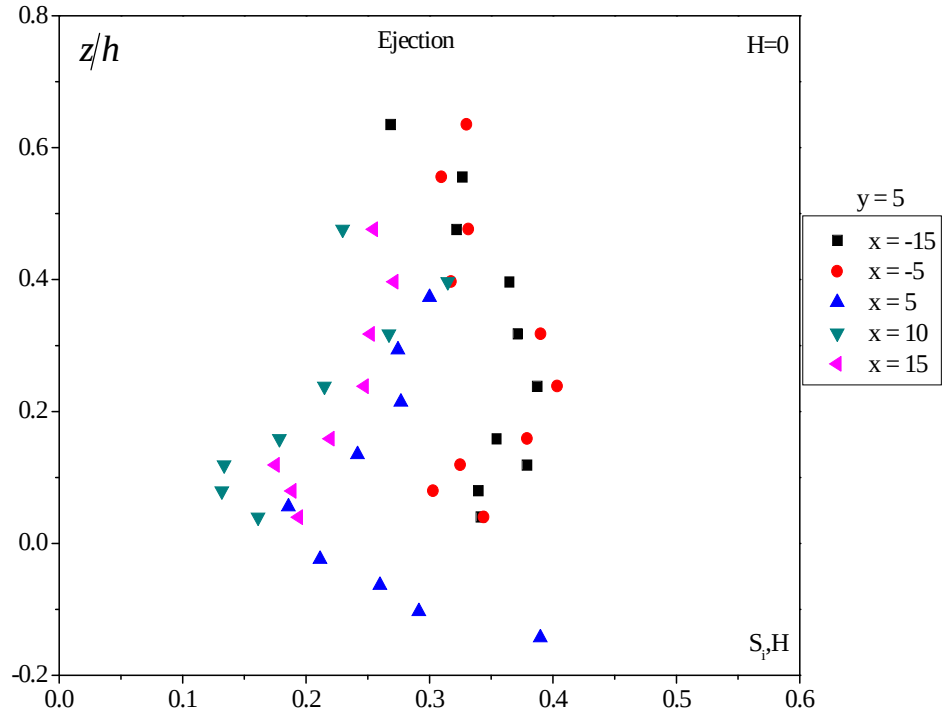

Fig. 5.70 (a) Distribution of ejection event at various measuring nodes around the submerged dike at y = 5cm

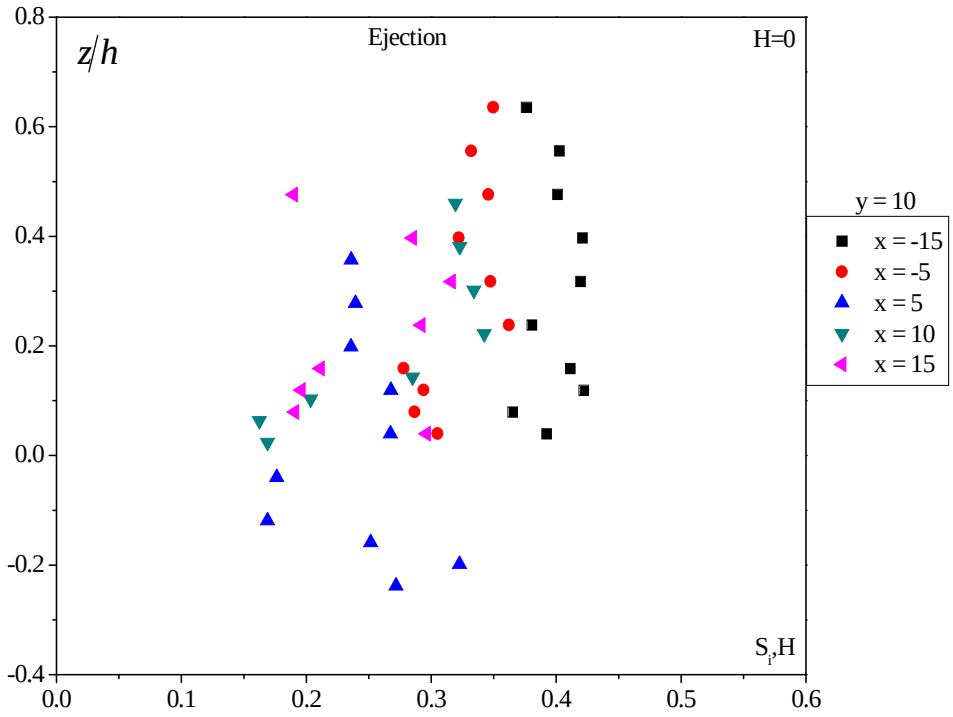

Fig. 5.70 (b) Distribution of ejection event at various measuring nodes around the submerged dike at y = 10cm

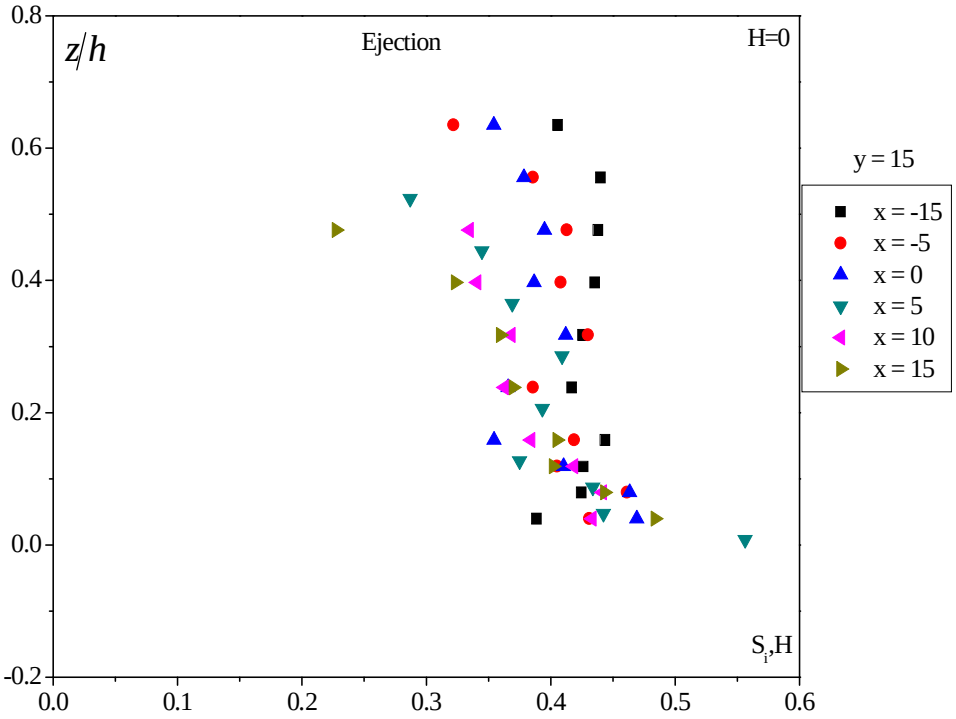

Fig. 5.70 (c) Distribution of ejection event at various measuring nodes around the submerged dike at y = 15cm

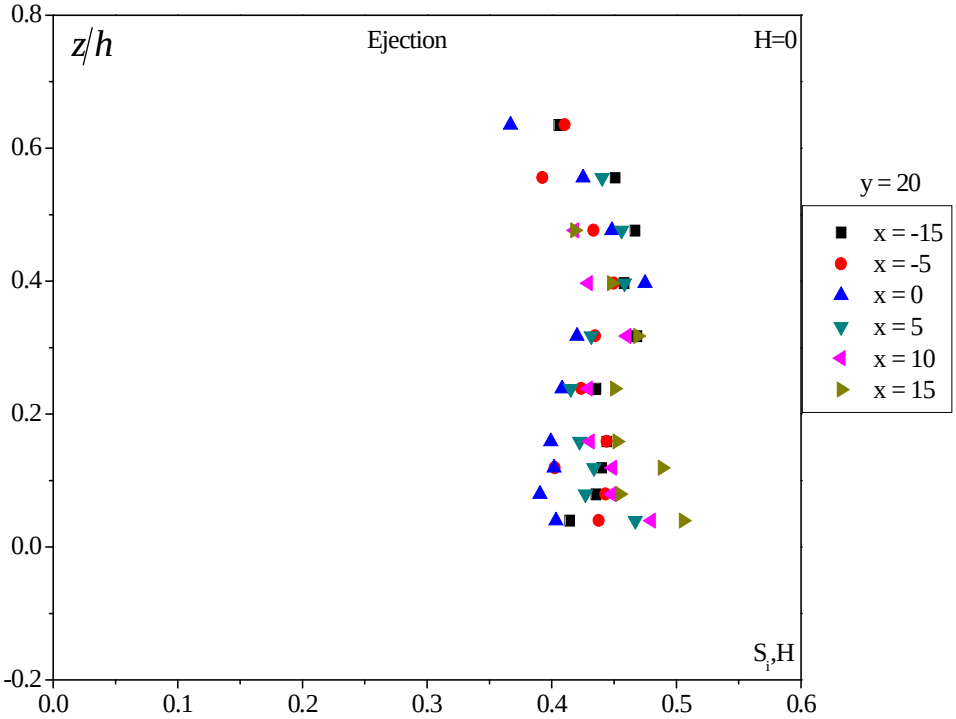

Fig. 5.70 (d) Distribution of ejection event at various measuring nodes around the submerged dike at y = 20cm

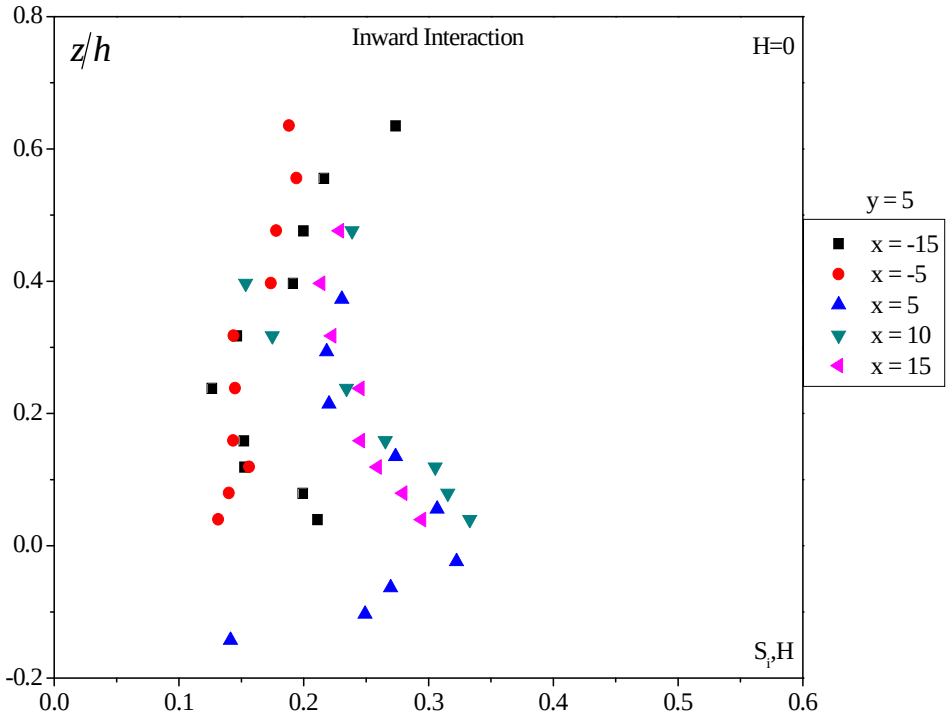

Fig. 5.71 (a) Distribution of inward interaction event at various measuring nodes around the submerged dike at y = 5cm

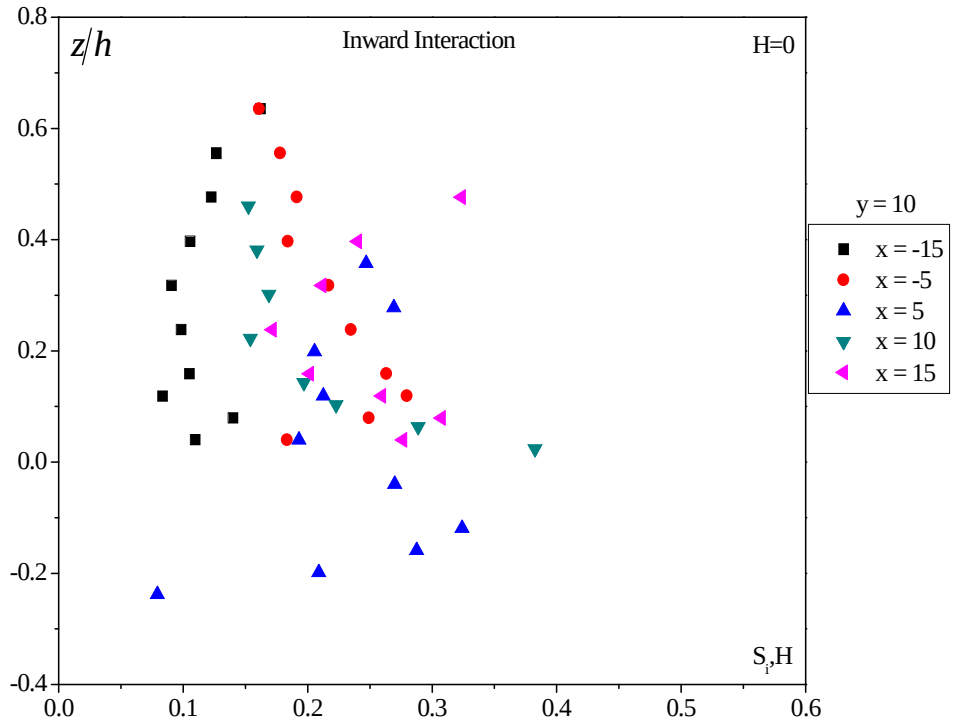

Fig. 5.71 (b) Distribution of inward interaction event at various measuring nodes around the submerged dike at y = 10cm

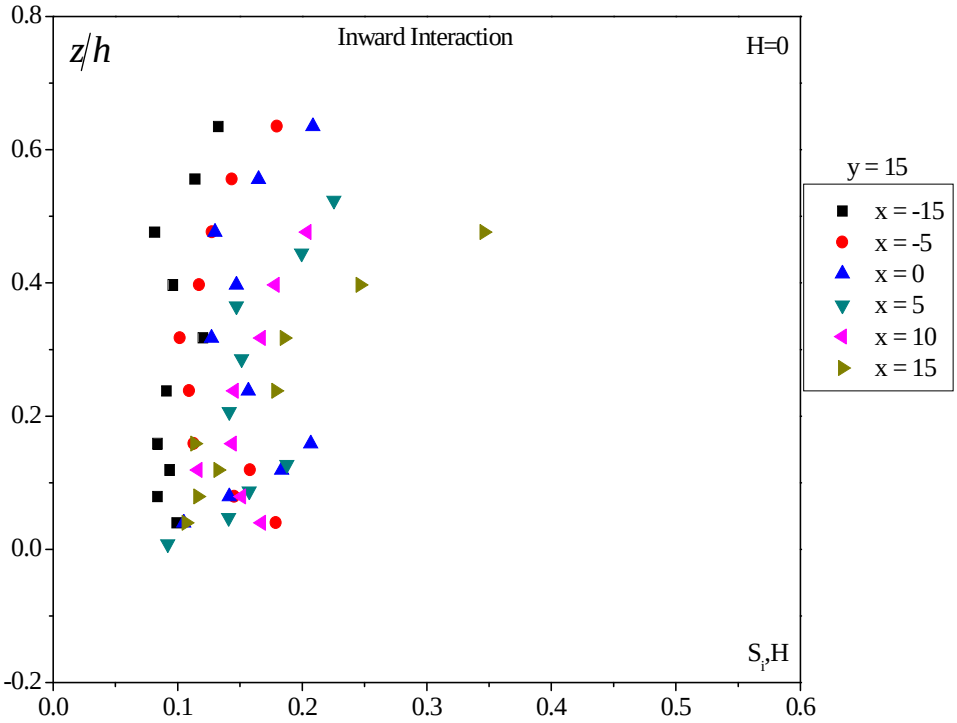

Fig. 5.71 (c) Distribution of inward interaction event at various measuring nodes around the submerged dike at y = 15cm

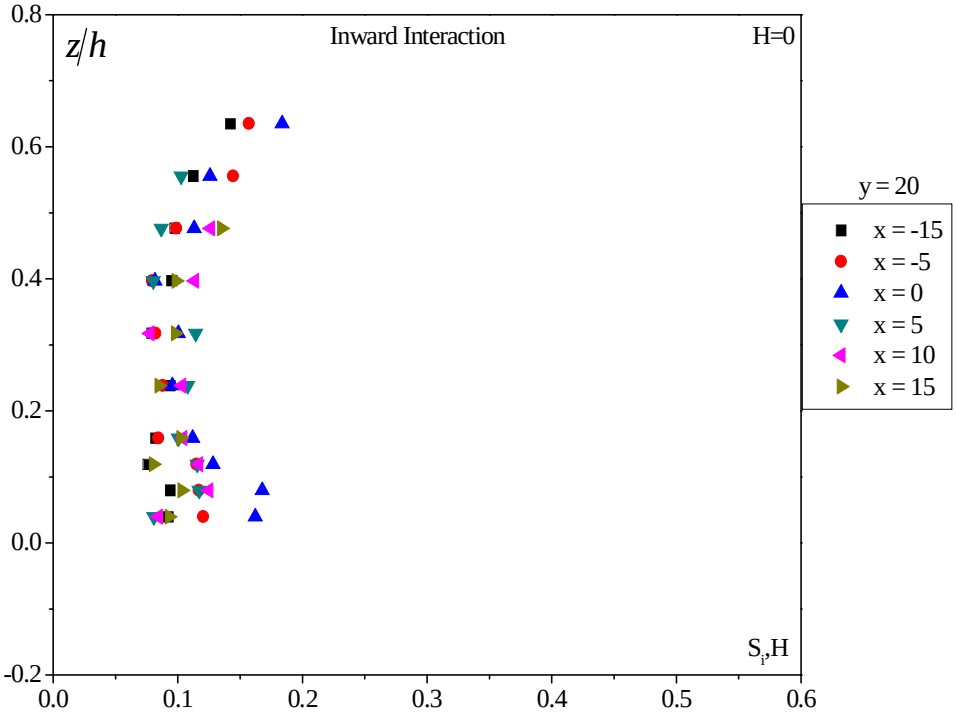

Fig. 5.71 (d) Distribution of inward interaction event at various measuring nodes around the submerged dike at y = 20cm

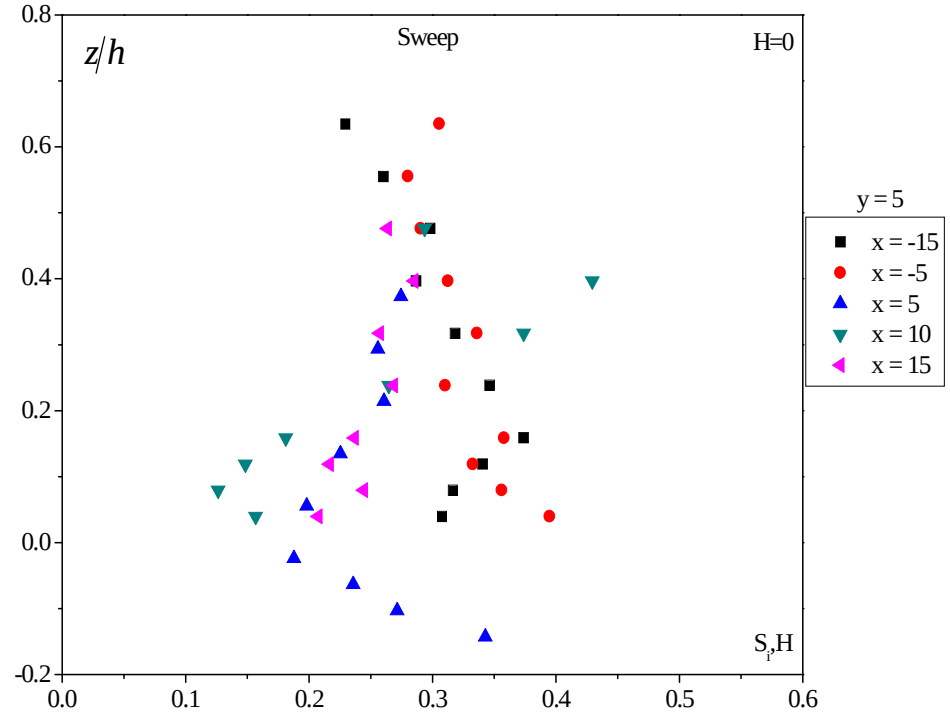

Fig. 5.72 (a) Distribution of sweep event at various measuring nodes around the submerged dike at y = 5cm

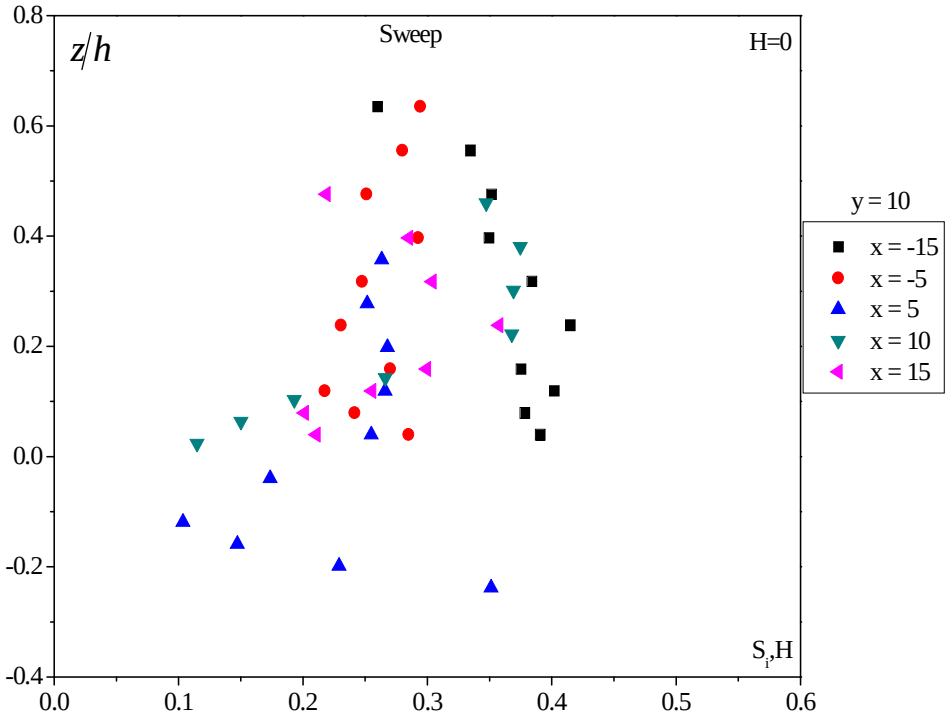

Fig. 5.72 (b) Distribution of sweep event at various measuring nodes around the submerged dike at y = 10cm

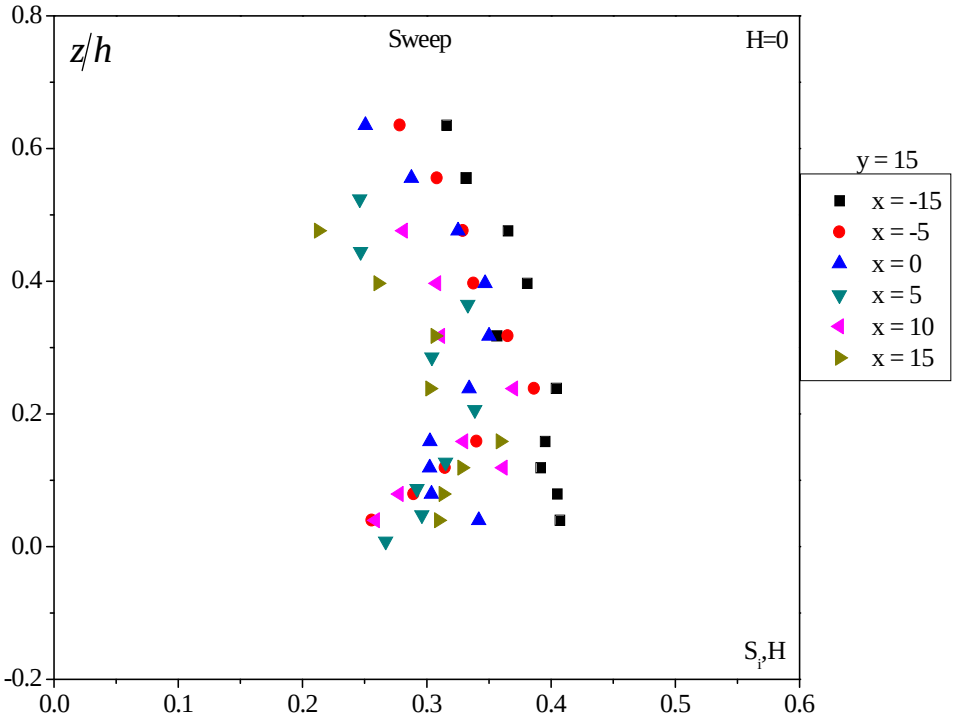

Fig. 5.72 (c) Distribution of sweep event at various measuring nodes around the submerged dike at y = 15cm

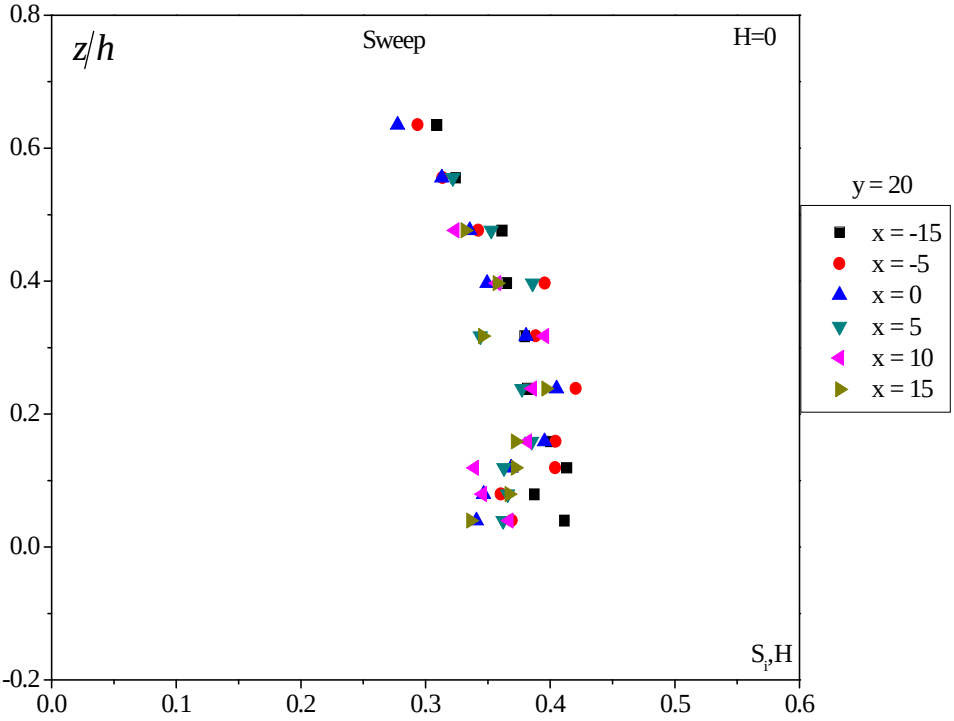

Fig. 5.72 (d) Distribution of sweep event at various measuring nodes around the submerged dike at y = 20cm

5.7 CONCLUDING REMARK

Visual analysis of process of scour around spur dike and pier in cohesive sediment mixtures formed by clay-gravel and clay-sand-gravel have been presented using the data collected in the present study. The extent, depth of scour and shape of scour hole were significantly different in cohesive sediments as compared to that in cohesionless sediments. Relationships were proposed to compute the temporal variation of depth of scour at nose and at the wake of the spur dikes (partially submerged and submerged) and at sides and in the wake zone of piers founded in clay-gravel and clay-sand-gravel sediment mixtures. The proposed relationships formulated in the Chapter-III were verified by the experimental data of depth of scour around partially submerged spur dike, submerged spur dike and pier in above mentioned cohesive sediment. Flow characteristics, turbulence intensities, Reynolds stresses and quadrant analysis of the flow around the spur dikes were also studied by measuring data at different grid points around the spur dikes. The study of flow and turbulence field signifies the sediment detachment and its transport by showing higher normalized velocity component, turbulence intensities and Reynolds stresses.

CHAPTER - VI

CONCLUSIONS

6.1 GENERAL

The main objective of present study was to investigate the influence of cohesion on the process of scour around spur dikes (partially submerged and submerged) and pier; and to study the flow characteristics around the spur dikes (partially submerged and submerged) founded in cohesive sediment consisting of clay-gravel and clay-sand-gravel mixtures. To achieve this, experiments were conducted to study the influence of cohesion on the above mentioned processes by varying the clay content in an organized manner. The experiments were conducted with two types of sediment mixtures; the first type was, fine gravel mixed with clay in varying proportions (10 to 50 %) and the second type was, fine gravel and fine sand in equal proportion by weight mixed with varying proportions of clay (10 to 50 %). For flow characteristics analysis ADV data was collected around the spur dikes after stabilization of scour hole. The working relationships were developed to compute the temporal variation of maximum depth of scour around spur dikes and piers in cohesive sediment mixtures.

The detailed conclusions derived from present study are summarized below.

6.2 COHESIVE PARAMETRS AFFECTING SCOURING PROCESS

The variables namely; proportion of clay fraction present in the mixture and unconfined compressive strength of the bed material were found to be significantly affecting the process of scour around spur dikes and pier. The value of observed depth of scour in cohesive sediment mixtures appeared to be much smaller in case of cohesive sediments compared to depth of scour in same sized cohesionless sediment. It was also found to decrease with an increase in the clay percentage and unconfined compressive strength of sediment bed. Based on dimensional consideration a functional relationship (Eq. 3.7) was derived in the present study for the estimation of depth of scour around the spur dikes and pier in clay-gravel and clay-sand-gravel mixtures.

6.3 SCOUR AROUND PARTIALLY SUBMERGED SPUR DIKE

The process of scour around partially submerged dike in cohesive sediment mixtures was found to be significantly different from that in cohesionless sediment. In cohesionless sediment, the scouring started from the nose of the spur dike immediately after the beginning of each experimental run and the maximum depth of scour was observed at the junction of wall and spur dike. However, in case of cohesive sediment bed, the scouring started from the wake region of the spur dike as shown in Figs. 5.1(a) and 5.1(b) and the maximum depth of scour was observed in the wake region of the spur dike (Figs. 5.2–5.4).

Relationships in the form of Eq. (5.4) and Eq. (5.5) were proposed to estimate the depth of scour at nose and at the wake of the partially submerged spur dike founded in cohesive sediment mixtures. The observed values of depth of scour at nose and at the wake of the partially submerged spur dike were compared against their corresponding values computed by the proposed relationship as shown in Figs. 5.17 and 5.18 respectively. The proposed relationship yielded satisfactory outcome with maximum error of two folds for 92.5% of total data for nose and 90.5% of the total data for the wake of the partially submerged spur dike. The scatterness of results by the proposed method as seen in Figs. 5.17 and 5.18 and similar other figures albeit was large, but is acceptable in the context of similar results generally reported in the literature on transport studies of the cohesive and cohesionless sediments.

Using the Eq. (2.17) as the basis, a computational procedure was proposed to determine the temporal variation of depth of scour in cohesive sediment consisting of clay-gravel and clay-sand gravel mixture. The proposed methodology was schematically described in Fig. 3.1 by illustrating the steps to be followed in the computations. Relationships described in Eq. (5.4) and Eq. (5.5) were proposed for the prediction of depth of scour at nose and at the wake of partially submerged spur dike. The graphical comparison of observed values of temporal variation of depth of scour with that computed by the proposed model revealed that proposed model very well predicted the depth of scour in such cohesive sediment mixtures (Figs. 5.19 to 5.22). The proposed method shall be useful in obtaining design value of depth of scour for hydraulic design of new bridges.

6.4 SCOUR AROUND SUBMERGED SPUR DIKE

The scouring initiates from the downstream corner of the submerged spur dike at the wake region (Fig. 5.23) and the maximum depth of scour was also observed at the wake of the dike. These results are very similar to partially submerged dike observations.

The relationships described in Eq. (5.17) and Eq. (5.18) were used to estimate the depth of scour at nose and at the wake of the submerged spur dike founded in cohesive sediment mixtures. The observed values of depth of scour at nose and at the wake of the submerged spur dike were compared against their corresponding values computed by the proposed relationship as shown in Figs. 5.36 and 5.37 respectively. The proposed relationships yielded satisfactory outcome with maximum error of two folds for 97.7% of the total data for nose and 95.9% of total data for wake of the submerged dike respectively.

The methodology is schematically described in Fig. 3.1 by illustrating the steps to be followed in the computations of depth of scour in cohesive sediment mixture. Relationships described in Eq. (5.17) and Eq. (5.18) were proposed to predict depth of scour at nose and at the wake of submerged spur dike. The graphical comparison of observed values of temporal variation of depth of scour with that computed by the proposed model revealed that proposed model very well predicted the depth of scour in such cohesive sediment mixtures (Figs. 5.38 to 5.41).

6.5 SCOUR AROUND PIER

In Cohesionless sediment, the process of scour started from the sides of the pier immediately after the commencement of each experimental run and the scour hole extended towards the nose of the pier. The maximum depth of scour was observed at the nose of the pier. However, in case of cohesive sediment bed the scouring started from the side of the pier at a point where separation of flow occured as shown in Figs. 5.42(a) and 5.42(b) and the maximum depth of scour observed at the sides of the pier.

Relationships described in Eq. (5.22) and Eq. (5.23) are used to estimate the depth of scour at sides and at the wake of the pier founded in cohesive sediment mixtures consisting of clay-gravel and clay-sand-gravel mixtures. The observed values of depth of scour at sides and at the wake of the pier were compared against their corresponding

values computed by the proposed relationships as depicted in Figs. 5.57 and 5.58. The proposed relationships yielded satisfactory outcome with maximum error of two folds for 92.57% of the total data for side and 94% of total data for wake of the pier respectively.

6.6 FLOW CHARACTERISTICS AROUND THE PARTIALLY SUBMERGED AND SUBMERGED SPUR DIKES

The flow characteristics around the partially submerged and submerged spur dike in the clay-gravel were analyzed in the form of mean velocity, turbulence intensity, Reynolds stresses and turbulence kinetic energy. Quadrant analysis was also carried out to quantify the contribution of outward interaction, ejection, inward interaction and sweep events out of whole data for a particular z/h value. Specific conclusions on flow characteristics are as follows

(i) At locations (5, 5), (5,10), (10,5) and (10,10) in the flow field of partially submerged and submerged spur dikes, very small values of longitudinal velocity component u (negative) were obtained whereas, larger values of u were obtained within the flow field bounded by the region x = 5 to 20cm and y = 15 to 25cm.

At the point (5, 15) the value of u varied from 1.24 to 1.48 times the approaching flow velocity for partially submerged dike and 1.07 to 1.38 times the approaching flow velocity for submerged dike (velocity profile were measured from bed surface to water surface).

(ii) The maximum value of longitudinal component of turbulence intensity occured near the original bed level (z/h = 0.3 to -0.3) just behind the partially submerged spur dike within the region x = 5 to 20cm and y = 5 to 10cm. Whereas, in the case of submerged spur dike, maximum value of longitudinal component of turbulence intensity was observed to occur near the original bed level (z/h = 0.5 to -0.25) just behind the submerged spur dike within the region x = 5 to 20cm and y = 5 to 10cm.

(iii) The maximum value of Reynolds stress component $\overline{u'w'}$ was observed to occur in the wake zone of partially submerged and submerged spur dikes [Figs. 5.62 (a - b)]. The value of Reynolds stresses component $\overline{u'w'}$ is larger for partially submerged spur dike than that for submerged spur dike whereas, the Reynolds stress component $\overline{v'w'}$ did not

show significant value around the spur dikes (partially submerged and submerged) [Figs. 5.63 (a - b)].

(iv) The maximum value of turbulence kinetic energy was observed to occur in the wake zone (bounded by the region x = 5 to 20cm and y = 5 to 10cm) of partially submerged and submerged dike [Figs. 5.64(a - b)]. Outside the scour hole, the values of the turbulence kinetic energy were larger for submerged spur dike than those for partially submerged dike while, within the scour hole the values of turbulence kinetic energy were larger for partially submerged dike than those observed for submerged spur dike.

(v) Quadrant analysis of ADV data showed that the values of outward and inward interaction were higher within the scour hole in partially submerged spur dike as compared to the values of ejection and sweep events, while outside of the scour hole the values of ejection and sweep events were higher as compared to the values of outward and inward interaction events. It was also observed that value of outward and inward interactions increases toward the lower most regions within the scour hole in case of partially submerged dike.

(vi) In case of submerged spur dike, the values of outward and inward interaction events were higher at the downstream of the submerged dike (x = 5, 10 and 20cm) than its upstream (x = -15 and -5cm) at an azimuthal plane of y = 5 and 10cm. The trend observed for ejection and sweep events around the submerged spur dike was also similar to that observed around partially submerged spur dike. At outside of the scour hole, small values of ejection and sweep events were measured at the downstream of the submerged dike (x = 10 and 20cm) than its upstream (x = -15 and -5cm) at an azimuthal plane of y = 5 and 10cm. While, within the scour hole at (5, 5) and (5, 10) the ejection and sweep events have maximum value at lower most level and decreases near initial bed level.

REFERENCES

Abou-seida, M. M., Elsaeed, G. H., Mostafa, T. M., and Elzahry, E. F. (2012). "Local scour at bridge abutments in cohesive soil." *J. Hydraul. Res., IAHR*, 50(2), 171–180.

Ahmad, M. F., Dong, P., Mamat, M., Nik, W. B. W., and Mohd, M. H. (2011). "The critical shear stresses for sand and mud mixture." *Applied Mathematical Sciences*, 5 (2), 53 – 71.

Ahmed, F. and Rajratnam, N. (1998). "Flow around bridge piers." *J. Hydraul. Eng., ASCE*, 124(3), 288-300.

Ahmed, M. F., and Rajaratnam, N. (2000). "Observations on flow around bridge abutment." *J. Eng. Mech.*, 126, 51-59.

Almediej, J. H. and Diplas, P. (2003). "Bed load transport in gravel bed streams with unimodel sediment." *J. Hydraul. Eng., ASCE*, Vol. 129(11), 896-904.

Ali, K. H. M., and Lim, S. Y. (1986). "Local scour caused by submerged wall jets." *Proceedings of Institution of Civil engineers*, Part 2, 81(4), 607-645.

Annandale, G. W. (1995). "Erodibility." *J. Hydraul. Res., IAHR*, 33 (4), 471-493.

Ansari, S. A. (1999). "Influence of cohesion on local scour." *Ph. D. Thesis, Department of Civil Engineering, Indian Institute of Technology, Roorkee* (Formerly University of Roorkee, Roorkee), India, pp. 189.

Ansari, S. A., Kothyari, U. C., and Ranga Raju, K. G. (2002). "Influence of cohesion on scour around bridge piers." *J. Hydraul. Res., IAHR*, 40(6), 717–729.

Ansari, S. A., Kothyari, U. C., and Ranga Raju, K. G. (2003). "Influence of cohesion on scour under submerged circular vertical jet." *J. Hydraul. Eng., ASCE*, 129(12), 1014-1019.

Ansari, S. A., Kothyari, U. C., and Ranga Raju, K. G. (2007). "Incipient motion characteristics of cohesive sediments." *ISH Journal of Hydraulic Engineering*, 13(2), 108-121.

Ballio, F., Radice, A. and Dey, S. (2010). "Temporal scales for live-bed scour at abutments." *Journal of Hydraulic Engineering, ASCE*, Vol. 136(7), 395-402.

Barbhuiya, A. K., and Chakma, T. (2012). "Effect of consolidation on local scour around bridge pier in cohesive soil." *International Journal of Engineering Research & Technology*, Vol. 1 (7), 1-9.

Barbhuiya, A. K., and Dey, S. (2003). "Vortex flow field in a scour hole around abutments." *Int. J. Sediment Res.*, 18(4), 310-325.

Barbhuiya, A. K., and Dey, S. (2004). "Velocity and turbulence at a wing-wall abutment." *Sadhana*, 29(1), 35-56.

Brandimarte, L., Montanari, A., Briaud, J. L., and D'odorico, P. (2006). "Stochastic flow analysis for predicting scour of cohesive soils." *J. Hydraul. Eng., ASCE*, Vol. 132(5), 493–500.

Briaud J. L., Ting F. C. K., Chen S. C., Gudavalli R., Perugu S., and Wei G. (1999). "SRICOS: Prediction of scour rate in cohesive soils at bridge piers." *Journal of Geotechnical and Geoenvironmental Engineering*, Vol. 125 (4), 237-246.

Briaud, J. L., Chen, H. C., Kwak, K. W., Han, S. W., and Ting, F. C. K. (2001). "Erosion function apparatus for scour rate predictions." *Journal of Geotechnical and Geoenvironmental Engineering*, 127 (2), 105-113.

Cardoso, A. H., and Bettess, R., (1999), "Effects of time and channel geometry on scour at bridge abutments." *J. Hydraul. Eng., ASCE*, Vol. 125 (4), 388-399.

Cava, D., Katul, G. G., Scrimieri, A., Poggi, D., Cescatti, A., and Giostra, U. (2006). "Buoyancy and the sensible heat flux budget within dense canopies." *Boundary Layer Meteorol*., 118, 217–240.

Cellino, M., and Lemmin, U. (2004). "Influence of coherent flow structure on the dynamics of suspended sediment transport in open channel flows." *J. Hydraul. Eng., ASCE*, 130(11), 1077-1088.

Chaudhuri, S., and Debnath, K. (2013). "Observations on initiation of pier scour and equilibrium scour hole profiles in cohesive sediments." *J. Hydraul. Eng., ASCE*, 19 (1), 27-37.

Chen, X. (2008). "Numerical study of abutment scour in cohesive soils." Ph.D. Thesis, Texas A&M University, College Station, TX.

Chang, W., Lai, J., and Yen, C. (2004). "Evolution of Scour Depth at Circular Bridge Piers." *J. Hydraul. Eng., ASCE*, Vol. 130(9), 905–913.

Debnath, K., and Chaudhuri, S. (2010,a). "Laboratory experiments on local scour around cylinder for clay and clay-sand mixed beds." *Engineering Geology*, 111, 51–61.

Debnath, K., and Chaudhuri, S. (2010,b). "Bridge pier scour in clay-sand mixed sediments at near-threshold velocity for sand." *J. Hydraul. Eng., ASCE*, 136(9), 597–609.

Debnath, K., Chaudhuri, S., and Manik, M., K. (2014). "Local scour around abutment in clay/sand-mixed cohesive sediment bed." *ISH Journal of Hydraulic Engineering*, 20(1), 46-64.

Dey, S., and Barbhuiya, A. K. (2004). "Clear-water scour at abutments in thinly armored beds." *J. Hydraul. Eng., ASCE*, 130, 622-634.

Dey, S., and Barbhuiya, A. K. (2005, a). "Time variation of scour at abutments." *J. Hydraul. Eng., ASCE*, 131, 11-23.

Dey, S., and Barbhuiya, A. K. (2005, b). "Flow field at a vertical-wall abutment." *J. Hydraul. Eng., ASCE*, 131(12), 1126–1135.

Dey, S., and Barbhuiya, A. K. (2006). "3D flow field in a scour hole at a wing-wall abutment." *J. Hydraul. Res., IAHR*, 44(1), 33-50.

Dey, S., Bose, S. K. and Sastry, G. L. N. (1995). "Clear water local scour at complex piers." *J. Hydraul. Eng., ASCE*, 121(9), 635-643.

Dey, S., Helkjær, A., Sumer, B. M., and Fredsøe, J. (2011). "Scour at vertical piles in sand-clay mixtures under waves." *Journal of Waterway, Port, Coastal, and Ocean Engineering*, Vol. 137(6), 334-331.

Dey, S. and Raiker, R. V. (2007). "Characteristics of horseshoe vortex in developing scour holes at piers." *J. Hydraul. Eng., ASCE*, 133(4), 399-413.

Dou, G. R. (1999). "Incipient motion of coarse and fine sediment." *J. Sediment Res.* (in Chinese), 6, 1-9.

Duan, J. (2009). "Mean flow and turbulence around a laboratory spur dike." *J. Hydraul. Eng., ASCE,* 135 (10), 803–811.

Duan, J., He, L., Fu, X., and Wang, Q. (2009). "Mean flow and turbulence around experimental spur dike." *Advances in Water Resources*, 32, 1717-1725.

Duan, J., He, L., Wang, G., and Fu, X. (2011). "Turbulent burst around experimental spur dike." *Int. J. Sediment Res.*, 26, 471-486.

Dunn, I. S. (1959). "Tactive resiatance of cohesive channels." *Journal of Soil Mechanics and Foundation Division, ASCE*, Vol. 85(SM-3), 1-24.

Elawady, E., Michiue, M., and Hinokidani, O. (2001). "Movable bed scour around submerged spur-dikes." *Annual Journal of Hydraulic Engineering*, 45, 373-378.

Ettema, R. (1980). "Scour at bridge piers." *Report No. 216, Department of Civil Eng., University of Auckland, Auckland, New Zealand.*

Ettema, R. and Muste, M. (2004). "Scale effects in flume experiments on flow around a spur dike in flat bed channel." *J. Hydraul. Eng., ASCE*, 130, 635-646.

Ezzeldin, M. M., Saafan, T. A., Rageh, O. S., and Nejm, L. M. (2007). "Local scour around spur dikes." *Eleventh International Water Technology Conference (IWTC11)*, Sharm El-Sheikh, Egypt, 779-795.

Fazli, M., Ghodsian, M., and Neyshabouri, S. A. A. S. (2008). "Scour and flow field around a spur dike in a 90° bend." *Int. J. Sediment Res.*, 23(1), 56-68.

Federal Highway Adminisration, (2001). "Evaluating scour at bridges." *National Highway Institute, Publication No. FHWA NHI 01-001, HEC No. 18*, U. S.

Fukuoka, S., Tomita, K., Hotta, T., and Miyagawa, T. (1994). "Practical numerical simulation of local scour around a bridge pier." *Journal of Hydraulic, Coastal and Environmental Engineering, JSCE*, No.497/II-28, 71-80. (In Japanese)

Fukuoka, S., Miyagawa, T. and Toboishi, M.(1997). "Measurements of flow and bed geometry around a cylindrical pier and calculation of its fluid forces." *Annual Journal of Hydraulic Engineering, JSCE*, 729-734. (in Japanese)

Garde, R. J., Subramanya, K., Nambudripad, K. D. (1961). “Study of scour around spur dikes.” *ASCE Journal of the Hydraulics Division*, 87(HY6), 23-37.

Garde, R. J., and Ranga Raju K. G. (2006). “Mechanics of Sediment Transport and Alluvial Stream Problems.” *3rd ed., New Age International Publisher, New Delhi*, pp 686.

Ghodsian, M., and Vaghefi, M. (2009). “Experimental study on scour and flow field in a scour hole around a T-shaped spur dike in a 90^{o} bend.” *Int. J. Sediment Res.*, 24, 145-158.

Gill, M. A. (1972). “Erosion of sand beds around spur dikes.” *J. Hydraul. Div., ASCE*, 98(9), 1587–1602.

Giri, S. (2010). “Clear-water scour development at bridge abutments.” *J. Hydraul. Res., IAHR*, 43 (4), 445-448.

Giri, S., and Shimizu, Y. (2004). “Observation on bed variation in a meandering like flume with river training structures.” *Annual Journal of Hydraulic Engineering, JSCE*, 48, 1069-1074.

Giri, S., and Shimizu, Y. (2005). “A method for local scour prediction at river structures considering time factor.” *Annual Journal of Hydraulic Engineering, JSCE*, 48, 1069-1074.

Goring, D. G., and Nikora, V. I. (2002). “Despiking acoustic doppler velocimeter data.” *J. Hydraul. Eng., ASCE*, 128 (1), 117–126.

Graf, W. H (1984). “Hydraulics of sediment transport.” *Water Resources Publications, Highlands Ranch, Colorado*.

Graf, W. H. and Istiarto, I. (2002). “Flow pattern in the scour hole around a cylinder.” *J. Hydraul. Res., IAHR*, 40(1), 13-20.

Graf, W. H., and Yulistiano, B. (1998). “Experiments on flow around a cylinder: the velocity and velocity fields.” *J. Hydraul. Res., IAHR*, 36(4), 637-653.

Grim, R. E. (1962). “Applied Clay Mineralogy.” McGraw-Hill Book Company, New York.

Hager, W. H. and Unger, J. (2010). “Bridge pier scour under flood waves.” *J. Hydraul. Eng., ASCE*, 136(10), 842-847.

Hanson, G. J. (1990). “Surface erodibility of earthen channels at high stresses. Part 1, Open channel testing.” *Trans. ASAE*, 33(1), 127–131.

Hanson, G. J., and Hunt, S. L. (2006). “Lessons learned using laboratory jet method to measure soil erodibility of compacted soils.” *Appl. Eng. Agric.*, 23(3), 305–312.

Hjorth, P. (1975). “Studies on the nature of local scour.” *Bulletin No. 46, Dept. of Water Resources Eng., University of London.*

Hong, R. J., and Xu, S. S. (1991). "Experimental study on incipient of mud in a fluid." *J Tianjin Univ* (in Chinese), (suppl): 79-85.

Hosny, H. M. (1995). "Experimental study of local scour around circular bridge piers in cohesive soils." *Ph.D. Thesis. Civil Eng. Dept., Colorado State University, Fort Collins CO.*

Hayter, E.J. (1983). "Prediction of Cohesive Sediment Movement in Estuarial Waters," *Ph.D. Thesis, The University of Florida, Gainesville.*

IS:1498. (1970). "Classification and identification of soils for general engineering purposes." Simco Printing Press, Delhi, India, 6–17.

IS:2720-10. (1991). "Methods of test for soil - Part X: Determination of unconfined compressive strength." Reprography Unit, BIS, New Delhi, India, 1–4.

IS:2720-29. (1975). "Methods of test for soil - Part XXIX: Determination of dry density of soils in-place." Prabhat Offset Press, Delhi, India, 4–8.

Jain, R. K. (2007). "Influence of cohesion on detachment and transport of clay-sand-gravel mixtures." *Ph.D. Thesis, Indian Institute of Technology, Roorkee, India,* pp. 247.

Jain, R. K., and Kothyari, U. C. (2009). "Cohesion influences on erosion and bed load transport." *Water Resour. Res.*, 45(6), W06410.

Jain, R. K. and Kothyari, U. C. (2010). "Influence of cohesion on suspended load transport of non-uniform sediments." *J. Hydraul. Res.*, IAHR, 48(1), 33-43.

Jain, R. K., Kumar, A., and Kothyari, U. C. (2015). "Turbulence statistics of flow through degraded channel bed of sandegravel mixture." *J. Hydro-envir. Res.*, (xx), 1-11. (in press)

Jiang, C. B., Bai, Y. C., Jiang, N. S., and Hu, S. X. (2001). "Incipient motion of cohesive silt in the Haihe River estuary." *Shuili Xuebao*, 6: 51-56. (In Chinese).

Kamojjala, S. Gattu, N. P., Parola, A. C. and Hagerty, D. J. (1995). "Analysis of 1993 Upper Mississippi Flood Highway Damage." *Proceedings 1st International Conference on Water Resources Engineering, San Antonio, Texas*, 14-18 Aug, Vol. 2, pp. 1061-1065.

Kamphuis, J. W., and Hall, K. R. (1983). "Cohesive material erosion by unidirectional current." *J. Hydraul. Eng., ASCE*, 109, 39-62.

Kand, C.V. (1993). "Pier scour in sand, clay and boulders." *Bridge Engineering* (India) Vol. IX and X.

Kessel, T. V., and Blom, C., (1998), "Rheology of Cohesive Sediments: Comparison Between a Natural and an Artificial Mud." *J. Hydraul. Res., IAHR*, Vol. 36(4), 591-612.

Kho, K. T. (2004). "An experimental study of local scour around circular bridge piers in cohesive soils." *Ph.D. Thesis, University of Newcastle upon Tyne*, pp. 228.

Koken, M. (2011). “Coherent structures around isolated spur dikes at various approach flow angles.” *J. Hydraul. Res., IAHR*, 49(6), 736-743.

Koken, M., and Constantinescu, G. (2014). “Flow and turbulence structure around abutments with sloped sidewalls.” *J. Hydraul. Eng., ASCE*, 04014031-13.

Kothyari, U. C. (1989). “Scour around bridge piers.” *Ph.D. Thesis, Univ. of Roorkee, Roorkee, India*.

Kothyari, U. C. (2007). “Indian practice on estimation of scour around bridge piers-A comment.” *Sadhana*, 32(3), 187–197.

Kothyari, U. C., Garde, R. J. and Ranga Raju, K. G. (1992, a). “Temporal variation of scour around circular bridge piers.” *J. Hydraul. Eng., ASCE*, 118(8), 1091-1106.

Kothyari, U. C., Garde, R. J. and Ranga Raju, K. G. (1992, b). “Live bed scour- around cylindrical bridge piers.” *J. Hydraul. Res., IAHR*, 30(5), 701-715.

Kothyari, U. C., Hager, W. H. and Oliveto, G. (2007). “Generalized approach for clear-water scour at bridge foundation elements.” *J. Hydraul. Eng., ASCE*, 133(11), 1229-1240.

Kothyari, U. C. and Jain, R. K. (2006). “Detachment of clay-gravel mixtures by channel flow.” *Proceedings of ICFMAE-06*, ISI Kolkata, India, pp.152-157.

Kothyari, U. C., and Jain, R. K. (2008). “Influence of cohesion on the incipient motion condition of sediment mixtures.” *Water Resour. Res.*, 44(4), W04410.

Kothyari, U. C., and Jain, R. K. (2010). “Erosion characteristics of cohesive sediment mixtures.” *River Flow*, 815-820.

Kothyari, U. C., and Kumar, A. (2010). "Temporal variation of scour around circular bridge piers." *ISH Journal of Hydraulic Engineering*, (Sup1.), 16, 35-48.

Kothyari, U. C., and Kumar, A. (2012) “Temporal variation of scour around circular bridge piers.” *ISH Journal of Hydraulic Engineering*, (Suppl 1), 18(3), 272-273.

Kothyari, U. C., Kumar, A., and Jain, R. K. (2014). “Influence of cohesion on river bed scour in wake region of piers.” *J. Hydraul. Eng., ASCE*, 140(1), 1-13.

Kothyari, U. C., and Ranga Raju, K. G. (2001). “Scour around spur dikes and bridge abutments.” *J. Hydraul. Res., IAHR*, 39 (4), 367-374.

Kraus, N.C., Lohrmann, A., and Cabrea, R. (1994). “New acoustic meter for measuring 3D laboratory flows.” *J. Hydraul. Eng., ASCE*, 120(3), 406-412.

Kuhnle, R. A., Alonso, C. V. and Shields F. D. (1999). “Geometry of scour hole associated with 90^{o} spur dikes.” *J. Hydraul. Eng., ASCE*, 125(9), 972-978.

Kuhnle, R. A., Alonso, C. V. and Shields F. D. (2002). “Local scour associated with angled spur dikes.” *J. Hydraul. Eng., ASCE*, 128(12), 1087-1093.

Kuhnle, R. A., Jia, Y., and Alonso, C. V. (2008). “Measured and simulated flow near a submerged spur dike.” *J. Hydraul. Eng., ASCE*, 134(7), 916-924.

Kumar, A. (2007). “Scour around circular compound bridge piers.” *Ph.D. Thesis, Indian Institute of Technology, Roorkee, India*.

Kumar, A. (2012). “Comparative study of Three-dimensional flow characteristics at Exposed nonuniform circular pier.” *Proc. Conf. on Hydraulics and Water Resources-HYDRO 2012*, 7-8 Dec, IIT Bombay, Mumbai, India

Kumar, A. (2011). “Scour around circular piers founded in clay-sand-gravel sediment mixtures.” *Ph.D. Thesis, Indian Institute of Technology, Roorkee, India*.

Kumar, A., and Kothyari, U. C. (2012). “Three-dimensional flow characteristics within the scour hole around circular uniform and compound piers.” *J. Hydraul. Eng., ASCE*, 138(5), 420–429.

Kumar, A., Kothyari, U. C., and Ranga Raju, K. G. (2012). “Flow structure and scour around circular compound bridge piers - A review.” *Journal of Hydro-Environment Research*, 6 (4), 251-265.

Kuti, E. O. and Yen, C. (1976). “Scouring of cohesive soils.” *J. Hydraul. Res., IAHR*, 14, 195-206.

Laflen, J. M., and Beasley, R. P. (1960). “Effect of compaction on critical tractive forces in cohesive soils.” *Res. Bull. 749, Agric. Exp. Stat. Univ. of Mo., Columbia.*

Lim, S. Y. (1997). “Equilibrium clear-water scour around an abutment.” *J. Hydraul. Eng., ASCE*, 123, 237–243.

Link, O. (2006). “Time scale of scour around a cylindrical pier in sand and gravel.” *Third Chinese-German Joint Symposium on Coastal and Ocean Engineering*, National Cheng Kung University, Tainan, November 8-16, 2006.

Link, O., Klischies, K., Montalva, G., and Dey, S. (2013). “Effects of bed compaction on scour at piers in sand-clay mixtures.” *J. Hydraul. Eng., ASCE*, 139(9), 1013-1019.

Liriano, S. L. and Day, R. A.(2000). “Structures of turbulent flow in scour holes downstream of submerged jets, in stochastic hydraulics.” In: Wang, and Hu (eds.), Balkema, Rotterdam.

Lu, J. Y. Z. S. Z., Hong, J. H., Lee, J. J., and Raikar, R. V. (2011). “Temporal variation of scour depth at non-uniform cylindrical piers.” *J. Hydraul. Eng., ASCE*, 137(1), 45-56.

Lu, S. S., and Willmarth, W. W. (1973). “Measurements of the structure of the Reynolds stress on a turbulent boundary layer.” *J. Fluid Mech.*, 60, 480-511.

Lundkvist, M., Grue, M., Friend, P. L., and Flindt, M. R. (2007). “The relative contributions of physical and microbiological factors to cohesive sediment stability.” *Continental Shelf Research*, 27(8), 1143-1152.

Mahapatra, P. K., and Murty, B. S. (1994). “Bed level variation in channel expansions with movable beds.” *J. Irrig. Drain. Eng., ASCE*, 120(6), 1114-1121.

Masjedi, A., Dehkordi, V., Alinejadi, M., and Taeedi, A. (2010a). “Experimental study on scour depth in around a T-shape spur dike in a 180 degree bend.” *World Appl. Sci. J.*, 10(10), 1046-1052.

Masjedi, A., Bejestan, M. S., and Rahnavard, P. (2010,b). “Reduction of local scour at single T-shape spur dike with wing shape in a 180 degree flume bend.” *World Appl. Sci. J.*, 8(9), 1122-1128.

Masjedi, A., and Foroushani, E. P. (2012). "Investigation of hydrodynamics on local scour by shape of single spur dike in river bend."*26th IAHR Symposium on Hydraulic Machinery and Systems, IOP Conf. Series: Earth and Environmental Science*, 15, 1-5.

Mazurek, K. A., Rajaratnam, N., and Sego D. C. (2001). “Scour of cohesive soil by submerged circular turbulent impinging jets.” *J. Hydraul. Eng., ASCE*, 127: 598–606.

Mazurek, K. A., Rajaratnam, N., and Sego, D. C. (2003). “Scour of a cohesive soil by submerged plane turbulent wall jets.” *J. Hydraul. Res., IAHR*, 41, 195–206.

Mazumder, B. S. and Ojha, S. P. (2007). “Turbulence statistics of flow due to wave-current interaction.” *Flow Measurement and Instrumentation*, 18, 129-138.

Mazumder, B. S. Pal, D. K., Ghoshal, K., and Ojha, S. P. (2006). “Contribution of burst-sweep cycles to the Reynolds shear stresses over the waveform structures.” *ISH Journal of Hydraulic Engineering*, 12 (2), 66-77.

Melville, B. W. (1975). “Scour at bridge sites.” *Rep. No. 117, Univ. of Auckland, Auckland, New Zealand*.

Melville, B. W. (1992), “Local Scour at Bridge Abutments.” *J. Hydraul. Eng., ASCE*, Vol. 118(4), 615-631.

Melville, B. W. (1997). “Pier and abutment scour: integrated approach.” *J. Hydraul. Eng., ASCE*, 123(2), 125-136.

Melville, B. W. and Chiew, Y. M. (1999). “Time Scale for Local Scour at Bridge Piers.” *J. Hydraul. Eng., ASCE*, 125(1), 59-65.

Melville, B. W. and Coleman, S. E. (2000). “Bridge Scour.” *Water Resources Publication, Highlands Ranch, Colo*.

Melville B. W., and Raudkivi, A. J. (1977). “ Flow characteristics in local scour at bridge piers.” *J. Hydraul. Res., IAHR*, 15: 373–380.

Melville, B. W. and Sutherland, A. J. (1988). “Design method for local scour in bridge piers.” *J. Hydraul. Eng., ASCE*, 114 (10), 1210–1226.

Mia, M. F. and Nago, H. (2003). “Design method of time -dependent local scour at circular bridge pier.” *J. Hydraul. Eng., ASCE*, 129(6), 420-427.

Mirtskaoulava, T. E. (1991). “Scouring by flowing of water of cohesive and non-cohesive beds.” *J. Hydraul. Res., IAHR*, 29 (3), 341–354.

Mitchell, J. K. (1993). "*Fundamentals of soil behavior.*" 2nd Ed. Wiley, New York.

Mohammadpour, R., Ghani, A. AB., and Azamathulla H. M. (2013). "Estimation of dimension and time variation of local scour at short abutment." *International Journal of River Basin Management*, 11(1), 121-135.

Molinas, A., Jones, S., and Hosny, M. (1999). "Effects of cohesive material properties on local scour around piers." *Transportation Research Record 1690, Transportation Research Board, Washington, DC*.

Molinas, A., and Reiad N. Y. (1999). "Effect of cohesion on bridge abutment scour." Publication No. FHWA-RD-99-187, *Federal Highway Administration, U.S. Department of Transportation, McLean, VA.*

Mostafa, T.M.S. (2003). "Experimental modeling of local scour in cohesive soils." *PhD dissertation. University of South Carolina, Columbia SC.*

Murty, B. S. and Chaudhry, M. H. (1991). "Numerical modeling of aggradation and degradation in alluvial channels". *J. Hydraul. Eng., ASCE*, 117(9), 1145-1164.

Muzzammil, M., and Gangadhariah, T. (2003). "The mean characteristics of horseshoe vortex at a cylindrical pier." *J. Hydraul. Res.,IAHR*, 41(3), 285–297.

Nasrollahi, A., Ghodsian, M. and Salehi Neyshabouri S. A. A. (2008). "Local scour at Permeable spur dikes." *J. Appl. Sci.*, 8(19), 3398-3406.

Nelson, J. M., Shreve, R. L., McLean, S. R., and Drake, T. G. (1995). "Role of near-bed turbulence structure in bed load transport and bed form mechanics." *Water Resour. Res.*, 31 (8), 2071-2086.

Nezu, I., and Nakagawa, H. (1993). "Turbulence in open channel flows." *IAHR Monograph, Balkema*, Rotterdam, the Netherlands.

Nortek (2000). "Nortek 10 MHz Velocimeter: Operations Manual." *NDV Operations Manual*, Document No., N3000-100/Rev.b/10.08.2000.

Oh, S., Chen, X., Briaud, J., Chang, K., and Chen, H. (2007). "The effect of abutment length for abutment scour in cohesive soil: initial results." *Geotechnics of Soil Erosion*, 1-10.

Ojha, S. P., and Majumder, B. S. (2008). "Turbulence characteristics of flow region over a series of 2-D dune shaped structure." *J. Advances in Water Resources*, 31, 561-576.

Ojha, S. P., and Mazumder, B. S. (2010). "Turbulence characteristics of flow over a series of 2-D bed forms in the presence of surface waves." *Journal of Geophysical Research*, 115, 1-15.

Oliveto, G., and Hager, W. H., (2002). "Temporal Evolution of clear-water pier and abutments scour." *J. Hydraul. Eng., ASCE*, 128 (9), 811-820.

Oliveto, G. and Hager, W. H. (2005). "Further results to time dependent local scour at bridge elements." *J. Hydraul. Eng., ASCE*, 131, 97-105.

Pagliara, S. and Carnacina, I. (2011, a). “Influence of large woody debris on sediment scour at bridge piers.” *Int. J. Sediment Res.*, 26, 121-136.

Pagliara, S., and Carnacina, I. (2011,b). “Influence of wood debris accumulation on bridge pier scour.” *J. Hydraul. Eng., ASCE,* 137(2), 254–261.

Pagliara, S., Carnacina, I., and Cigni, F. (2010). “Sills and gabions as countermeasures at bridge pier in presence of debris accumulation.” *J. Hydraul. Res., IAHR,* 48(6), 764–774.

Pagliara, S., Palermo, M. and Azizi, R. (2014). “Scour control at bridge piers using macro-roughness elements.” *Water Management*, 1-15.

Papanicolaou, A. N., Diplas, P., Dancy, C. L., and Balakrishnan, M. (2001). “Surface roughness effects in near-bed turbulence: Implication to sediment entrainment.” *Journal of Engineering Mechanics,* 127 (3), 211–218.

Parola, A. C., Hagerty, D. J., Mueller, D. S., Melville, B. W., Parker, G., Usher, J. S. (1997) “The Need for Research on Scour at Bridge Crossings.” *Proceedings of the 27th Congress of the International Association for Hydraulic Research, San Francisco,*CA, 10-15 Aug, Vol. 1, pp. 124-129.

Partheniades, E. (2007). “Engineering properties and hydraulic behavior of cohesive sediments.” *Boca Raton,* Florida.

Patel, P. L., Porey, P. D., Ghare, A. D. and Patel, B. S. (2009,a). “Entrainment characteristics of nonuniform unimodel and bimodal sediments.” *KSCE Journal of Civil Engineering,* 13 (3), 189-194.

Patel, P. L., Porey, P. D., and Patel, B. S. (2009,b). “Critical tractive stresses of representative sizes in nonuniform sediments.” *ISH Journal of Hydraulic Engineering*, 15 (3), 40-50.

Patel, P. L., and Rati, D. R. (2006). “Critical tractive stress of nonuniform and bimodal sediments.” *ISH Journal of Hydraulic Engineering,* 12 (1), 39-51.

Proctor, R. R. (1933). “Fundamental Principles of Soil Compaction,” *First of Four Articles on the Design and Construction of Rolled-Earth Dams,* Engineering News-Record, Volume 111, Number 9, New York, New York.

Raiker, R. V., and Dey, S. (2005). “Scour of gravel beds at bridge piers and abutments.” *Water Management,* WM4, 157-162.

Ramesh, R., Datta, B., Murty, B. S. and Narayana, A. (2000). “Optimal estimation of roughness in open channel flows.” *J. Hydraul. Eng., ASCE,* 126(4), 299-303.

Ram Babu, M., Rao, N. S., and sunder, V. (2002). “A simplified instrumentation for measuring scour in silty clay around a vertical pile.” *Applied Ocean research,* 24, 355-360.

Ram Babu, M., Sunder, V., and Rao, N. S. (2003). “Measurement of scour in cohesive soils around a vertical pile-simplified instrumentation and regression analysis.” *IEEE Journalof Ocean Engineering,* 28 (1), 106-116.

Rashedipoor, A., Masjedi, A., and Shojaenjad, A. (2012). “Investigation on local scour around spur dike in a 180 degree flume bend.” *World Appl. Sci. J.*, 19(7), 924-928.

Raudkivi, A. J. (1990). “Loose Boundary Hydraulics.” 3rd ed., Pergamon, New York.

Raudkivi, A. J., and Ettema, R. (1983). “Clear-water scour at cylindrical piers.” *J. Hydraul. Eng., ASCE,* 109 (3), 338–350.

Raudkivi, A. J., and Tan, S.K. (1984). “Erosion of cohesive sediments.” *J. Hydraul. Res., IAHR,* 22(4), 217-233.

Reddy, H.A., Roussinova, V., Balachandar, R., and Bolisetti, T. (2012). “Higher order moments of velocity fluctuations in an open channel flow with mobile bedforms.” *River Flow Murillo (Ed.)*

Richardson, E. V., Harrison, L. J., and Davis, S. R. (1991). “Evaluating Scour at Bridges.” *HEC-18, Report FHWA-IP-90-017,* Washington, D.C.

Robinson, K. M., and Hanson, G. J. (1995). “Large scale headcut erosion testing.” *Trans. ASAE,* 38(2), 429-434.

Rodrigue-Grevais, K., Biron, P. M., and Lapointe, M. F. (2011). “Temporal development of scour holes around submerged stream deflectors.” *J. Hydraul. Eng., ASCE,* 137(7), 781-785.

Sarma, A. K. and Das, M. M. (2001). “Mathematical Model for Simulating Flood Propagation on Downstream of River Dike.” *Proc. of International Conference on Mathematical Modelling,* Roorkee, 29-31st January, 2001, 569- 573.

Sarma, A. K., and Das, M. M., (2003). “Analytical solution of flood-wave resulting from dike failure.” *Journal of Water and Maritime Engineering,* ICE, 156, 41-45.

Sarma, A. K., and Roy. S., (2001). “Mathematical simulation of gradual river dike failure.” *Geotechnical Conference IGC2001,* Indoor, 14-16th Dec, 2001, 359-362.

Shan, H. (2010). “Experimental study on incipient motion of non-cohesive and cohesive sediments.” *Ph.D. Dissertation, University of Nebraska, Lincoln, Nebraska.*

Sheppard, D.M., Odeh, M., and Glasser, T. (2004). “Large scale clear-water local pier scour experiments.” *J. Hydraul. Eng., ASCE,* 130 (10), 957–963.

Smerdon, E. T., and Beasley, R. P. (1961). “The tractive force theory applied to stability of open channels in cohesive soils.” *Missouri Univ. Agri. Expt. Sta. Res. Bulletin,* 715.

Smerdon, E. T., and Beasley, R. P. (1961). “Critical tractive forces in cohesive soils.” *Agric. Eng.*, 42, 26–29.

Srivastava, R. (1982). “Effect of free stream turbulence on the characteristics of a turbulent boundary layer on a flat plate. M. E. Dissertation. India: University of Roorkee

Srivastava, R. (2008). “Flow through open channels.” *Oxford University Press*, pages 410.

Srivastava, R., and Contractor, D. N. (1992.) “Bed-load and suspended load transport of nonuniform sediments.” *J. Hydraul. Eng., ASCE*, 118, 948-949.

Srivastava, R., and Ranga Raju, K. G. (1983). “Effect of free-stream turbulence on characteristics of a turbulent boundary layer on a flat plate.” *Proceedings, Twelfth National Conference on Fluid Mechanics and Fluid Power*, New Delhi, India, 241-246.

Storm, K. B., and Papanicolaou, A. N. (2007). “ADV Measurements around a cluster microform in a shallow mountain stream.” *J. Hydraul. Eng., ASCE*, 133(12), 1379-1389.

Sukhodolov, A., Engelhardt, C., Kruger, A., and Bungartz, Z. (2004). “Case study: turbulent flow and sediment distributions in a groyne field.” *J. Hydraul. Eng., ASCE*, 130 (1), 1-9.

Sundborg, A. (1956). “The River Klarelven; A study of fluvial processes.” *Geografiska annalen Stockholm, Sweden.*

Ting, F. C. K., Briaud, J. L, Chen, H. C., Guada Valli, R., Perugu, S., and Wei, G. (2001). “Flume tests for scour in clay at circular piers.” *J. Hydraul. Eng., ASCE*, 127 (11), 969–978.

Thompson, D. M. (2002). ‘‘Channel-bed scour with high versus low deflectors.’’ *J. Hydraul. Eng., ASCE*, 128(6), 640–643.

Uchida, T., and Fukuoka, S. (2010). “A semi-direct computation method of bed surface velocity by horizontal vorticity for estimating local scouring around a pier.” *Annual Journal of Hydraulic Engineering, JSCE*, 54, 841-846. (In Japanese)

Uddin, M. J., and Hosain M. M. (2011). “Local scour around non-submerged bell mouth groin.” *Int. J. Eng. & Appl. Sci.*, 3(2), 37-51.

Uddin, M. J., Hossain, M. M., and Ali, M. S. (2011). “Local scour around submerged bell mouth groin for different orientations.” *J. Civil Eng.*, 39(1), 1-17.

Uijttewaal, W. S. J. (2005). “Effect of groyne layout on the flow in groyne fields: Laboratory experiments.” *J. Hydraul. Eng.*, 131(9), 782-791.

Vaghefi, M., Ghodsian, M., and Neyshaboori, S. A. A. S. (2009). “Experimental study on the effect of a T- shaped spur dike length on scour in a 90° channel bend.” *The Arabian Journal for Science and Engineering*, 34 (2B), 337-348.

Voulgaris, G. and Trowbridge, J. H. (1998). “Evaluation of Acoustic Doppler Velocimeter (ADV) for turbulence measurement.” *Journal of Atmospheric and Oceanic Technology*, 15, 272-289.

Wang, Z., Huang, J., and Su, D. (1997). “Scour rate formula.” *Int. J. Sediment Res.*, 12(3), 11-20.

Wallece, J. M., Eckelmann, H., and Brodkey, R. S. (1972). “The wall region in turbulent shear flow.” *J. Fluid Mechanics*, 54, 39-48.

Yaeger, M. A. (2009). “Mean flow and turbulence around two series of experimental dikes.” *M.Sc. Thesis, The University of Arizona*.

Yalin, M. S. (1977). “Mechanics of sediment transport.” 2nd Ed. Pergamon, Oxford, England.

Yang, C. T., Molinas, A., and Wu, B. (1996). “Sediment transport in the Yellow River.” *J. Hydraul. Eng., ASCE*, 122(5), 237–244.

Yanmaz, A. M., (2006). “Temporal Variation of Clear Water Scour at Cylindrical Bridge Piers.” *Canadian Journal of Civil Engineering*, 33, 1098-1102.

Yanmaz, A. M. and Altinbilek, H. D. (1991). “Study of time-dependent local scour around bridge piers.” *J. Hydraul. Eng., ASCE*, 117 (10), 1247–1268.

Yanmaz, A. M., and Cicekdag, O. (2001). “Composite reliability model for local scour around cylindrical bridge piers.” *Can. J. Civ. Eng.*, 28, 520–535.

Zaghloul, N. A. (1983). “Local scour around spur-dikes.” *Journal of Hydrology*, 60, 123-140.

Zhang, L. D. (2000). “Study on starting velocity of cohesive sediment.” *J Hydrodynamics*, Ser A (in Chinese), 15(1), 82-88.

Zhang, H. and Nakagawa, H.(2008). “Scour around spur dyke: recent advances and future researches.” *Annuals of the Disaster Prevention Research Institute*, Kyoto University.

Zhang, H., Nakagawa, H., and Mizutani, H. (2012). “Bed morphology and grain size characteristics around a spur dyke.” *Int. J. Sediment Res.*, 27(2), 141-157.

APPENDIX- A

Sediment and hydraulic parameters for experimental runs of partially submerged spur dike in cohesionless sediments

Run	da (mm)	h (m)	b (m)	d_{une} (m)	d_{uje} (m)	Time (min)
D_pG1	2.70	0.125	0.1152	0.180	0.197	2160
D_pG2	2.70	0.125	0.089	0.147	0.162	1440
D_pG3	2.70	0.125	0.061	0.106	0.115	1440
D_pSG1	1.47	0.112	0.1152	0.122	0.117	1200
D_pSG2	1.47	0.112	0.089	0.096	0.081	1200
D_pSG3	1.47	0.112	0.061	0.073	0.073	1200

APPENDIX- B

Sediment and hydraulic parameters for experimental runs of partially submerged spur dike founded in cohesive sediment formed by clay-gravel sediments mixture

Run No.	P_c (%)	d_a (mm)	W (%)	γ_d (kN/m^3)	UCS (kN/m^2)	e	h (m)	U_o (m/s)	S_o	b (m)	d_{cune} (m)	d_{cuwe} (m)	Time (min)
D_pCG1.1	10	2.431	6.17	15.58	0.00	0.79	0.120	0.578	0.003	0.1152	0.149	0.128	960
D_pCG1.2	10	2.431	5.95	14.15	0.00	0.83	0.118	0.588	0.003	0.0890	0.112	0.102	960
D_pCG1.3	10	2.431	5.59	13.22	0.00	0.92	0.115	0.603	0.003	0.0610	0.094	0.086	960
D_pCG2.1	20	2.163	7.68	14.88	2.11	0.76	0.122	0.690	0.003	0.1152	0.110	0.118	1200
D_pCG2.2	20	2.163	6.62	14.82	2.16	0.74	0.120	0.693	0.003	0.0890	0.093	0.100	1800
D_pCG2.3	20	2.163	7.27	15.05	2.60	0.71	0.117	0.702	0.003	0.0610	0.067	0.077	1560
D_pCG3.1	30	1.894	9.50	15.50	9.14	0.64	0.122	0.717	0.003	0.1152	0.071	0.100	2400
D_pCG3.2	30	1.894	11.00	15.35	9.95	0.67	0.119	0.735	0.003	0.0890	0.052	0.083	2400
D_pCG3.3	30	1.894	12.06	16.19	10.11	0.66	0.117	0.747	0.003	0.0610	0.027	0.072	2400
D_pCG4.1	40	1.626	11.61	17.90	16.22	0.45	0.094	0.936	0.005	0.1152	0.033	0.071	2400
D_pCG4.2	40	1.626	11.76	18.26	16.22	0.42	0.091	0.967	0.005	0.0890	0.023	0.052	2400
D_pCG4.3	40	1.626	11.83	18.10	16.76	0.43	0.072	1.222	0.005	0.0610	0.021	0.043	2400
D_pCG5.1	50	1.357	17.12	17.44	14.60	0.50	0.095	0.926	0.005	0.1152	0.012	0.047	2400
D_pCG5.2	50	1.357	15.28	17.13	15.14	0.49	0.078	1.128	0.005	0.0890	0.010	0.037	2400
D_pCG5.3	50	1.357	17.51	17.33	14.60	0.51	0.078	1.128	0.005	0.0610	0.000	0.017	2400

APPENDIX- C

Sediment and hydraulic parameters for experimental runs of partially submerged spur dike founded in cohesive sediment formed by clay-sand-gravel sediments mixture

Run No.	P_c (%)	d_a (mm)	W (%)	γ_d (kN/m^3)	UCS (kN/m^2)	e	h (m)	U_o (m/s)	S_o	b (m)	d_{csne} (m)	d_{cswe} (m)	Time (min)
D_pCSG1.1	10	1.324	8.46	17.49	0.00	0.49	0.126	0.504	0.003	0.1152	0.150	0.148	960
D_pCSG1.2	10	1.324	8.74	17.29	0.00	0.50	0.126	0.504	0.003	0.0890	0.130	0.116	960
D_pCSG1.3	10	1.324	8.97	16.82	0.00	0.55	0.126	0.504	0.003	0.0610	0.103	0.085	840
D_pCSG2.1	20	1.179	10.19	18.34	11.52	0.42	0.114	0.657	0.003	0.1152	0.102	0.131	1560
D_pCSG2.2	20	1.179	12.38	17.42	13.73	0.49	0.121	0.619	0.003	0.0890	0.088	0.101	1560
D_pCSG2.3	20	1.179	11.07	17.55	11.73	0.48	0.119	0.629	0.003	0.0610	0.058	0.075	1560
D_pCSG3.1	30	1.033	12.04	18.80	41.63	0.38	0.134	0.681	0.003	0.1152	0.060	0.083	1800
D_pCSG3.2	30	1.033	11.99	19.11	40.39	0.36	0.135	0.676	0.003	0.0890	0.042	0.056	1800
D_pCSG3.3	30	1.033	11.85	18.85	40.60	0.38	0.119	0.767	0.003	0.0610	0.020	0.028	1680
D_pCSG4.1	40	0.888	11.71	18.98	48.77	0.37	0.099	0.824	0.005	0.1152	0.017	0.051	1800
D_pCSG4.2	40	0.888	12.35	18.80	53.53	0.38	0.085	1.003	0.005	0.0890	0.010	0.031	1800
D_pCSG4.3	40	0.888	11.99	18.65	53.42	0.39	0.071	1.201	0.005	0.0610	0.006	0.016	1800
D_pCSG5.1	50	0.742	13.43	18.13	50.82	0.43	0.072	1.184	0.005	0.1152	0.012	0.032	2400
D_pCSG5.2	50	0.742	13.52	18.45	52.45	0.41	0.072	1.184	0.005	0.0890	0.003	0.017	2400
D_pCSG5.3	50	0.742	13.70	18.42	51.90	0.41	0.071	1.201	0.005	0.0610	0.000	0.005	2400

APPENDIX- D

Data on temporal variation of scour depth at nose (d_{cun}) and at the wake (d_{cuw}) of the partially submerged dike in clay-gravel (CG) and clay-sand-gravel (CSG) sediment mixtures

Run No. D_PCG 1.1

Time (min.)	d_{cun} (m)	Time (min.)	d_{cuw} (m)
1	0.008	2	0.005
4	0.024	5	0.020
10	0.045	11	0.051
15	0.049	16	0.059
30	0.067	31	0.065
60	0.087	61	0.078
120	0.096	121	0.094
240	0.114	241	0.104
360	0.14	361	0.12
480	0.141	481	0.123
600	0.143	601	0.126
720	0.146	721	0.127
840	0.149	841	0.128
960	0.149	961	0.128

Run No. D_PCG 1.2

Time (min.)	d_{cun} (m)	Time (min.)	d_{cuw} (m)
1	0.005	2	---
4	0.009	5	0.006
10	0.016	11	0.023
15	0.027	16	0.027
30	0.031	31	0.038
60	0.042	61	0.056
120	0.052	121	0.066
240	0.061	241	0.078
360	0.083	361	0.088
480	0.097	481	0.093
600	0.111	601	0.098
720	0.111	721	0.102
840	0.112	841	0.102
960	0.112	961	0.102

Run No. D_PCG 1.3

Time (min.)	d_{cun} (m)	Time (min.)	d_{cuw} (m)
1	0.003	2	0.000
4	0.005	5	0.004
10	0.009	11	0.009
15	0.018	16	0.020
30	0.027	31	0.035
60	0.037	61	0.050
120	0.048	121	0.060
240	0.055	241	0.070
360	0.075	361	0.079
480	0.087	481	0.084
600	0.091	601	0.085
720	0.092	721	0.085
840	0.094	841	0.086
960	0.094	961	0.086

Run No. D_PCG 2.1

Time (min.)	d_{cun} (m)	Time (min.)	d_{cuw} (m)
3	0.003	5	0.005
5	0.009	11	0.011
10	0.016	16	0.018
15	0.021	31	0.024
30	0.025	61	0.030
60	0.031	121	0.035
120	0.037	241	0.041
240	0.044	361	0.049
360	0.05	481	0.057
480	0.059	601	0.067
600	0.068	721	0.076
720	0.084	841	0.090
840	0.102	961	0.109
960	0.109	1081	0.115
1080	0.110	1201	0.118
1200	0.110	1321	0.118

Run No. D_PCG 2.2

Time (min.)	d_{cun} (m)	Time (min.)	d_{cuw} (m)
3	---	4	0.004
5	0.004	6	0.007
10	0.008	11	0.012
15	0.011	16	0.018
30	0.016	31	0.026
60	0.022	61	0.033
120	0.029	121	0.038
240	0.036	241	0.045
360	0.044	361	0.054
480	0.053	481	0.061
600	0.061	601	0.067
720	0.065	721	0.072
840	0.070	841	0.078
960	0.074	961	0.083
1080	0.079	1081	0.087
1200	0.084	1201	0.091
1320	0.088	1321	0.096
1440	0.091	1441	0.098
1560	0.093	1561	0.100
1680	0.093	1681	0.100
1800	0.093	1801	0.100

Run No. D_PCG 2.3

Time (min.)	d_{cun} (m)	Time (min.)	d_{cuw} (m)
5	0.000	6	0.003
10	0.002	11	0.005
15	0.005	16	0.008
30	0.009	31	0.013
60	0.014	61	0.019
120	0.019	121	0.025
240	0.025	241	0.032
360	0.033	361	0.040
480	0.040	481	0.047
600	0.048	601	0.056
720	0.056	721	0.063
840	0.060	841	0.066
960	0.063	961	0.069
1080	0.065	1081	0.071
1200	0.066	1201	0.074
1320	0.067	1321	0.076
1440	0.067	1441	0.077
1560	0.067	1561	0.077

Run No. D_PCG 3.1

Time (min.)	d_{cun} (m)	Time (min.)	d_{cuw} (m)
10	0.000	11	0.003
15	0.000	16	0.004
30	0.000	31	0.007
60	0.002	61	0.009
120	0.003	121	0.011
240	0.005	241	0.014
360	0.009	361	0.018
480	0.012	481	0.020
600	0.017	601	0.024
720	0.020	721	0.029
840	0.023	841	0.035
960	0.027	961	0.041
1080	0.031	1081	0.048
1200	0.035	1201	0.058
1320	0.040	1321	0.067
1440	0.046	1441	0.072
1560	0.051	1561	0.078
1680	0.056	1681	0.085
1800	0.060	1801	0.090
1920	0.065	1921	0.094
2040	0.068	2041	0.097
2160	0.070	2161	0.098
2280	0.071	2281	0.100
2400	0.071	2401	0.100

Run No. D_PCG 3.2

Time (min.)	d_{cun} (m)	Time (min.)	d_{cuw} (m)
15	0.000	16	0.003
30	0.000	31	0.003
60	0.000	61	0.005
120	0.002	121	0.008
240	0.003	241	0.010
360	0.004	361	0.013
480	0.007	481	0.017
600	0.011	601	0.021
720	0.014	721	0.026
840	0.018	841	0.030
960	0.021	961	0.036
1080	0.026	1081	0.043
1200	0.032	1201	0.052
1320	0.036	1321	0.059
1440	0.041	1441	0.066
1560	0.044	1561	0.070
1680	0.047	1681	0.073
1800	0.048	1801	0.076
1920	0.05	1921	0.080
2040	0.051	2041	0.082
2160	0.051	2161	0.083
2280	0.052	2281	0.083
2400	0.052	2401	0.083

Run No. D_PCG 3.3

Time (min.)	d_{cun} (m)	Time (min.)	d_{cuw} (m)
30	0.000	31	0.002
60	0.000	61	0.004
120	0.000	121	0.006
240	0.002	241	0.007
360	0.002	361	0.010
480	0.004	481	0.012
600	0.005	601	0.015
720	0.008	721	0.017
840	0.011	841	0.021
960	0.014	961	0.027
1080	0.017	1081	0.033
1200	0.020	1201	0.040
1320	0.020	1321	0.048
1440	0.021	1441	0.057
1560	0.021	1561	0.064
1680	0.022	1681	0.067
1800	0.022	1801	0.069
1920	0.025	1921	0.071
2040	0.026	2041	0.071
2160	0.026	2161	0.072
2280	0.027	2281	0.072
2400	0.027	2401	0.072

Run No. D_PCG 4.1

Time (min.)	d_{cun} (m)	Time (min.)	d_{cuw} (m)
120	0.000	121	0.004
240	0.000	241	0.007
360	0.004	361	0.009
480	0.006	481	0.011
600	0.006	601	0.014
720	0.007	721	0.016
840	0.008	841	0.018
960	0.009	961	0.022
1080	0.011	1081	0.026
1200	0.012	1201	0.034
1320	0.014	1321	0.041
1440	0.018	1441	0.049
1560	0.023	1561	0.055
1680	0.023	1681	0.058
1800	0.027	1801	0.062
1920	0.029	1921	0.066
2040	0.032	2041	0.067
2160	0.032	2161	0.069
2280	0.033	2281	0.070
2400	0.033	2401	0.071

Run No. D_PCG 4.2

Time (min.)	d_{cun} (m)	Time (min.)	d_{cuw} (m)
120	0.000	121	0.003
240	0.000	241	0.005
360	0.000	361	0.006
480	0.003	481	0.009
600	0.003	601	0.011
720	0.005	721	0.014
840	0.006	841	0.016
960	0.007	961	0.018
1080	0.007	1081	0.023
1200	0.008	1201	0.029
1320	0.011	1321	0.033
1440	0.011	1441	0.037
1560	0.013	1561	0.040
1680	0.016	1681	0.044
1800	0.018	1801	0.047
1920	0.020	1921	0.048
2040	0.021	2041	0.050
2160	0.022	2161	0.051
2280	0.023	2281	0.051
2400	0.023	2401	0.052

Run No. D_PCG 4.3

Time (min.)	d_{cun} (m)	Time (min.)	d_{cuw} (m)
360	0.000	361	0.002
480	0.000	481	0.003
601	0.000	601	0.005
720	0.002	721	0.007
840	0.002	841	0.009
960	0.004	961	0.009
1080	0.006	1081	0.012
1200	0.007	1201	0.014
1320	0.009	1321	0.018
1440	0.01	1441	0.023
1560	0.013	1561	0.029
1680	0.016	1681	0.037
1800	0.018	1801	0.039
1920	0.020	1921	0.042
2040	0.020	2041	0.042
2160	0.021	2161	0.043
2280	0.021	2281	0.043
2400	0.021	2401	0.043

Run No. D_PCG 5.1

Time (min.)	d_{cun} (m)	Time (min.)	d_{cuw} (m)
240	0.000	241	0.003
360	0.000	361	0.004
480	0.000	481	0.006
600	0.000	601	0.009
720	0.000	721	0.011
840	0.002	841	0.012
960	0.003	961	0.013
1080	0.005	1081	0.015
1200	0.006	1201	0.018
1320	0.007	1321	0.020
1440	0.008	1441	0.024
1560	0.008	1561	0.029
1680	0.011	1681	0.036
1800	0.011	1801	0.041
1920	0.011	1921	0.042
2040	0.012	2041	0.045
2160	0.012	2161	0.046
2280	0.012	2281	0.046
2400	0.012	2401	0.047

Run No. D_PCG 5.2

Time (min.)	d_{cun} (m)	Time (min.)	d_{cuw} (m)
240	0.000	361	0.003
360	0.000	481	0.003
480	0.000	601	0.005
600	0.000	721	0.007
720	0.000	841	0.008
1080	0.003	961	0.011
1200	0.003	1081	0.013
1320	0.004	1201	0.016
1440	0.004	1321	0.022
1560	0.007	1441	0.027
1680	0.007	1561	0.029
1800	0.007	1681	0.030
1920	0.009	1801	0.030
2040	0.009	1921	0.032
2160	0.010	2041	0.034
2280	0.010	2161	0.035
2400	0.010	2281	0.037

Run No. D_PCG 5.3

Time (min.)	d_{cuw} (m)
601	0.002
721	0.003
841	0.005
961	0.005
1081	0.007
1201	0.009
1321	0.009
1441	0.011
1561	0.013
1681	0.014
1801	0.014
1921	0.016
2041	0.017
2161	0.017
2281	0.017
2401	0.017

Run No. D_PCSG 1.1

Time (min.)	d_{cun} (m)	Time (min.)	d_{cuw} (m)
1	0.025	2	0.037
4	0.069	5	0.054
10	0.079	11	0.063
15	0.089	16	0.068
30	0.098	31	0.081
60	0.112	61	0.092
120	0.121	121	0.105
240	0.131	241	0.124
360	0.138	361	0.135
480	0.143	481	0.141
600	0.148	601	0.145
720	0.149	721	0.147
840	0.150	841	0.148
960	0.150	961	0.148

Run No. D_PCSG 1.2

Time (min.)	d_{cun} (m)	Time (min.)	d_{cuw} (m)
1	0.014	2	0.025
4	0.040	5	0.040
10	0.065	11	0.052
15	0.078	16	0.066
30	0.086	31	0.075
60	0.099	61	0.082
120	0.107	121	0.091
240	0.113	241	0.099
360	0.119	361	0.106
480	0.125	481	0.110
600	0.128	601	0.114
720	0.128	721	0.115
840	0.130	841	0.116
960	0.130	961	0.116

Run No. D_PCSG 1.3

Time (min.)	d_{cun} (m)	Time (min.)	d_{cuw} (m)
1	0.01	2	0.017
4	0.025	5	0.033
10	0.032	11	0.045
15	0.058	16	0.051
30	0.07	31	0.062
60	0.079	61	0.067
120	0.085	121	0.072
240	0.092	241	0.076
360	0.095	361	0.079
480	0.1	481	0.082
600	0.102	601	0.084
720	0.103	721	0.085
840	0.103	841	0.085

Run No. D_PCSG 2.1

Time (min.)	d_{cun} (m)	Time (min.)	d_{cuw} (m)
4	--	5	0.004
10	0.005	11	0.008
15	0.008	16	0.010
30	0.013	31	0.015
60	0.019	61	0.024
120	0.028	121	0.033
240	0.039	241	0.045
360	0.048	361	0.058
480	0.058	481	0.073
600	0.069	601	0.084
720	0.078	721	0.096
840	0.084	841	0.105
960	0.090	961	0.112
1080	0.094	1081	0.120
1200	0.098	1201	0.126
1320	0.101	1321	0.129
1440	0.102	1441	0.131
1560	0.102	1561	0.131

Run No. D_PCSG 2.2

Time (min.)	d_{cun} (m)	Time (min.)	d_{cuw} (m)
10	0.003	11	0.005
15	0.006	16	0.009
30	0.009	31	0.013
60	0.014	61	0.019
120	0.020	121	0.028
240	0.03	241	0.039
360	0.041	361	0.051
480	0.054	481	0.062
600	0.062	601	0.075
720	0.070	721	0.081
840	0.075	841	0.085
960	0.079	961	0.090
1080	0.082	1081	0.094
1200	0.085	1201	0.097
1320	0.087	1321	0.099
1440	0.087	1441	0.100
1560	0.088	1561	0.101

Run No. D_PCSG 2.3

Time (min.)	d_{cun} (m)	Time (min.)	d_{cuw} (m)
10	0.000	11	0.003
15	0.002	16	0.005
30	0.004	31	0.009
60	0.007	61	0.015
120	0.011	121	0.020
240	0.016	241	0.029
360	0.023	361	0.04
480	0.030	481	0.049
600	0.036	601	0.055
720	0.041	721	0.061
840	0.044	841	0.065
960	0.047	961	0.068
1080	0.051	1081	0.070
1200	0.053	1201	0.072
1320	0.056	1321	0.074
1440	0.057	1441	0.075
1560	0.058	1561	0.075

Run No. D_PCSG 3.1

Time (min.)	d_{cun} (m)	Time (min.)	d_{cuw} (m)
10	0.000	11	0.003
15	0.002	16	0.005
30	0.004	31	0.007
60	0.006	61	0.010
120	0.009	121	0.014
240	0.012	241	0.018
360	0.014	361	0.021
480	0.017	481	0.024
600	0.022	601	0.029
720	0.026	721	0.033
840	0.033	841	0.039
960	0.040	961	0.050
1080	0.046	1081	0.061
1200	0.051	1201	0.072
1320	0.054	1321	0.076
1440	0.057	1441	0.080
1560	0.059	1561	0.082
1680	0.060	1681	0.083
1800	0.060	1801	0.083

Run No. D_PCSG 3.2

Time (min.)	d_{cun} (m)	Time (min.)	d_{cuw} (m)
15	0.000	16	0.002
30	0.000	31	0.003
60	0.003	61	0.005
120	0.005	121	0.007
240	0.007	241	0.010
360	0.010	361	0.013
480	0.012	481	0.015
600	0.015	601	0.019
720	0.019	721	0.024
840	0.024	841	0.030
960	0.029	961	0.036
1080	0.035	1081	0.042
1200	0.038	1201	0.047
1320	0.040	1321	0.051
1440	0.041	1441	0.053
1560	0.042	1561	0.054
1680	0.042	1681	0.056
1800	0.042	1801	0.056

Run No. D_PCSG 3.3

Time (min.)	d_{cun} (m)	Time (min.)	d_{cuw} (m)
30	0.000	31	0.002
60	0.002	61	0.003
120	0.004	121	0.005
240	0.005	241	0.008
360	0.007	361	0.010
480	0.008	481	0.012
600	0.011	601	0.012
720	0.011	721	0.016
840	0.014	841	0.017
960	0.017	961	0.020
1080	0.019	1081	0.023
1200	0.019	1201	0.024
1320	0.019	1321	0.026
1440	0.020	1441	0.028
1560	0.020	1561	0.028
1680	0.020	1681	0.028

Run No. D_PCSG 4.1

Time (min.)	d_{cun} (m)	Time (min.)	d_{cuw} (m)
30	0.000	31	0.005
60	0.000	61	0.008
120	0.003	121	0.0100
240	0.005	241	0.012
360	0.006	361	0.014
480	0.007	481	0.017
600	0.007	601	0.021
720	0.008	721	0.023
840	0.010	841	0.028
960	0.012	961	0.034
1080	0.014	1081	0.039
1200	0.015	1201	0.043
1320	0.016	1321	0.046
1440	0.017	1441	0.048
1560	0.017	1561	0.049
1680	0.017	1681	0.050
1800	0.017	1801	0.051

Run No. D_PCSG 4.2

Time (min.)	d_{cun} (m)	Time (min.)	d_{cuw} (m)
60	0.000	61	0.004
120	0.000	121	0.006
240	0.002	241	0.009
360	0.003	361	0.010
480	0.005	481	0.013
600	0.007	601	0.015
720	0.007	721	0.016
840	0.007	841	0.019
960	0.008	961	0.020
1080	0.008	1081	0.023
1200	0.008	1201	0.026
1320	0.009	1321	0.028
1440	0.009	1441	0.030
1560	0.010	1561	0.030
1680	0.010	1681	0.031
1800	0.010	1801	0.031

Run No. D_PCSG 4.3

Time (min.)	d_{cun} (m)	Time (min.)	d_{cuw} (m)
60	0.000	61	0.002
120	0.000	121	0.003
240	0.000	241	0.005
360	0.000	361	0.006
480	0.002	481	0.006
600	0.002	601	0.009
720	0.003	721	0.009
840	0.003	841	0.010
960	0.006	961	0.011
1080	0.006	1081	0.012
1200	0.006	1201	0.013
1320	0.006	1321	0.014
1440	0.006	1441	0.015
1560	0.006	1561	0.016
1680	0.006	1681	0.016
1800	0.006	1801	0.016

Run No. D_PCSG 5.1

Time (min.)	d_{cun} (m)	Time (min.)	d_{cuw} (m)
120	0.000	121	0.003
240	0.000	241	0.004
360	0.000	361	0.004
480	0.002	481	0.006
600	0.003	601	0.007
720	0.006	721	0.008
840	0.007	841	0.01
960	0.007	961	0.01
1080	0.008	1081	0.011
1200	0.009	1201	0.014
1320	0.009	1321	0.016
1440	0.009	1441	0.019
1560	0.01	1561	0.02
1680	0.01	1681	0.023
1800	0.011	1801	0.027
1920	0.011	1921	0.029
2040	0.011	2041	0.031
2160	0.012	2161	0.032
2280	0.012	2281	0.032
2400	0.012	2401	0.032

Run No. D_PCSG 5.2

Time (min.)	d_{cuw} (m)
361	0.002
481	0.002
601	0.004
721	0.005
841	0.006
961	0.006
1081	0.008
1201	0.010
1321	0.011
1441	0.011
1561	0.014
1681	0.014
1801	0.015
1921	0.015
2041	0.017
2161	0.017
2281	0.017
2401	0.017

Run No. D_PCSG 5.3

Time (min.)	d_{cuw} (m)
721	0.001
841	0.003
961	0.003
1081	0.003
1201	0.003
1321	0.003
1441	0.004
1561	0.004
1681	0.004
1801	0.004
1921	0.005
2041	0.005
2161	0.005
2281	0.005
2401	0.005

APPENDIX- E

Sediment and hydraulic parameters for experimental runs of submerged spur dike founded in cohesive sediment formed by clay-gravel and clay-sand-gravel sediment mixtures

Run No.	P_c (%)	d_a (mm)	W (%)	γ_d (kN/m^3)	UCS (kN/m^2)	e	h (m)	U_o (m/s)	S_o	b (m)	d_{csne} (m)	d_{cswe} (m)	Time (min)
D_sCG1.1	10	2.431	5.57	13.98	0.00	0.86	0.125	0.555	0.003	0.1152	0.120	0.109	960
D_sCG2.1	20	2.163	7.46	15.41	3.30	0.69	0.118	0.653	0.003	0.1152	0.076	0.081	1560
D_sCG3.1	30	1.894	8.84	16.11	9.19	0.61	0.126	0.694	0.003	0.1152	0.066	0.088	2400
D_sCG4.1	40	1.626	12.71	16.89	15.14	0.54	0.080	1.099	0.005	0.1152	0.025	0.06	2400
D_sCG5.1	50	1.357	16.80	20.54	14.06	0.27	0.077	1.142	0.005	0.1152	0.010	0.036	2400
D_sCSG1.1	10	2.431	8.58	17.17	0.00	0.51	0.130	0.489	0.003	0.1152	0.134	0.132	960
D_sCSG2.1	20	2.163	11.19	17.60	11.84	0.48	0.122	0.577	0.003	0.1152	0.073	0.096	1560
D_sCSG3.1	30	1.894	12.27	18.91	39.09	0.37	0.128	0.713	0.003	0.1152	0.031	0.067	1800
D_sCSG4.1	40	1.626	12.19	18.56	51.90	0.40	0.088	0.969	0.005	0.1152	0.006	0.039	1800
D_sCSG5.1	50	1.357	13.92	18.33	54.61	0.42	0.084	1.015	0.005	0.1152	0.003	0.026	2400

APPENDIX- F

Data on temporal variation of scour depth at nose (d_{csn}) and at the wake (d_{csw}) of the submerged spur dike in clay-gravel (CG) and clay-sand-gravel (CSG) sediment mixtures

Run No. D_SCG 1.1

Time (min.)	d_{csn} (m)	Time (min.)	d_{csw} (m)
1	0.005	2	0.004
4	0.010	4	0.008
10	0.033	6	0.020
15	0.051	11	0.034
30	0.062	16	0.048
60	0.084	31	0.064
120	0.095	61	0.075
240	0.108	121	0.093
360	0.114	241	0.100
480	0.117	361	0.105
600	0.119	481	0.107
720	0.119	601	0.108
840	0.120	721	0.109
960	0.120	841	0.109

Run No. D_SCG 2.1

Time (min.)	d_{csn} (m)	Time (min.)	d_{csw} (m)
5	0.007	6	0.010
10	0.012	11	0.018
15	0.015	16	0.025
30	0.022	31	0.034
60	0.031	61	0.044
120	0.039	121	0.051
240	0.046	241	0.057
360	0.052	361	0.060
480	0.056	481	0.063
600	0.059	601	0.066
720	0.064	721	0.068
840	0.068	841	0.070
960	0.070	961	0.073
1080	0.073	1081	0.076
1200	0.075	1201	0.078
1320	0.076	1321	0.080
1440	0.076	1441	0.081
1560	0.076	1561	0.081

Run No. D_SCG 3.1

Time (min.)	d_{csn} (m)	Time (min.)	d_{csw} (m)
30	0.000	31	0.003
60	0.002	61	0.005
120	0.003	121	0.007
240	0.005	241	0.009
360	0.007	361	0.012
480	0.010	481	0.015
600	0.011	601	0.02
720	0.013	721	0.023
840	0.016	841	0.027
960	0.021	961	0.032
1080	0.027	1081	0.038
1200	0.036	1201	0.045
1320	0.046	1321	0.057
1440	0.051	1441	0.065
1560	0.053	1561	0.070
1680	0.057	1681	0.073
1800	0.06	1801	0.081
1920	0.061	1921	0.084
2040	0.063	2041	0.086
2160	0.065	2161	0.087
2280	0.065	2281	0.088
2400	0.066	2401	0.088

Run No. D_SCG 4.1

Time (min.)	d_{csn} (m)	Time (min.)	d_{csw} (m)
120	0.000	121	0.003
240	0.003	241	0.004
360	0.005	361	0.006
480	0.006	481	0.008
600	0.006	601	0.011
720	0.009	721	0.013
840	0.011	841	0.016
960	0.012	961	0.020
1080	0.012	1081	0.027
1200	0.016	1201	0.033
1320	0.019	1321	0.039
1440	0.021	1441	0.044
1560	0.024	1561	0.047
1680	0.024	1681	0.05
1800	0.025	1801	0.054
1920	0.025	1921	0.056
2040	0.025	2041	0.058
2160	0.025	2161	0.059
2280	0.025	2281	0.060
2400	0.025	2401	0.060

Run No. D_SCG 5.1

Time (min.)	d_{csn} (m)	Time (min.)	d_{csw} (m)
360	0.000	361	0.003
480	0.000	481	0.003
601	0.000	601	0.005
720	0.000	721	0.006
840	0.002	841	0.009
960	0.002	961	0.011
1080	0.004	1081	0.013
1200	0.005	1201	0.016
1320	0.005	1321	0.021
1440	0.006	1441	0.024
1560	0.007	1561	0.024
1680	0.007	1681	0.028
1800	0.009	1801	0.029
1920	0.009	1921	0.031
2040	0.010	2041	0.034
2160	0.010	2161	0.034
2280	0.010	2281	0.035
2400	0.010	2401	0.036

Run No. D_SCSG 1.1

Time (min.)	d_{csn} (m)	Time (min.)	d_{csw} (m)
1	0.014	2	0.019
4	0.026	5	0.025
10	0.043	11	0.041
15	0.055	16	0.049
30	0.075	31	0.068
60	0.087	61	0.075
120	0.099	121	0.084
240	0.112	241	0.104
360	0.121	361	0.108
480	0.125	481	0.123
600	0.129	601	0.131
720	0.133	721	0.132
840	0.134	841	0.132
960	0.134	961	0.132

Run No. D_SCSG 2.1

Time (min.)	d_{csn} (m)	Time (min.)	d_{csw} (m)
10	---	11	0.002
15	0.003	16	0.003
30	0.006	31	0.007
60	0.009	61	0.011
120	0.013	121	0.016
240	0.016	241	0.022
360	0.018	361	0.028
480	0.024	481	0.036
600	0.031	601	0.047
720	0.040	721	0.060
840	0.049	841	0.073
960	0.057	961	0.082
1080	0.064	1081	0.087
1200	0.069	1201	0.091
1320	0.073	1321	0.094
1440	0.073	1441	0.096
1560	0.073	1561	0.096

Run No. D_SCSG 3.1

Time (min.)	d_{csn} (m)	Time (min.)	d_{csw} (m)
30	0.000	31	0.004
60	0.003	61	0.006
120	0.004	121	0.010
240	0.006	241	0.012
360	0.008	361	0.015
480	0.011	481	0.018
600	0.013	601	0.022
720	0.016	721	0.031
840	0.018	841	0.043
960	0.021	961	0.049
1080	0.025	1081	0.053
1200	0.028	1201	0.056
1320	0.029	1321	0.060
1440	0.03	1441	0.063
1560	0.031	1561	0.065
1680	0.031	1681	0.067
1800	0.031	1801	0.067

Run No. D_SCSG 4.1

Time (min.)	d_{csn} (m)	Time (min.)	d_{csw} (m)
240	0.000	241	0.003
360	0.002	361	0.006
480	0.002	481	0.009
600	0.003	601	0.011
720	0.004	721	0.016
840	0.005	841	0.025
960	0.005	961	0.031
1080	0.006	1081	0.031
1200	0.006	1201	0.034
1320	0.006	1321	0.036
1440	0.008	1441	0.037
1560	0.008	1561	0.039
1680	0.008	1681	0.039
1800	0.008	1801	0.039

Run No. D_SCSG 5.1

Time (min.)	d_{csw} (m)
481	0.003
601	0.003
721	0.005
841	0.005
961	0.007
1081	0.009
1201	0.010
1321	0.013
1441	0.015
1561	0.018
1681	0.020
1801	0.021
1921	0.023
2041	0.025
2161	0.026
2281	0.026
2401	0.026

APPENDIX- G

Sediment and hydraulic parameters for experimental runs of pier founded in cohesionless sediments

Run	d_a (mm)	h (m)	D (m)	d_{pne}(m)	Time (min)
PG1	2.70	0.125	0.1152	0.166	2160
PG2	2.70	0.125	0.089	0.140	1440
PG3	2.70	0.125	0.061	0.094	1440
PSG1	1.47	0.115	0.1152	0.090	1200
PSG2	1.47	0.115	0.089	0.068	1200
PSG3	1.47	0.115	0.061	0.048	1200

APPENDIX- H

Sediment and hydraulic parameters for experimental runs of bridge pier founded in cohesive sediment formed by clay-gravel sediments mixture

Run No.	P_c (%)	d_a (mm)	W (%)	γ_d (kN/m^3)	UCS (kN/m^2)	e	h (m)	U_o (m/s)	S_o	D (m)	d_{cps} (m)	d_{cpw} (m)	Time (min)
PCG1.1	10	2.431	5.76	13.08	0.00	0.99	0.121	0.573	0.003	0.1152	0.124	0.083	1800
PCG1.2	10	2.431	5.46	12.76	0.00	1.04	0.117	0.593	0.003	0.089	0.101	0.076	1800
PCG2.1	20	2.163	8.09	15.78	3.68	0.65	0.114	0.716	0.003	0.1152	0.101	0.065	1800
PCG2.2	20	2.163	7.49	15.49	2.92	0.68	0.113	0.722	0.003	0.089	0.080	0.049	1560
PCG3.1	30	1.894	9.14	16.18	9.08	0.61	0.115	0.760	0.003	0.1152	0.087	0.049	2400
PCG3.2	30	1.894	8.18	16.41	9.14	0.58	0.113	0.774	0.003	0.089	0.030	0.013	1440
PCG4.1	40	1.626	11.97	17.93	15.68	0.45	0.125	0.704	0.005	0.1152	0.050	0.037	2400
PCG4.2	40	1.626	12.82	18.10	16.11	0.44	0.115	0.765	0.005	0.089	0.034	0.025	2400
PCG5.1	50	1.357	17.36	16.71	14.06	0.56	0.087	1.011	0.005	0.1152	0.041	0.034	2400
PCG5.2	50	1.357	17.30	16.76	14.60	0.55	0.087	1.011	0.005	0.089	0.029	0.020	2400

APPENDIX- I

Sediment and hydraulic parameters for experimental runs of bridge pier founded in cohesive sediment formed by clay-sand-gravel sediments mixture

Run No.	P_c (%)	d_a (mm)	W (%)	γ_d (kN/m^3)	UCS (kN/m^2)	e	h (m)	U_o (m/s)	S_o	D (m)	d_{cps} (m)	d_{cpw} (m)	Time (min)
PCSG1.1	10	1.324	8.37	17.34	0.00	0.50	0.119	0.534	0.003	0.1152	0.140	0.111	962
PCSG1.2	10	1.324	8.99	17.54	0.00	0.48	0.118	0.538	0.003	0.089	0.122	0.094	962
PCSG2.1	20	1.179	10.19	18.34	11.30	0.42	0.122	0.614	0.003	0.1152	0.107	0.051	1560
PCSG2.2	20	1.179	9.63	17.78	11.08	0.46	0.127	0.589	0.003	0.089	0.085	0.039	1560
PCSG3.1	30	1.033	10.44	18.80	36.33	0.38	0.117	0.780	0.003	0.1152	0.056	0.041	1800
PCSG3.2	30	1.033	11.09	19.61	41.09	0.33	0.116	0.786	0.003	0.089	0.034	0.030	1800
PCSG4.1	40	0.888	11.81	19.07	54.07	0.36	0.101	0.844	0.005	0.1152	0.032	0.032	1800
PCSG4.2	40	0.888	11.45	18.50	51.47	0.40	0.087	0.980	0.005	0.089	0.025	0.019	1800
PCSG5.1	50	0.742	13.61	18.27	52.34	0.42	0.099	0.861	0.005	0.1152	0.028	0.025	2400
PCSG5.2	50	0.742	13.88	18.39	53.09	0.41	0.080	1.066	0.005	0.089	0.020	0.018	2400

APPENDIX- J

Data on temporal variation of scour depth at sides (d_{cps}) and at the wake (d_{cpw}) of the pier in clay-gravel (CG) and clay-sand-gravel (CSG) sediment mixtures

Run No. PCG 1.1

Time (min.)	d_{cps} (m)	Time (min.)	d_{cpw} (m)
1	0.005	2	0.003
3	0.012	4	0.006
5	0.022	6	0.018
10	0.030	11	0.025
15	0.046	16	0.031
30	0.053	31	0.044
60	0.061	61	0.052
120	0.070	121	0.061
240	0.075	241	0.066
360	0.091	361	0.070
480	0.098	481	0.074
600	0.104	601	0.076
720	0.115	721	0.079
840	0.120	841	0.081
960	0.124	961	0.082
1080	0.124	1081	0.083

Run No. PCG 1.2

Time (min.)	d_{cps} (m)	Time (min.)	d_{cpw} (m)
1	0.003	2	----
3	0.008	4	0.004
5	0.012	6	0.009
10	0.022	11	0.016
15	0.027	16	0.021
30	0.032	31	0.028
60	0.041	61	0.034
120	0.049	121	0.046
240	0.057	241	0.054
360	0.062	361	0.061
480	0.081	481	0.063
600	0.088	601	0.068
720	0.089	721	0.071
840	0.094	841	0.073
960	0.101	961	0.075
1080	0.101	1081	0.076

Run No. PCG 2.1

Time (min.)	d_{cps} (m)	Time (min.)	d_{cpw} (m)
3	0.003	4	0.000
5	0.006	6	0.000
10	0.010	11	0.002
15	0.014	16	0.005
30	0.020	31	0.009
60	0.026	61	0.014
120	0.031	121	0.020
240	0.037	241	0.024
360	0.042	361	0.029
480	0.048	481	0.036
600	0.053	601	0.043
720	0.063	721	0.049
840	0.074	841	0.055
960	0.081	961	0.059
1080	0.088	1081	0.064
1200	0.093	1201	0.064
1320	0.097	1321	0.064
1440	0.099	1441	0.065
1560	0.100	1561	0.065
1680	0.101	1681	0.065
1800	0.101	1801	0.065

Run No. PCG 2.2

Time (min.)	d_{cps} (m)	Time (min.)	d_{cpw} (m)
5	0.002	6	0.000
10	0.004	11	0.003
15	0.007	16	0.005
30	0.011	31	0.007
60	0.016	61	0.011
120	0.022	121	0.016
240	0.029	241	0.019
360	0.035	361	0.021
480	0.042	481	0.026
600	0.053	601	0.034
720	0.06	721	0.038
840	0.064	841	0.040
960	0.069	961	0.043
1080	0.073	1081	0.045
1200	0.075	1201	0.047
1320	0.078	1321	0.048
1440	0.079	1441	0.049
1560	0.08	1561	0.049

Run No. PCG 3.1

Time (min.)	d_{cps} (m)	Time (min.)	d_{cpw} (m)
10	0.003	11	0.000
15	0.003	16	0.000
30	0.006	31	0.002
60	0.008	61	0.003
120	0.011	121	0.005
240	0.015	241	0.008
360	0.017	361	0.011
480	0.021	481	0.013
600	0.025	601	0.015
720	0.028	721	0.019
840	0.031	841	0.021
960	0.035	961	0.022
1080	0.041	1081	0.025
1200	0.049	1201	0.029
1320	0.057	1321	0.032
1440	0.065	1441	0.036
1560	0.072	1561	0.038
1680	0.077	1681	0.041
1800	0.081	1801	0.041
1920	0.084	1921	0.043
2040	0.086	2041	0.047
2160	0.087	2161	0.047
2280	0.087	2281	0.049
2400	0.087	2401	0.049

Run No. PCG 3.2

Time (min.)	d_{cps} (m)	Time (min.)	d_{cpw} (m)
10	0.002	11	0.000
15	0.004	16	0.000
30	0.005	31	0.002
60	0.007	61	0.002
120	0.01	121	0.004
240	0.012	241	0.006
360	0.016	361	0.007
480	0.019	481	0.008
600	0.021	601	0.008
720	0.022	721	0.009
840	0.023	841	0.010
960	0.026	961	0.010
1080	0.028	1081	0.011
1200	0.030	1201	0.012
1320	0.030	1321	0.012
1440	0.030	1441	0.013

Run No. PCG 4.1

Time (min.)	d_{cps} (m)	Time (min.)	d_{cpw} (m)
120	0.002	120	0.000
240	0.003	241	0.002
360	0.005	361	0.004
480	0.008	481	0.007
600	0.010	601	0.008
720	0.012	721	0.010
840	0.015	841	0.012
960	0.017	961	0.013
1080	0.020	1081	0.015
1200	0.025	1201	0.017
1320	0.029	1321	0.018
1440	0.033	1441	0.022
1560	0.037	1561	0.025
1680	0.041	1681	0.028
1800	0.044	1801	0.030
1920	0.045	1921	0.032
2040	0.047	2041	0.034
2160	0.049	2161	0.036
2280	0.050	2281	0.037
2400	0.050	2401	0.037

Run No. PCG 4.2

Time (min.)	d_{cps} (m)	Time (min.)	d_{cpw} (m)
120	0.002	121	0.000
240	0.003	241	0.003
360	0.005	361	0.003
480	0.007	481	0.005
600	0.010	601	0.006
720	0.011	721	0.009
840	0.013	841	0.010
960	0.016	961	0.012
1080	0.018	1081	0.013
1200	0.020	1201	0.015
1320	0.023	1321	0.016
1440	0.026	1441	0.018
1560	0.028	1561	0.019
1680	0.028	1681	0.021
1800	0.031	1801	0.023
1920	0.032	1921	0.024
2040	0.033	2041	0.025
2160	0.034	2161	0.025
2280	0.034	2281	0.025
2400	0.034	2401	0.025

Run No. PCG 5.1

Time (min.)	d_{cps} (m)	Time (min.)	d_{cpw} (m)
360	0.004	361	0.003
480	0.004	481	0.004
600	0.006	601	0.004
720	0.009	721	0.006
840	0.011	841	0.009
960	0.014	961	0.012
1080	0.017	1081	0.014
1200	0.020	1201	0.016
1320	0.022	1321	0.019
1440	0.025	1441	0.021
1560	0.028	1561	0.025
1680	0.031	1681	0.028
1800	0.034	1801	0.029
1920	0.036	1921	0.031
2040	0.039	2041	0.032
2160	0.040	2161	0.034
2280	0.041	2281	0.034
2400	0.041	2401	0.034

Run No. PCG 5.2

Time (min.)	d_{cps} (m)	Time (min.)	d_{cpw} (m)
360	0.003	361	0.002
480	0.004	481	0.002
600	0.005	601	0.003
720	0.005	721	0.004
840	0.006	841	0.005
960	0.006	961	0.007
1080	0.009	1081	0.008
1200	0.011	1201	0.010
1320	0.013	1321	0.012
1440	0.016	1441	0.013
1560	0.020	1561	0.015
1680	0.023	1681	0.016
1800	0.025	1801	0.018
1920	0.027	1921	0.019
2040	0.028	2041	0.020
2160	0.028	2161	0.020
2280	0.029	2281	0.020
2400	0.029	2401	0.020

Run No. PCSG 1.1

Time (min.)	d_{cps} (m)	Time (min.)	d_{cpw} (m)
2	0.024	3	0.028
5	0.041	6	0.033
11	0.052	12	0.039
16	0.064	17	0.045
31	0.081	32	0.051
61	0.090	62	0.053
121	0.108	122	0.066
241	0.119	242	0.078
361	0.125	362	0.091
481	0.132	482	0.096
601	0.137	602	0.104
721	0.139	722	0.108
841	0.140	842	0.110
961	0.140	962	0.111

Run No. PCSG 1.2

Time (min.)	d_{cps} (m)	Time (min.)	d_{cpw} (m)
2	0.022	3	0.016
5	0.030	6	0.021
11	0.042	12	0.036
16	0.055	17	0.041
31	0.064	32	0.052
61	0.079	62	0.055
121	0.092	122	0.060
241	0.099	242	0.073
361	0.116	362	0.086
481	0.119	482	0.09
601	0.12	602	0.092
721	0.122	722	0.093
841	0.122	842	0.094
961	0.122	962	0.094

Run No. PCSG 2.1

Time (min.)	d_{cps} (m)	Time (min.)	d_{cpw} (m)
4	0.004	5	----
10	0.007	11	0.003
15	0.009	16	0.004
30	0.012	31	0.006
60	0.016	61	0.009
120	0.021	121	0.011
240	0.026	241	0.015
360	0.035	361	0.017
480	0.047	481	0.021
600	0.062	601	0.025
720	0.072	721	0.028
840	0.078	841	0.033
960	0.086	961	0.039
1080	0.091	1081	0.045
1200	0.097	1201	0.048
1320	0.103	1321	0.049
1440	0.107	1441	0.050
1560	0.107	1561	0.051

Run No. PCSG 2.2

Time (min.)	d_{cps} (m)	Time (min.)	d_{cpw} (m)
10	0.003	11	0.000
15	0.005	16	0.002
30	0.008	31	0.003
60	0.010	61	0.006
120	0.013	121	0.008
240	0.017	241	0.011
360	0.02	361	0.013
480	0.026	481	0.016
600	0.032	601	0.018
720	0.042	721	0.022
840	0.053	841	0.025
960	0.065	961	0.030
1080	0.076	1081	0.034
1200	0.082	1201	0.037
1320	0.084	1321	0.039
1440	0.085	1441	0.039
1560	0.085	1561	0.039

Run No. PCSG 3.1

Time (min.)	d_{cps} (m)	Time (min.)	d_{cpw} (m)
15	0.003	16	0.002
30	0.005	31	0.002
60	0.006	61	0.004
120	0.008	121	0.006
240	0.011	241	0.007
360	0.013	361	0.010
480	0.016	481	0.012
600	0.018	601	0.016
720	0.023	721	0.02
840	0.027	841	0.025
960	0.033	961	0.029
1080	0.039	1081	0.033
1200	0.043	1201	0.036
1320	0.048	1321	0.038
1440	0.051	1441	0.039
1560	0.054	1561	0.040
1680	0.055	1681	0.040
1800	0.056	1801	0.041

Run No. PCSG 3.2

Time (min.)	d_{cps} (m)	Time (min.)	d_{cpw} (m)
30	0.002	31	0.000
60	0.002	60	0.000
120	0.005	121	0.000
240	0.006	241	0.003
360	0.008	361	0.004
480	0.011	481	0.006
600	0.014	601	0.009
720	0.018	721	0.013
840	0.023	841	0.016
960	0.026	961	0.020
1080	0.028	1081	0.023
1200	0.029	1201	0.027
1320	0.032	1321	0.029
1440	0.032	1441	0.029
1560	0.033	1561	0.030
1680	0.034	1681	0.030
1800	0.034	1801	0.030

Run No. PCSG 4.1

Time (min.)	d_{cps} (m)	Time (min.)	d_{cpw} (m)
60	0.002	61	0.003
120	0.004	121	0.003
240	0.006	241	0.005
360	0.006	361	0.007
480	0.009	481	0.008
600	0.011	601	0.009
720	0.013	721	0.012
840	0.016	841	0.015
960	0.019	961	0.015
1080	0.021	1081	0.019
1200	0.025	1201	0.022
1320	0.028	1321	0.026
1440	0.030	1441	0.028
1560	0.031	1561	0.031
1680	0.032	1681	0.031
1800	0.032	1801	0.032

Run No. PCSG 4.2

Time (min.)	d_{cps} (m)	Time (min.)	d_{cpw} (m)
60	0.003	61	0.002
120	0.005	121	0.003
240	0.005	241	0.006
360	0.006	361	0.006
480	0.008	481	0.008
600	0.009	601	0.008
720	0.011	721	0.011
840	0.015	841	0.012
960	0.016	961	0.013
1080	0.017	1081	0.014
1200	0.018	1201	0.016
1320	0.021	1321	0.016
1440	0.023	1441	0.017
1560	0.024	1561	0.019
1680	0.024	1681	0.019
1800	0.025	1801	0.019

Run No. PCSG 5.1

Time (min.)	d_{cps} (m)	Time (min.)	d_{cpw} (m)
480	0.002	481	0.002
600	0.002	601	0.003
720	0.004	721	0.003
840	0.007	841	0.005
960	0.009	961	0.008
1080	0.011	1081	0.010
1200	0.012	1201	0.013
1320	0.015	1321	0.016
1440	0.017	1441	0.018
1560	0.020	1561	0.022
1680	0.022	1681	0.022
1800	0.025	1801	0.024
1920	0.027	1921	0.024
2040	0.028	2041	0.025
2160	0.028	2161	0.025
2280	0.028	2281	0.025
2400	0.028	2401	0.025

Run No. PCSG 5.2

Time (min.)	d_{cps} (m)	Time (min.)	d_{cpw} (m)
480	0.003	481	0.000
600	0.003	601	0.002
720	0.004	721	0.004
840	0.006	841	0.007
960	0.008	961	0.007
1080	0.009	1081	0.008
1200	0.010	1201	0.009
1320	0.011	1321	0.009
1440	0.011	1441	0.012
1560	0.014	1561	0.013
1680	0.016	1681	0.015
1800	0.017	1801	0.017
1920	0.019	1921	0.017
2040	0.019	2041	0.018
2160	0.020	2161	0.018
2280	0.020	2281	0.018
2400	0.020	2401	0.018